

4-6-2010

Crosslinked conventional size and nanoparticle size acrylic latexes and their blends: Investigation of the effects of crosslinking, particle size and distribution, glass transition temperature and blending on film formation, properties and morphology

Ravi Ghanshyambhai Joshi

Follow this and additional works at: <http://commons.emich.edu/theses>

 Part of the [Polymer and Organic Materials Commons](#)

Recommended Citation

Joshi, Ravi Ghanshyambhai, "Crosslinked conventional size and nanoparticle size acrylic latexes and their blends: Investigation of the effects of crosslinking, particle size and distribution, glass transition temperature and blending on film formation, properties and morphology" (2010). *Master's Theses and Doctoral Dissertations*. 283.

<http://commons.emich.edu/theses/283>

This Open Access Dissertation is brought to you for free and open access by the Master's Theses, and Doctoral Dissertations, and Graduate Capstone Projects at DigitalCommons@EMU. It has been accepted for inclusion in Master's Theses and Doctoral Dissertations by an authorized administrator of DigitalCommons@EMU. For more information, please contact lib-ir@emich.edu.

Crosslinked Conventional Size and Nanoparticle Size Acrylic Latexes and Their Blends:
Investigation of the Effects of Crosslinking, Particle Size and Distribution, Glass Transition
Temperature and Blending on Film Formation, Properties and Morphology

by

Ravi Ghanshyambhai Joshi

Doctoral Thesis

Submitted to School of Engineering Technology in College of Technology

Eastern Michigan University

in partial fulfillment of the requirements for the degree of

DOCTOR OF PHILOSOPHY

in

Technology with a concentration in Polymers and Coatings

Thesis Committee:

Vijaykumar Mannari, PhD, Chair

Frank N. Jones, PhD

Mary L. Brake, PhD

Weidian Shen, PhD

Theodore Provder, PhD (Additional Member)

April 6, 2010

Ypsilanti, Michigan

Dedication

Almighty God

&

My family

Acknowledgements

- PhD Program at College of Technology, Eastern Michigan University
- Doctoral Fellowship Program, Graduate School, Eastern Michigan University
- Surface Science Research Center at Eastern Michigan University
- Rene Crombez and Malik C. Nagolu for SPM work
- Dr. Weihua (Marshall) Ming for guidance and help with experimental of modified microemulsion process
- Sarjak Amin, Paul Ziemer, Ninad Dixit, Chirag Patel, Elodie Lefereve, Achin Goel, and Kumaril Kapadia for valuable technical discussions, experimental lab set-up
- Dr. Bruce Weiner (Brookhaven Instruments) troubleshooting with nanoparticle size measurements
- Dr. Fred Willard and Marty D., CASMI Labs for lab supplies & ASTM test methods
- Madhavi Joshi for valuable technical discussions, nanoparticle synthesis plan, experimental set up, end-use properties testing, and samples preparation for mechanical and thermal analysis testing

Abstract

Synthetic latexes have many product applications including functioning as a binder in paints and coatings. For many years, researchers in industry as well as in academe have been exploring various strategies to improve performance of acrylic latexes mainly to replace traditionally used solvent borne coatings due to increasing environmental concerns and strict governmental regulations. The main goal of the study is to investigate the effects of type (pre-coalescence or post-coalescence) and level of crosslinking, particle size (nano particle size ~ 20-25 nm vs. conventional particle size ~ 120-130 nm) and distribution, glass transition temperature (T_g), and blending on latex film formation process, properties and latex morphology. Films cast from these latexes were characterized using specific end use tests and fundamental properties using advanced instruments such as a dynamic mechanical analyzer (DMA), thermogravimetric analyzer (TGA), modulated differential scanning calorimeter (MDSC), nano-indenter, and atomic force microscope (AFM). The results showed significant improvements in acrylic latex performance proposing coatings near zero VOC and forming basis for exploring potential commercial applications of functional nanosize latexes and their blends.

TABLE OF CONTENTS

Dedication.....	ii
Acknowledgements.....	iii
Abstract.....	iv
List of Tables.....	vii
List of Figures.....	x
Chapter 1: Introduction.....	1
References.....	8
Chapter 2: Historical Overview.....	12
References.....	22
Chapter 3: Effects of pre-coalescence or post-coalescence crosslinking and glass transition temperature.....	26
Introduction.....	26
Experimental Details.....	28
Characterization of Latexes.....	32
Results and Discussion.....	36
Conclusions.....	76
References.....	80
Chapter 4: Synthesis and characterization of nanosize acrylic latex and comparison to their conventional sized counterparts.....	82
Introduction.....	82
Experimental Details.....	86
Characterization of Latexes.....	90

Results and Discussion.....	102
Conclusions.....	122
References.....	125
Chapter 5: Blends of conventional size and nanoparticle size acrylic latexes.....	129
Introduction.....	129
Experimental Details.....	132
Characterization of Latexes.....	136
Results and Discussion.....	141
Conclusions.....	199
References.....	201
Chapter 6: Conclusions.....	204

LIST OF TABLES

<u>Table</u>	<u>Page</u>
3.1 Characteristics of 1, 3-BGDMA Pre-coalescence Crosslinked Latexes.....	38
3.2 Characteristics of DAA Externally Crosslinkable Latexes.....	39
3.3 Empirical properties of films cast from internally crosslinked latexes.....	55
3.4 Empirical properties of films cast from externally crosslinked latexes.....	55
3.5 Results of Stress-Strain Analysis.....	58
3.6 Comparison of DMA values with MDSC T _g values.....	66
4.1 Composition table for nanosize latexes (with or without functional group).....	89
4.2 Characteristics of nanosize (with or without crosslinker) latexes.....	96
4.3 Characteristics of conventional (with or without crosslinker) latexes.....	96
4.4 End use properties of films cast from conventional latexes.....	110
4.5 End use properties of films cast from nanosize latexes.....	110
4.6 Comparison of surface smoothness and gloss values of nanoparticle latexes and their conventional counter parts.....	110
4.7 Results of stress-strain analysis of nanosize latexes.....	113
4.8 Results of stress-strain analysis of conventional size latexes.....	113
4.9 Comparison of DMA values with MDSC T _g values of conventionally size pre-coalescence or post-coalescence crosslinked latexes.....	119
4.10 Comparison of DMA values with MDSC T _g values of nano size pre-coalescence or post-coalescence crosslinked latexes.....	119

5.1	Characteristics of conventionally sized (with or without crosslinker) latexes.....	134
5.2	Characteristics of nanosize (with or without crosslinker) latexes.....	134
5.3	Characteristics of ten most representative latex blends.....	135
5.4(a)	MFT crack point (MFTc) of latex blends.....	148
5.4(b)	MFT knife point (MFTk) of latex blends.....	149
5.5	MDSC T _g of latex blends.....	149
5.6	Cross- cut Adhesion (ASTM D 3359) of latex blends.....	151
5.7	Pencil Hardness (ASTM D 3363) of latex blends.....	151
5.8	Solvent Resistance (MEK 2 Rub) of latex blends.....	151
5.9	Elevated Temperature Block Resistance (ASTM D 4946) of latex blends.....	152
5.10	Acid - Open Spot Test (ASTM D 1308) of latex blends.....	152
5.11	Water - Open Spot Test (ASTM D 1308) of latex blends.....	153
5.12	Specular Gloss (ASTM D 523) of latex blends.....	153
5.13	Formulation matrix based on end-use properties results.....	166
5.14	Latex blend series L0_nL0.....	167
5.15	Latex blend series L0_nIL4.....	168
5.16	Latex blend series L0_nEL2.....	168
5.17	Latex blend series H0_nL0.....	168
5.18	Latex blend series H0_nIL2.....	169
5.19	Latex blend series H0_nEL5.....	169
5.20	Latex blend series EL5_nL0.....	169
5.21	Latex blend series IL4_nL0.....	170
5.22	Latex blend series EH5_nL0.....	170

5.23	Latex blend series IH4_nL0.....	170
5.24	Latex blend series L0_nL0.....	194
5.25	Latex blend series L0_nIL4.....	194
5.26	Latex blend series L0_nEL2.....	195
5.27	Latex blend series H0_nL0.....	195
5.28	Latex blend series H0_nIL2.....	196
5.29	Latex blend series H0_nEL5.....	196
5.30	Latex blend series EL5_nL0.....	197
5.31	Latex blend series IL4_nL0.....	197
5.32	Latex blend series EH5_nL0.....	198
5.33	Latex blend series IH4_nL0.....	198

LIST OF FIGURES

<u>Figure</u>	<u>Page</u>
3.A Schematic representation of 1, 3-BGDMA.....	37
3.B Schematic representation of the latex film formation process.....	40
3.C Schematic representation of DAA & ADDH crosslinking reaction.....	43
3.D Representative friction images of morphological changes observed by AFM contact mode during the film formation.....	50
3.1 Gel Content of Pre-coalescence Crosslinked Latex Films.....	45
3.2 Gel Content of Post-coalescence Crosslinked Latex Films.....	45
3.3 20 $\mu\text{m} \times 20 \mu\text{m}$ AFM topographic image (left) and frictional image (right) of Sample IH-4.....	46
3.4 5 $\mu\text{m} \times 5 \mu\text{m}$ AFM topographic image and frictional images of Sample IH-4.....	47
3.5 AFM topographic Images of Sample EL-1 (top) and IH-4 (bottom). The two images have different Z scales, and surface of EL-1 is much rougher than that of IH-4.....	48
3.6 Comparison of hardness of samples in groups EL and IL with different crosslinker levels. The hardness was measured under a normal force of 1 mN.....	51
3.7 Comparison of moduli of samples in groups EL and IL with different crosslinker levels. The modulus was measured under a normal force of 1 mN.....	52
3.8 Comparison of hardness of samples in groups EH and IH with different crosslinker levels. The hardness was measured under a normal force of 1 mN.....	53
3.9 Comparison of modulus of samples in groups EH and IH with different crosslinker	

levels. The modulus was measured under a normal force of 1 mN.....	53
3.10 Optical Images of the Residual Indentation in films cast from latexes IL-1.2 and IH-1.2 (1000x).....	54
3.11 Average Stress-Strain Curves for Post-Coalescence Series: Low T_g	59
3.12 Average Stress-Strain Curves for Post-Coalescence Series: High T_g	60
3.13 Average Stress-Strain Curves for Pre-Coalescence Series: Low T_g	61
3.14 Average Stress-Strain Curves for Pre-Coalescence Series: High T_g	62
3.15 Storage and Loss modulus curves of Post-coalescence Crosslinked Latexes: High T_g	63
3.16 Storage and Loss modulus curves of Post-coalescence Crosslinked Latexes: Low T_g	64
3.17 Tan delta curves of Post-coalescence Crosslinked Latexes: High T_g	67
3.18 Tan delta curves of Post-coalescence Crosslinked Latexes: Low T_g	68
3.19 Tan delta curves of Pre-coalescence Crosslinked Latexes: Low T_g	70
3.20 Tan delta curves of Pre-coalescence Crosslinked Latexes: High T_g	71
3.21(a) Representative curves showing 1 st day vs. 7 th day comparison of stress-strain analysis of EL series.....	72
3.21(b) Representative curves showing 1 st day vs. 7 th day comparison of stress-strain analysis of IL series.....	72
3.22(a) Representative tan delta curves showing 1 st day vs. 7 th day comparison of DMA studies of EL-2.....	73
3.22(b) Representative tan delta curves showing 1 st day vs. 7 th day comparison of DMA studies of IL- 1.2 samples.....	74
3.23(a) Time based stress-strain analysis of EH-0 at ambeint conditions.....	75
3.23(b) Time based DMA analysis of EH-0 at ambeint conditions.....	75

4.1	Particle Size Analysis Graphs of nanoparticle latexes (Brookhaven Instruments 90 plus Particle Size Software Output)	
	(a) Nanoparticle latex with no crosslinker, nL0.....	97
	(b) Nanoparticle latex with 2% post-coalescence crosslinker, nEL2.....	98
	(c) Nanoparticle latex with 5% post-coalescence crosslinker, nEL5.....	99
	(d) Nanoparticle latex with 2% pre-coalescence crosslinker, nIL2.....	100
	(e) Nanoparticle latex with 4% pre-coalescence crosslinker, nIL4.....	101
4.2	Crosslinking reaction for DAA monomer.....	105
4.3(a)	Comparison of gel content of pre-coalescence crosslinked nanosize vs. conventional latexes.....	107
4.3(b)	Comparison of gel content of post-coalescence crosslinked nanosize vs. conventional latexes.....	107
4.4	AFM tapping mode phase images of (a) nL0, (b) nIL4, and (c) nEL5 at image size of 1um X 1um.....	111
4.5	AFM tapping mode height images of (a) nL0, (b) nIL4, and (c) nEL5 at image size of 1um X 1um.....	111
4.6	AFM tapping mode height images of (a) L0, (b) nIL4, and (c) nEL5 at image size of 2um X 2um.....	112
4.7	Comparison of surface smoothness and gloss values of nanoparticle latexes and their conventional counter parts.....	112
4.8	Comparison of average stress-strain curves for pre-coalescence crosslinked nanosize latex series.....	115
4.9	Comparison of average stress-strain curves for post-coalescence crosslinked	

nanosize latex series.....	115
4.10 Comparison of average stress-strain curves for post-coalescence crosslinked conventional latex series.....	116
4.11 Comparison of average stress-strain curves for post-coalescence crosslinked conventional latex series.....	116
4.12 Comparison of storage and loss modulus curves of pre-coalescence crosslinker nanoparticle latex series.....	117
4.13 Comparison of storage and loss modulus curves of post-coalescence crosslinker nanoparticle latex series.....	117
5. A Volleyball (conventional particles ~120-130nm) vs. golf ball (nanoparticles ~ 20-25 nm).....	179
5.1 Comparison of gel content of (a) pre-coalescence crosslinked nanosize vs. conventional latexes and (b) post-coalescence crosslinked nanosize vs. conventional latexes.....	135
5.2 Crosslinking reactions for DAA monomer.....	144
5.3 L0_nL0 (from left to right - nanolatex concentration: 0%, 15%, 30%, 50%, 70%, and 100%).....	158
5.4 L0_nIL4 (from left to right - nanolatex concentration: 0%, 15%, 30%, 50%, 70%, and 100%).....	158
5.5 L0_nEL2 (from left to right - nanolatex concentration: 0%, 15%, 30%, 50%, 70%, and 100%).....	158
5.6 H0_nL0 (from left to right - nanolatex concentration: 0%, 15%, 30%, 50%, 70%, and 100%).....	158

5.7	H0_nIL2 (from left to right - nanolatex concentration: 0%, 15%, 30%, 50%, 70%, and 100%).....	159
5.8	H0_nEL5 (from left to right - nanolatex concentration: 0%, 15%, 30%, 50%, 70%, and 100%).....	159
5.9	EL5_nL0 (from left to right - nanolatex concentration: 0%, 15%, 30%, 50%, 70%, and 100%).....	159
5.10	IL4_nL0 (from left to right - nanolatex concentration: 0%, 15%, 30%, 50%, 70%, and 100%).....	159
5.11	EH5_nL0 (from left to right - nanolatex concentration: 0%, 15%, 30%, 50%, 70%, and 100%).....	160
5.12	IH4_nL0 (from left to right - nanolatex concentration: 0%, 15%, 30%, 50%, 70%, and 100%).....	160
5.13	Plots of relative average surface smoothness and specular gloss at 20° and 60° vs. % nanoparticles by weight (L0_nL0 series).....	161
5.14	Plots of relative average surface smoothness and specular gloss at 20° and 60° vs. % nanoparticles by weight (L0_nIL4 series)	161
5.15	Plots of relative average surface smoothness and specular gloss at 20° and 60° vs. % nanoparticles by weight (L0_nEL2 series)	162
5.16	Plots of relative average surface smoothness and specular gloss at 20° and 60° vs. % nanoparticles by weight (H0_nL0 series)	162
5.17	Plots of relative average surface smoothness and specular gloss at 20° and 60° vs. % nanoparticles by weight (H0_nIL2 series)	163
5.18	Plots of relative average surface smoothness and specular gloss at 20° and 60°	

vs. % nanoparticles by weight (H0_nEL5 series)	163
5.19 Plots of relative average surface smoothness and specular gloss at 20° and 60°	
vs. % nanoparticles by weight (EL5_nIL0 series)	164
5.20 Plots of relative average surface smoothness and specular gloss at 20° and 60°	
vs. % nanoparticles by weight (EH5_nIL0 series)	164
5.21 Plots of relative average surface smoothness and specular gloss at 20° and 60°	
vs. % nanoparticles by weight (IL4_nIL0 series)	165
5.22 Plots of relative average surface smoothness and specular gloss at 20° and 60°	
vs. % nanoparticles by weight (IH4_nIL0 series).....	165
5.23 Comparison of average stress-strain curves for L0_nL0 series.....	173
5.24 Comparison of average stress-strain curves for L0_nIL4 series.....	173
5.25 Comparison of average stress-strain curves for L0_nEL2 series.....	174
5.26 Comparison of average stress-strain curves for H0_nL0 series.....	174
5.27 Comparison of average stress-strain curves for H0_nIL2 series.....	175
5.28 Comparison of average stress-strain curves for H0_nEL5 series.....	175
5.29 Comparison of average stress-strain curves for IL4_nL0 series.....	176
5.30 Comparison of average stress-strain curves for EL5_nL0 series.....	176
5.31 Comparison of average stress-strain curves for EH5_nL0 series.....	177
5.32 Comparison of average stress-strain curves for IH4_nL0 series.....	177
5.33 (a) Comparison of loss modulus curves and (b) Comparison of storage modulus curves for L0_nL0 series.....	184
5.34 (a) Comparison of loss modulus curves and (b) Comparison of storage modulus curves for L0_nIL4 series.....	185

5.35	(a) Comparison of loss modulus curves and (b) Comparison of storage modulus curves for L0_nEL2 series.....	186
5.36	(a) Comparison of loss modulus curves and (b) Comparison of storage modulus curves for H0_nL0 series.....	187
5.37	(a) Comparison of loss modulus curves and (b) Comparison of storage modulus curves for H0_nIL2 series.....	188
5.38	(a) Comparison of loss modulus curves and (b) Comparison of storage modulus curves for H0_nEL5 series.....	189
5.39	(a) Comparison of loss modulus curves and (b) Comparison of storage modulus curves for EL5_nL0 series.....	190
5.40	(a) Comparison of loss modulus curves and (b) Comparison of storage modulus curves for IL4_nL0 series.....	191
5.41	(a) Comparison of loss modulus curves and (b) Comparison of storage modulus curves for EH5_nL0 series.....	192
5.42	(a) Comparison of loss modulus curves and (b) Comparison of storage modulus curves for IH4_nL0 series.....	193

Chapter 1

Introduction

Latexes have been important to industry for many decades due to their performance and in a number of applications in a wide variety of products in daily human life. Examples can be found in detergents, cosmetics, paints and coatings, and newspapers. For more than 90 years many publications, patents and literature reviews have covered the numerous useful properties of latexes and their application areas.¹⁻³ The literature¹⁻³ reported that almost 7% of the world polymer production is produced as a polymer dispersion which corresponds to 10^7 tons.

A latex is a dispersion of polymer particles in water. It can be described or referred to as an aqueous polymeric dispersion. It should be noted here that the term *aqueous polymeric dispersion* is broad and constitutes a variety of polymeric dispersions. In addition to latexes, prepared by several techniques, for example, there are polyurethane dispersions prepared by a step growth polymerization process. Historians report that the word *latex* in Latin means “liquid” or “fluid” that originally comes from a Greek word “látax” which means a “droplet.”⁴ Natural latexes are produced by plants, notably by the rubber tree. Synthetic latexes are typically synthesized using various heterophase polymerization techniques. More than 10 million tons of latexes or aqueous polymeric dispersions are produced worldwide using heterophase polymerization techniques.^{2, 3, 5}

In the literature¹⁻³ heterophase polymerization is classically described as a polymerization reaction under non-homogeneous conditions. For latex it can be simply described as a process resulting in polymer dispersion, where polymers are finely dispersed meaning mainly insoluble or immiscible in a continuous phase. Any liquid can be a dispersion medium or a continuous phase provided it is a non-solvent for the dispersed material. Most of the heterophase

polymerization techniques are reported to be carried out in water as a dispersion medium or a continuous phase.¹⁻³ Further, the most commonly used dispersing medium for latexes is water due to safety and environmental reasons. However, other volatile organic solvents, stabilizers, and plasticizers are typically present in the dispersion composition. Antonietti and Tauer¹ provided a masterful overview of several heterophase polymerization techniques. Among all those polymerization techniques (a) emulsion polymerization and (b) microemulsion polymerization techniques are the main study of interest.

Emulsion polymerization is widely known and the most commonly used heterophase polymerization technique. The emulsion polymerization technique is used to prepare the majority of commercial synthetic latexes by a free radical-initiated chain growth polymerization process where one or more monomer species is added to aqueous surfactant mixtures, in the presence of an initiator, to form a dispersion of finely divided polymer particles, such as latex. Most latexes are stabilized by surfactants. The surfactants used in the process contribute to stability, and additional stabilizing structures may be formed during the emulsion polymerization process or added later.^{1,6} Further, most of the commercial latexes are produced by a *semicontinuous batch process* where the polymerization is started in the presence of seed latex and monomers and initiators are added in the proportions and rates such that rapid polymerization occurs. In this way, the monomer concentration at any time is low and the polymerization is said to be carried out under monomer starved conditions. The *semicontinuous* emulsion polymerization process and its highlights are covered in great detail in the literature.⁶

In this study a seeded semi-continuous emulsion polymerization was used to prepare acrylic latexes having average particle diameters of 120-140 nm referred to as conventional latexes. The conventional latexes were prepared from commonly used monomers such as n-butyl

acrylate (n-BA), n-butyl methacrylate (n-BMA), and methacrylic acid (MAA). For crosslinking, functional or crosslinkable monomers were used, such as 1-3-butylene glycol dimethacrylate (1-3-BGDMA) was used for pre-coalescence crosslinking and diacetone acrylamide (DAA) used for post-coalescence crosslinking with adipic dihydrazide (ADH).

Microemulsion polymerization was first reported by Stoffer and Bone^{7,8} and Atik and Thomas⁹⁻¹¹ in 1980. Since then a great deal of research has been devoted in the area of making polymeric nanoparticles using microemulsion polymerization processes.^{5,7-27} As reported in the literature^{5,7-27} in the traditional microemulsion polymerization technique the monomer must be slightly water soluble to form a separate phase in the shape of so called spherical droplets. The size of these droplets is mainly controlled by a proper choice of physical dispersing techniques in combination with chemical stabilization systems.^{5,7-27} It has also been reported that due to design of the recipes for microemulsion polymerization processes the polymerization takes place mainly inside the preformed monomer droplets.^{5,7-27} Further details and mechanisms of microemulsion polymerization techniques can be found in several references.^{5,7-27}

Since its introduction many tried to establish the commercial microemulsion process by addressing its classically known limitations – (a) higher surfactant concentrations to form stable polymer microlatexes and (b) low final polymer content. The above two so-called limitations of the microemulsion polymerization technique restricted its proposed viable uses to some extent in coatings, drug delivery, microencapsulation, and many other applications where lower surfactant loading and higher polymer content is desired.

In late 1990s, Ming et al.^{28,29} reported laboratory scale modified microemulsion polymerization producing high solids content nanosize polymer latexes. Ming and his coworkers modified the traditional microemulsion process to produce nano particles with diameters of 10-

30 nm and final polymer content ranging from 10-30 wt. %. The details of the process are covered in later sections. Briefly, in Ming's modified microemulsion polymerization process the original microemulsion was composed of the entire amount of surfactant, a co-surfactant (if required), and a very small portion of monomers and water. The rest of the monomers were added dropwise into the polymerizing microemulsion.

In the present research, Ming's modified microemulsion process was further improved to enable use of a variety of monomers including functional or crosslinkable monomers. The improved modified microemulsion process was developed to produce acrylic nanoparticle latexes having average particle diameters of 15-30 nm referred as nanoparticle latexes. The nanoparticles latexes were prepared using the same monomers used to prepare the conventional size latexes. In other words, the nanoparticle latexes were prepared from commonly used monomers such as n-butyl acrylate (n-BA), n-butyl methacrylate (n-BMA), and methacrylic acid (MAA). For crosslinking, functional or crosslinkable monomers were used, such as 1-3-butylene glycol dimethacrylate (1-3-BGDMA) was used for pre-coalescence crosslinking and diacetone acrylamide (DAA) used for post-coalescence crosslinking with adipic dihydrazide (ADH).

For many years both the emulsion and microemulsion polymerization techniques and their respective mechanisms have been extensively explored by many researchers in academe and in industry, covered in the following section – Historical Overview.

As described earlier, latexes have many applications including functioning as a film former or a binder in paints and coatings – our main area of interest. Traditionally a film former or a binder, commonly considered as the “engine” in a typical paint formulation, is combined with pigments, extenders, and several other additives. In a typical paint formulation, a binder is the main factor that determines the physical, mechanical, and chemical properties of the coating

film.⁶ According to a market report and 2007 – Census Bureau Data,³⁰ aqueous polymeric dispersions (or latexes) in the United States market are the largest of all coatings, mainly used in architectural paints, amounting to an annual sales of more than \$8 billion in the U.S. Further, they contribute to 60% of all sales, mainly in the architectural coatings market segment.³⁰

Despite the environmental benefits of latex paints, however, large sectors of the coatings industry do not use latex paints extensively because latex films typically cannot achieve the strength, hardness, and gloss of enamels and solvent-based paints. Accordingly, latex paints are not widely used in the automotive coatings or marine coatings market segments. Similarly, latex paints have not been widely adopted as protective coatings for metal structures which are exposed to the elements (bridges, refineries, ships, storage tanks, water towers, etc.)

For many years, researchers in industry as well as in academia have been exploring various strategies³¹ to improve latex film properties, such as ultimate mechanical properties (film modulus, tensile strength, elongation at break, etc.) and solvent resistance. The goal of this research is to replace traditionally used solvent-borne coatings due to increased environmental concerns and strict governmental regulations.³² The solvent-borne coatings usually contain substantial amounts of volatile organic compounds (VOCs), which participate in atmospheric photochemical reactions, contributing to the formation of smog and the depletion of the ozone layer.³²

An exhaustive review of the literature^{1, 6, 31, 33, 34} showed that the latex film properties depend upon many factors. These factors include, for example, the chemistries of latex backbone monomers, the polymer glass transition temperatures (T_g), molecular weights, and crosslinking densities of backbone polymers, latex particle size and distribution, surfactant level, the extent of particle coalescence, particle surface functional groups, interfacial crosslinking, film-forming

and curing temperatures and conditions, and so on. By carefully considering these factors, possible approaches^{1, 6, 12, 28, 29, 31, 33-58} to be able to either control or improve latex film properties are (a) imparting a crosslinkable functionality: either externally (between two particles) or internally (within the particle), and/or (b) making polymeric particles nanosize (average particle diameter ~ 15-30 nm), or (c) blending polymer nanoparticle latexes with conventional (average particle diameters ~ 120-140 nm) latexes. The above three approaches form the basic subject of this thesis research.

The main goal of the present study is to investigate the effect(s) of (a) type (pre-coalescence or post-coalescence) and level of crosslinking, (b) particle size and distribution, (c) glass transition temperature (T_g), and (d) blends of conventional and nanoparticle latexes and their different weight ratios on latex film formation process, end-use properties, fundamental thermal and mechanical properties, and latex morphology. As described earlier, in the present research the conventional latexes were prepared using a seeded semi-continuous emulsion polymerization technique, and nanoparticle latexes were prepared using an improved modified microemulsion polymerization technique.^{28, 29} The films cast from the individual conventional and nanoparticle latexes and their respective blends were characterized for physical and mechanical properties, using a variety of end-use tests and advanced instruments such as a Nano-indenter, Dynamic Mechanical Analyzer (DMA), Thermogravimetric Analyzer (TGA), Modulated Differential Scanning Calorimeter (MDSC), and an Atomic Force Microscope (AFM). Information from such tests should greatly enhance our understanding of the relationship between the physical, morphological, and end-use properties of coatings.

This dissertation is divided into six chapters. Chapter 1 includes the introduction, in order to put emulsion and microemulsion produced latexes in their appropriate perspective; a historical

overview of the developments of emulsion and microemulsion polymerization techniques is presented in Chapter 2. Chapter 3 focuses on the effects of precoalescence or postcoalescence crosslinking and glass transition temperature (T_g) on conventional size latex film formation, properties, and latex morphology. Chapter 4 reports synthesis of nanoparticle latexes using improved modified microemulsion process using similar acrylic monomers used for making conventional latexes, including functional (pre-coalescence and post-coalescence) monomers, nanoparticle latex film formation, properties, latex morphology and their comparisons to conventional size counterparts. Chapter 5 covers formulating various blends of selected conventional latexes (Chapter 3) and selected nanoparticle latexes (Chapter 4) in different weight ratios between 7.5/92.5 to 70/30 nanoparticle latex to conventional latex particles and studying the effects blending and blend ratios on latex film formation, properties; and latex morphology. The overall conclusion and scope of future research is covered in Chapter 6.

This study will serve as a fundamental and practical contribution to latex and latex blend research and form a basis for exploring potential commercial applications of crosslinked conventional latexes, nanoparticle latexes, and their respective blends.

References:

1. Antonietti, M.; Tauer, K., 90 Years of Polymer Latexes and Heterophase Polymerization: More vital than ever. *Macromolecular Chemistry and Physics* 2003, 204, (2), 207-219.
2. DeFusco, A. J.; Sehgal, K. C.; Bassett, D. R., Overview of uses of polymer latexes In *NATO ASI Series, Series E: Applied Sciences (Polymeric Dispersions: Principles and Applications)*, Asua, J. M., Ed. Kluwe Academic Publishers: Dordrecht, Boston, London, 1997; Vol. 335, pp 379-396.
3. Distler, D., *Wäßrige Polymerdispersionen: Synthese, Eigenschaften, Anwendungen*. Wiley-VCH: Weinheim, 1999.
4. Blackley, D. C., *Polymer Latices*. 2nd ed.; Chapman & Hall: London, 1997; Vol. 1.
5. Antonietti, M.; Bremser, W.; Muschenborn, D.; Rosenauer, C.; Schupp, B.; Schmidt, M., Synthesis and size control of polystyrene latexes via polymerization in microemulsion *Macromolecules* 1991, 24, (25), 6636-43.
6. Wicks, Z. W.; Jones, F. N.; Pappas, P. S.; Wicks, D. A., *Organic Coatings : science and technology*. 3rd Edition ed.; John Wiley & Sons: Hoboken, New Jersey, 2007.
7. Stoffer, J. O.; Bone, T. J., Polymerization in Water-in-Oil Microemulsion Systems I. *Journal of Polymer Science, Polymer Chemistry Edition* 1980, 18, (8).
8. Stoffer, J. O.; Bone, T. J., Polymerization in water-in-oil microemulsion systems. II. SEM investigation of structure *Journal of Dispersion Science and Technology* 1980, 1, (4), 393-412.
9. Atik, S. S.; Thomas, J. K., Polymerized Microemulsions. *J. American Chemical Society* 1981, 103, (14), 4279-4280.
10. Atik, S. S.; Thomas, J. K., Photochemistry in polymerized microemulsion systems *Journal of the American Chemical Society* 1982, 104, (12), 5868-74.
11. Atik, S. S.; Thomas, J. K., Photoinduced reactions in polymerized microemulsions *Journal of the American Chemical Society* 1983, 105, (14), 4515.
12. Winnik, M. A., The formation and properties of latex films. In *Emulsion Polymerization and Emulsion Polymers*, Lovell, P. A. E.-A., M. S., Ed. Wiley: New York, 1997; pp 467-518.
13. Candau, F.; Leong, Y. S.; Fitch, R. M., Kinetic study of the polymerization of acrylamide in inverse microemulsion *Journal of Polymer Science, Polymer Chemistry Edition* 1985, 23, (1), 193-214.
14. Candau, F.; Leong, Y. S.; Fitch, R. M., Effect of solution components on the termination mechanism in acrylamide microemulsion polymerizations *Journal of Polymer Science, Part A: Polymer Chemistry* 1989, 27, (7), 2179-88.
15. Capek, I.; Potisk, P., Microemulsion polymerization of butyl acrylate. IV. Effect of emulsifier concentration *Journal of Polymer Science, Part A: Polymer Chemistry* 1995, 33, (10), 1675-83.
16. Corpart, J. M.; Selb, J.; Candau, F., Characterization of high charge density ampholytic copolymers prepared by microemulsion polymerization *Polymer* 1993, 34, (18), 3873-86.
17. Feng, L.; Ng, K. Y. S., In situ kinetic studies of microemulsion polymerizations of styrene and methyl methacrylate by Raman spectroscopy *Macromolecules* 1990, 23, (4), 1048-53.

18. Gan, L. M.; Chew, C. H.; Lee, K. C.; Ng, S. C., Polymerization of methyl methacrylate in ternary oil-in-water microemulsions *Polymer* 1993, 34, (14), 3064-9.
19. Gan, L. M.; Chew, C. H.; Lee, K. C.; Ng, S. C., Formation of polystyrene nanoparticles in ternary cationic microemulsions *Polymer* 1994, 35, (12), 2659-64.
20. Gan, L. M.; Chew, C. H.; Lian, N.; Li, G. Z., Polymerization of Styrene in a Winsor I-like System *Langmuir* 1994, 10, (7), 2197-201.
21. Gan, L. M.; Chew, C. H.; Lye, I.; Ma, L.; Li, G., Effect of water-soluble cosurfactants on microemulsion polymerization of styrene *Polymer* 1993, 34, (18), 3860-4.
22. Guo, J. S.; Sudol, E. D.; Vanderhoff, J. W.; El-Asser, M. S., Particle nucleation and monomer partitioning in styrene oil-in-water microemulsion polymerization *Journal of Polymer Science, Part A: Polymer Chemistry* 1992, 30, (5), 691-702.
23. Guo, J. S.; Sudol, E. D.; Vanderhoff, J. W.; El-Asser, M. S., Modeling of the styrene microemulsion polymerization *Journal of Polymer Science, Part A: Polymer Chemistry* 1992, 30, (5), 703-12.
24. Kuo, P. L.; Turro, N. J.; Tseng, C. M.; El-Aasser, M. S.; Vanderhoff, J. W., Photoinitiated polymerization of styrene in microemulsions *Macromolecules* 1987, 20, (6), 1216-21.
25. Rodriguez-G., L. A.; Mendizabal, E.; Puig, J. E.; Kaler, E. W., Polymerization of methyl methacrylate in 3-component cationic microemulsion *Journal of Applied Polymer Science* 1993, 48, (5), 775-86.
26. Texter, J.; Oppenheimer, L. E.; Minter, J. R., Microemulsion polymerization in the water, bis(2-ethylhexyl) sulfosuccinate sodium salt (Aerosol-OT), tetrahydrofurfuryl methacrylate system *Polymer Bulletin (Berlin, Germany)* 1992, 27, (5), 487-94.
27. Wu, C., Laser Light Scattering Determination of the Surfactant Interface Thickness of Spherical Polystyrene Microlatexes. *Macromolecules* 1994, 27, (24), 7099-102.
28. Ming, W.; Jones, F. N.; Fu, S., High solids-content nanosize polymer latexes made by microemulsion polymerization. *Macromolecular Chemistry and Physics* 1998, 199, (6), 1075-1079.
29. Ming, W.; Jones, F. N.; Fu, S., Synthesis of nanosize poly(methyl methacrylate) microlatexes with high polymer content by a modified microemulsion polymerization. *Polymer Bulletin* 1998, 40, (6), 749-756.
30. Challener, C., Environmentally Friendly Paints and Coatings: Making the world a Greener Place. *JCT Coatings Tech* July, 2006, pp 2-8.
31. Taylor, J. W.; Winnik, M. A., Functional Latex and Thermoset Latex Films. *Journal of Coatings Technology Research* 2004, 1, (3), 163-190.
32. Joshi, R.; Provder, T.; Kustron, K., Green coatings: a trend that is becoming the rule rather than the exception *JCT CoatingsTech* 2008, 5, (1), 38-43.
33. Lee, D., The effects of latex coalescence and interfacial crosslinking on the mechanical properties of latex films. *Polymer* 2005, 46, (4), 1287-1293.
34. Flory, P. J., Effects of molecular structure on physical properties of butyl rubber. *Industrial and Engineering Chemistry* 1946, 38, (4), 417-436.
35. Emmons, W. D. Ambient or low-temperature curable coatings. 4,210,565, 1980.
36. Jones, F. N.; Mao, W.; Ziemer, P. D.; Xiao, F.; Hayes, J.; M., G., Artist Paints –an overview and preliminary studies of durability. *Progress in Organic Coatings* 2005, 52, 9-20.
37. Geelhaar, H. J.; Penzel, E.; Ley, G. Binders for paints. 4267091 1981.

38. Robinson, G. F.; Shemancik, R. C.; Speight, R. D.; Wong, P. T.; Znidersic, K. M. Coating compositions and coatings formed therefrom. 6,605,359, 2003.
39. Winnik, M. A., Crosslinking and polymer interdiffusion in latex films. *Polymer Preprints* 2003, 44, (1), 100-101.
40. Park Y.; Monteiro, M. J. v. E. S. G. A. L., Effect of ambient crosslinking on the mechanical properties and film morphology of PSTY-P(BA-co-AAEMA) reactive composite latexes. *European Polymer Journal* 2001, 37, (5), 965-973.
41. Teng, G.; Soucek, M. D., Effect of introduction mode of hydroxyl functionality on morphology and film properties of cycloaliphatic diepoxide crosslinkable core-shell latex. *Journal of Polymer Science Part A: Polymer Chemistry* 2002, 40, 4256-4265.
42. Park, Y.; Kim, J.-H., Film formation form reactive latex particles : influence of interparticle crosslinking on mechanical properties. *Colloids and Surfaces A* 1999, 153, 583-590.
43. Zosel, A.; Ley, G., Influence of cross-linking on structure, mechanical properties, and strength of latex films. *Macromolecules* 1993, 26, 2222-2227
44. Winnik, M. A., Interdiffusion and crosslinking in Thermoset Latex Films. *Journal of Coatings Technology* 2002, 74, (925), 49-63.
45. Ghazaly, H. M.; Daniels; E.S.; Dimonie; V.L.; Klein, A.; Sperling, L. H.; El-Aasser, M. S., Properties of N-butyl methacrylate copolymer latex films derived from crosslinked latex particles. *Journal of Applied Polymer Science* 2003, 88, 42-49.
46. Bufkin, B.; Grawe, J. R., Survey of Applications, Properties, and Technology of Crosslinking Emulsions: Part I. *Journal of Coatings Technology* 1978, 50, (641), 41-55.
47. Bufkin, B.; Grawe, J. R., Survey of Applications, Properties, and Technology of Crosslinking Emulsions: Part III. *Journal of Coatings Technology* 1978, 50, (644), 83-109.
48. Bufkin, B.; Grawe, J. R., Survey of Applications, Properties, and Technology of Crosslinking Emulsions: Part IV. *Journal of Coatings Technology* 1978, 50, (645), 70-100.
49. Bufkin, B.; Grawe, J. R., Survey of Applications, Properties, and Technology of Crosslinking Emulsions: Part V. *Journal of Coatings Technology* 1978, 50, (647), 65-96.
50. Bufkin, B.; Grawe, J. R., Survey of the Applications, Properties, and Technology of Crosslinking Emulsions : Part II. *Journal of Coatings Technology* 1978, 50, (643), 67-83.
51. Ghazaly, H. M.; Daniels, E. S.; Dimonie, V. L.; El-Aasser, M. S.; Klein, A., Synthesis and characterization of a macromonomer crosslinker. *Journal of Applied Polymer Science* 2000, 77, 1362-1368.
52. Coleman, L. E.; Bork, J. F.; Wyman, D. P.; Hoke, D. I., Synthesis and polymerization of N[2-(2-methyl-4-oxopentyl)]-acrylamide-A new reactive vinyl monomer. *Journal of polymer Science Part A: General Papers* 1965, 3, (4), 1601-1608.
53. Huang, Y.; Jones, F. N., Synthesis of crosslinkable acrylic latexes by emulsion polymerization in the presence of etherified melamine-formaldehyde (MF) resins. *Progress in Organic Coatings* 1996, 28, 133-141.
54. Hahn, K.; Ley, G.; Schuller, H.; Oberthur, R., On Particle Coalescence in Latex Films. *Colloid & Polymer Science* 1986, 264, (12), 1092-1096.
55. El-Aasser, M. S.; Tang, J.; Wang, X.; Daniels, E. S.; Dimonie, V. L.; Sudol, E. D., Advances in Emulsion Polymerization for Coatings Applications: Latex Blends and Reactive Surfactants. *Journal of Coatings Technology* 2001, 73.
56. Winnik, M. A.; Feng, J., Latex Blends: An approach to Zero VOC Coatings. *Journal of Coatings Technology* 1996, 68, (852).

57. Eckersley, S. T.; Helmer, B. J., Mechanistic considerations of particle size effects on film properties of hard/soft latex blends. *Journal of Coatings Technology* 1997, 69, (864), 97-110.
58. Winnik, M. A.; Feng, J., Polymer Blend Latex Films: Morphology and Transparency. *Macromolecules* 1995, 28.

Chapter 2

Historical Overview

Paint and coatings technology can be classified as one of the oldest technologies in the history of mankind. Several historical reviews^{1,2} reported that the Egyptians and many of the ancient Asian and European cultures used a mixture of raw natural pigments (for example, turmeric) with plant oil or egg-yolk for decorative as well as protective purpose. In their masterful historical review on the historical development of heterophase polymerization techniques Antonietti and Tauer³ noted that the development of heterophase polymerization techniques has a strong connections to the history of synthetic rubber manufacturing. Historically, saps from trees were used to make elastic rubber balls, glue, or waterproofed clothes. Antonietti and Tauer³ further noted that the birth of emulsion polymerization claiming it as one of the key heterophase polymerization techniques goes back to 1912 when a pioneer researcher K. Gotlob filed the first patent on manufacturing synthetic rubber using naturally occurring materials via emulsion polymerization technique.^{3,4}

In the following 20 years, several companies in the United States and Germany extensively explored emulsion polymerization processes that led to some groundbreaking research studies including the development of catalyzed emulsion polymerization process and commercialization of synthetic latexes using emulsion polymerization process.^{3,4} Katz^{3,5,6} and Mark^{3,7,8} reported a comprehensive review on the early developments of emulsion polymerization processes. According to previous reports^{3,4} from the 1930s to 1950s; nearly two decades, the number of commercially available synthetic latexes made using an emulsion polymerization process increased from a few to nearly 200. Several manufacturers in the U.S.

and Germany soon recognized the value and merits of emulsion polymerization process in comparison to traditionally used the bulk polymerization process.

As reported in the literature⁹ during the World War II, C. S. Marvel led a synthetic rubber project supported by the US government involving 100 other chemists. Further, Marvel and his group were involved in a rush program to develop synthetic rubber because supplies of rubber from Asia were cut off. During the war, the group worked on several key issues and made huge contributions to the developing area of emulsion polymerization technique. The details of Marvel and his group's work during the war are reported in detail in the literature.⁹ The research by Marvel and his group was a major impetus for commercial development starting in 1945.

In their key historical overview, Winnik and Taylor⁴ report that in 1946 Dow Chemical Company commercialized the first styrene-butadiene (SBR) latex, followed by commercialization of AC-33 acrylic latex for coatings (Rohm & Haas) and vinyl acetate based latex - UCAR WC 130 (Union Carbide).^{3,4}

Prior to 1930 the majority of the research carried out in the emulsion polymerization area remained within the industrial domain in the form of trade secrets, patents, or non-public research reports. In their historical overview, Antonietti and Tauer³ report that there was only one report in form of an abstract on emulsion polymerization in the open literature before 1939. This was part of a talk by a German scholar Fikentscher during an annual plastic division meeting in Germany in 1938. In another example, Antonietti and Tauer³ report that after World War II, research scientists at Bayer published the first document on emulsion polymerization of butadiene using redox polymerization and chain transfer agents. It was around the 1950s when

researchers and scholars in academia and independent research institutes focused intensely on experimental and theoretical investigation of the emulsion polymerization process.

Harkins,¹⁰ Smith, and Ewart¹¹ reported the first theory of emulsion polymerization. A general mechanism of emulsion polymerization technique was reported by Harkins¹⁰ proposing two key features: (a) he considered two loci of particle formation (i) monomer swollen micelles and (ii) the aqueous phase. According to Harkins¹⁰ the aqueous phase becomes more and more important with decreasing emulsifier concentration, and (b) the monomer swollen polymer particles become the locus in which nearly all of the polymer is formed. Another key and perhaps the most important contribution came from Smith and Ewart¹¹ in 1948. They developed a quantitative theory of the kinetics of radical polymerization in monomer swollen polymer particles (isolated loci) where the free radicals are supplied to loci from the aqueous phase (external source). Further details of Smith and Ewart theory is covered extensively in the past by many researchers available in the literature elsewhere.^{3,4} In later years, many scientists studied the kinetics of emulsion polymerization technique based upon Smith-Ewart theory. Notably, Flory^{12,13} developed his theories on the swelling structures and gelation and made huge contributions to polymer science in general. The literature^{3,4} reports another significant contribution that came from Bradford and his co-workers publishing their dry-sintering theory of latex film formation.

The literature^{3,4,14} reports that during the early 1970s first Fitch and Tsai¹⁵⁻¹⁸ and later Hansen and Ugelstad¹⁹⁻²³ contributed and proposed the now famous HUFT,¹⁵ homogenous nucleation theory, in emulsion polymerization. Additionally, Hansen and Ugelstad¹⁹⁻²³ also contributed to general kinetics of emulsion polymerization in 1976. In later years, Napper,

Gilbert, and coworkers^{24, 25} made many important contributions towards understanding the emulsion polymerization mechanism.

To date, many quantitative theories for understanding mechanisms of emulsion polymerization have been proposed. Scholars have reported¹⁴ that none of the proposed mechanisms can be generally applied to all systems, because of the wide range of variables involved in the emulsion polymerization process. It should be noted here that many of the early studies were based on small-scale batch processes that cannot be used in large scale production. As a result, some of the earlier mentioned theories do not apply well for starved feed conditions. As reported in the review literature,^{3, 4, 14} various theories and mathematical models of emulsion polymerization have been concisely reviewed by Hansen et al.¹⁹⁻²³ and van Berkel et al.²⁶⁻²⁹ Also, as cited in Wicks et al.,¹⁴ Herrera-Ordonez et al. reviewed controversial issues related to mechanisms of emulsion polymerization technique.

Due to increasing commercial significance and focus on synthetic latexes many researchers worked on understanding film formation behavior of heterogeneous systems that ultimately influences film properties. As reported in the review literature^{3, 4, 14} Bradford and co-workers^{30, 31} proposed dry-sintering theory, concluding that the surface tension of the polymer plays a critical role in driving particle compaction to a fully dense film. Sheetz³² showed that evaporation of water from latex films produce stresses (osmotic) that compressed particles. Vanderhoff^{33, 34} proposed that water interfacial tension provides the necessary force for particle compression, ultimately producing particle deformation and densification. Vyoutskaa^{35, 36} suggested that autohesion or polymer diffusion was essential to the development of the mechanical properties of the latex films. Routh and Russel^{37, 38} provided an in-depth view of various film formation mechanisms and developed a model that explains the circumstances under

which each of the mechanisms may dominate. During the 1980s and 1990s, research efforts of the scholars in this area resulted in developments of two direct methods to measure interdiffusion of polymeric chains in latex film formation. Hahn and co workers^{39, 40} and Sperling and his group⁴¹⁻⁴³ monitored interdiffusion of poly (butyl methacrylate) and deuterated polystyrene using small angle neutron scattering (SANS). Winnik and coworkers^{4, 14} developed direct nonradiative energy transfer (DET) method and studied diffusion mechanisms latex polymers.^{4, 14}

Notably, one classical and well-known model of latex film formation by Winnik^{4, 14} describes the latex film formation in three steps (1) evaporation of volatiles (solvent), (2) particle deformation to a continuous film (coalescence), and (3) molecular interpenetration to knit the particles together (fusion). However, the three steps need not be distinct, and they may take place concurrently as the film forms. According to this classical model, varying the water and solvent composition of the latexes and size of the polymer particles will vary the properties of the resultant film. Additionally, the degree to which the polymers interpenetrate and bind together can be influenced by the inclusion of crosslinkers that bind separate polymer chains together to form a vast network of linked molecules. The detailed discussion of this is covered in Chapter 3.

Since 1950, the ongoing commercialization of synthetic polymer latex (or aqueous polymeric dispersions), however, created a need to develop and understand many new heterogeneous polymerization techniques. In addition it was critical to understand film formation process and other useful properties of heterogeneous particles when dispersed in water. All this was accelerated mainly due to increased environmental concerns, strict governmental regulations, and technological advancements that resulted in a continuous shift from traditionally used solvent based materials to aqueous polymeric dispersions.

Prior to 1960,⁴⁴ there were hardly any regulations or laws that specified or restricted the use of toxic substances or the amount of volatile organic solvents (VOCs) in paint manufacturing and application. For example, lead pigments (that are toxic in nature and hazardous to human health), were used without any regulations or mandated limits in commercial paint manufacturing.⁴⁴ Another example involves VOC levels. When a gallon of typical paint was used to coat a surface, approximately 900 grams of volatile organic compounds were released into the atmosphere.⁴⁴ When exposed to sunlight, these VOCs contributed to the formation of smog.⁴⁴ These compounds have been classically defined by the Environmental Protection Agency (EPA) as “any compound of carbon, excluding carbon monoxide, carbon dioxide, carbonic acid, metallic carbides or carbonates, and ammonium carbonate, which participates in atmospheric photochemical reactions”.⁴⁴ The above and many more similar examples raised concerns about product safety, health, and environmental friendliness. These concerns generated a need to develop regulatory standards for consumer products related to paints and coatings.

In 1966, California’s “Rule 66” was promulgated by the Los Angeles Air Pollution Control Department (LAAPC) regarding VOC emissions.⁴⁴ Rule 66 was among the first regulation in the country regarding VOC emissions.⁴⁴ It took effect in 1967. Since the passing of Rule 66, the federal government enacted the Clean Air Act in 1967 and established the Environmental Protection Agency (EPA).⁴⁴ The purpose of the law was to regulate the use of “toxic air pollutants which were hazardous to human health or the environment”.⁴⁴ The Clean Air Act was amended in 1977 and again in 1990.⁴⁴ In addition to nationwide laws, the states were also asked to develop State Implementation Plans (SIPs), “a collection of the regulations a state will use to clean up polluted areas”,⁴⁴ mandated by the 1990 Clean Air Act.⁴⁴ In 1978, the Consumer Product Safety Commission (CPSC)⁴⁵ became involved and issued a regulation to

restrict the use of lead pigment in commercial paint manufacturing. It should also be mentioned that during this period similar regulations – somewhat different in form – were being enacted in Europe.⁴⁴

The introduction of the federal and state regulations pushed the researchers in industries as well as in academe to think “outside the box”.⁴⁴ They started exploring new strategies to meet the mandated limits. As a result, many scientists in industry and academia started looking at various approaches to enhance the performance of synthetic latexes prepared using emulsion polymerization technique. In addition, a great deal of research efforts have been devoted to exploration and commercialization of several advanced polymerization techniques, such as microemulsion polymerization, miniemulsion polymerization, or microencapsulation. From all the advanced polymerization techniques developed in last 30 years, this dissertation focuses on microemulsion polymerization discussed below.

Broadly, the literature^{3, 14} describes microemulsion as a – “large amounts of two immiscible liquids (e.g. water and oil) brought into a single phase (macroscopically homogeneous but microscopically heterogeneous) by addition of an appropriate surfactant or a surfactant mixture.” Characteristically, microemulsions are classified as a unique class of optically clear, thermodynamically stable, and usually low-viscosity solutions.^{3, 14} The literature^{3, 14} reports two essential distinctions between the emulsion polymerization and the microemulsion polymerization: (a) particle size of the resulting latex polymers and (b) the stability feature of the process. Further, as referred in the literature^{3, 14} the emulsion polymerization process is characterized as a kinetically stable process, whereas microemulsion polymerization process is characterized as a thermodynamically stable process.

Microemulsion polymerization was first reported by Stoffer and Bone^{46, 47} and Atik and Thomas⁴⁸⁻⁵⁰ in 1980-82. The early microemulsion polymerization processes that were reported produced microlatexes with smaller particle diameters of 10-100 nm when compared to a conventional latex made using traditional emulsion polymerization technique with relatively larger particle diameters of 50 nm or higher. Antonietti et al.⁵¹ and Wu⁵² established a quantitative relation between particle size and the monomer to surfactant ratio for a range of compositions with the ratios ranging from 1/3 to 3/1 of monomer to surfactant. Many publications describing microemulsion polymerization of water insoluble⁵³⁻⁶⁴ and water soluble monomers⁶⁵⁻⁶⁷ subsequently followed. Many of these research publications, though not all of them, reported (a) higher surfactant concentrations to form stable polymer microlatexes, and (b) final polymer content of less than 10% wt. The removal of surplus surfactant was seldom undertaken, since it would be an expensive process. The above two or any other reported limitations of the traditional microemulsion process restricted its proposed viable and commercial uses to some extent in coatings, drug delivery, microencapsulation, and many other applications where lower surfactant loading and higher polymer content is desired.

In recent years, many research attempts⁵³⁻⁶⁴ were focused on addressing the above two as well as other limitations of the traditional microemulsion polymerization process. Gan et al.^{68, 69} reported polymerization of styrene and methyl methacrylate using cationic surfactants and relatively high weight ratios of polymer to surfactant (approximately 8/1 polymer/surfactant) and produced latexes with average particle diameters between 30-100 nm. Recently, He et al.⁷⁰ studied the preparation polystyrene (PS) nano particles using seeded polymerization method utilizing anionic surfactants. The resulting polymethacrylate/polystyrene (PMMA/PS) nanoparticles had an average particle diameter < 20 nm using lower amounts of surfactant. Kaiyi

and Zhaoqun⁷¹ demonstrated a novel microemulsion polymerization process and reported monodisperse polystyrene nanoparticles with average particle diameters < 20 nm using very low amount of surfactant. Several other research attempts are covered in great detail in previous literature.⁵³⁻⁶⁴

Notably, in late 1990s Ming et al.^{72, 73} reported laboratory scale modified microemulsion polymerization producing high solids content nanosize polymer latexes. Ming and his coworkers modified the traditional microemulsion process to produce nano particles with diameters of 10-30 nm and final polymer content ranging from 10-30 wt%. In this process the polymer/surfactant ratio was kept at 7:1 to 12:1. This ratio was significantly higher than a traditional microemulsion process that typically uses 1:1 polymer/surfactant or even lower as reported in many previous methods.^{51, 52} Briefly, in the modified microemulsion polymerization the original microemulsion was composed of the entire amount of surfactant, a co-surfactant (if required), a very small portion of monomer or monomer mixture, and water. The rest of the monomer or monomer mixture was added dropwise into the polymerizing microemulsion. The researchers^{72, 73} used anionic, cationic, non-ionic surfactants and their mixtures to produce high solids content nanosize latexes. The researchers also studied the particle size changes during the polymerization, the polymerization mechanism and some specific end-use properties. Promising results from Ming's modified technique opened up a wealth of opportunities for future research, particularly, exploration for potential applications in the area of polymers and coatings forming basis for this research.

In summary, for many years and at present a great deal of research has mainly focused on (a) emulsion polymerization techniques and (b) developing and understanding advanced

polymerization techniques (such as microemulsion polymerization) in order to ultimately produce latexes with enhanced performance properties for wide variety of applications.

References:

1. Martens, C. R., *Introduction of Coating Industry. Technology of Paints, Varnishes and Lacquers*. R.E.Krieger Publishing: New York, 1974; Vol. II, p 1-12.
2. Fischer, W. v., *Introduction to the Protective Coatings Industry. Paint and Varnish Technology*. Reinhold Publishing Corp.: New York, 1948; Vol. I, p 1-11.
3. Antonietti, M.; Tauer, K., 90 Years of Polymer Latexes and Heterophase Polymerization: More vital than ever. *Macromolecular Chemistry and Physics* 2003, 204, (2), 207-219.
4. Taylor, J. W.; Winnik, M. A., Functional Latex and Thermoset Latex Films. *Journal of Coatings Technology Research* 2004, 1, (3), 163-190.
5. Whitby, G. S.; Katz, M., Synthetic Rubber. *Ind. Eng. Chem.* 1933, 25, (12), 1338-1348.
6. Whitby, G. S.; Katz, M., Synthetic Rubber. *Ind. Eng. Chem.* 1933, 25, (11), 1204-1211.
7. Hohenstein, W. P.; Mark, H., Polymerization of olefins and diolefins in suspension and emulsion. I. *Journal of Polymer Science* 1946, 1, 127-45.
8. Hohenstein, W. P.; Mark, H., Polymerization of olefins and diolefins in suspension and emulsion. II. *Journal of Polymer Science* 1946, 1, 549-80.
9. Morris, P. J. T., *Polymer Pioneers: A Popular History of the Science and Technology of Large Molecules*. Diane Publishing Co: Darby, PA, 1986; p 88.
10. Harkins, W. D., A General Theory of the Mechanism of Emulsion Polymerization. *Journal of American Chemical Society* 1947, 69, 1428-1444.
11. Smith, W. V.; Ewart, R. H., Kinetics of Emulsion Polymerization. *J. Chem. Phys.* 1948, 16, (6), 592-599.
12. Flory, P. J., Effects of molecular structure on physical properties of butyl rubber. *Industrial and Engineering Chemistry* 1946, 38, (4), 417-436.
13. Flory, P. J., *Principles of Polymer Chemistry*. Cornell University Press: London, 1953; p 495-518.
14. Wicks, Z. W.; Jones, F. N.; Pappas, P. S.; Wicks, D. A., *Organic Coatings : science and technology*. 3rd Edition ed.; John Wiley & Sons: Hoboken, New Jersey, 2007.
15. Fitch, R. M., "Polymer Colloids: A Comprehensive Introduction". Academic Press: San Diego, London, Boston, New York, Sydney, Tokyo, 1997.
16. Fitch, R. M.; Tsai, C., Polymer colloids: particle formation in nonmicellar systems. *Journal of Polymer Science, Polymer Letters Edition* 1970, 8, (10), 703-10.
17. Fitch, R. M.; Tsai, C. H. In *Homogeneous nucleation of polymer colloids. IV. Role of soluble oligomeric radicals*, Polym. Colloids, Proc. Symp. , Storrs, CT, USA, 1971; Fitch, R. M., Ed. Dep. Chem.; Univ. Connecticut: Storrs, CT, USA, 1971; pp 103-16.
18. Fitch, R. M.; Tsai, C. H. In *Particle formation in polymer colloids. III. Prediction of the number of particles by a homogeneous nucleation theory*, Polym. Colloids, Proc. Symp., Storrs, CT, USA 1971; Fitch, R. M., Ed. Dep. Chem.; Univ. Connecticut: Storrs, CT, USA 1971; pp 73-102.
19. Hansen, F. K.; Ugelstad, J., Particle nucleation in emulsion polymerization. I. A theory for homogeneous nucleation. *Journal of Polymer Science, Polymer Chemistry Edition* 1978, 16, (8), 1953-79.

20. Hansen, F. K.; Ugelstad, J., Particle nucleation in emulsion polymerization. II. Nucleation in emulsifier-free systems investigated by seed polymerization. *Journal of Polymer Science, Polymer Chemistry Edition* 1979, 17, (10), 3033-45.
21. Hansen, F. K.; Ugelstad, J., Particle nucleation in emulsion polymerization. III. Nucleation in systems with anionic emulsifier investigated by seeded and unseeded polymerization. *Journal of Polymer Science, Polymer Chemistry Edition* 1979, 17, (10), 3047-67.
22. Hansen, F. K.; Ugelstad, J., Particle nucleation in emulsion polymerization. IV. Nucleation in monomer droplets. *Journal of Polymer Science, Polymer Chemistry Edition* 1979, 17, (10), 3069-82.
23. Ugelstad, J.; Hansen, F. K., Kinetics and mechanism of emulsion polymerization. *Rubber Chemistry and Technology* 1976, 49, (3), 536-609.
24. Gilbert, R. G.; Napper, D. H.; Lichti, G.; Ballard, M.; Sangster, D. F., Emulsion polymerization in seeded systems. *Organic Coatings and Plastics Chemistry* 1980, 43, 527-30.
25. Lichti, G.; Gilbert, R. G.; Napper, D. H. In *Molecular weight distributions of polymer formed in emulsion polymerization*, Polym. Colloids 2 [Two], [Proc. Symp. Phys. Chem. Prop. Colloidal Part.] Sydney, Australia 1980; Fitch, R. M., Ed. Plenum, New York, N. Y: Sydney, Australia 1980; pp 651-58.
26. Castro, J. V.; van Berkel, K. Y.; Russell, G. T.; Gilbert, R. G., General Solution to the Band-Broadening Problem in Polymer Molecular Weight Distributions. *Australian Journal of Chemistry* 2005, 58, (3), 178-181.
27. van Berkel, K. Y.; Russell, G. T.; Gilbert, R. G., Entry in Emulsion Polymerization: Effects of Initiator and Particle Surface Charge. *Macromolecules* 2003, 36, (11), 3921-3931.
28. van Berkel, K. Y.; Russell, G. T.; Gilbert, R. G., Molecular Weight Distributions and Chain-Stopping Events in the Free-Radical Polymerization of Methyl Methacrylate. *Macromolecules* 2005, 38, (8), 3214-3224.
29. van Berkel, K. Y.; Russell, G. T.; Gilbert, R. G., The dissociation rate coefficient of persulfate in emulsion polymerization systems. *Polymer* 2006, 47, (13), 4667-4675.
30. Dillion, R. E.; Matheson, L. A.; Bradford, E. B., Sintering of Synthetic Latex Particles. *J. Colloid Sci.* 1951, 6, 107-117.
31. Henson, W. A.; Taber, D. A.; Bradford, E. B., *Ind. Eng. Chem.* 1953, 45, 735.
32. Sheetz, D. P., Formation of films by drying of latex. *Journal of Applied Polymer Science* 1965, 9, (11), 3759-73.
33. Vanderhoff, J. W.; Bradford, E. B.; Tarkowski, H. L.; Wilkinson, B. W., High-energy irradiation in an investigation of the mechanism and kinetics of emulsion polymerization. *Journal of Polymer Science* 1961, 50, 265-86.
34. Vanderhoff, J. W.; Tarkowski, H. L.; Jenkins, M. C.; Bradford, E. B., Theoretical Consideration of the Interfacial Forces Involved in the Coalescence of Latex Particles. *J. Macromol. Sci. Chem.* 1966, 1, (2), 361-397.
35. Voyutskii, S. S., Autohesion and Adhesion of High Polymers. In *Polymer Reviews*, Saegusa, F. a., Ed. Wiley: NY, 1963; Vol. 4, p 272.
36. Voyutskii, S. S.; Ustinova, Z. M., Role of autohesion during film formation from the latex. *Journal of Adhesion* 1977, 9, (1), 39-50.
37. Routh, A. F.; Russel, W. B., Horizontal Drying Fronts in Evaporating Latex Films. *AICHE J.* 1998, 44, 2088.

38. Routh, A. F.; Russel, W. B., A Process Model for Altex Film Formation: Limiting Regimes for Individual Driving Forces. *Langmuir* 1999, 15, 7762-7773.
39. Hahn, K.; Ley, G.; Schuller, H.; Oberthur, R., On Particle Coalescence in Latex Films. *Colloid & Polymer Science* 1986, 264, (12), 1092-1096.
40. Hahn, K. G. Thermosetting Acrylic Latexes. 4,812,491 1989.
41. Linné, M. A.; Klein, A.; Miller, G. A.; Sperling, L. H., Film Formation from Latex: Hindered Initial Interdiffusion of Constrained Polystyrene Chains Characterized by Small-Angle Neutron Scattering. *J. Macromol. Sci., Phys.* 1988, B27, 217-231.
42. Sperling, L. H.; Klein, A.; Sambasivam, M.; Kim, K. D., Molecular Basis of Healing and Fracture at Polymer Interfaces. *Polym. Adv. Technol.* 1993, 5, 453-472.
43. Yoo, J. N.; Sperling, L. H.; Glinka, C. J.; Klein, A., Characterization of Film Formation from Polystyrene Latex Particles via SANS. I. Moderate Molecular Weight. *Macromolecules* 1990, 23, 3962-3967.
44. Joshi, R.; Provder, T.; Kustron, K., Green coatings: a trend that is becoming the rule rather than the exception *JCT CoatingsTech* 2008, 5, (1), 38-43.
45. NPCA, The Paint and Coatings Industry addresses Lead Issue. *Issue Backgrounder* 2000, pp 1-6.
46. Stoffer, J. O.; Bone, T. J., Polymerization in Water-in-Oil Microemulsion Systems I. *Journal of Polymer Science, Polymer Chemistry Edition* 1980, 18, (8).
47. Stoffer, J. O.; Bone, T. J., Polymerization in water-in-oil microemulsion systems. II. SEM investigation of structure *Journal of Dispersion Science and Technology* 1980, 1, (4), 393-412.
48. Atik, S. S.; Thomas, J. K., Polymerized Microemulsions. *J. American Chemical Society* 1981, 103, (14), 4279-4280.
49. Atik, S. S.; Thomas, J. K., Photochemistry in polymerized microemulsion systems *Journal of the American Chemical Society* 1982, 104, (12), 5868-74.
50. Atik, S. S.; Thomas, J. K., Photoinduced reactions in polymerized microemulsions *Journal of the American Chemical Society* 1983, 105, (14), 4515.
51. Antonietti, M.; Bremser, W.; Muschenborn, D.; Rosenauer, C.; Schupp, B.; Schmidt, M., Synthesis and size control of polystyrene latexes via polymerization in microemulsion *Macromolecules* 1991, 24, (25), 6636-43.
52. Wu, C., Laser Light Scattering Determination of the Surfactant Interface Thickness of Spherical Polystyrene Microlatexes. *Macromolecules* 1994, 27, (24), 7099-102.
53. Capek, I.; Potisk, P., Microemulsion polymerization of butyl acrylate. IV. Effect of emulsifier concentration *Journal of Polymer Science, Part A: Polymer Chemistry* 1995, 33, (10), 1675-83.
54. Feng, L.; Ng, K. Y. S., In situ kinetic studies of microemulsion polymerizations of styrene and methyl methacrylate by Raman spectroscopy *Macromolecules* 1990, 23, (4), 1048-53.
55. Gan, L. M.; Chew, C. H.; Lee, K. C.; Ng, S. C., Polymerization of methyl methacrylate in ternary oil-in-water microemulsions *Polymer* 1993, 34, (14), 3064-9.
56. Gan, L. M.; Chew, C. H.; Lye, I.; Ma, L.; Li, G., Effect of water-soluble cosurfactants on microemulsion polymerization of styrene *Polymer* 1993, 34, (18), 3860-4.
57. Gan, L. M.; Chew, C. H.; Lee, K. C.; Ng, S. C., Formation of polystyrene nanoparticles in ternary cationic microemulsions *Polymer* 1994, 35, (12), 2659-64.

58. Guo, J. S.; Sudol, E. D.; Vanderhoff, J. W.; El-Asser, M. S., Particle nucleation and monomer partitioning in styrene oil-in-water microemulsion polymerization *Journal of Polymer Science, Part A: Polymer Chemistry* 1992, 30, (5), 691-702.
59. Guo, J. S.; Sudol, E. D.; Vanderhoff, J. W.; El-Asser, M. S., Modeling of the styrene microemulsion polymerization *Journal of Polymer Science, Part A: Polymer Chemistry* 1992, 30, (5), 703-12.
60. Larpent, C.; Tadros, T. F., Preparation of microlatex dispersions using oil-in-water microemulsions *Colloid & Polymer Science* 1991, 269, (11), 1171-83.
61. Ming, W.; Zhao, J.; Lu, X.; Wang, C.; Fu, S., Novel Characteristics of a Polystyrene Microsphere Prepared by Microemulsion Polymerization *Macromolecules* 1996, 29, (24), 7678-7682.
62. Rodriguez-G., L. A.; Mendizabal, E.; Puig, J. E.; Kaler, E. W., Polymerization of methyl methacrylate in 3-component cationic microemulsion *Journal of Applied Polymer Science* 1993, 48, (5), 775-86.
63. Texter, J.; Oppenheimer, L. E.; Minter, J. R., Microemulsion polymerization in the water, bis(2-ethylhexyl) sulfosuccinate sodium salt (Aerosol-OT), tetrahydrofurfuryl methacrylate system *Polymer Bulletin (Berlin, Germany)* 1992, 27, (5), 487-94.
64. Kuo, P. L.; Turro, N. J.; Tseng, C. M.; El-Asser, M. S.; Vanderhoff, J. W., Photoinitiated polymerization of styrene in microemulsions *Macromolecules* 1987, 20, (6), 1216-21.
65. Candau, F.; Leong, Y. S.; Fitch, R. M., Kinetic study of the polymerization of acrylamide in inverse microemulsion *Journal of Polymer Science, Polymer Chemistry Edition* 1985, 23, (1), 193-214.
66. Candau, F.; Leong, Y. S.; Fitch, R. M., Effect of solution components on the termination mechanism in acrylamide microemulsion polymerizations *Journal of Polymer Science, Part A: Polymer Chemistry* 1989, 27, (7), 2179-88.
67. Corpart, J. M.; Selb, J.; Candau, F., Characterization of high charge density ampholytic copolymers prepared by microemulsion polymerization *Polymer* 1993, 34, (18), 3873-86.
68. Gan, L. M.; Chew, C. H.; Lian, N.; Li, G. Z., Polymerization of Styrene in a Winsor I-like System *Langmuir* 1994, 10, (7), 2197-201.
69. Loh, S. E.; Gan, L. M.; Chew, C. H.; Ng, S. C., Polymerization of methyl methacrylate in Winsor I-like system *Journal of Macromolecular Science, Pure and Applied Chemistry* 1996, A33, (3), 371-84.
70. He, G.; Pan, Q., Synthesis of Polystyrene and Polystyrene/Poly (methyl methacrylate) Nanoparticles. *Macromolecular Rapid Communications* 2004, 25, (17), 1545-1548.
71. Kaiyi, L.; Zhaoqun, W., A novel method for preparing monodispersed polystyrene nanoparticles. *Front.Chem.China* 2007, 2, (1), 17-20.
72. Ming, W.; Jones, F. N.; Fu, S., High solids-content nanosize polymer latexes made by microemulsion polymerization. *Macromolecular Chemistry and Physics* 1998, 199, (6), 1075-1079.
73. Ming, W.; Jones, F. N.; Fu, S., Synthesis of nanosize poly(methyl methacrylate) microlatexes with high polymer content by a modified microemulsion polymerization. *Polymer Bulletin* 1998, 40, (6), 749-756.

Chapter 3

Effects of pre-coalescence or post-coalescence crosslinking and glass transition temperature*

Introduction

In 1978 Bufkin and Grawe^{1(a-e)} published a series of review articles on crosslinking latexes with several thousand references. These articles provided an extensive overview of the various crosslinking chemistries available before 1978. Many thousands of patents and publications on crosslinkable latexes have appeared since then. For examples of recent publications, see references²⁻⁹ and patents, see references.¹⁰⁻¹³

As Jones¹⁴ points out, crosslinker mechanisms for latexes include the use of carbodiimides and aziridine crosslinkers as well as the autoxidation mechanism. The autoxidation mechanism can allow the crosslinking of latexes at room temperature following which the latexes are storage stable for long periods of time. This approach includes the use of allylic functionality in the latex, alkyd-acrylic latexes, latexes incorporating soya oil in the polymer backbone or side chain, and the use of small amounts of diene monomers (e.g., butadiene, pentadiene) in the latex.¹⁵ The main disadvantage of the autoxidation mechanism is the tendency for films to discolor upon aging (crosslinking) at room temperature. The review paper of Winnik and Taylor² covers advancements in crosslinking technology, various crosslinking chemistries, and a masterful overview on their film formation mechanisms.

*Winner of the “Best Student Research Poster” at 2006 International Coatings Expo, sponsored by Federation of Societies for Coatings Technology, in New Orleans, USA.

*Finalist of the “Prestigious Roon Foundation Award” at 2007 FutureCoat! Conference sponsored by Federation of Societies for Coatings Technology, in Toronto, Ontario, Canada.

Surprisingly few, if any, of the thousands of publications contain systematic comparisons of film properties of “pre-coalescence” (internal) and “post-coalescence” (external) crosslinked latexes, the subject of this research. The main goal of the present study is to compare the effects of type and level of crosslinking on latex fundamental and end-use properties and on the film formation process and resulting morphology.

The conventional latexes presented in this study are prepared using n-butyl acrylate/n-butyl methacrylate copolymers. A third monomer, methacrylic acid (2 wt %) was included to enhance latex stability. The original goal of the conventional latex project was synthesis of improved latexes for artist paints.¹⁶ Previous work¹⁶ showed that n-Butyl acrylate/n-butyl methacrylate latexes with small amounts of crosslinker proved to be good candidates for artist paints. This study extended to the research to include crosslinked latexes.

“Pre-coalescence crosslinked latexes” are referred as latexes that are prepared by emulsion polymerization of conventional monomers such as mono-acrylates, mono-methacrylates or styrene in combination with di- or poly-functional monomers such as di-methacrylates or divinyl benzene which cause a degree of crosslinking within the latex particles. It is sometimes called “*intraparticle crosslinking*”. The crosslinking reaction takes place before the coalescence of the particles. In this study 1, 3-butylene glycol dimethacrylate (1, 3-BGDMA) was used as the pre-coalescence crosslinker.

“Post-coalescence crosslinked latexes” are referred as latexes that are prepared with reactive sites such as hydroxyl groups and are crosslinked during film formation by a crosslinker that is added to the coating formulation but not co-polymerized in the latex. Another term is “*interparticle crosslinking*.” Many combinations of reactive sites and crosslinkers have been described in literature.² In this study, diacetone acrylamide (DAA) was used as the monomer to

place reactive sites within the latex and adipic dihydrazide (ADDH) as the post-coalescence crosslinker. This combination of site and crosslinker has been described in trade literature⁸ and in numerous patents¹⁰⁻¹³ and is being utilized by some major coatings and ink companies.

In this study, comparable latexes containing 0 – 4 wt. % of pre-coalescence crosslinker (1, 3-BGDMA) and 0 – 5 wt. % of reactive monomer for post-coalescence crosslinker (DAA) was investigated. Both the pre-coalescence and post-coalescence latex series were prepared by semi-continuous emulsion polymerization using target glass transition temperatures (T_g) of 7 °C and 22 °C. The films cast from these latexes were characterized using a variety of end-use tests and advanced instruments such as a Nano-indenter, Dynamic Mechanical Analyzer (DMA), Modulated Differential Scanning Calorimeter (MDSC), and an Atomic Force Microscope (AFM). Information from such instruments greatly enhanced our understanding of the relationship between the physical and morphological properties of coatings. The main goal of the research was to understand the relationships between level and type of crosslinker and the resultant fundamental and end-use film properties and film morphology.

Experimental Details

Materials

Materials with sources of supply utilized in this study are listed below:

Deionized Water, *n*-Butyl Methacrylate (*nBMA*, 99+%, 10-55 ppm MEHQ from Sigma-Aldrich), Methacrylic Acid (MAA, 99%, 250 ppm MEHQ from Sigma-Aldrich), *n*-Butyl Acrylate (*nBA*), 99%, 10-55 ppm MEHQ from Sigma-Aldrich), 1,3-Butylene glycol dimethacrylate (1,3-BGDMA 99%, 200 ppm MEHQ from Sigma-Aldrich), Diacetone acrylamide (DAA, 99% from Sigma-Aldrich), Adipic dihydrazide (ADDH, 98% from Sigma-

Aldrich), Sodium Lauryl Sulfate (SLS, RHODAPON UB (30%) from Rhone-Poulenc], Ammonium Persulfate (APS, Certified A.C.S, from Fisher Scientific), 2,2'-Azobis [2-(2-imidazolin-2-yl)propane] (VA-061 from Wako Pure Chemical Industries, Ltd.), Anhydrous Sodium Carbonate (Certified A.C.S from Fisher Scientific), "Proxyl GXL" (from Avecia Biocides), 2-Amino-2-methyl-1-propanol ("AMP-95" from Angus Chemical Company), Ammonium Hydroxide (NH₄OH, 29.2% from Fisher Scientific), Sodium Iodide (99.5%, Certified A.C.S from Sigma-Aldrich), 2-Propanol (99.5+% from Sigma-Aldrich), Acetic Acid, (99.8% from Sigma-Aldrich), Sodium Thiosulfate volumetric standard (0.1040N Solution in water from Sigma-Aldrich), Acetone (99.5+% from Aldrich), Methyl Ethyl Ketone (MEK, 99.5% from Sigma-Aldrich), 2-Butoxyethanol (Butyl Cellosolve, 99% from Sigma-Aldrich), "SURFYNOL 104BC" (from Air Products).

Latex Synthesis

Latexes were synthesized with varying levels of pre-coalescence crosslinker (internal) and post-coalescence (external) crosslinkable sites. Two sets of latexes were prepared, one with target glass transition temperatures (T_g) of about 7 °C and the other with target T_g of about 22 °C. Compositions and characteristics of these latexes are shown in Tables 3.1 and 3.2. The latexes are coded I for pre-coalescence or internal, E for post-coalescence or external, L for low T_g , H for high T_g , and a number for the weight % of crosslinker or reactive site in the monomer line up. Thus, for example, IL-2 means an internally (or pre-coalescence) crosslinked, low T_g latex with 2.0 wt. % of 1, 3-BGDMA and EH-1 means an externally (or post-coalescence) crosslinked, high T_g latex with 1.0 wt. % of DAA.

Representative procedure for synthesis of latex IL-2

The procedure was essentially previously published but is included here for completeness.¹⁶ Polymerization was performed under a nitrogen atmosphere in a 5-L, 4-neck flask (“kettle”) equipped with a mechanical stirrer (fitted with a 125 mm crescent Teflon blade), a temperature control system, an inlet for a monomer emulsion fed by an FMI peristaltic pump, an inlet for an initiator solution stream fed by a syringe pump, and a reflux condenser. The temperature control system was a thermometer immersed in the reaction mixture electronically linked to a heating mantle and a pneumatic jack. The jack automatically raised or lowered the heating mantle to increase or reduce heat. A jet of room temperature air was directed at the flask for cooling when the mantle was lowered. By these means, the temperature was controlled within ± 1 °C. Steps in the process were:

1. The kettle was charged with 773 g of DI water and 6.67 g of SLS.
2. In a graduated beaker with a magnetic stirrer was placed 369 g of DI water, 167 g of SLS, 353 g of *n*BA, 1260 g of *n*BMA, 33.6 g of 1,3-BGDMA, and 33.6 g of MAA; stirring gave a white monomer emulsion.
3. Separately, a solution of 3.37 g of ammonium persulfate in 178 g of DI water was prepared.
4. To make a “pre-form” (seed latex), the kettle contents were heated to 80 – 82 °C and stirred as the following ingredients were added sequentially: (a) 44.5 g of the monomer emulsion, (b) 47.5 g of DI water, (c) a solution of 5.83 g of anhydrous sodium carbonate in 47.5 g of DI water, and (d) a solution of 4.98 g of ammonium persulfate in 47.5 g of DI water. The mixture was stirred at 80 – 82 °C for 20 minutes.

5. Addition of the main charges was then started by simultaneously pumping the monomer emulsion (step 2) using the peristaltic pump and the initiator solution (step 3) using the syringe pump, with continuous stirring of the reaction flask and the monomer emulsion in the beaker. The monomer emulsion was added at a rate of 450 mL/hr for the first 20 minutes and at a rate of 900 mL/hr for the next 160 minutes. The rate of decrease of the volume of monomer emulsion in the graduated beaker measured the feed rate. The initiator solution was added throughout the process at a rate of 60 mL/hr using a calibrated syringe pump. Throughout the 3-hr. addition, the reactor temperature was maintained at 80 – 82 °C, and this temperature was maintained for 30 min after addition was complete.
6. As step 5 approached completion, a solution of 1.6 g of 2, 2'-azobis [2-(2-imidazolin-2-yl) propane] in 320 g of DI water was prepared with heating to about 70 °C.
7. With the kettle temperature at 80 – 82 °C, the 2, 2'-azobis 2, 2'-azobis [2-(2-imidazolin-2-yl) propane] solution was added all at once. Temperature was increased to 91 – 93 °C and held for 2 h with continued stirring.
8. The latex in the kettle was cooled to about 60 °C, and a 50/50 wt./wt, solution of 2-amino-2-methyl-1-propanol in DI water (about 30 mL) was added with continued stirring to adjust the pH to 9.2 – 9.5.
9. The kettle temperature was reduced to about 40 °C, and a solution 1.44 g of “Proxyl GXL,” a bio-stabilizer, in 14 g of water was added and stirred in.
10. The latex was filtered through a tared 200-mesh sieve.
11. Coagulum was assessed by drying the sieve and weighing the material collected.

The characteristics of the resulting latexes are shown in Table 3.1. Coagulum was negligible. The other latexes described in Tables 3.1 and 3.2 were made by essentially identical procedures with the compositions adjusted as shown in Tables 3.1 and 3.2. In the case of making pre-coalescence crosslinked latexes, the functional monomer was included in the monomer mixture recipe. In the case of the post-coalescence crosslinkable latexes, (a) crosslinkable monomer was added at the end of the monomer addition and (b) aqueous ammonia was used to adjust the pH of the product instead of 2-amino-2-methyl-1-propanol to reduce the potential for interference with the crosslinking reaction.

It should be noted that the syntheses were repeated by different operators with essentially similar results. This demonstrated the robustness of the process, if followed carefully, in terms of repeatability and reproducibility.

Characterization of Latexes

Latex Properties

The weight percentage of non-volatile solids content (% NVM) was measured using ASTM D 4758-87. Viscosity was measured by ASTM D 4287 at 20 °C using a Brookfield Viscometer, Model DV-1, using Spindle #4 at 20 rpm. pH was measured with a Fischer Acumet Model 620 pH meter and with pH paper.

For particle size (diameter) and particle size distribution measurements, each latex was diluted to a transmission factor of 0.5-1.0 (about 0.05-0.1 wt% solids) and measured at 25 °C using the light-scattering instrument, MICROTAC Series 9200. Three tests were performed within 180 sec. to obtain an average value of a volume distribution.

For gel content measurements, an empty extraction thimble was dried at 85 °C in an oven for 2 hours, cooled in a desiccator overnight, and weighed. Latex films (prepared on glass and detached) were dried in a desiccator overnight, cut into small pieces, weighed, and put into the thimble. After a 12-hour extraction with acetone in a Soxhlet extractor, the thimble was dried in an oven at 85°C for 2 hours, cooled in a desiccator overnight, and weighed. The gel content was calculated from the initial and final weights, assuming that gelled material remained in the thimble. The results are shown in Figures 3.1 and 3.2, and in Tables 3.1 and 3.2.

Film Properties

Specimens were prepared on aluminum panels by drawing the latexes down using a square wet film applicator (Paul N. Gardner Co., Inc.) with 0.2 mm (wet) clearance on aluminum panels. The panels were placed in at 55 °C in oven overnight then stored at normal room conditions for a week before testing. No coalescing solvents were used. Dry film thicknesses were approximately 50 µm. Before casting these films, a stoichiometric amount of adipic dihydrazide (ADDH) was added to the E-series latexes.

Dry film thickness was measured at 25°C by Elcometer-345-Digital Coating thickness Gauge (Elcometer Instruments Ltd.). Solvent resistance was determined by methyl ethyl ketone (MEK) rubbing. Load was applied by a ball peen hammer with a 448 g head wrapped with cheesecloth soaked with MEK. The reported end point was the number of double rubs required to break through the film, exposing bare metal.

Chemical resistance tests were conducted at 25 °C following ASTM D 1308. A 1-mL sample of each test reagent (water, dilute sulfuric acid at pH 3) was pipeted (a 5-mL pipet graduated in 0.1 mL) onto the horizontal panel and immediately covered with a watch glass.

After an interval, the spot was wiped clean and the film was examined immediately for defects. Intervals used were 15 min, 1 h, and 16 h.

Pencil hardness was tested at 25 °C following the procedure of ASTM 3363. Tape adhesion was measured by ASTM D 3359. The films were cut with a cross-cut kit (Precision Gage & Tool Company) before testing.

Thermal and Mechanical Properties

For glass transition temperature (T_g) measurement, specimens were prepared on glass panels by drawing the latexes down using a square wet film applicator (Paul N. Gardner Co., Inc) with 0.25 mm (wet) clearance on glass panels. The panels were dried in an oven at 55 °C and 50% humidity. The films were then stored at a normal room conditions for a week before testing. The T_g of the dried films were determined by TA instrument - TA 2920 MDSC with Liquid Nitrogen Cooling Accessory System (LNCS) under nitrogen purge at flow rate of 50 ml/min. For testing, the samples were kept in closed aluminum non-hermetic pans. Temperature scans were done from -100 °C to 100 °C at 2 °C/min with modulation of +/- 1.00 °C at every 60 seconds under nitrogen. The MDSC equilibrated at -100 °C for 5 min.

Dynamic Mechanical Analyses were conducted using TA Instruments Model Q800 Dynamic Mechanical Analyzer (DMA) with LNCS accessory. Specimens for stress-strain and dynamic mechanical studies were prepared on glass panels as described in MDSC studies section. A film cutter (supplied by TA instruments) was used to cut, at constant depth, rectangular specimens about 15-20 mm long, 3-6 mm wide, and 0.1-0.2 mm thick from the cured films.

The stress-strain studies were performed at room temperature (~25°C) in air on the Q800 DMA with the thin film tension clamp in a controlled force mode with a ramped force of 3

N/min. up to 18 N/min., and the resultant % strain was observed. DMA measurements of dried specimen were done at 1 Hz with a thin film tension clamp over the temperature range of -100 °C to 100 °C, using liquid nitrogen as a coolant. The flow rate of liquid nitrogen into the DMA depends upon the starting temperature desired and is controlled by the ramp rate or heating rate of 3 °C/min.

Measurements with the Nanoindenter

The nanoindentation or nanoscratch tester used in this study was a computer controlled “Nanoindenter XP,” made by MTS. Its operation was described in detail in a previous paper by Shen et al.¹⁷

In the present study, a Berkovich diamond tip with an angle of 142.4° was used for the indentation experiments. The tests were performed by applying an increasing normal force (loading) at a constantly increasing rate to a pre-determined maximum load in 15 seconds, holding at the maximum force for 30 seconds to check visco creep if any, and then decreasing the force to zero (unloading) in 15 seconds. The temperature during the indentation tests was 26 – 28 °C. The maximum applied force was determined, depending on the hardness of the tested specimens. The instrument plots a curve of applied force versus the indentation depth during loading, holding, and unloading after the test. Usually, the tip continues to indent into the surface at the fixed maximum force during the holding period due to viscous creep of the material. Also, usually, the unloading curve does not coincide with the loading curve, reflecting a residual plastic deformation. The instrument automatically calculates the hardness (H), defined as applied normal force divided by projected contact area,

$$H = \frac{F}{A} \quad (1)$$

and the elastic modulus (E), using the formula

$$E = \frac{\sqrt{\pi}}{2} \frac{S}{\sqrt{A}}. \quad (2)$$

where A is the contact area projected on the original surface under the maximum normal force and S is the slope of the tangential of the unloading curve at the turning point. Note that A increases with the indentation depth as explained by Oliver and Pharr.¹⁸ The interpretation of H and E values measured in the indentation tests was discussed by Shen et al.¹⁷

Measurements with Atomic Force Microscope

An Atomic Force Microscope (NanoScope III, Digital Instruments) was used to observe surface morphology and friction property of the specimens. The contact mode was used to obtain surface morphology and friction force images. Both surface morphology and friction force images were obtained at sizes of 20 $\mu\text{m} \times 20 \mu\text{m}$ and 5 $\mu\text{m} \times 5 \mu\text{m}$. The 100 $\mu\text{m} \times 100 \mu\text{m}$ surface morphology images were also studied. For time evolution study, both surface morphology and friction force images were captured at image sizes of 2 $\mu\text{m} \times 2 \mu\text{m}$ and 5 $\mu\text{m} \times 5 \mu\text{m}$; two sets for each sample.

Results and Discussion

Latex Synthesis and Characterization

“Pre-coalescence” crosslinked latexes were synthesized by a straightforward semi-continuous emulsion polymerization process with varying levels of a crosslinking monomer. Compositions and characteristics of the latexes are shown in Tables 3.1 and 3.2. As shown in Table 3.1, addition of up to 4 wt. % of 1, 3-BGDMA has minimal effect on the characteristics of the latexes except that T_g is increased at the 4 % level. In the synthesis 2, 2'-Azobis [2-(2-imidazolin-2-yl) propane] was used as a “chaser” to consume unreacted monomers at the end of

the polymerization rather than the more conventional tert-butyl hydroperoxide. A previous study¹⁶ showed that the azo-chaser was associated with a much lower rate of hydroperoxide build up during QUV-A exposure.

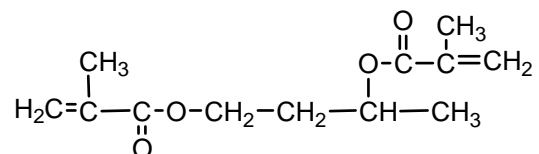


Figure 3.A. Schematic representation of 1, 3-BGDMA

Table 3.1. Characteristics of 1,3-BGDMA pre-coalescence crosslinked latexes

Latex	Composition	% Non-Volatiles	Particle Size, μm	Glass Transition Temp. ($^{\circ}\text{C}$) by MDSC	pH	Gel Content	Viscosity η ($\text{mPa}\cdot\text{s}$)
IL-0	<i>n</i> BA/ <i>n</i> BMA/1,3-BGDMA/MAA=21/77/0/2	47.1	0.130	6	9.3	0.00	100
IL-0.25	<i>n</i> BA/ <i>n</i> BMA/1,3-BGDMA/MAA=21/76.75/0.25/2	47.7	0.129	8	9.3	46.1	90
IL-0.6	<i>n</i> BA/ <i>n</i> BMA/1,3-BGDMA/MAA=21/76.4/0.6/2	47.5	0.128	5	9.2	56.2	100
IL-1.2	<i>n</i> BA/ <i>n</i> BMA/1,3-BGDMA/MAA=21/75.8/1.2/2	47.4	0.127	6	9.3	52.8	90
IL-2	<i>n</i> BA/ <i>n</i> BMA/1,3-BGDMA/MAA=21/75/2/2	44.6	0.118	5	9.0	57.1	80
IL-4	<i>n</i> BA/ <i>n</i> BMA/1,3-BGDMA/MAA=21/73/4/2	46.8	0.123	13	9.2	64.2	70
IH-0	<i>n</i> BA/ <i>n</i> BMA/1,3-BGDMA/MAA=9/89/0/2	46.9	0.126	21	9.1	0.0	120
IH-0.25	<i>n</i> BA/ <i>n</i> BMA/1,3-BGDMA/MAA=9/88.75/0.25/2	46.6	0.134	25	9.3	10.1	120
IH-0.6	<i>n</i> BA/ <i>n</i> BMA/1,3-BGDMA/MAA=9/88.4/0.6/2	46.9	0.129	25	9.4	10.3	120
IH-1.2	<i>n</i> BA/ <i>n</i> BMA/1,3-BGDMA/MAA=9/87.8/1.2/2	47.5	0.126	24	9.1	15.6	120
IH-2	<i>n</i> BA/ <i>n</i> BMA/1,3-BGDMA/MAA=9/87/2/2	47.8	0.125	13	9.3	61.3	100
IH-4	<i>n</i> BA/ <i>n</i> BMA/1,3-BGDMA/MAA=9/85/4/2	47.6	0.125	33	9.2	62.9	120

Table 3.2 Characteristics of DAA externally crosslinkable latexes

Latex	Composition	% Non-Volatiles	Particle Size, μm	Glass Transition Temperature ($^{\circ}\text{C}$) by MDSC	pH	Gel Content	Viscosity η ($\text{mPa}\cdot\text{s}$)
EL-0	<i>n</i> BA/ <i>n</i> BMA/DAA/MAA=21/77/0/2	47.0	0.134	6	9.8	0.0	280
EL-1	<i>n</i> BA/ <i>n</i> BMA/DAA/MAA=21/76/1/2	46.4	0.128	9	9.8	91.3	390
EL-2	<i>n</i> BA/ <i>n</i> BMA/DAA/MAA=21/75/2/2	46.6	0.133	7	9.8	98.1	560
EL-5	<i>n</i> BA/ <i>n</i> BMA/DAA/MAA=21/72/5/2	46.3	0.137	5	9.7	100.0	1320
EH-0	<i>n</i> BA/ <i>n</i> BMA/DAA/MAA=9/89/0/2	47.3	0.135	22	9.8	0.00	260
EH-1	<i>n</i> BA/ <i>n</i> BMA/DAA/MAA=9/88/1/2	45.6	0.128	25	9.8	90.0	230
EH-2	<i>n</i> BA/ <i>n</i> BMA/DAA/MAA=9/87/0/2	45.8	0.133	25	9.8	97.4	230
EH-5	<i>n</i> BA/ <i>n</i> BMA/DAA/MAA=9/84/5/2	46.0	0.129	23	9.8	97.9	1010

In a similar process, emulsion copolymerization with diacetone acrylamide (DAA) at up to 2 wt. % levels also had negligible effect on the measured characteristics of the latexes (See Table 3.2). At the 5 wt. % level a substantial increase in latex viscosity was observed along with a slight effect on T_g . It should be noted here that the surfactant/monomer wt. ratio used in the synthesis is 3/100.

Film Formation by “Pre-coalescence” Crosslinked Latexes

Films were cast from the internally (pre-coalescence) crosslinked latexes by conventional means. No coalescing solvent was used; film formation was accelerated by warming the films at 55 $^{\circ}\text{C}$ overnight. Film thicknesses were about 50 μm .

A useful model of film formation by latexes²⁻⁴ involves three major overlapping stages: (1) evaporation of volatiles, (2) particle deformation to a continuous film (usually referred as “coalescence”), and (3) molecular interpenetration to knit the particles together (also called “fusion” or “further coalescence”). The third stage is critical to achieving full potential film properties. A schematic diagram of the latex film formation process is shown below.²⁻⁴

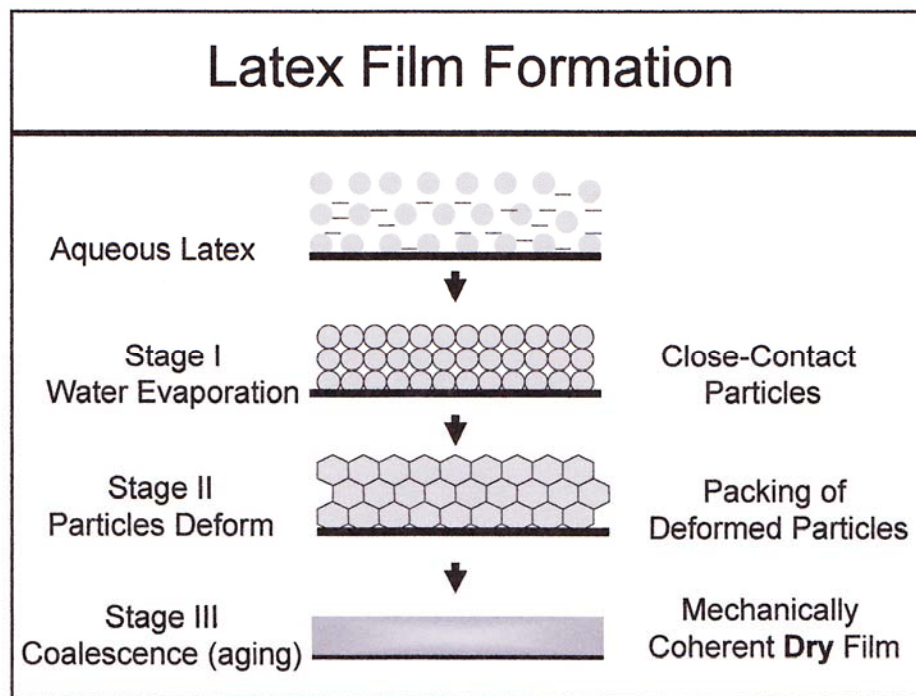


Figure 3.B. Schematic representation of the latex film formation process²⁻⁴

The third stage of film formation involves interdiffusion of polymer chains from different latex polymers. Interdiffusion knits vestigial particles together and is essential if the polymer film is to realize the mechanical properties of which its composition is capable. Complete interdiffusion is not necessary, however; it is only necessary for the molecules from adjacent particles to interpenetrate to a distance comparable to the root-mean-square radius of gyration (R_G) of the individual molecules,⁴ typically a smaller distance than the diameters of the original latex particles.

In this model, latexes with very low levels of internal crosslinking are able to coalesce to form good films. Presumably, dangling ends of crosslinked molecules and any unreacted molecules present are able to interdiffuse. But how much internal crosslinking can be tolerated before interdiffusion is impeded sufficiently that the film cannot approach the mechanical film properties of uniformly crosslinked latex of that composition? Previous studies offer insight into this question.

Zosel and Ley⁵ used swelling, dynamic mechanical analysis, and small angle neutron scattering to study poly (*n*-butyl acrylate) (PNBA) and poly (*n*-butyl methacrylate) (PNBMA) latexes with 0 to 2 wt. % of an internal crosslinker, methallyl methacrylate (MAMA). Their results present a complex picture. Films that contain 2 wt. % of MAMA remain brittle even after annealing at 90 °C, while films with smaller amounts of MAMA become tougher and more elastic when annealed. The results are discussed in terms of the relationship between the mean molar mass between crosslinks (M_c) and the entanglement length (M_e). When crosslink density is high enough that $M_c = M_e$, a critical concentration, is reached, above which the films are incapable of sufficient interdiffusion to fully knit the vestigial particles. Below that level, good knitting is possible, but the rate of interdiffusion at a given temperature decreases as the critical level is approached. The critical concentration of MAMA is about 0.7 wt. % for PNBA and about 1.5 wt. % for PNBMA. Of course, these levels might vary widely with other compositions.

Tamai, Pinenq, and Winnik,¹⁹ whose research was built on the work of Zosel and Ley,⁵ studied the effect of crosslinking on polymer diffusion in Poly (butyl methacrylate-co-butyl acrylate-co-ethylene glycol dimethacrylate) latex films primarily by fluorescent energy-transfer measurements and AFM. Their results showed that the presence of crosslinks in the latex

particles limits the extent of polymer interdiffusion with increasing levels of crosslinking. At 4 mol% of ethylene glycol dimethacrylate, significant polymer diffusion occurred. This was attributed primarily to intercellular mixing caused by the diffusion of dangling polymer chains anchored in the crosslinked network. The crosslinked particles formed tough elastomeric films with high tensile strength and substantial elongation to break but with expected poor solvent resistance. Aradian, Raphael, and de Gennes²⁰ developed a theoretical mode to account for the competition between interdiffusion and cross-linking at polymer interfaces largely inspired by the experimental work of Winnik and coworkers.¹⁹

A series of papers by Ghazaly et al.²¹⁻²⁴ provides further insight. These authors used miniemulsion polymerization to prepare NBMA copolymers with three crosslinkers, ethylene glycol dimethacrylate (EGDMA) and two polymeric diacrylates with M_n of roughly 4000. The mole ratio of NBMA to the crosslinkers was 500:1. Studies of swelling and tensile properties of materials cast from polymers at 120 °C showed wide differences in properties, with one of the polymeric diacrylate crosslinkers giving the best tensile properties and EGDMA giving brittle materials. In one case, the choice of initiator for the polymerization also affected properties. The differences were attributed to differences in the way the network microstructures evolved during miniemulsion polymerization. Ghazaly et al.'s²¹⁻²⁴ study illustrates the complexities inherent in studies of internally or pre-coalescence crosslinked latexes.

Film Formation by “Post-coalescence” Crosslinked Latexes

The DAA-containing latexes are combined with a stoichiometric amount of adipic dihydrazide (ADDH) crosslinker. Then the films were cast under the same conditions as for internally crosslinked latexes. Before the film is cast, premature reaction of ADDH with the reactive sites in the latex is minimal.^{2, 3, 8, 9, 24, 25} The crosslinking reaction for the DAA monomer

is shown below. The ADDH is water soluble, and almost all of it remains separated from the reactive sites in the serum where it is. The relatively high (9 – 9.5) pH also suppresses the reaction. When the film is cast, however, the water evaporates, forcing ADDH to come in contact with the latex polymer surfaces when close packing of the latex particles has occurred; ammonia evaporates, lowering the pH to about 6.5; and then crosslinking accelerates.²⁴

The crosslinking reaction, illustrated for DAA monomer is as follows:

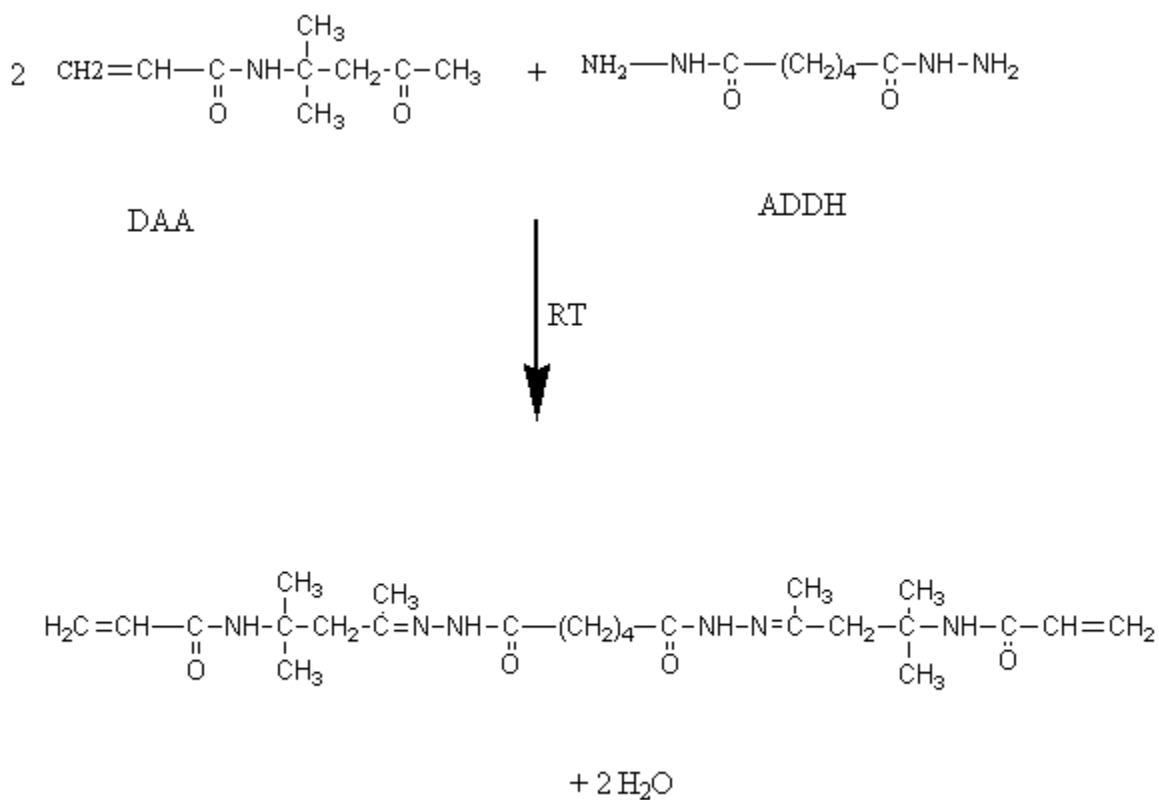


Figure 3.C. Schematic representation of DAA & ADDH crosslinking reaction

After the film is cast, the crosslinking reaction is known to proceed at a useful rate at room temperature.¹⁰ In this study we baked the films overnight at 55°C to assure a high level of conversion before testing and to avoid the use of coalescing solvents. Among the factors that influence final properties of the films are the composition of the latexes and the relative rates of

- mixing of the crosslinker with the polymer,
- interdiffusion of the polymer molecules that originated in different latex particles,
- the chemical crosslinking reactions and diffusion of ADDH into the polymer,¹⁰ and
- T_g of latex at a specific composition.

To reach a high level of conversion, the bake temperature should be well above the T_g of the specific latex composition. In this study, this is true for the low T_g latex (both pre-coalescence and post-coalescence crosslinked latexes). However, it may be borderline for high T_g latex (both pre-coalescence and post-coalescence crosslinked latexes). This will be discussed further later in the paper.

If the rate of the crosslinking reaction is too fast relative to mixing and interdiffusion, coalescence and interdiffusion will be slowed and perhaps retarded prematurely. The likely result will be excessively non-uniform films and less than optimal film properties. Some literature reports^{2, 8, 10-13} suggest that the DAA/ADDH crosslinking combination has satisfactory relative rates and good film properties can be attained. A patent,¹¹ however, indicates that film properties can be improved by incorporating a retarder chosen from wide variety of substances, many of them salts of weak acids with stronger bases.

Gel Content Results

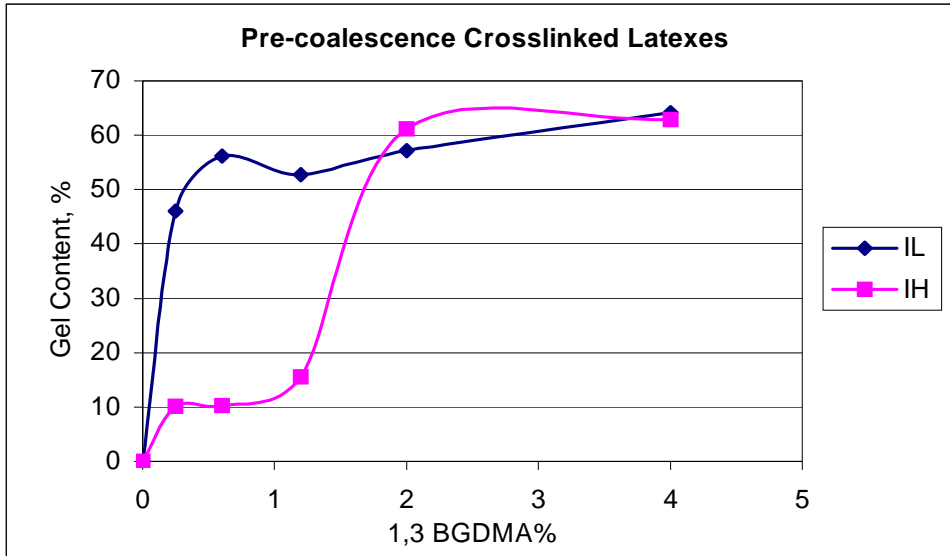


Figure 3.1 Gel Content of Pre-coalescence Crosslinked Latex Films

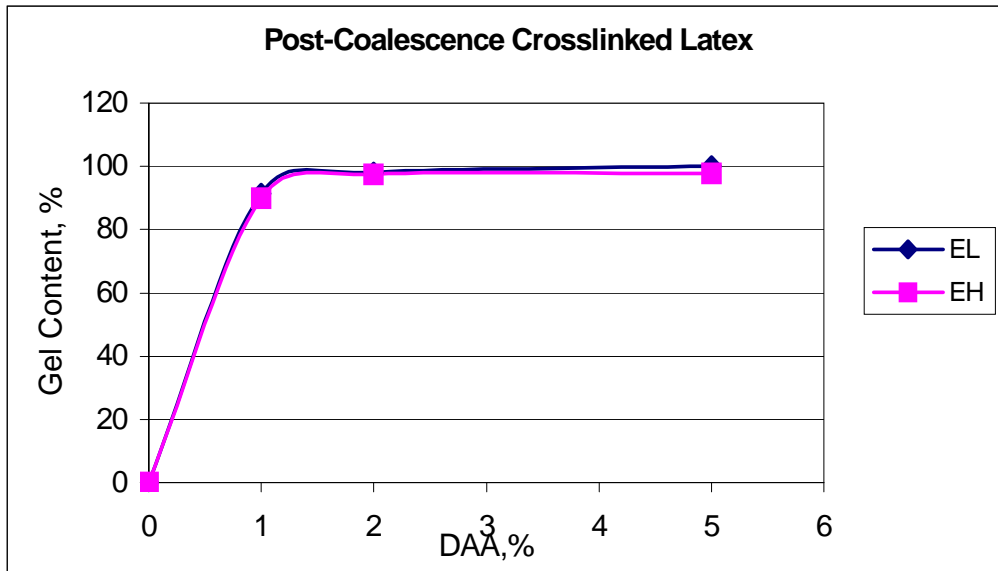


Figure 3.2 Gel Content of Post-coalescence Crosslinked Latex Films

Acetone extraction was employed to measure the gel content of the films, with the results shown in Figures 3.1 and 3.2. For post-coalescence (externally) crosslinked films, not surprisingly, the gel content was about 90% for films containing 1 wt.% of DAA reactive site and approaches 100% for films with higher levels of crosslinking. For pre-coalescence (internally) crosslinked films, however, the gel content measured in this way never rises much higher than 60%. From 0.25 to 1.2 wt. % internal crosslinker, the low T_g films have much higher gel fractions than the high T_g films. It is speculated that the gel content of these latexes are actually much higher. The low values recorded here may reflect incomplete knitting of the pre-coalescence (internally) crosslinked latex particles during film formation, allowing small pieces to break loose and pass through the filter.

Atomic Force Microscope Results

Atomic Force Microscope images of the surface of a film cast from latex IH-4 (Figure 3.3 and 2.4) show ball-like features in both the topographic and frictional images. In addition, the frictional images show dark areas suggestive of deposits of some contaminant on the surface, cracks, or some other surface defects. In the frictional images, bright indicates low friction and dark indicates high friction. The physical significance of these dark areas is not known. The fact that they are high friction areas discourages the notion that they are shrinkage cracks or voids.

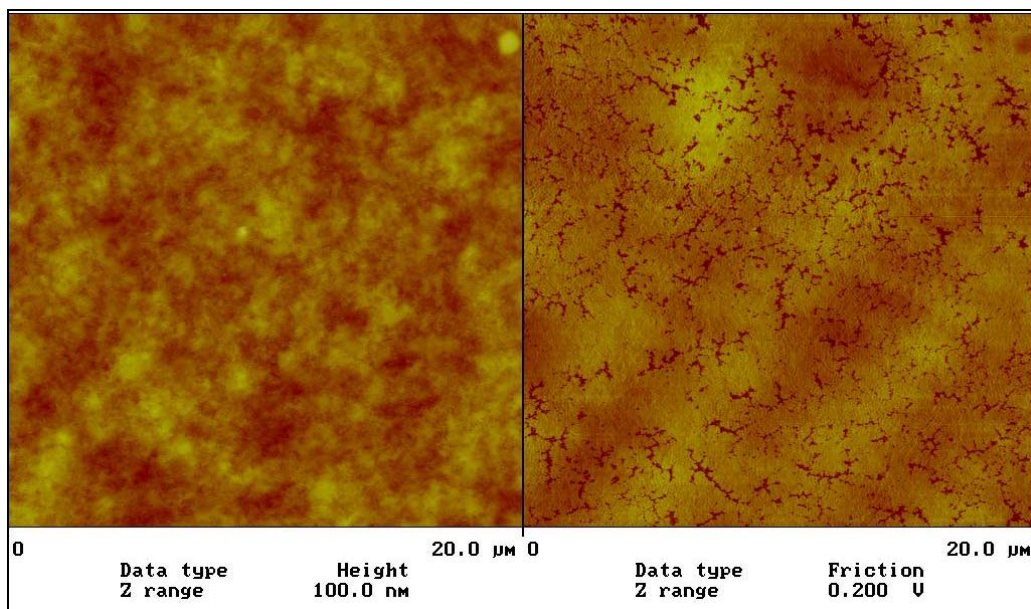


Figure 3.3 20 μm × 20 μm AFM topographic image (left) and frictional image (right) of Sample IH-4

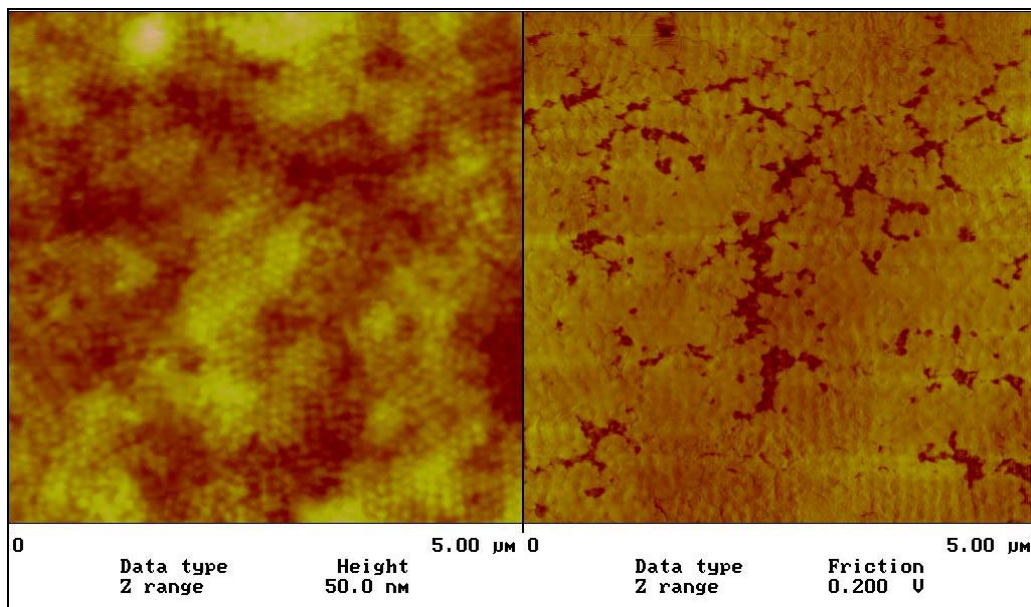


Figure 3.4 5 μm × 5 μm AFM topographic image and frictional images of Sample IH-4

The AFM images, with higher magnified z scale, of surfaces of the films cast from latexes EL-1 and IH-4 (Figure 3.5) show the topographic variation of the surfaces with lateral dimensions of the same order of magnitude as the original latex particles, as commonly observed

with films cast from latexes. Note that the height of the peaks at the surface of the EL-1 film is an order of magnitude larger than the height of the peaks in the IH-4 film. This observation suggests that the rate of the crosslinking reaction was fast enough to significantly retard the homogenization of the film, at least near the surface. This observation is consistent with the previously mentioned report by Geelhaar et al.¹¹ that retarders can improve film properties with this type of crosslinking, presumably by slowing the rate of the chemical crosslinking reaction.

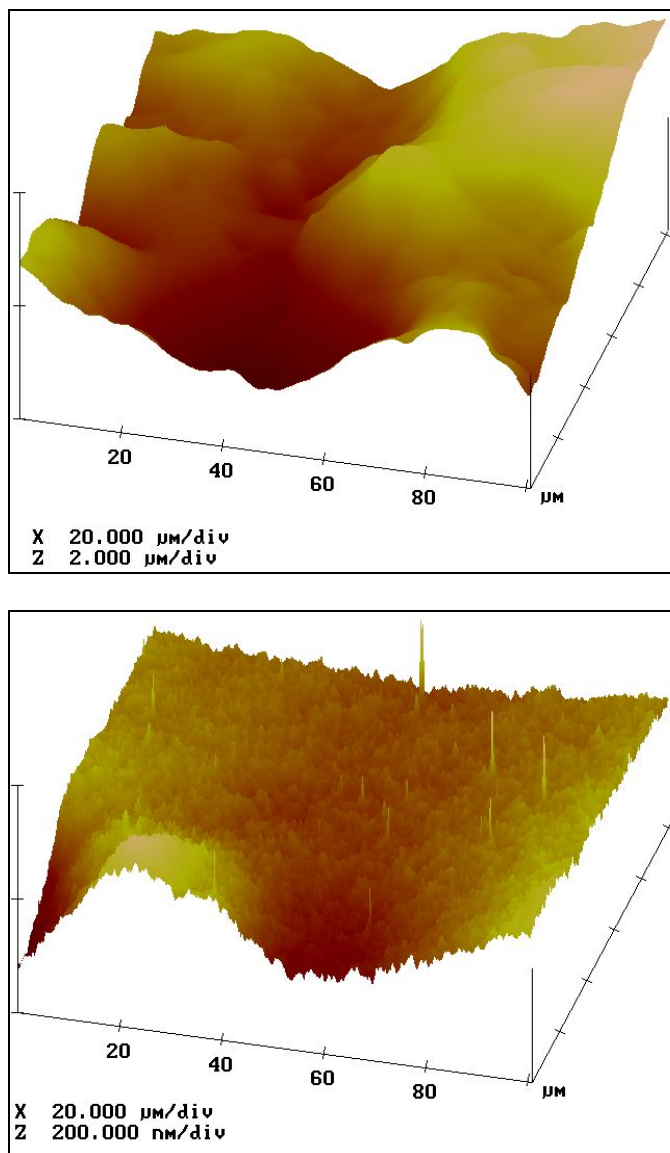


Figure 3.5 AFM topographic Images of Sample EL-1 (top) and IH-4 (bottom). The two images have different Z scales, and surface of EL-1 is much rougher than that of IH-4

Time Evolution of Morphology by AFM

Figure 3.D shows morphological changes observed in the frictional images by AFM operated in the contact mode during the film formation. The latex films were applied at room temperature, and film formation was studied at regular time-intervals. The film formation process is clearly evident in AFM images shown in Figure 3.D. The effect of T_g on film formation can be clearly seen when the images of EL-5 and EH-5 are compared. The EL-5 films appear smooth and homogenous compared to EH-5 at similar time interval. The effect of level of crosslinking can also be seen when the images of EH-0 and EH-5 are compared. Looking at EH-5, images latex particles interdiffusion can be clearly observed. The rate of crosslinking here certainly affects the rate of interdiffusion of particles. Also, effect of type of crosslinking can also be seen when comparing the film formation images of EL-5 and IH-4. The image of EL-5 shows more homogenous structure when compared to IH-4 images at similar time intervals.

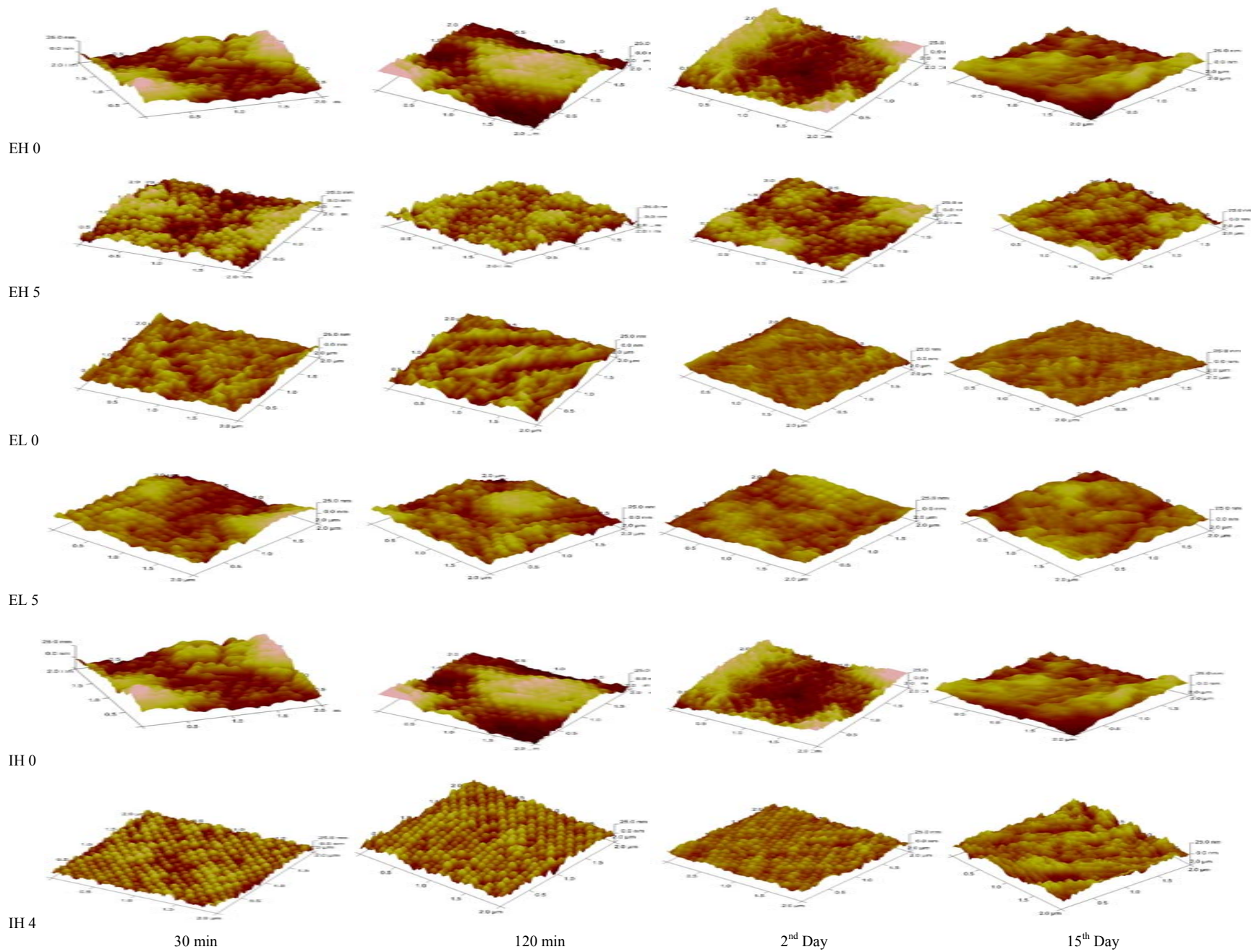


Figure 3.D. Representative friction images of morphological changes observed by AFM contact mode during the film formation

Indentation tests with the nano-indenter

Conditions for preparation and testing of un-pigmented latex films are described in the Experimental Section. As detailed in previous publications¹⁶⁻¹⁷ and in the Experimental Section each test produces a load-displacement curve from which hardness and modulus were calculated.

For the low- T_g films, hardnesses and elastic moduli at varying crosslinker levels are compared in Figures 3.6 and 3.7. For hardness, it can be seen that in post-coalescence crosslinking, the value increases from 0% to 5%, but in the case of pre-coalescence crosslinking going from 0% to 4%, it appears to have little effect on hardness values. Elastic modulus, post-coalescence crosslinking caused a modest increase. Pre-coalescence crosslinking may also have increased modulus, although scatter in the data make interpretation of the data less certain.

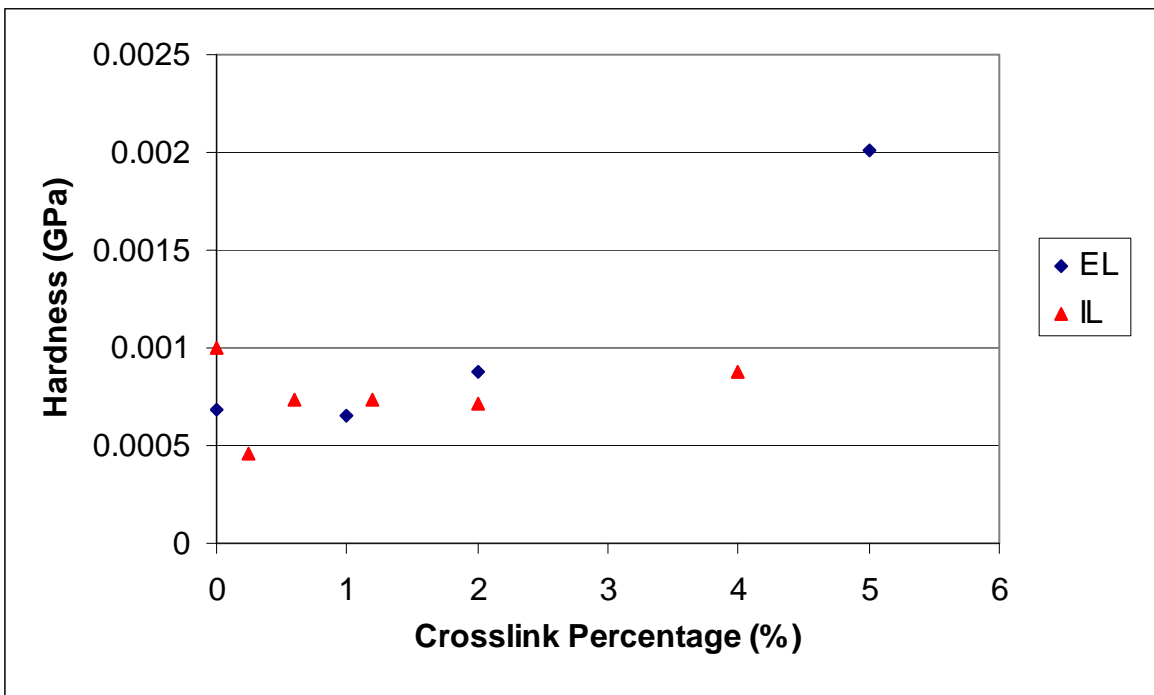


Figure 3.6. Comparison of hardness of samples in groups EL and IL with different crosslinker levels. The hardness was measured under a normal force of 1 mN.

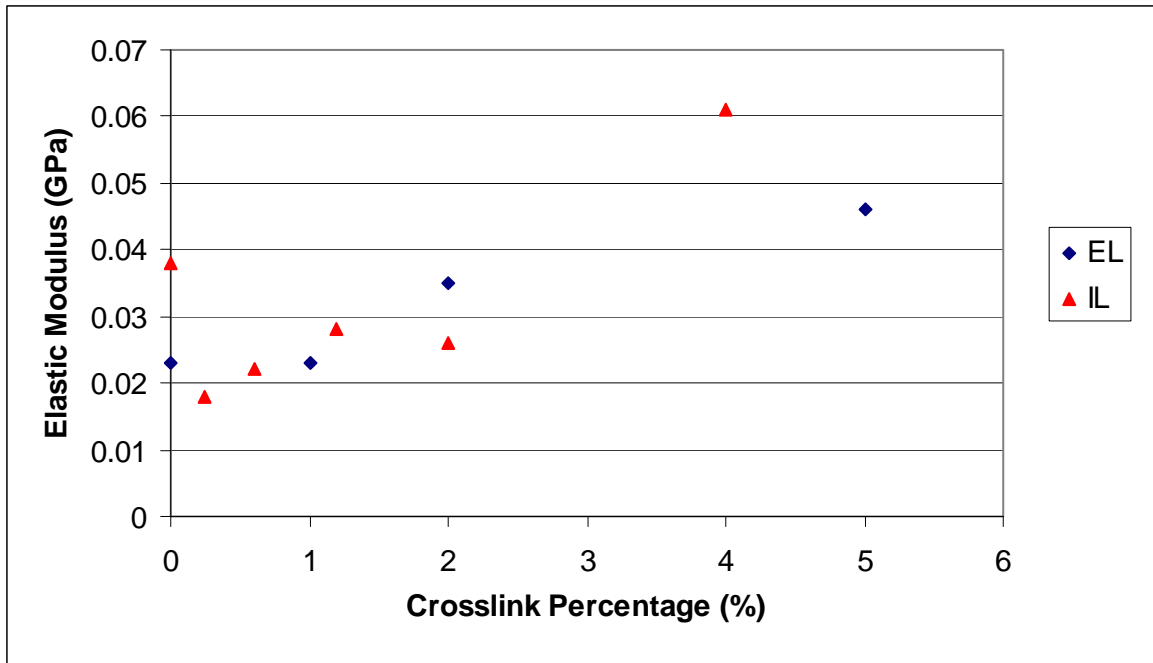


Figure 3.7. Comparison of moduli of samples in groups EL and IL with different crosslinker levels. The modulus was measured under a normal force of 1 mN.

For high- T_g films, hardnesses and elastic moduli are compared in Figures 3.8 and 3.9. As expected, high- T_g films are harder than low- T_g films at equal crosslinker levels. In this case, hardness increases as the levels of both pre-coalescence and post-coalescence crosslinkers increase. The elastic modulus of the pre-coalescence crosslinker increases with the level of crosslinker, but does not increase very much with the level of post-coalescence crosslinking. The latter result is surprising. In addition, high T_g latex films show higher hardness and elastic modulus, but less instant elastic recovery, than those low T_g latex films. The instant elastic recovery increased slightly with the increasing crosslinker percentage.

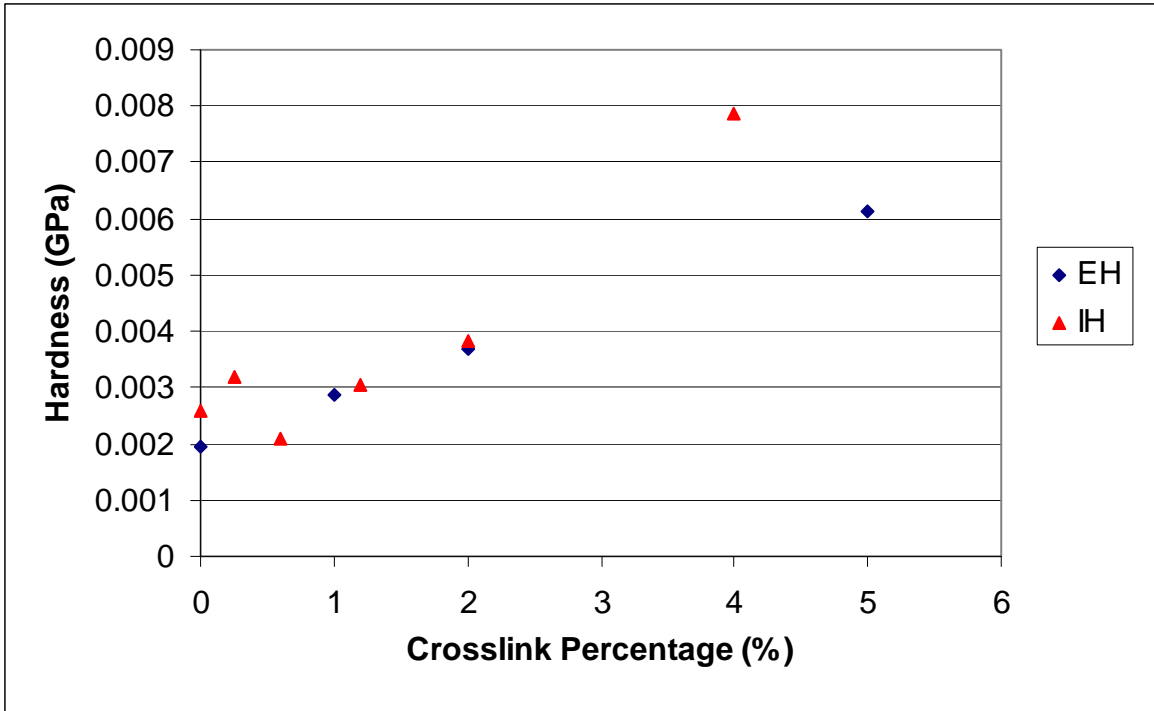


Figure 3.8. Comparison of hardness of samples in groups EH and IH as a function of crosslinker percentage. The hardness was measured under a normal force of 1 mN.

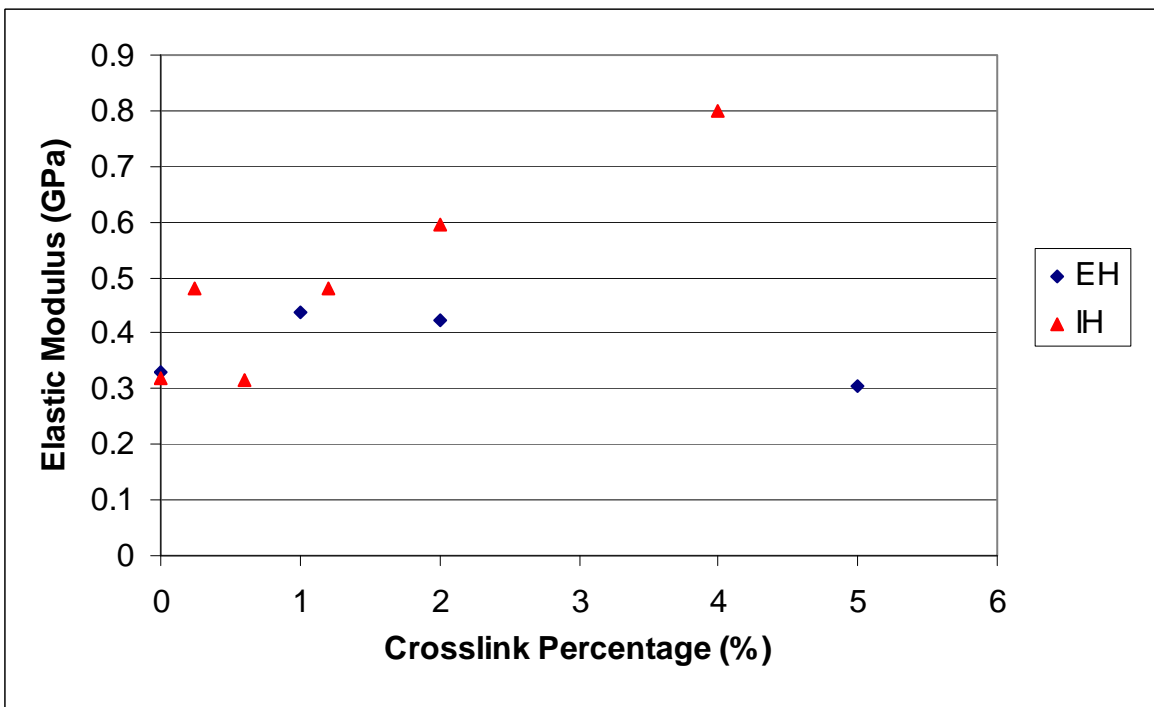


Figure 3.9. Comparison of modulus of samples in groups EH and IH as a function of crosslinker percentage. The modulus was measured under a normal force of 1 mN.

The dents made by the nano-indenter largely heal with time, as illustrated by the optical images (1000x) in Figure 10 for IL-1.2 and IH-1.2, pre-coalescence crosslinked films. Note the rough surface of film IL-1.2 Surface roughness may account for the difficulty of obtaining clear-cut results with these specimens. As shown in Figure 3.10, the images of indent recovery in samples IL-1.2 and IH-1.2 were taken at the intervals of 1, 4, 8, and 12 minutes.

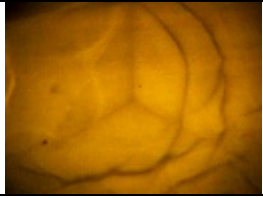
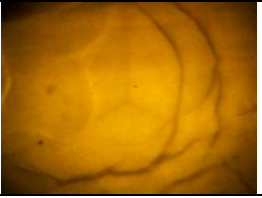
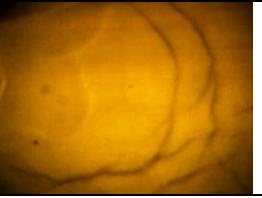
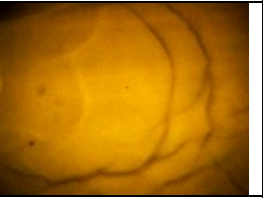




Time after indent	1 minute	4 minutes	8 minutes	12 minutes
IL-1.2				
IH-1.2				

Figure 3.10. Optical Images of the Residual Indentation in films cast from latexes IL-1.2 and IH-1.2. (1000x)

In general, the hardness and elastic modulus increase with increasing crosslinker percentage. However, in low T_g pre-coalescence crosslinked latexes, the one with no crosslinker (0% 1, 3-BGDMA) is harder and has higher modulus value than those that contain crosslinkers less than 4%. In high T_g post-coalescence crosslinked latexes, EH-4 of 4% DDA/ADDH exhibits lower modulus value than EH-0. These results are not easily explainable. However, based on stress-strain data later in the results and discussion section, nano-indentation results are consistent with modulus results from stress-strain data on bulk samples.

End-use film properties

Both types of latexes were cast on aluminum panels and kept at 55 °C overnight. The end-use film properties correlated to crosslink density such as solvent resistance, hardness, adhesion, and chemical resistance were studied. Results are presented in Table 3.3 and Table 3.4.

Table 3.3. Empirical properties of films cast from internally crosslinked latexes

Latexes		IL-0	IL-0.25	IL-0.6	IL-1.2	IL-2	IL-4	IH-0	IH-0.25	IH-0.6	IH-1.2	IH-2	IH-4
Tape Adhesion		4B	4B	3B	3B	5B	3B	4B	4B	3B	5B	4B	3B
Pencil Hardness		5B	4B	4B	4B	4B	4B	4B	4B	4B	4B	4B	5B
MEK 2 Rub Resistance		4	6	6	6	6	6	3	4	4	4	4	4
D.I. Water 2 Rub Resistance		200	200	200	200	200	200	200	200	200	200	200	200
H ₂ SO ₄ Spot Test, pH=3.1	15 min	E	E	E	E	E	E	E	E	E	E	E	E
	1 h	E	G	G	G	G	G	G	G	G	G	E	G
	16 h	F	F	F	F	F	F	F	P	P	P	P	P
Distilled Water Spot Test	15 min	E	E	E	E	E	E	E	E	E	E	E	E
	1 h	E	E	E	E	E	E	E	E	E	E	E	E
	16 h	G	F	F	F	F	F	F	P	P	P	P	P

E: Excellent, no change; G: Good, slightly white, but recovered quickly

F: Fair, whitening, becomes transparent after 24 hours; P: Poor, permanent damage

Table 3.4. Empirical properties of films cast from externally crosslinked latexes

Latexes		EL-0	EL-1	EL-2	EL-5	EH-0	EH-1	EH-2	EH-5
Tape Adhesion		4B	5B	4B	4B	3B	4B	5B	5B
Pencil Hardness		4B	HB	2B	2B	4B	HB	2B	B
MEK 2 Rub Resistance		5	18	42	83	7	14	16	106
D.I. Water 2Rub Resistance		200	200	200	200	200	200	200	200
H ₂ SO ₄ Spot Test (pH=3.1)	15 min	G	E	E	E	G	E	E	E
	1 h	G	E	E	E	G	G	G	G
	16 h	F	F	F	G	F	P	P	F
Distilled Water Spot Test	15 min	E	E	E	E	E	E	E	E
	1 h	G	E	E	E	E	G	G	G
	16 h	G	G	G	E	G	G	G	G

E, G, F, P as in Table 3.3.

Higher DAA/ADDH in post-coalescence crosslinked latexes generally improves adhesion, MEK solvent resistance, hardness, and chemical resistance as expected for post-coalescence crosslinking. In contrast, the pre-coalescence crosslinked latexes exhibited opposite phenomena. The higher amount of 1,3-BGDMA, the worse the adhesion. All pre-coalescence crosslinked films had poor solvent resistance, and within probable experimental error, there was no significant difference in film hardness. For pre-coalescence crosslinked latexes, chemical spot resistance results average one grade down than the post-coalescence crosslinked ones. These results indicate that, while very low levels of pre-coalescence crosslinking may improve certain properties, the affect on properties at higher levels is generally deleterious. Thus, in case of pre-coalescence crosslinking, the interdiffusion is impeded as too much crosslinking occurs before sufficient coalescence.

Summarizing the end-use test results, it appears that pre-coalescence crosslinked latexes can provide some good properties but cannot satisfy the full spectrum of film properties needed for many paints. On the other hand, post-coalescence crosslinked latexes provide dramatic improvement in chemical resistance and mechanical properties. They improve film toughness, provide solvent resistance and reduce dirt pick-up. As the crosslinker level in pre-coalescence crosslinked latexes increases, the particles are increasingly resistant to interdiffusion and perhaps to coalescence, resulting in inferior films. On the other hand, post-coalescence crosslinked latexes of the type studied here are apparently able to coalesce and interpenetrate adequately before the crosslink density is high enough to impede formation of desirable films. These observations are in harmony with the studies of Winnik and his colleagues on thermoset latex film formation.²⁴⁻²⁶

Fundamental Mechanical Properties

- *Stress-Strain Curves*

Average stress-strain curves for postcoalescence low and high T_g latex samples are shown in Figures 3.11 and 3.12, respectively, while the stress-strain curves for low and high T_g pre-coalescence latex samples are shown in 2.13 and 2.14, respectively. Each stress-strain curve represents an average of 5-6 replicates. Stress-strain data give information about the ultimate mechanical properties of materials. The values of Young's modulus, area under the stress-strain curve, strain-at-break, and stress at break are summarized in Table 3.5. The area under the stress-strain curve is a measure of the flexibility and toughness of the film. As the area decreases, the film becomes less flexible and more brittle.

Table 3.5. Results of Stress-Strain Analysis

Sample	Gel Content	Young's Modulus (E')	Area Under Curve	Strain at Break(ϵ_b)	Stress at Break(ϵ_b)
		(MPa)		(%)	(MPa)
IL-0	0.00	8.9 ± 0.6	172 ± 11	95.7 ± 6	2.7 ± 0.9
IL-0.25	46.1	13.9 ± 0.9	261 ± 21	109 ± 5.4	5.35 ± 0.6
IL-0.6	56.2	16.7 ± 1.2	299 ± 12	106 ± 5.4	5.78 ± 0.5
IL-1.2	52.8	16.2 ± 2.7	271 ± 40	107 ± 15	5.65 ± 0.8
IL-2	57.1	18.1 ± 0.9	311 ± 14	106 ± 12	6.00 ± 0.2
IL-4	64.2	49.7 ± 9.2	222 ± 6.3	57.9 ± 1.2	7.7
IH-0	0.0	15.9 ± 1.1	175 ± 2.8	98.8 ± 0.1	3.55
IH-0.25	10.1	55.5 ± 4.6	415 ± 68	74.7 ± 9.6	8.66 ± 0.6
IH-0.6	10.3	55.5 ± 4.6	415 ± 68	74.7 ± 9.6	8.66 ± 0.6
IH-1.2	15.6	59.9 ± 1.3	459 ± 25	75.5 ± 4.6	9.67 ± 0.3
IH-2	61.3	15.2 ± 1.6	257 ± 28	105 ± 11	5.04 ± 0.4
IH-4	62.9	213 ± 5.7	186	38.2	9.83
EL-0	0.0	8.9 ± 0.6	172 ± 11	95.7 ± 6	2.7 ± 0.9
EL-1	91.3	19.5 ± 0.5	318 ± 57	93.2 ± 11	6.71 ± 0.6
EL-2	98.1	24.2 ± 1.5	221 ± 50	62.9 ± 9.1	6.63 ± 0.8
EL-5	100.0	45.3	196.5 ± 11	41.8 ± 0.7	9.5 ± 0.5
EH-0	0.0	15.9 ± 1.1	175 ± 2.8	98.8 ± 0.1	3.55
EH-1	90.0	68.9 ± 10	364 ± 66	61.8 ± 7.6	8.71 ± 0.8
EH-2	97.4	69.9 ± 4.1	361 ± 35	60.8 ± 4.1	8.84 ± 0.3
EH-5	97.9	159 ± 11	174 ± 11	38.8 ± 1.5	8.9 ± 0.2

Figure 3.11 shows that with increasing levels of post-coalescence or external crosslinking, Young's modulus increases as expected for low T_g latex. However, a significant decrease in area under the curve and strain at break is observed. The sample becomes more brittle. Going from 0% to 1% crosslinker for the low T_g latex shows hardly any difference in Young's modulus. However, from 1 to 5% of crosslinker Young's modulus values go from

approximately 70 MPa to 159 MPa. This also has been observed by nano-indentation characterization, which shows that the Elastic modulus values for 0% and 1% crosslinker remain similar while there has been a significant build-up in modulus values as crosslinker levels go from 1% to 5% crosslinker. However, it should be noted that nano-indentation gives a surface modulus value while stress-strain characterization gives a bulk modulus value.

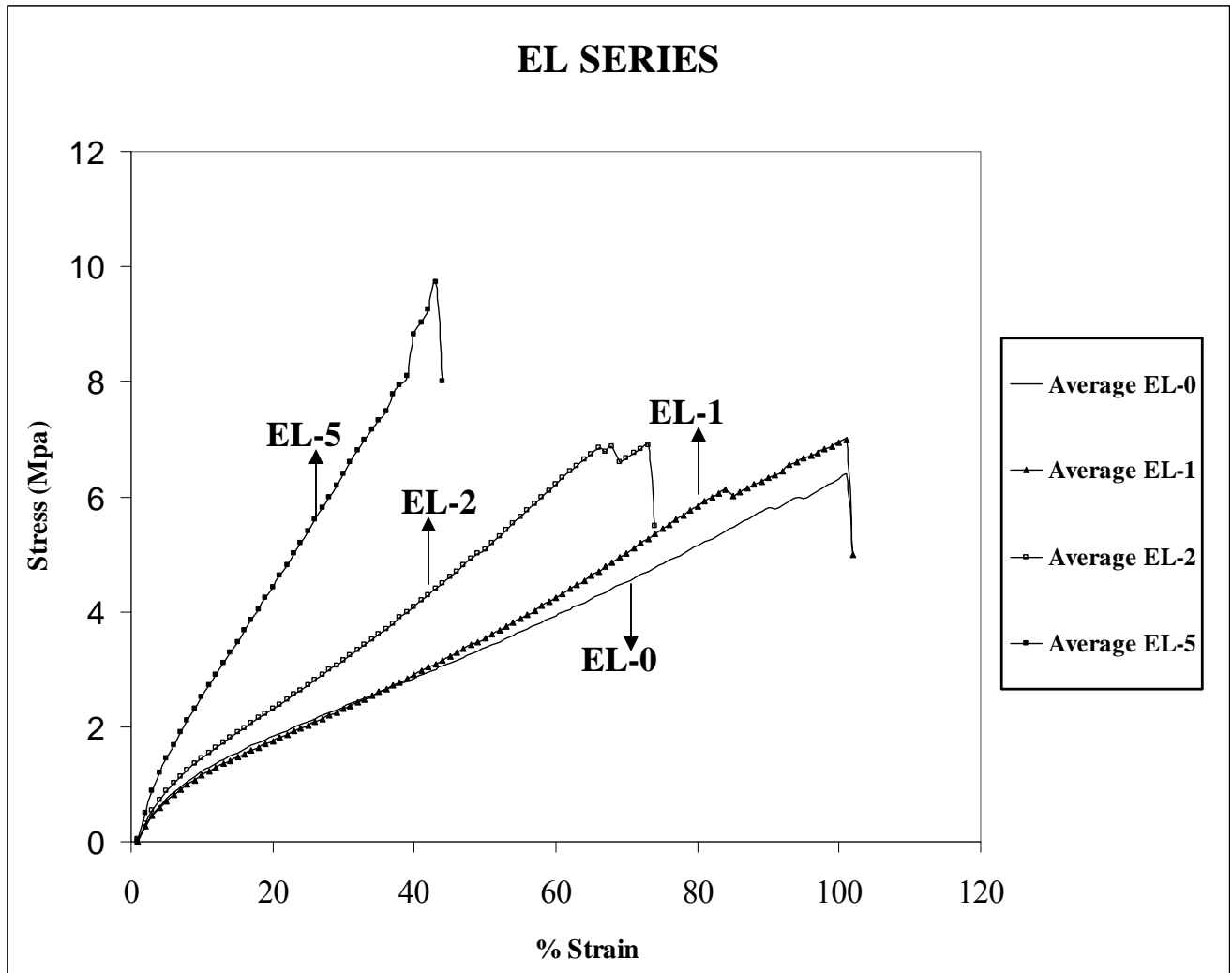


Figure 3.11. Average Stress-Strain Curves for Post-Coalescence Series: Low T_g

Figure 3.12 shows that for post-coalescence crosslinked high T_g latexes, the modulus values increase with the level of crosslinking and the samples become more brittle. The modulus values are higher than the low T_g counterparts, showing the effect of high glass transition

temperature with crosslinking. In contrast to low T_g samples, the high T_g samples shows a significant change in modulus value as the crosslinking level goes from 0% to 1%. Both stress-strain and nano-indenter data at 1% and 2% show a similar build up in modulus value compared to 0% crosslinking. However, in the nano-indentation test, samples with 5% crosslinker show a significant drop in elastic modulus in contrast to Young's modulus by stress-stain. This difference may reflect the different measurement methods.

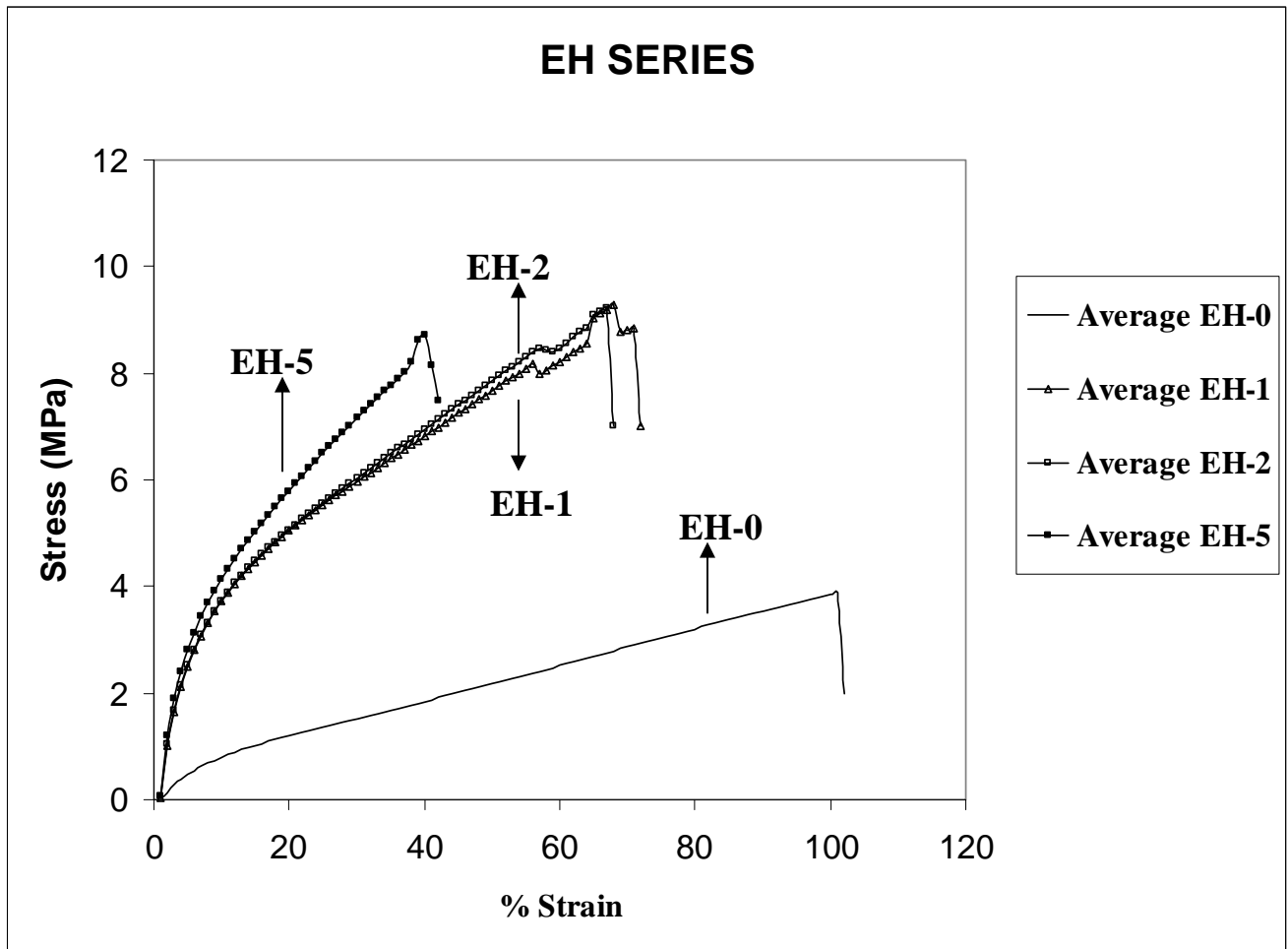


Figure 3.12. Average Stress-Strain Curves for Post-Coalescence Series: High T_g

Figure 3.13 shows that in the case of pre-coalescence crosslinking, as the level of crosslinking increases, interdiffusion of particles is retarded by crosslinking. It is observed that between 0.25% to 2% crosslinker, the modulus value is comparatively lower than 0%

crosslinking. At 4% of crosslinking the sample builds up the modulus value but becomes more brittle. The same trend is observed with the nano-indenter data where it is evident that the 0% crosslinker sample has a higher modulus value than the modulus values corresponding to 0.25% and 2% crosslinker. However, at highest level of crosslinking the Young's modulus value is the highest.

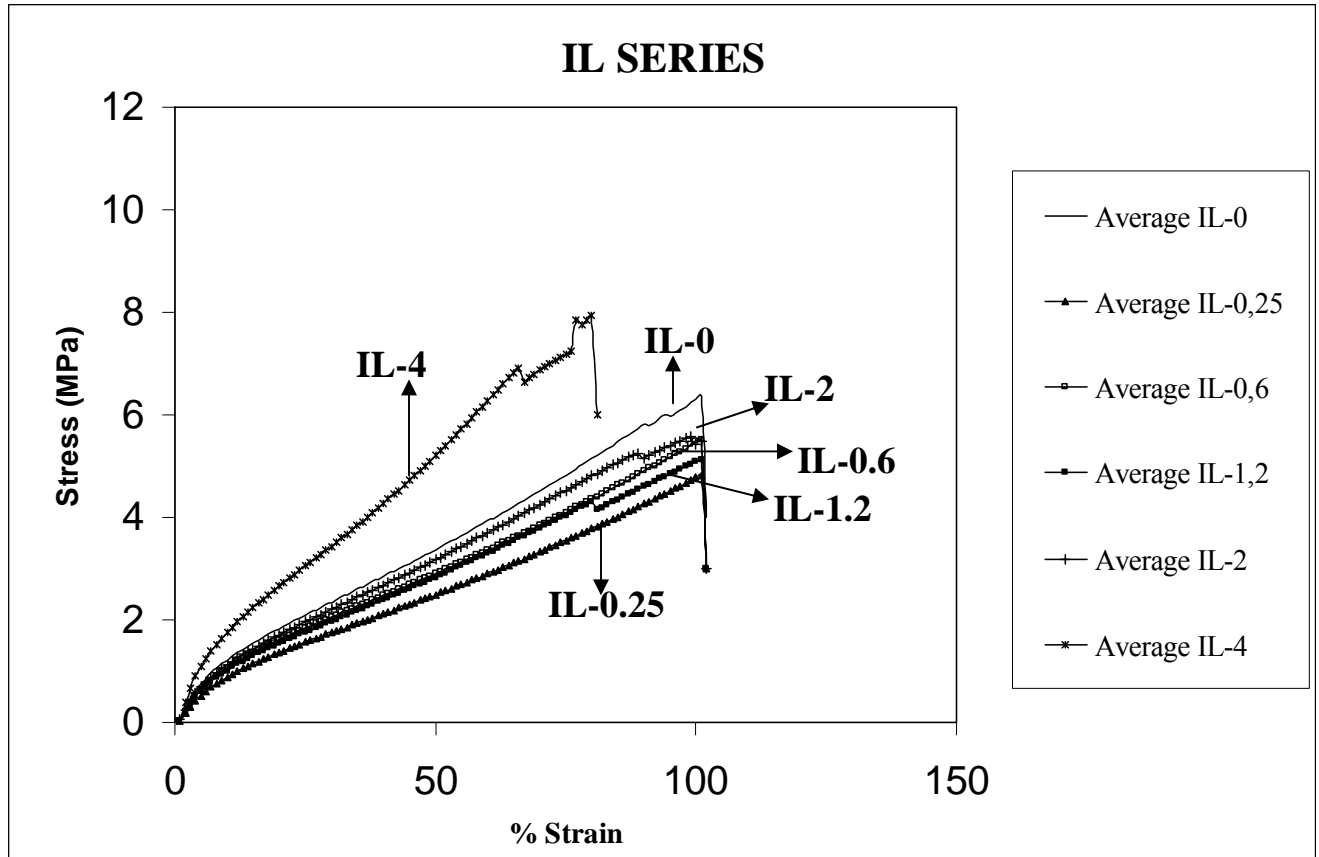


Figure 3.13. Average Stress-Strain Curves for Pre-Coalescence Series: Low T_g

Figure 3.14 shows that for high T_g pre-coalescence crosslinked latexes as the crosslinker level increases from 0-1.2%, the modulus values increase. However, the modulus value then decreases at 2% but significantly increases at 4%. The drop in modulus value at 2% could be due to retarded interdiffusion of polymer chains between particles. At 4% the increase in modulus

may be due to significantly increasing intra-particle crosslinking without further interrupting interdiffusion of polymer chains compared to 2%.

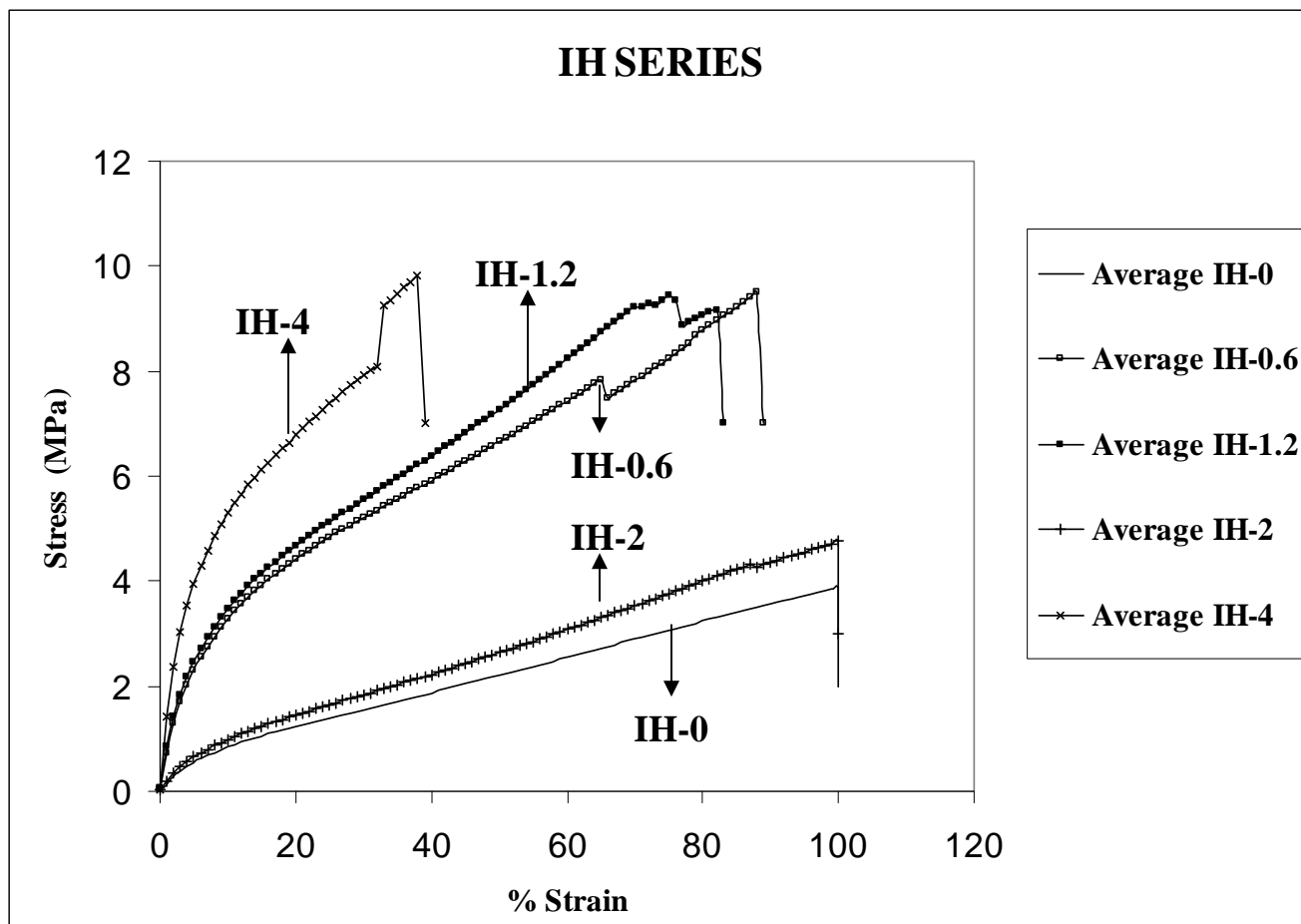


Figure 3.14. Average Stress-Strain Curves for Pre-Coalescence Series: High T_g

- *Dynamic Mechanical Properties*

Dynamic Mechanical characterization of heterogeneous polymers is dependent not only on the chemical composition of a material but also on physical or structural arrangement of the phases in a bulk polymer. DMA analysis gives an insight into intrinsic mechanical properties of a polymer. Figure 3.15 and Figure 3.16 show representative temperature scan graphs of the post-coalescence crosslinked latexes, high T_g and low T_g , respectively.

EH SERIES

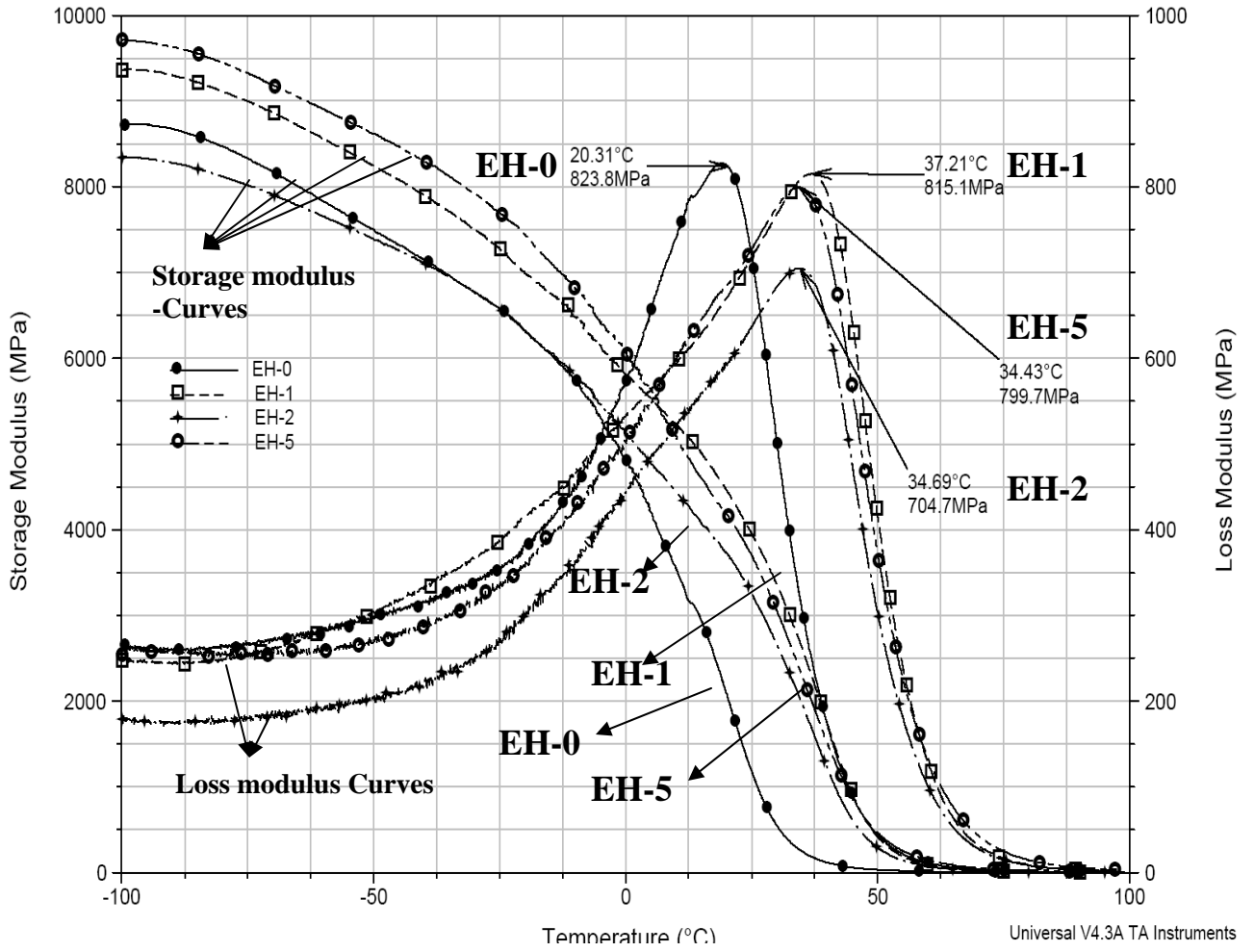


Figure 3.15: Storage and Loss modulus curves of Post-coalescence Crosslinked Latexes: High T_g

EL SERIES

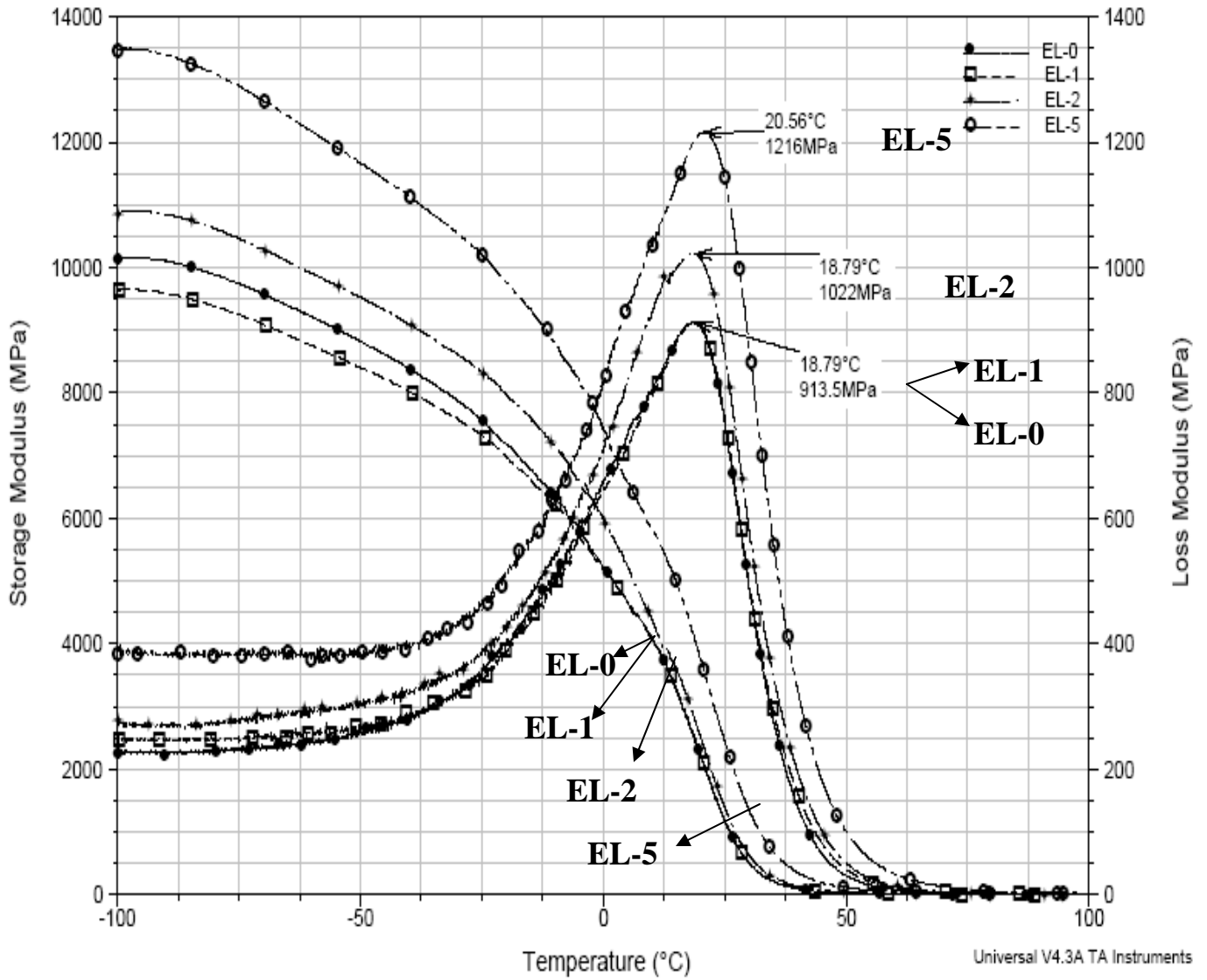


Figure 3.16 Storage and Loss modulus curves of Post-coalescence Crosslinked Latexes: Low T_g

DMA provides information about the viscoelastic properties (storage modulus and loss modulus) of a polymer as a function of frequency and temperature. The inflection point of the storage modulus is related to the T_g of the polymer. It should be noted that the temperature

corresponding to the inflection point of the tan delta curve is higher than the T_g value determined by MDSC, which is commonly observed. The tan delta curve is calculated as ratio of the loss modulus and storage modulus. The point where the storage modulus curve flattens is an indicator of the rubbery plateau. Hill²⁷ points out that “for unpigmented crosslinked coating films the level of the storage modulus, E' , in the rubbery plateau region above T_g is an indication of crosslink density”. Hill²⁷ further points out that a wide variation in E' values have been observed from 4MPa for lightly crosslinked systems to 200MPa for very highly crosslinked films. For the EH series latex films in the 80 to 90°C temperature range, the values of E' are as follows: EH0, $E' = 1$ MPa; EH1, $E' = 2$ MPa; EH2, $E' = 2$ MPa and EH5, $E' = 9$ MPa. For the EL series latex films in the 80 to 90°C temperature range the values of E' are as follows: EL0, $E' = 1$ MPa; EL1, $E' = 3$ MPa; EL2, $E' = 3$ MPa and EL5, $E' = 10$ MPa. Therefore, according to Hill's²⁷ criteria, the rubbery plateau modulus values indicate that at 5% crosslinker level, films from both EH and EL latexes are very lightly crosslinked systems.

Table 3.6 compares the MDSC T_g , DMA storage modulus inflection point, DMA loss peak temperature, tan delta peak temperature, and half width/half height of tan delta peak.

Table 3.6 Comparison of DMA values with MDSC T_g values

Samples	MDSC (T _g)	DMA	DMA	DMA	(L)HWHH	(R)HWHH
		Storage modulus inflection point	Loss peak temperature	Tan delta peak temperature	DMA Tan delta	DMA Tan delta
EL-0	6	13.5	18.7	42.5	10.0	12.6
EL-1	9	16.0	18.7	42.7	11.0	14.2
EL-2	7	18.9	18.7	43.9	11.6	14.2
EL-5	5	21.4	20.6	44.4	13.1	16.8
IL-0	6	13.5	18.5	42.4	10	12.6
IL-0.25	8	16.7	17.6	42.7	10.8	12.9
IL-0.6	5	20.0	17.6	43.3	11.0	13.7
IL-1.2	6	17.0	19.1	43.0	10.5	12.9
IL-2	5	18.7	18.2	42.7	10.0	13.1
IL-4	13	23.4	25.1	50.4	10.5	13.4
EH-0	22	31.2	20.3	41.6	11.3	14.2
EH-1	25	38.4	37.2	61.4	11.0	12.1
EH-2	25	37.1	34.6	61.4	11.3	13.7
EH-5	23	36.4	34.4	59.1	12.6	16.3
IH-0	21	31.2	32.8	41.9	11.3	14.2
IH-0.25	25	31.0	35.0	62.2	10.5	13.2
IH-0.6	25	31.0	35.0	62.2	10.5	13.2
IH-1.2	24	20.3	36.6	62.0	10.5	12.4
IH-2	13	20.4	26.0	48.1	11.0	13.1
IH-4	33	*	*	*	*	*

* indicates – sample was too brittle to test

- **Tan delta Curves**

In the case of post-coalescence crosslinked latexes, with increasing % crosslinker, clear broadening and shifting of tan delta peak to higher temperatures is evident in Figure 3.17. Going from 0% to 1% or 2% shows a shift in tan delta peak to higher temperatures but the clear broadening of the tan delta peak can be seen at the 5 % crosslinker level. However, in the case of low T_g latexes in Figure 3.18, the shifting in tan delta peaks is negligible, but at the highest level of crosslinking, broadening as well as a decrease in peak height can be seen very clearly. The

above observations are also reflected in half width and half height values of tan delta curves as shown in Table 3.6. The broadening of the tan delta peak is an indication of the development of a heterogeneous network structure and morphology as the crosslinker level increases.²⁷

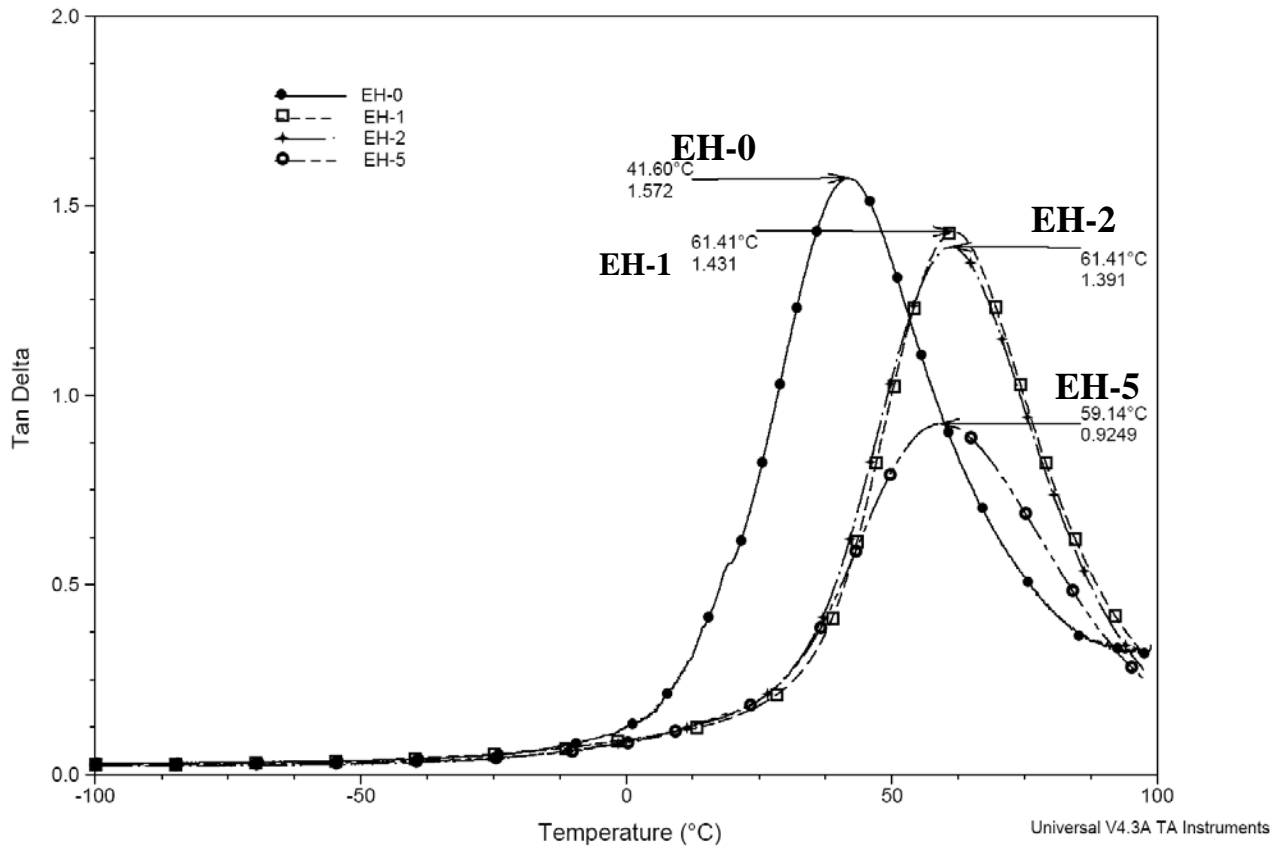


Figure 3.17 Tan delta curves of Post-coalescence Crosslinked Latexes: High T_g

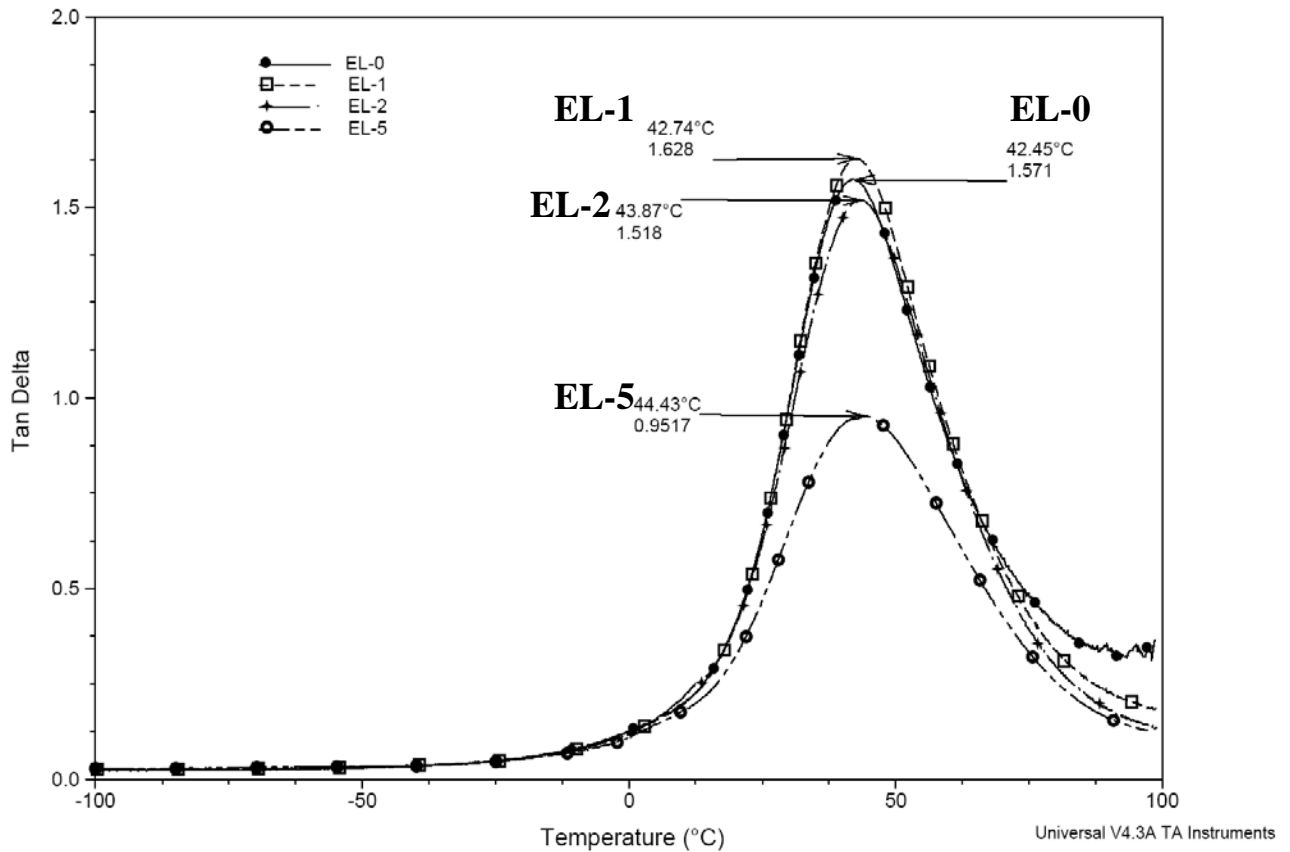


Figure 3.18 Tan delta curves of Post-coalescence Crosslinked Latexes: Low T_g

Figures 3.17 and 3.18 show that the decrease of the tan delta peak can be seen for both high T_g and low T_g post-coalescence crosslinker latex samples, particularly at the 5% level. This can be directly attributed to increased crosslinking. As the level of crosslinking increases, the Young's modulus value increases at measurement temperatures of 25°C as shown in Figures 3.11 and 3.12 and Table 3.5. Also, the tan delta peaks become broader (increase of half width and half height, Table 3.6), and the tan delta peak value decreases, an indication of the development of a more heterogeneous network structure and morphology. Thus, as the crosslinking level increases, the elastic modulus level obtained from stress-strain measurements increases and the DMA tan delta peak broadens. The rubbery plateau modulus obtained from

DMA measurements increases at the 5% level indicating a lightly crosslinked latex film. It should be noted that the MEK double rub resistance does increase as a function of crosslinking level and the pencil hardness also increases with crosslinking level (see Table 3.3). These results lead us to conclude that at the appropriate crosslinker levels an optimized hardness-flexibility balance can be achieved. Clearly the postcoalescence crosslinked latex particles are able to coalesce, interdiffuse, and interpenetrate adequately before the crosslink density is high enough to impede the formation of films with desirable properties.

In the case of the pre-coalescence crosslinked latex samples, shifting of the tan delta peak to higher temperature can be seen for low T_g latex samples at the highest crosslinking level in Figure 3.19 with minimal broadening of the tan delta peak. In the case of higher T_g latex samples in Figure 3.20, shifting of the tan delta peak to higher temperatures can be seen for all crosslinker levels with minimal broadening of the tan delta peak. This would indicate that with increasing crosslinker level, a more heterogeneous structure is not developing at least up to crosslinker levels of 4%. However, as the crosslinking level increases, the elastic modulus level obtained from stress-strain measurements increases at the 4% level. For IL latex films, the rubbery plateau modulus obtained from DMA measurements increases to 9MPa for IL0.6 and then declines to about 1MPa for IL2. This indicates as the level of precoalescence crosslinker increases internal particle crosslinking increases and inhibits interdiffusion and interparticle chain entanglement. For IH latex films the rubbery plateau modulus obtained from DMA measurements does not increase above 3MPa for all levels of crosslinker. This indicates that for all levels of precoalescence crosslinker, internal particle crosslinking inhibits interdiffusion and interparticle chain entanglement. It should be noted that the MEK double rub resistance does not increase as a function of crosslinking level, and the pencil hardness appears to be essentially independent of

crosslinking level (see Table 3.3). These results indicate that the pre-coalescence particles are indeed internally crosslinked but do not improve the properties of the latex films. These results lead to the conclusion that higher crosslink levels will not affect the rubbery plateau modulus for these high molecular weight, high T_g latex polymer chains. Thus, in case of pre-coalescence crosslinking, the interdiffusion is impeded because too much crosslinking occurs before sufficient interparticle chain entanglement and particle coalescence can occur.

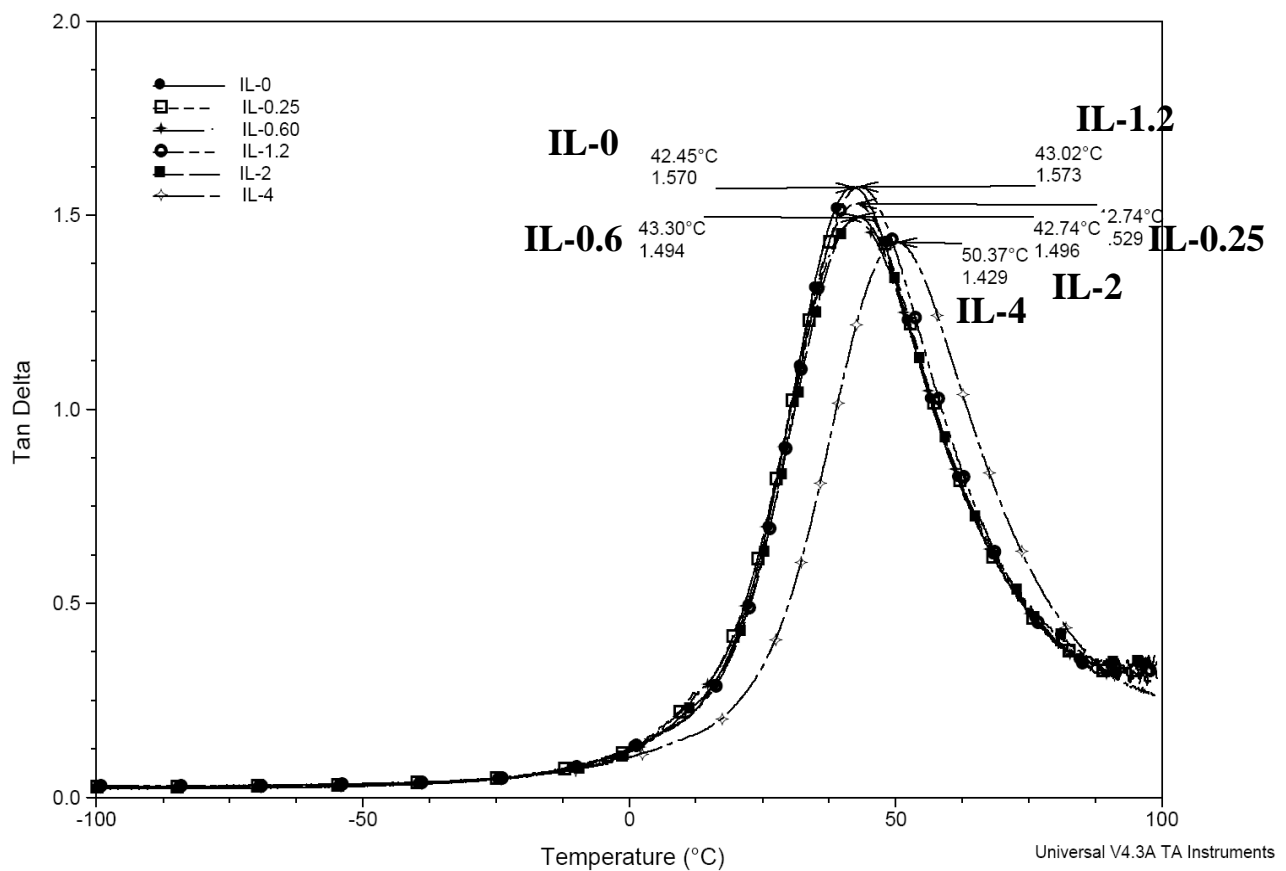


Figure 3.19 Tan delta curves of Pre-coalescence Crosslinked Latexes: Low T_g

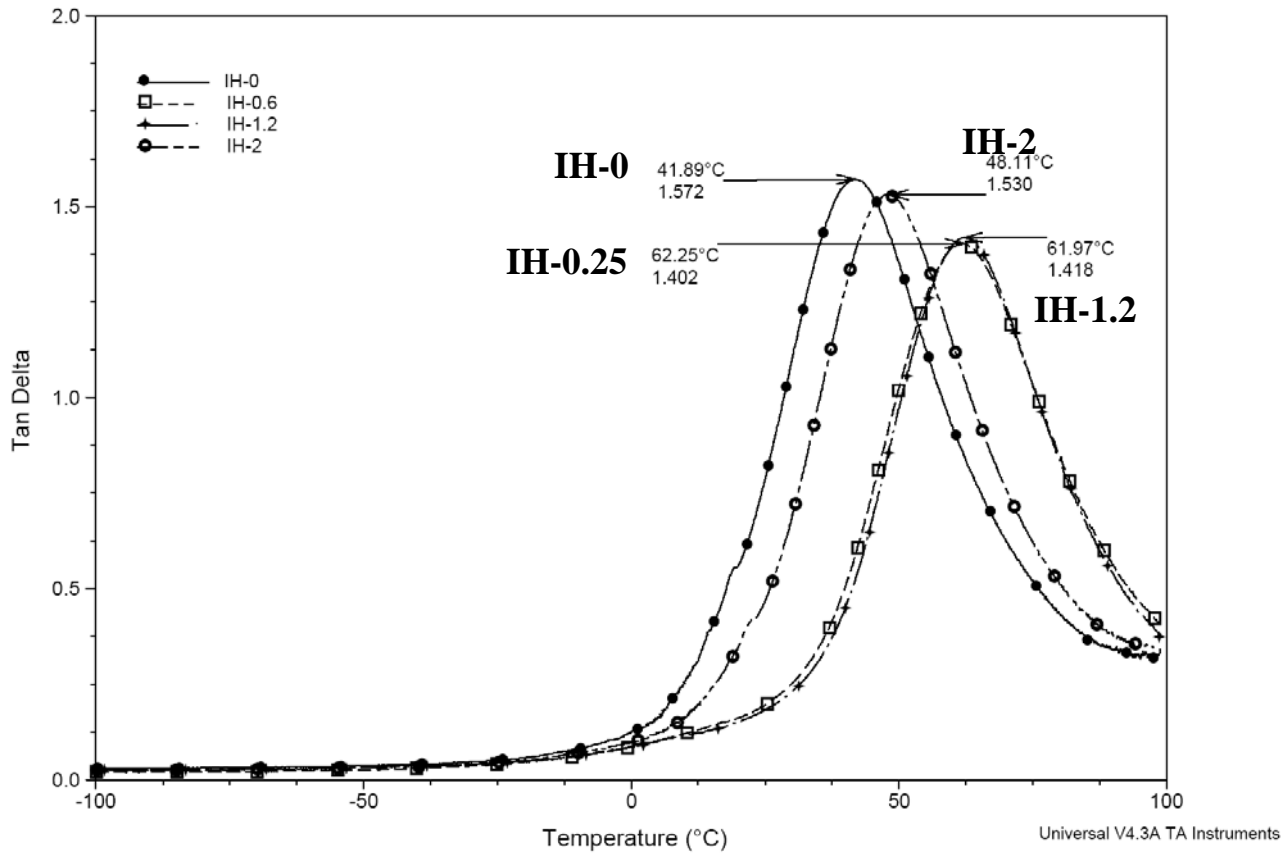


Figure 3.20 Tan delta curves of Pre-coalescence Crosslinked Latexes: High T_g

Comparison of DMA results of latex samples: 1st day (after oven cured) vs. 7th day (after oven curing):

Two sets of studies were performed: (1) on the first day (at the end of overnight cure into the oven), and (2) on the 7th day (7 days of ambient cure after overnight cure into the oven). The results from the 1st and 7th day studies were compared. Comparison between the first day studies and the 7th day studies were done. Figure 3.21 (a, b) shows Young's modulus vs. % gel of EL and IL samples of 1st vs. 7th day studies. Figure 3.22 (a, b) shows representative tan delta curves of EL2 and IL-1.2 samples of 1st vs. 7th day studies. The comparison showed that similar trend is

observed when comparing the results obtained in 1st and 7th day for stress-strain results and dynamic mechanical analysis. The values are not identical but these are very close (with in the experimental error or standard deviations) and the curves show the same inflection.

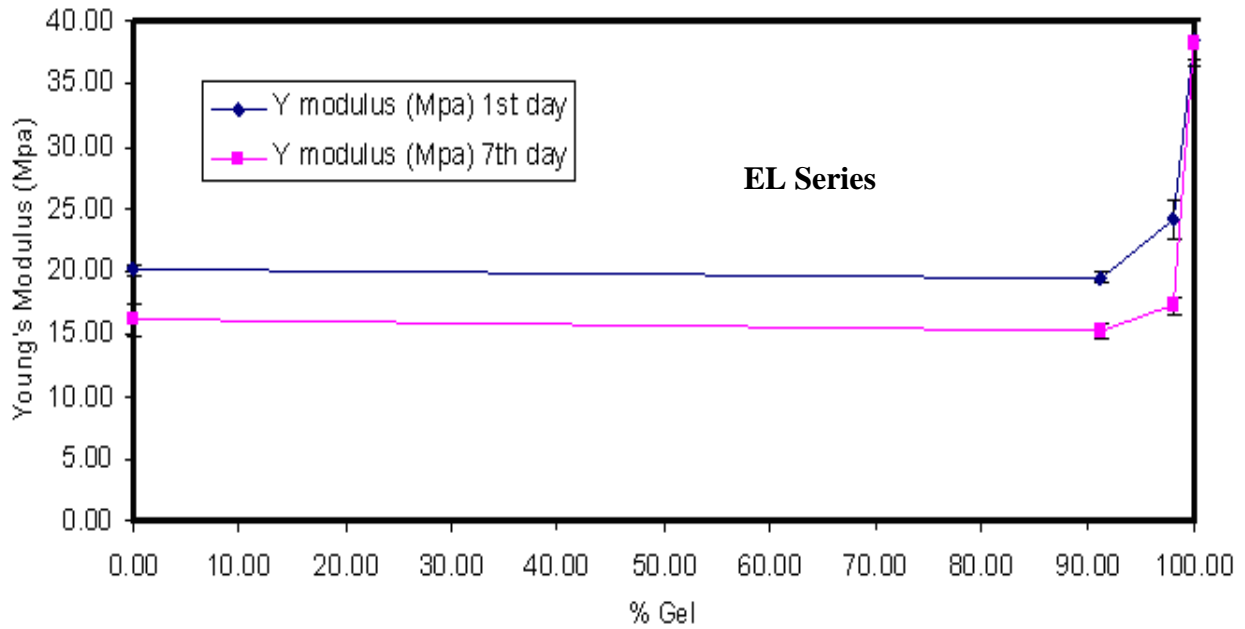


Figure 3.21 (a) Representative curves showing 1st day vs. 7th day comparison of stress-strain analysis of EL series

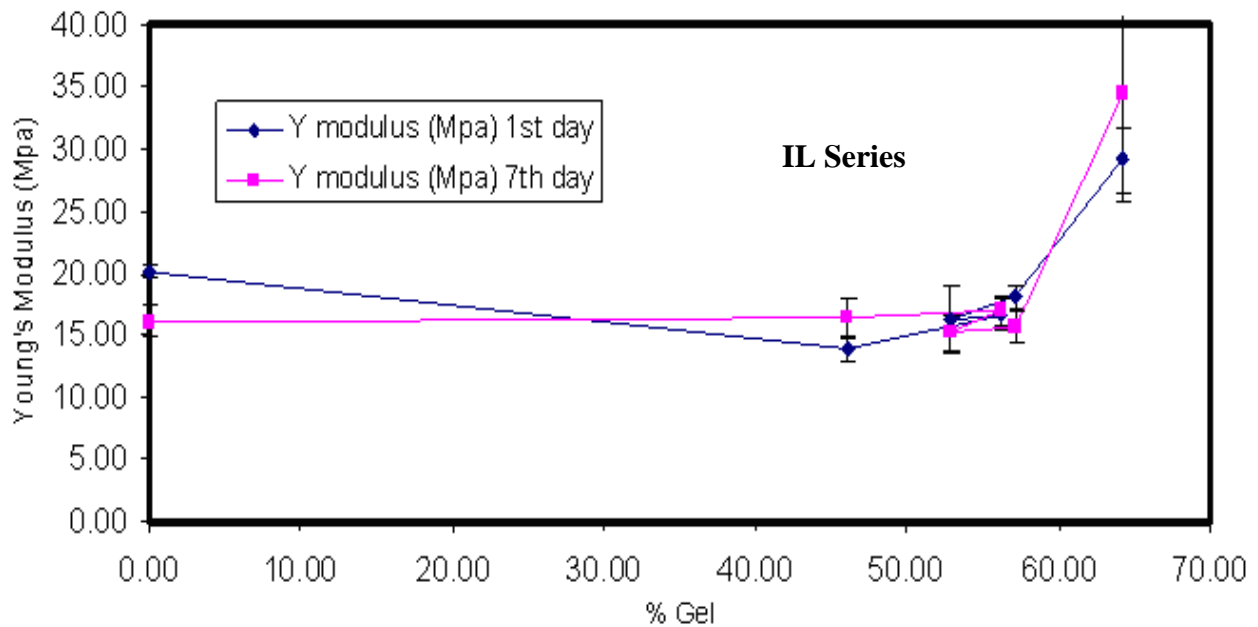


Figure 3.21 (b) Representative curves showing 1st day vs. 7th day comparison of stress-strain analysis of IL series

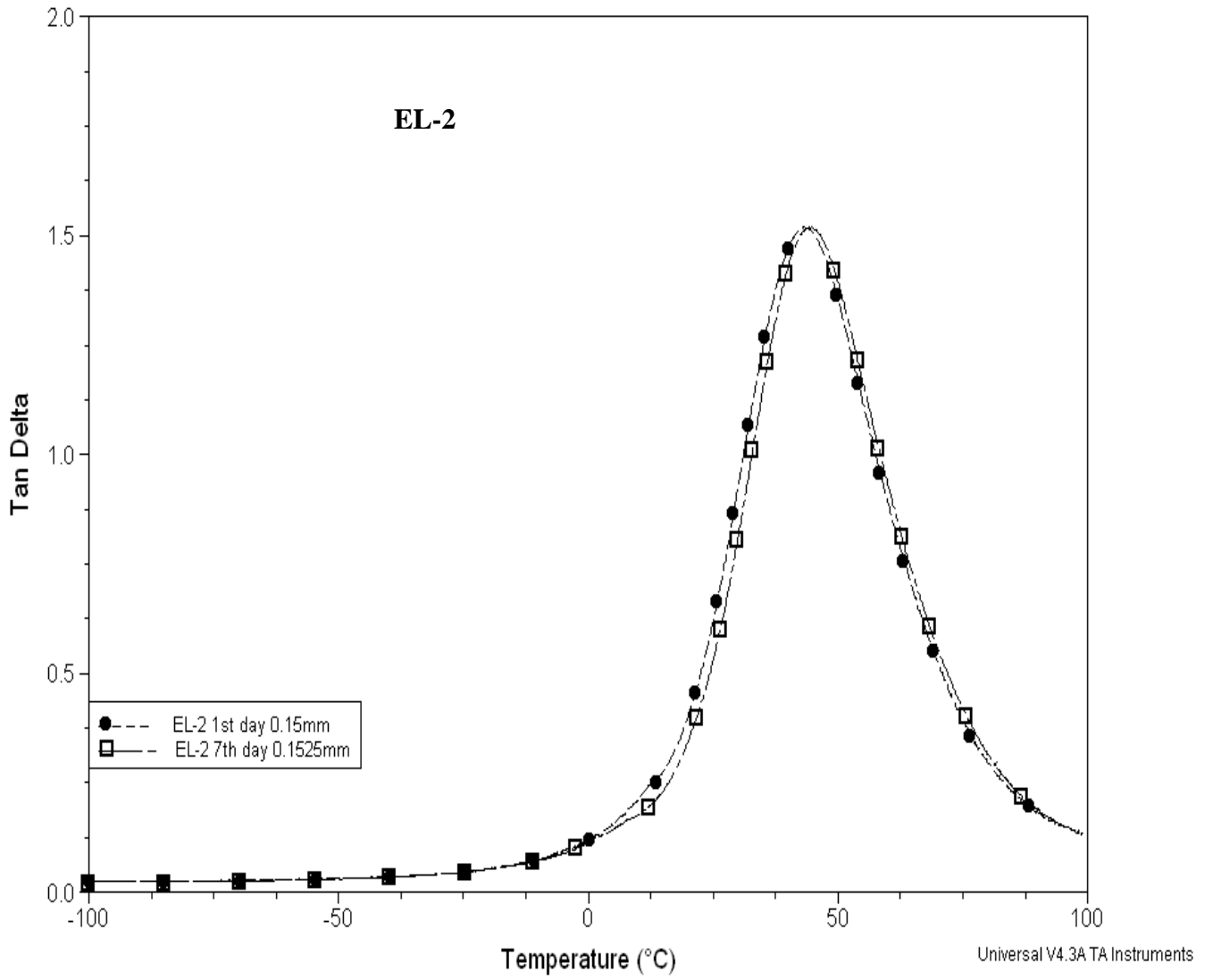


Figure 3.22 (a) Representative tan delta curves showing 1st day vs. 7th day comparison of DMA studies of EL-2

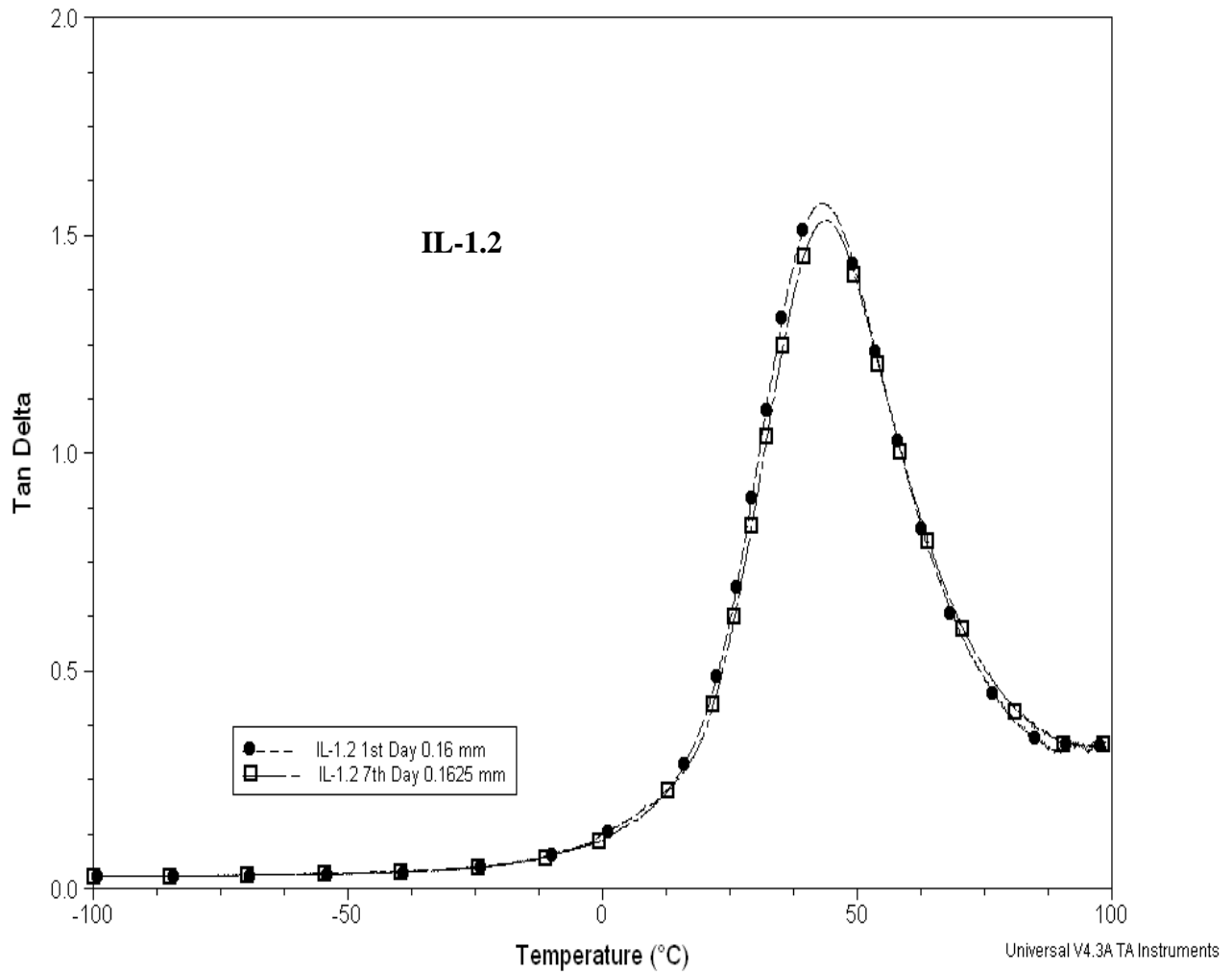


Figure 3.22 (b) Representative tan delta curves showing 1st day vs. 7th day comparison of DMA studies of IL- 1.2 samples

Time-evolution of mechanical properties

The liquid coating samples were applied and cured on glass panels at room temperature. The stress-strain and DMA analysis of samples of dried coatings at specified time intervals from 1st day to 10th day were done. Figure 3.23 (a-b) shows representative stress-strain average curves and Storage & Loss modulus curves of sample EH-0. The graph shows clear evidence of build up in mechanical properties as a function of time. Going from the first day to second day to fifth day, the mechanical properties show significant build-up.

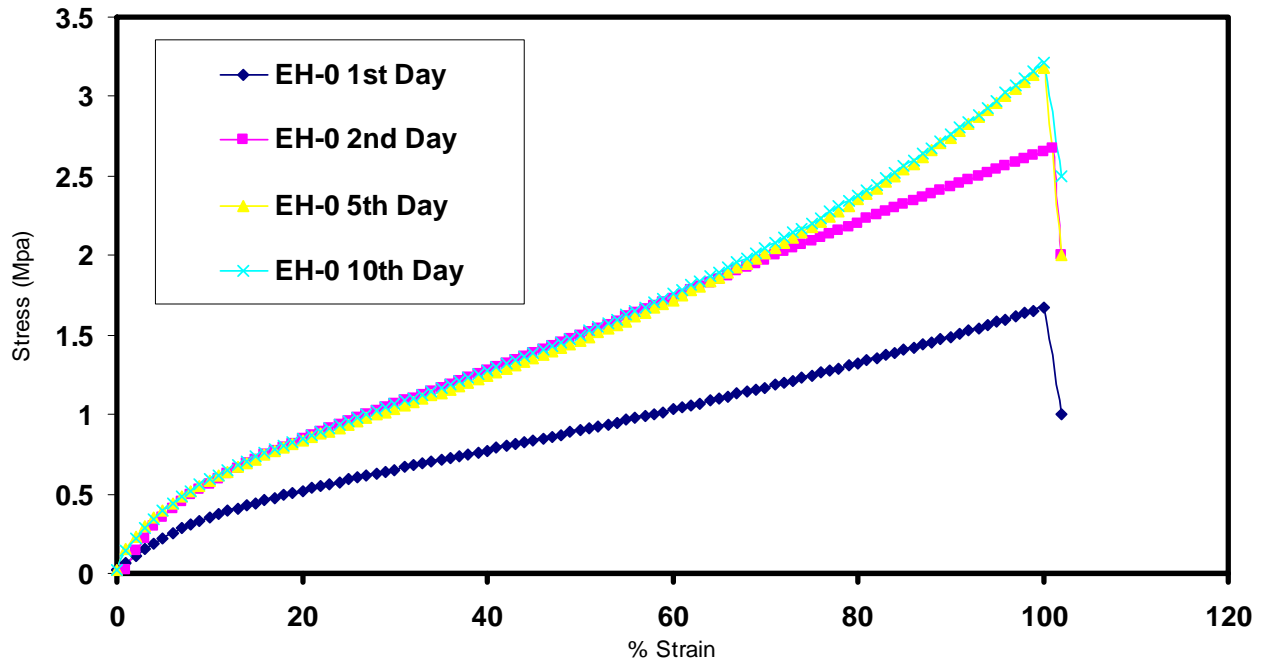


Figure 3.23 (a) Time-based stress-strain analysis of EH-0 at ambient conditions

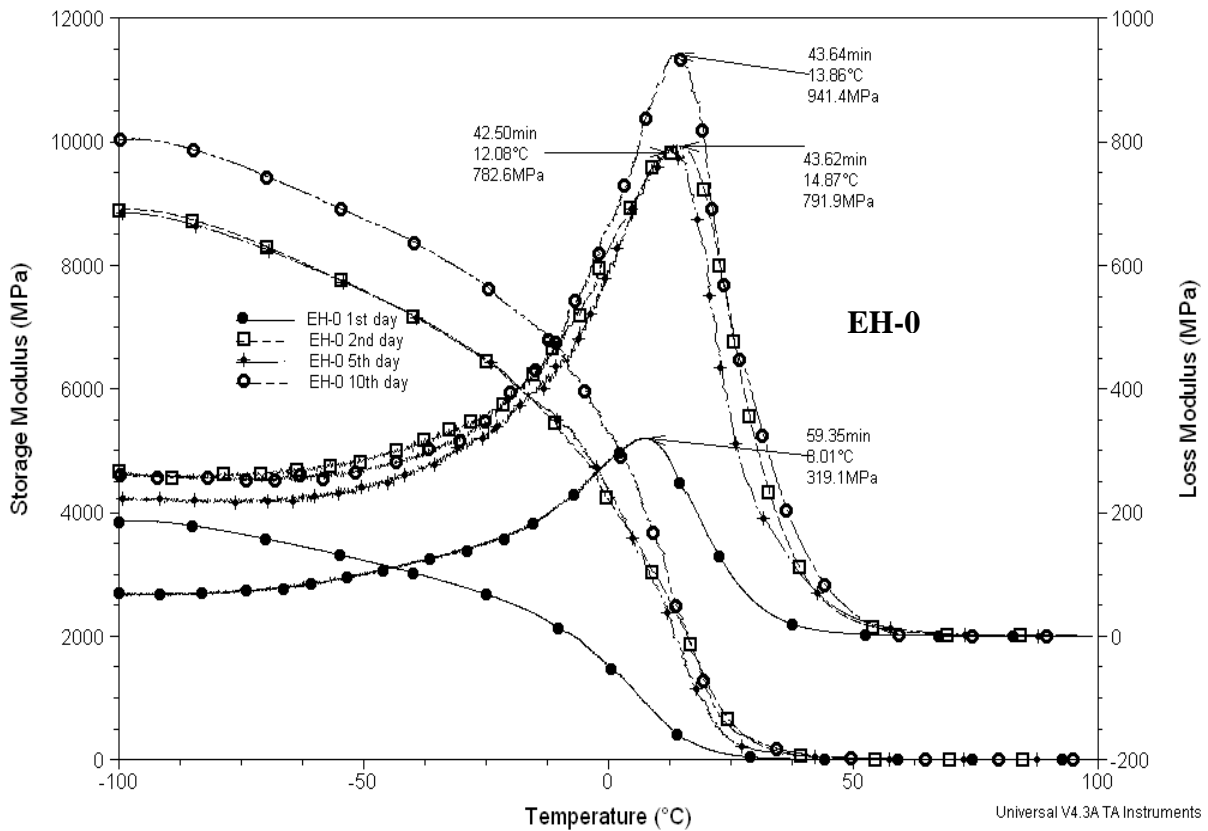


Figure 3.23(b) Time-based DMA analysis of EH-0 at ambient conditions

Conclusions

The present research is one of the few, if any, systematic comparisons of both pre-coalescence vs. post-coalescence crosslinking. The key findings of the research are summarized below:

- Up to 4 wt. % of 1, 3-BGDMA has a minimal effect on the end-use properties of the pre-coalescence crosslinked latexes except that T_g is increased at the 4 % (highest) level. In the case of post-coalescence crosslinked latexes, at the 5 wt. % level (highest) a substantial increase in latex viscosity was observed along with a slight effect on T_g .
- The post-coalescence crosslinked latexes showed higher % gel compared to pre-coalescence crosslinked latexes. The low values recorded for pre-coalescence crosslinked latexes may reflect incomplete knitting of the pre-coalescence crosslinked latex particles during film formation, allowing small pieces to break loose and pass through the extraction filter.
- AFM images of the films cast from latexes showed that the height variation at the surface of the low T_g post-coalescence latex at the 1% crosslinker level is an order of magnitude larger than the height variation at the surface of high T_g pre-coalescence latex at the 4% level of crosslinker. This observation suggests that the rate of the crosslinking reaction for high T_g pre-coalescence latex at the 4% level was fast enough to significantly impede interdiffusion and retard particle coalescence and the homogenization of the film, at least near the surface.
- With the use of AFM the film formation as a function of time can clearly be seen through evolution of mechanical properties and morphological changes with time for post-coalescence and pre-coalescence crosslinking.

- Hardness values of low T_g post-coalescence crosslinked latexes increased with increasing crosslinker level, while hardness values of low T_g pre-coalescence crosslinked latexes were independent of crosslinker level. Hardness values of high T_g pre-coalescence and post-coalescence crosslinked latexes increased with increasing levels of crosslinker. As expected, high T_g films were harder than low T_g films at equal crosslinker levels. The elastic modulus for post-coalescence crosslinked latexes showed a modest increase with the increase of the level of crosslinker, while the pre-coalescence crosslinked latexes had an increased elastic modulus at increasing crosslinker levels. At the 4% (the highest) level of crosslinker for pre-coalescence crosslinked latexes, the elastic modulus was the highest. Surprisingly, for the high T_g post-coalescence latexes the elastic modulus did not increase very much. In addition, the high T_g latex films showed higher hardness and elastic modulus but less instant elastic recovery than the low T_g latex films. The instant elastic recovery increased slightly with increasing levels of crosslinker.
- For pre-coalescence crosslinking, as the level of crosslinking increased the interdiffusion of polymer chains between particles was retarded by increasing levels of crosslinker. The same trend was observed when results were corroborated with the nano-indenter data where it was evident that the 0% crosslinker level sample had a higher modulus value than samples with 0.25% to 2% crosslinker levels. However, at the highest level of crosslinking, the modulus value was at its highest value. For high T_g pre-coalescence crosslinked latexes, the tan delta peak shifts to higher temperatures with increasing levels of crosslinker. For the low T_g pre-coalescence crosslinked latex samples, shifting of tan delta peak to higher temperatures occurs at the highest crosslinking level. The rubbery

plateau modulus values indicate that at 0.6% crosslinker, these systems are lightly crosslinked.

- For post-coalescence crosslinking, with increasing levels of post-coalescence crosslinker, Young's modulus increased for both high and low T_g latexes as expected. However, a decrease in area under the curve and strain at break was observed, clearly indicating that the samples become more brittle. Both high and low T_g post-coalescence crosslinker latex samples exhibited a decrease and broadening of the tan delta peak with increasing levels of crosslinker, indicating an increase in heterogeneous network structure and morphology. At the 5% crosslinker level for both high and low T_g samples, the rubbery plateau modulus values indicate that these systems are lightly crosslinked.
- Samples with higher DAA/ADDH levels for post-coalescence crosslinked latexes exhibited improved adhesion, MEK solvent resistance, hardness, and chemical resistance, as expected. In contrast, the pre-coalescence crosslinked latexes showed generally deleterious properties at high levels. At very high levels of 1, 3 – BGDMA, the films had poor solvent resistance and no significant difference in film hardness; adhesion became worse; and chemical spot resistance results averaged one grade down compared to the post-coalescence crosslinked samples. These results indicated that the effect of higher crosslinker levels on end-use properties was generally deleterious for pre-coalescence crosslinking. However up to 0.6% and may be up to 1.2% level of 1,3 BGDMA, the latex samples showed may be neutral or even favorable for overall properties. Thus, as the crosslinker level in pre-coalescence crosslinked latexes increased, the polymer chains within particles became increasingly resistant to interdiffusion between particles and perhaps to coalescence, resulting in inferior film properties. In contrast post-coalescence

crosslinked latexes of the type studied here had sufficient interdiffusion of polymer chains between particles to interdiffuse and interpenetrate adequately before the cross-link density was high enough to impede the formation of films with desirable end-use properties.

References:

1. a. Bufkin, B. G. and Grawe, J. R., "Survey of the applications, properties, and technology of crosslinking emulsions. Part I", *Journal of Coatings Technology-Research* 1978, 50, (641), 41-55.
- b. Grawe, J. R. and Bufkin, B. G., "Survey of the applications, properties, and technology of crosslinking emulsions. Part II", *Journal of Coatings Technology-Research* 1978, 50, (643), 67-83.
- c. Bufkin, B. G. and Grawe, J. R., "Survey of the applications, properties, and technology of crosslinking emulsions. Part III", *Journal of Coatings Technology-Research* 1978, 50, (644), 83-109.
- d. Grawe, J. R. and Bufkin, B. G., "Survey of the applications, properties, and technology of crosslinking emulsions. Part IV", *Journal of Coatings Technology-Research* 1978, 50, (645), 70-100.
- e. Bufkin, B. G. and Grawe, J. R., "Survey of the applications, properties, and technology of crosslinking emulsions. Part V", *Journal of Coatings Technology-Research* 1978, 50, (647), 65-96.
2. Taylor J.W. and Winnik M.A., "Functional Latex and Thermoset Latex Films," *Journal of Coatings Technology-Research* 2004, 1, (3), 163-190 and references therein.
3. a) Winnik, M.A., "Interdiffusion and crosslinking in Thermoset Latex Films," *Journal of Coatings Technology-Research* 2002, 74, (925), 49-63 and references therein.
b) Winnik, M.A., "Crosslinking and polymer interdiffusion in latex films," *Polym. Prep.* 2003, 44(1), 100-101.
4. Winnik, M.A., "The formation and properties of latex films," in Lovell, P.A. and El-Aasser, M. S., In *Emulsion Polymerization and Emulsion Polymers*, Wiley, New York, 1997, 467-518.
5. Zosel, A. and Ley, G., "Influence of crosslinking on structure, mechanical properties, and strength of latex films," *Macromolecules* 1993, 26, 2222-2227.
6. Huang, Y. and Jones, F.N., "Synthesis of crosslinkable acrylic latexes by emulsion polymerization in the presence of etherified melamine-formaldehyde (MF) resins," *Prog. Org. Coat.* 1996, 28, 133-141.
7. Teng, G. and Soucek, M.D., "Effect of introduction mode of hydroxyl functionality on morphology and film properties of cycloaliphatic diepoxide crosslinkable core-shell latex," *J. Polym. Sci. Part A: Polymer Chemistry* 2002, 40, 4256-4265.
8. Technical information sheet, "Diacetone acrylamide, N-(1,1dimethyl-3-oxobutyl)-acrylamide," Kyowa Hakko U.S.A. Inc., p 4.
9. Coleman, L.E.; Bork, J. F.; Wyman, D. P.; Hoke, D. I., "Synthesis and polymerization of N-[2-(2-methyl-4-oxopentyl)]-acrylamide (diacetone acrylamide)--a new reactive vinyl monomer", *Journal of Polymer Science, Part A: General Papers* 1965, 3, (4), 1601-1608.
10. Emmons, W.D., (to Rohm and Haas) "Ambient or low-temperature curable coatings," U.S. Patent 4,210,565, 1980.
11. Geelhaar, H.J., Penzel, E., and Ley, G., (to BASF) "Binders for paints," U.S. Patent 4,267,091, 1981.

12. Krajnik, J.M., Lam, V.H., Sabo, L. O., Camerson, J.M., Mittleman, M.L., and Wise, K.M., (to Sherwin-Williams) "Waterborne coating compositions," U.S. Patent Application 20020103278, 2002.
13. Robinson, G.F., Shemancik, R.C., Speight, R.D., Wong, P.T., and Znidersic, K.M. (to Akzo Nobel), U.S. Patent 6,605,359, 2003.
14. Wicks, Jr. Z.W., Jones, F. N., and Pappas, S. P., *Organic Coatings Science and Technology*, Third Edition, Wiley-Interscience, New York 2007, 195-196.
15. Baghdachi, J., Eastern Michigan University, private communication.
16. Jones, F.N., Mao, W., Ziemer, P.D., Xiao, F., Hayes, J., and Golden M., "Artist Paints –an overview and preliminary studies of durability", *Prog. In Organic Coatings* 2005, 52, 9-20.
17. Shen, W., Sun, J., Liu, Z., Mao, W., Nordstrom, J.D., Ziemer, P. D., and Jones, F.N., "Methods for study of mechanical and Tribological properties of hard and soft coatings with a nano-indenter," *J. Coat. Tech. Research* 2004, 1(2), 117-125.
18. Oliver, W.C. and Pharr, G.M., "An improved technique for determining hardness and elastic modulus using load and displacement sensing indentation", *J. Mater. Res.* 1992, 7, (6), 1564-1583.
19. Tamai, T., Pinenq, P., and Winnik, M.A. "Effect of cross-linking on polymer diffusion in poly(butyl methacrylate-co-butyl acrylate) latex films", *Macromolecules* 1999, 32, 6102-6110.
20. Aradian, A., Raphael, E., and de Gennes, P.G., "A scaling theory of the competition between interdiffusion and cross-linking at polymer interfaces", *Macromolecules* 2002 35, 4036-4043.
21. Ghazaly, H.M., Daniels, E.S., Dimonie, V.L., Klein, A., Sperling, L.H., and El-Aasser, M.S., "Properties of N-butyl methacrylate copolymer latex films derived from crosslinked latex particles" *J. Appl. Polym. Sci.* 2003, 88, 42-49.
22. Ghazaly, H.M., Daniels, E.S., Dimonie, V.L., Klein, A., and El-Aasser, M.S., "Miniemulsion copolymerization of n-butyl methacrylate with crosslinking monomers," *J. Appl. Polym. Sci.* 2001, 81, 1721-1730.
23. Ghazaly, H.M., Daniels, E.S., Dimonie, V.L., El-Aasser, M.S., and Klein, A., "Synthesis and characterization of a macromonomer crosslinker," *J. Appl. Polym. Sci.* 2000, 77, 1362-1368.
24. Winnik, M. A. and Feng, J., *J. Coat. Tech. Research* 1996, 68, (852), 39-47.
25. Kessel, N., Illsley, D.R., and Keddie, J.L., "The influence of interdiffusion and crosslinking in the film formation of an acrylic latex", *Journal of Coatings Technology-Research* 2008, 5, (3), 285-297.
26. Feng, J., Pham, H., Macdonald, P., Winnik, M. A., Geurts, J. M., Zirkzee, H., Vn Es, S., and German, A. L., *J. Coat. Tech. Research* 1998, 70, (881), 57-68.
27. Hill, L. W., "Dynamic Mechanical and Tensile Properties" in Koleske, J.V. Ed., *Paint and Coatings Testing Manual: Fourteenth Edition of the Gardner-Sward Handbook* 1995, ASTM, Ann Arbor, MI, 534-546.

Chapter 4

Synthesis and Characterization of Nanosize Acrylic Latex and Comparison to Their Conventional sized Counterparts

Introduction

In recent years a great deal of research has been devoted to the nano-structured materials. Many publications have appeared dealing with metal, ceramic, semiconductor nanoparticles,¹⁻³ and polymer related nano-structured materials.⁴ Nevertheless, until now there have been a few descriptions⁵⁻⁸ of direct synthesis of polymer nanoparticles (especially with diameters < 30 nm), which are speculated to be potential candidates for various application fields, such as drug delivery carriers, microencapsulation, electric materials, catalysts, high performance polymers and coatings.⁵⁻⁸

In the early 1980s Stoffer and Bone^{9, 10} and Atik¹¹⁻¹³ first reported microemulsion polymerization process. Since then researchers around the globe explored the process and sought commercial applications of microemulsion polymerization process.¹⁴⁻³⁰ As Jones points out, it is now widely recognized that the method can be used to prepare latexes with particle diameters in the nanoparticle region. In late 1990s, Liu et al.^{31, 32} published the preparation of nano-spheres by dispersing a block copolymer [poly (2-cinnamoyl ethyl methacrylate)-block-polyacrylic acid] in an appropriate solvent mixture. However, this approach involved the synthesis of a block copolymer and a photo-crosslinking reaction. Jiang et al.³³ reported preparation of stable colloidal nanoparticles from randomly carboxylated polystyrene ionomers. In both the above methods the resultant final solids content were fairly low. In 1997, Okubo et al.^{34, 35} reported preparation of nanoparticles by “dissolution” of submicron sized ionized copolymer particles of

* 2 Patents filed, Joshi, R.G. et al., “Conventional Latex/Nanolatex Blends”, US (12578442) and PCT (60536) on Oct 13, 2009 (Eastern Michigan University)

styrene-methacrylic acid (MAA) in nonionic emulsifier solution; but the final polymer content was as low as 2.2 g/L.

The above and several other research reports¹⁴⁻³⁰ demonstrated that the microemulsion polymerization showed great potential for broad application areas since it can produce nanosize particles. However, it had two major limitations as reported in the literature – (1) the traditional microemulsion process demanded higher surfactant to produce lower particle diameters and (2) resultant polymers were produced at very low solids content. The above two limitations of traditional microemulsion process restricted its proposed viable and commercial uses to some extent in coatings, drug delivery, microencapsulation, and many other applications where lower surfactant loading and higher polymer content is desired.

In the last decade, many research attempts were focused on addressing the classically known limitations of traditional microemulsion polymerization process. Gan et al.^{36,37} reported polymerization of styrene and methyl methacrylate using cationic surfactants and relatively high weight ratios of polymer to surfactant (approximately 8/1 polymer/surfactant) and produced latexes with particle diameters between 30-100 nm. Recently, He et al.⁸ studied the preparation polystyrene (PS) nano particles using particular seeded polymerization method utilizing anionic surfactants. The resulting polymethamethacrylate/polystyrene (PMMA/PS) nanoparticles had an average particle diameter <20 nm using lower amount of surfactant. In another recent report, Kaiyi and Zhaoqun⁷ demonstrated a novel method of producing monodisperse polystyrene (PS) nanoparticles having average particle diameters <20 nm using very low amount of surfactant. Several other research attempts are covered in great detail in previous literature.^{17, 19-29}

Notably, in late 1990s Ming et al.^{27, 38, 39} reported laboratory scale modified microemulsion polymerization producing high solids content nanosize polymer latexes. Ming and his group modified the traditional microemulsion process to produce nano particles with diameters of 10-30 nm and final polymer content ranging from 10-30 wt%. In this process the polymer/surfactant ratio was kept from 7:1 to 12:1. The ratio in the process was significantly higher than the traditional microemulsion process that typically uses 1:1 polymer/surfactant or even lower as reported in many previous methods.^{14, 30} Briefly, in the modified microemulsion polymerization, the original microemulsion was composed of the entire amount of surfactant, a co-surfactant (if required), a very small portion of monomer or monomer mixture, and all water. The rest of the monomer or monomer mixture was added dropwise into the polymerizing microemulsion. The researchers used anionic, cationic, non-ionic surfactants and their mixtures to produce high solids content nanosize latexes. The researchers also studied the particle size changes during the polymerization, the polymerization mechanism, and some specific end-use properties. As reported,^{14, 30} this method can also be used to make nanosize latexes that are crosslinked within the particles and/or bear reactive groups that can crosslink later. Promising results from Ming's modified technique^{14, 30} opened up a wealth of opportunities for future research, particularly exploration for potential applications in the area of polymers and coatings forming basis for this research.

In the present research, Ming's modified microemulsion^{14, 30} process was further improved to enable the use of a variety of monomers including functional or crosslinkable monomers. The improved modified microemulsion process was developed to produce acrylic nanoparticle latexes having average particle diameters of 15-30 nm referred to as nanoparticle latexes. For pre-coalescence crosslinking: 0-4 wt% of 1, 3 butylene glycol dimethacrylate (1, 3-

BGDMA), and for post-coalescence crosslinking: 0-5 wt% of diacetone acrylamide (DAA) as reactive monomer and adipic dihydrazide (ADH) as crosslinker were used. Both the pre-coalescence and post-coalescence nano-size polymeric latex series were prepared using a target glass transition temperature (T_g) of about 7 to 9 °C. The nanoparticle latexes were compared with respective conventional latexes (of similar compositions) with average particle diameters of 120-140 nm made using seeded semi-continuous emulsion polymerization process (described in Chapter 3). The films cast from these latexes were characterized using a variety of end-use tests and advanced instruments such as a Dynamic Mechanical Analyzer (DMA), Modulated Differential Scanning Calorimeter (MDSC), and an Atomic Force Microscope (AFM). Information from such instruments should greatly enhance our understanding of the relationship between the physical and morphological properties of coatings. The main goals of the research described in this chapter are (a) an improved method of making nanoparticle latexes using a variety of monomers including functional monomers and (b) an understanding of the relationships between particle size and distribution and the resultant fundamental and end-use film properties and film morphology.

Experimental Details

Preparation of nanoparticle latexes using improved modified microemulsion

copolymerization: ⁴⁰⁻⁴³

Nanosize latexes were synthesized with varying levels of pre-coalescence (internal) and post-coalescence (external) crosslinkable sites. The latexes were prepared with the target glass transition temperature (T_g) of 5 °C. Composition and characteristics of these latexes are shown in Tables 3.1 and 3.2 respectively. Further, the nanosize latexes are coded n for nanosize, I for pre-coalescence or internal, E for post-coalescence or external, L for low T_g , and a number for the weight % of the crosslinker or reactive site in the monomer line up. Thus, for example, nIL-2 means pre-coalescence crosslinked latex with 2 wt. % of 1, 3-BGDMA, and nEL-5 means post-coalescence crosslinked latex with 5 wt. % of DAA.

Materials

Materials with sources of supply to be utilized in this study are listed below:

Deionized (DI) Water, *n*-Butyl Methacrylate (99+%), 10-55 ppm MEHQ (*nBMA*) (Aldrich), Methacrylic Acid (99%), 250 ppm MEHQ (MAA) (Aldrich), *n*-Butyl Acrylate (99%), 10-55 ppm MEHQ (*nBA*) (Aldrich), Sodium dodecyl Sulfate (SDS) [95.5%], Ammonium Persulfate (Certified A.C.S) (Fisher Scientific), N,N,N',N'- tetramethylethylenediamine (TMEDA), 1-pentanol (Aldrich), 2-Amino-2-methyl-1-propanol ("AMP-95," Angus Chemical Company), Ammonium Hydroxide (NH₄OH, 29.2%) (Fisher Scientific), 1, 3-Butylene glycol dimethacrylate, 200 ppm MEHQ (1, 3-BGDMA) (Aldrich), Diacetone acrylamide, 99 %, (DAA) (Aldrich), Adipic dihydrazide, 98 % (ADDH) (Aldrich).

(a) Representative procedure for synthesis of nL0 (nanoparticle size latexes with no functional group):

A nanolatex, comprising a 21/77/2 ratio of nBA/nBMA/MAA monomers, having a $T_g = 5-10\text{ }^\circ\text{C}$, was prepared under a nitrogen atmosphere in a 250 mL, 3-neck flask (Ace Glass, Vineland, N. J.) equipped with a reflux condenser, a thermometer, an addition funnel, and a nitrogen gas inlet and outlet. The flask was heated and stirred with a stirring hotplate (Fisher Scientific, Waltham MA) using a 25mm x 8mm magnetic stirrer. Using the above setup, the nanolatex was prepared in the following steps:

STEP 1: A microemulsion formulation was formed by mixing 0.3 g of a 21/77/2 (wt/wt/wt) mixture of nBA/nBMA/MAA monomers, 1 g of SDS (monomer to surfactant ratio 10.5:1), 0.1 g of 1-pentanol (Sigma-Aldrich, St. Louis, MO), 78.7 g of DI water and 10-14 drops of aqueous ammonia (30% in water, Sigma-Aldrich, St. Louis, MO). After addition of the ammonia solution, the formulation had a pH of 9-10.

STEP 2: The microemulsion was heated at $40\text{ }^\circ\text{C}$ with stirring and purged by bubbling nitrogen through the formulation for 5 minutes.

STEP 3: A solution of 0.0464 g of N,N,N',N' - tetramethylethylenediamine (TMEDA) (Sigma-Aldrich, St. Louis, MO) in 5 g of D.I. water (4mM) was added to the microemulsion via addition funnel, followed by a solution of 0.0912 g of ammonium persulfate in 5 g of water (4mM), which initiated the polymerization.

STEP 4: An additional 9.7 g 21/77/2 (wt/wt/wt) mixture of nBA/nBMA/MAA monomers was added dropwise via addition funnel (~ 6 drops/min.) into the microemulsion formulation over the course of 90-120 mins. During addition, the temperature of the formulation was maintained at

40 +/- 1 °C, a slow flow of nitrogen was maintained, and the reaction mixture was stirred at a rate of approximately 600 revolutions per minute.

STEP 5: After addition was complete, stirring was continued for another 2-3 hours at 40 °C to essentially complete the conversion of the monomer mixture. A 50/50 wt/wt solution of 2-amino-2-methyl-1-propanol (in DI water (about 3 mL) was added with continued stirring. The resulting latex had the characteristics shown in Table 4.3.

(b) Representative procedure for synthesis of nEL or nIL (nanoparticle size latexes with functional groups):

The pre-coalescence and the post-coalescence nano crosslinkable latexes, described in the Table 4.1, were made by essentially identical procedures as described above. In case of making pre-coalescence crosslinked nano latexes, the functional monomers were included in the monomer mixture recipe. In case of the post-coalescence nano crosslinkable latexes (a) crosslinkable monomer was added at the end of the monomer addition and (b) aqueous ammonia was used to adjust the pH of the product instead of 2-amino-2-methyl-1-propanol to reduce the potential for interference with the crosslinking reaction. The resulting latexes had the characteristics shown in Table 4.2.

Table 4.1: Composition table for nanosize latexes (with or without functional group)

Nano Latex	Original Microemulsion in Step 1 (in g.)				Monomer Mixture added in Step 2 (in g.)	Monomer Composition	Monomer/Surfactant ratio
	Monomer	SDS	1-pentanol	Water (pH= 9-10)			
nL0	0.3 (monomer mixture – M ₁)	1.0	0.1	78.7	9.7 (monomer mixture – M ₂) + 0.1 g. 1-pentanol	<i>n</i> BA/ <i>n</i> BMA//MAA=21/77/2	10.5
nEL2	0.3 (M ₁)	1.0	0.1	77.7	(a) 8.7 g. (M ₂) + 0.1 g. 1-pentanol (b) 0.8 g. (monomer mixture-M ₃) + 0.2 g. DAA	<i>n</i> BA/ <i>n</i> BMA/DAA/MAA=21/75/2/2	10.5
nEL5	0.3 (M ₁)	1.0	0.1	77.7	(a) 7.7 g. (M ₂) + 0.1 g. 1-pentanol (b) 1.5 g. (M ₃) + 0.5 g. DAA	<i>n</i> BA/ <i>n</i> BMA/DAA/MAA=21/72/5/2	10.5
nIL2	0.3 (M ₁)	1.0	0.1	77.7	(a) 9.7 g. (M ₂) + 0.1 g. 1-pentanol	<i>n</i> BA/ <i>n</i> BMA/1,3-BGDMA/MAA=21/75/2/2	10.5
nIL4	0.3 (M ₁)	1.0	0.1	78.7	(a) 9.7 g. (M ₂) + 0.1 g. 1-pentanol	<i>n</i> BA/ <i>n</i> BMA/1,3-BGDMA/MAA=21/73/4/2	10.5

Preparation of conventional pre-coalescence or post-coalescence crosslinked conventional latexes^{44, 45} (described in Chapter 3):

The conventional latex samples employed here have been described previously.³¹ In brief, latexes were synthesized with varying levels of pre-coalescence crosslinker (internal) and post-coalescence (external) crosslinkable sites. For comparisons, the conventional latexes were prepared with a target glass transition temperature (T_g) of about 7°C. Compositions and characteristics of these latexes are shown in Table 4.3. The latexes are coded I for pre-coalescence or internal, E for post-coalescence or external, L for low T_g , and a number for the weight % of crosslinker or reactive site in the monomer line up. Thus, for example, IL-4 means an internally (or pre-coalescence) crosslinked, low T_g latex with 4.0 wt. % of 1, 3-BGDMA and EL-5 means an externally (or post-coalescence) crosslinked, low T_g latex with 5.0 wt. % of DAA. It also should be noted that in terms of composition, both nanoparticle latexes and selected conventional latexes were similar for the purpose of the study as described earlier.

Characterization of Latexes

Latex Properties

(a) Conventional Latexes (with or without functional groups):^{44, 45}

The weight percentage of non-volatile solids content (% NVM) was measured using ASTM D 4758-87. Viscosity was measured by ASTM D 4287 at 20 °C using a Brookfield Viscometer, Model DV-1, using Spindle #4 at 20 rpm. pH was measured with a Fischer Acumet Model 620 pH meter and with pH paper.

For particle size (diameter) and particle size distribution measurements, each latex was diluted to a transmission factor of 0.5-1.0 (about 0.05-0.1 wt% solids) and measured at 25 °C using the light-scattering instrument, MICROTAC Series 9200. Three tests were performed

within 180 sec. to obtain an average value of a volume distribution. The results are shown in Table 4.3.

For gel content measurements, an empty extraction thimble was dried at 85°C in an oven for 2 h, cooled in a desiccator overnight, and weighed. Latex films (prepared on glass and detached) were dried in a desiccator overnight, cut into small pieces, weighed, and put into the thimble. After a 12-h extraction with acetone in a Soxhlet extractor, the thimble was dried in an oven at 85°C for 2 h, cooled in a desiccator overnight, and weighed. The gel content was calculated from the initial and final weights, assuming that gelled material remained in the thimble. The results are shown in Figure 4.3(a, b) and Table 4.3.

(b) Nanoparticle latexes (with or without functional groups):

The weight percentage of non-volatile solids content (% NVM) was measured using ASTM D 4758-87. Viscosity was measured by ASTM D 4287 at 25 °C using a Brookfield Viscometer, model CAP 2000+, using Spindle #1 at 113 rpm. pH was measured with a Fischer Acumet Model 620 pH meter and with pH paper.

Particle size (diameter) and particle size distribution of nanosize latexes were determined using dynamic light scattering method with a 90 PLUS Particle Analyzer (Brookhaven Instruments Co.) at room temperature, before which the nanosize latex samples were diluted to a solid content of about 0.1 wt.%. A 10 MM potassium nitrate (KNO₃) solution was used as diluent. The latex samples were filtered using Whatman Puradisc 25 AS filters with 200nm pore size before running for particle size analysis. For each sample at least 3 runs (each run of 10 min. duration) for a total of 30 min. were done. The average effective diameters and polydispersity from the intensity distribution were obtained directly from the measurement results and reported.

The results are shown in Table 4.2 and the particle size distribution graphs are shown in 3.1 (a-e).

For gel content measurements of nanosize latexes, the same procedure was followed as described earlier for gel content measurements of conventional latex. The results are shown in Figure 4.3(a, b) and Table 4.2.

Film Properties of conventional latexes and nanoparticle latexes:

The minimum film formation temperature (MFFT), crack point and knife point, was determined using a Rhopoint MFFT Bar - 90, Rhopoint Instruments. Briefly, the instrument was equilibrated over a specific temperature range (determined based on the glass transition temperature of latex sample) for about 20 minutes. Five replicates are laid down in quick succession using a 75- micron (3 mils) one-inch cube applicator. The tracks were laid down left to right. A clearly defined limit of coalescence will show in about 90-120 minutes, and the MFFT temperature can then be read using the cursor scale. The crack point, the temperature onset of formation that is crack-free, was determined using a fingernail. The knife point, the temperature onset of film integrity, where the film no longer cracks upon disturbing or peeling the film was determined using a plastic or metallic spatula by carefully peeling away the film, starting from the crack point.

Specimens were prepared on aluminum panels by drawing the latexes down using a square wet film applicator (Paul N. Gardner Co., Inc.) with 0.25 mm (wet) clearance on aluminum panels. The panels were dried in an oven at 70 °C and 50% humidity for 24 hours and then stored at normal room conditions for a week before testing. No coalescing solvents were used. Dry film thicknesses were approximately 50 µm. Before casting these films, a stoichiometric amount of adipic dihydrazide (ADDH) was added to the E-series latexes.

Dry film thickness was measured at 25°C by Elcometer-345-Digital Coating thickness Gauge (Elcometer Instruments Ltd.).

Solvent resistance was determined by methyl ethyl ketone (MEK) rubbing. Load was applied by a ball peen hammer with a 448 g head wrapped with cheesecloth soaked with MEK. The reported end point was the number of double rubs required to break through the film, exposing bare metal.

Chemical resistance tests were conducted at 25 °C following ASTM D 1308. A 1-mL sample of each test reagent (water, dilute sulfuric acid at pH 3) was pipeted (a 5-mL pipet graduated in 0.1 mL) onto the horizontal panel and immediately covered with a watch glass. After an interval, the spot was wiped clean and the film was examined immediately for defects. Intervals used were 15 min, 1 h, and 16 h.

Pencil hardness was tested at 25 °C following the procedure of ASTM 3363.

Tape adhesion was measured by ASTM D 3359. The films were cut with a cross-cut kit (Precision Gage & Tool Company) before testing.

Block Resistance was measured by ASTM D 4946. Briefly, latex films were cast on a sealed test chart and the films were dried in an oven at 70 °C and 50% humidity for 8-10 hours and then stored at normal room conditions for a week before testing. After conditioning, six 3.8 X 3.8 cm. sections from the films were exactly cut as mentioned in the ASTM method. 3 sets of 2 film squares facing each other were placed in oven, exactly as described in the ASTM method, at 50 °C for 30 minutes. The specimens were cooled at room temperature for about 30 min. and blocking was measured. An average of three reading with standard deviation is reported.

Specular Gloss at 20° and 60° was measured using ASTM D 523 test method. Latex films were applied to glass panels, conditioned in an oven at 70 °C and 50% humidity for 8-10

hours and then stored at normal room conditions for a week before testing. Gloss was measured using BYK Gardner, BYK micro-TRI-gloss meter.

Thermal and Mechanical Properties of conventional latexes and nanoparticle latexes:

For glass transition temperature (T_g) measurement specimens were prepared as follows: (a) nanoparticle latexes were prepared using a rectangular Teflon block about 50mm long, 10 mm wide and 3 mm deep (or thick), and (b) conventional latexes were prepared on glass panels by drawing the latexes down using a square wet film applicator (Paul N. Gardner Co., Inc) with 0.30 mm (wet) clearance on glass panels. The glass panels and Teflon blocks were dried in an oven at 70 °C and 50% humidity for 8-10 hours and then stored at normal room conditions for a week before testing. The T_g of the dried films were determined by TA instrument - TA 2920 MDSC with RCS (Refrigerant Cooling System) accessory under nitrogen purge at flow rate of 50 mL/min. For testing, the samples were kept in closed Aluminum non-hermetic pans. Temperature scans were done from -90 °C to 100 °C at 2 °C/min with modulation of +/- 1.00 °C at every 60 seconds under nitrogen. The MDSC equilibrated at -90 °C for 5 min.

Dynamic Mechanical analyses were conducted using TA Instruments Model Q800 Dynamic Mechanical Analyzer (DMA) with the LNCS accessory. Specimens for stress-strain and dynamic mechanical studies were prepared on glass panels and Teflon blocks accordingly as described in MDSC studies section. A film cutter (supplied by TA instruments) was used to cut, at constant depth, rectangular specimens about 15-20 mm long, 3-6 mm wide and 0.1-0.2 mm thick from the cured films.

The stress-strain studies were done at the room temperature (~25 °C) in air on the Q800 DMA with the thin film tension clamp in a controlled force mode with a ramped force of 3N/min up to 18N/min and the resultant % strain was observed. DMA measurements of dried specimen

were done at 1 Hz with a thin film tension clamp over the temperature range of -100°C to 120°C, using liquid nitrogen as a coolant. The flow rate of liquid nitrogen into the DMA depends upon the starting temperature desired and is controlled by the ramp rate or heating rate of 3 °C/min.

Measurements with AFM of conventional latexes and nanoparticle latexes:

A Digital Instruments Multimode SPM with a Nanoscope IIIa controller and an E-scanner (X-Y scanning limit of 15 µm and a Z limit of 2 µm), operated in the tapping mode, was used to observe surface morphologies of selected specimens. The latex samples were conditioned in an oven at 70 °C and 50% humidity for 8-10 hours and then stored at normal room conditions for a week before imaging. Both height and phase data were captured at image size of 1 × 1 µm (for conventional and nanoparticle latexes). For every sample, two sets of images were captured.

Table 4.2: Characteristics of nanosize (with or without crosslinker) latexes

Nanoparticle latex	Composition	% Non-Volatiles	Avg. Particle Size, nm	Polydispersity	Glass Transition Temperature (°C) using MDSC	Glass Transition Temperature (°C) using Fox Equation	pH	Gel Content	Viscosity η (mPa•s)
nL0	<i>nBA/nBMA//MAA=21/77/2</i>	10.8	23.2	0.09	4.77	5.06	9.3	0.0	13
nEL2	<i>nBA/nBMA/DAA/MAA=21/75/2/2</i>	10.7	23	0.087	3.13	---	9.7	98.1	13
nEL5	<i>nBA/nBMA/DAA/MAA=21/72/5/2</i>	10.6	21.7	0.12	5.15	---	9.5	99.9	17
nIL2	<i>nBA/nBMA/1,3-BGDMA/MAA=21/75/2/2</i>	10.9	23.2	0.089	4.67	---	9.1	63.8	13
nIL4	<i>nBA/nBMA/1,3-BGDMA/MAA=21/73/4/2</i>	10.9	22.2	0.1	10.9	---	9.8	97.4	15

Table 4.3: Characteristics of conventional (with or without crosslinker) latexes

Conventional Latex	Composition	% Non-Volatiles	Avg. Particle Size, nm	Glass Transition Temp. (°C) by MDSC	Glass Transition Temperature (°C) using Fox Equation	pH	Gel Content	Viscosity η (mPa•s)
IL-0	<i>nBA/nBMA/MAA=21/77/2</i>	47.1	130	6	5.06	9.3	0.00	100
IL-2	<i>nBA/nBMA/1,3-BGDMA/MAA=21/75/2/2</i>	44.6	118	5	---	9.0	57.1	80
IL-4	<i>nBA/nBMA/1,3-BGDMA/MAA=21/73/4/2</i>	46.8	123	13	---	9.2	64.2	70
EL-2	<i>nBA/nBMA/DAA/MAA=21/75/2/2</i>	46.6	133	7	---	9.8	98.1	560
EL-5	<i>nBA/nBMA/DAA/MAA=21/72/5/2</i>	46.3	137	5	---	9.7	100.0	1320

Figure 4.1. Particle Size Analysis Graphs of nanoparticle latexes (Brookhaven Instruments 90

Plus Particle Size Software Output):

(a) Nanoparticle latex with no crosslinker, nL0:



Brookhaven Instruments Corp.
90Plus Particle Sizing Software Ver. 3.47

Date: Apr 3, 2008

Time: 17:54:57

Batch: 0

Sample ID **nL0 (Combined)**

Operator ID **RJ**

Notes

Measurement Parameters:			
Temperature	= 25.0 deg. C	Runs Completed	= 3
Liquid	= Aqueous	Run Duration	= 00:10:00
Viscosity	= 0.890 cP	Total Elapsed Time	= 00:30:00
Ref.Index Fluid	= 1.330	Average Count Rate	= 1.2 Mcps
Angle	= 90.00	Ref.Index Real	= 1.483
Wavelength	= 661.0 nm	Ref.Index Imag	= 0.000
		Dust Filter	= On

nL0 (Combined)	
Effective Diameter:	23.2 nm
Polydispersity:	0.090
Sample Quality:	9.3/ 97.88%
Elapsed Time:	00:30:00

Correlation Function

Run	Eff. Diam. (nm)	Half Width (nm)	Polydispersity	Sample Quality
1	23.1	7.1	0.094	9.5 / 94.06%
2	23.2	6.6	0.082	9.6 / 100.00%
3	23.1	7.1	0.095	8.7 / 99.57%
Mean	23.2	7.0	0.090	9.3 / 97.88%
Std. Error	0.0	0.2	0.004	0.3 / 1.91
Combined	23.2	7.0	0.090	9.3 / 97.88%

(b) Nanoparticle latex with 2% post-coalescence crosslinker, nEL2:



Brookhaven Instruments Corp.
90Plus Particle Sizing Software Ver. 3.47

Date: Apr 3, 2008
Time: 20:23:34
Batch: 0

Sample ID **nEL-2 (Combined)**

Operator ID **RJ**

Notes

Measurement Parameters:			
Temperature	= 25.0 deg. C	Runs Completed	= 3
Liquid	= Aqueous	Run Duration	= 00:10:00
Viscosity	= 0.890 cP	Total Elapsed Time	= 00:30:00
Ref.Index Fluid	= 1.330	Average Count Rate	= 1.2 Mcps
Angle	= 90.00	Ref.Index Real	= 1.483
Wavelength	= 661.0 nm	Ref.Index Imag	= 0.000
		Dust Filter	= On

nEL-2 (Combined)	
Effective Diameter:	23.0 nm
Polydispersity:	0.087
Sample Quality:	9.3/ 99.44%
Elapsed Time:	00:30:00

Lognormal Distribution

Run	Eff. Diam. (nm)	Half Width (nm)	Polydispersity	Sample Quality
1	22.9	6.5	0.080	9.5 / 99.57%
2	23.0	7.0	0.092	9.2 / 99.14%
3	23.0	6.8	0.088	9.3 / 99.60%
Mean	23.0	6.8	0.087	9.3 / 99.44%
Std. Error	0.0	0.1	0.004	0.1 / 0.15
Combined	23.0	6.8	0.087	9.3 / 99.44%

(c) Nanoparticle latex with 5% post-coalescence crosslinker, nEL5:

BI Brookhaven Instruments Corp.
90Plus Particle Sizing Software Ver. 3.47

Date: Apr 3, 2008
Time: 21:39:57
Batch: 0

Sample ID **nEL-5 (Combined)**

Operator ID **RJ**

Notes

Measurement Parameters:			
Temperature	= 25.0 deg. C	Runs Completed	= 3
Liquid	= Aqueous	Run Duration	= 00:10:00
Viscosity	= 0.890 cP	Total Elapsed Time	= 00:30:00
Ref.Index Fluid	= 1.330	Average Count Rate	= 1.4 Mcps
Angle	= 90.00	Ref.Index Real	= 1.483
Wavelength	= 661.0 nm	Ref.Index Imag	= 0.000
		Dust Filter	= On

nEL-5 (Combined)		<p>Multimodal Size Distribution</p>
Effective Diameter:	21.7 nm	
Polydispersity:	0.120	
Sample Quality:	9.6/ 99.15%	
Elapsed Time:	00:30:00	

Run	Eff. Diam. (nm)	Half Width (nm)	Polydispersity	Sample Quality
1	21.8	7.4	0.115	9.7 / 99.60%
2	21.7	7.6	0.124	9.4 / 98.71%
3	21.7	7.6	0.121	9.6 / 99.14%
Mean	21.7	7.5	0.120	9.6 / 99.15%
Std. Error	0.0	0.1	0.003	0.1 / 0.26
Combined	21.7	7.5	0.120	9.6 / 99.15%

(d) Nanoparticle latex with 2% pre-coalescence crosslinker, nIL2:



Brookhaven Instruments Corp.
90Plus Particle Sizing Software Ver. 3.47

Date: Apr 3, 2008

Time: 18:32:19

Batch: 0

Sample ID **nIL-2 (Combined)**

Operator ID **RJ**

Notes

Measurement Parameters:			
Temperature	= 25.0 deg. C	Runs Completed	= 3
Liquid	= Aqueous	Run Duration	= 00:10:00
Viscosity	= 0.890 cP	Total Elapsed Time	= 00:30:00
Ref.Index Fluid	= 1.330	Average Count Rate	= 1.3 Mcps
Angle	= 90.00	Ref.Index Real	= 1.483
Wavelength	= 661.0 nm	Ref.Index Imag	= 0.000
		Dust Filter	= On

nIL-2 (Combined)		<p style="text-align: center;">Correlation Function</p>
Effective Diameter:	23.2 nm	
Polydispersity:	0.089	
Sample Quality:	9.7 / 99.29%	
Elapsed Time:	00:30:00	

Run	Eff. Diam. (nm)	Half Width (nm)	Polydispersity	Sample Quality
1	23.4	6.7	0.082	9.8 / 98.27%
2	23.3	7.0	0.090	9.3 / 99.60%
3	23.1	7.1	0.094	9.2 / 100.00%
Mean	23.3	6.9	0.089	9.4 / 99.29%
Std. Error	0.1	0.1	0.003	0.2 / 0.52
Combined	23.2	6.9	0.089	9.7 / 99.29%

(e) Nanoparticle latex with 4% pre-coalescence crosslinker, nIL4:

BIC Brookhaven Instruments Corp.
90Plus Particle Sizing Software Ver. 3.47

Date: Apr 3, 2008

Time: 19:38:51

Batch: 0

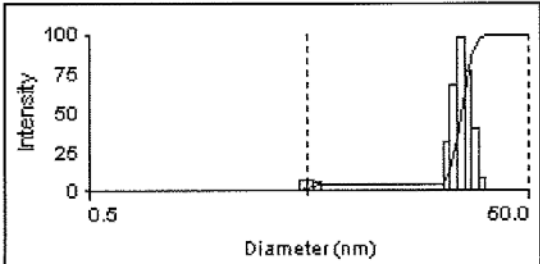
Sample ID **nIL-4 (Combined)**

Operator ID **RJ**

Notes

Measurement Parameters:			
Temperature	= 25.0 deg. C	Runs Completed	= 3
Liquid	= Aqueous	Run Duration	= 00:10:00
Viscosity	= 0.890 cP	Total Elapsed Time	= 00:30:00
Ref.Index Fluid	= 1.330	Average Count Rate	= 1.4 Mcps
Angle	= 90.00	Ref.Index Real	= 1.483
Wavelength	= 661.0 nm	Ref.Index Imag	= 0.000
		Dust Filter	= On

nIL-4 (Combined)	
Effective Diameter:	22.2 nm
Polydispersity:	0.100
Sample Quality:	9.2/100.00%
Elapsed Time:	00:30:00



Run	Eff. Diam. (nm)	Half Width (nm)	Polydispersity	Sample Quality
1	22.2	6.9	0.098	9.3 / 100.00%
2	22.2	7.0	0.099	9.1 / 100.00%
3	22.2	7.1	0.102	9.2 / 100.00%
Mean	22.2	7.0	0.100	9.2 / 100.00%
Std. Error	0.0	0.1	0.001	0.1 / 0.00
Combined	22.2	7.0	0.100	9.2 / 100.00%

Results and discussion

Nanosize latex synthesis and characterization

Both pre-coalescence and post-coalescence crosslinked nanosize latexes were synthesized by an improved modified microemulsion process with varying levels of crosslinking monomers. Composition and characteristics of these latexes are shown in Tables 4.2 and 3.3. In general, Ming et al.'s⁴⁰⁻⁴³ modified microemulsion process was used as a starting point of the present work to make nanosize latexes.⁴⁰⁻⁴³ The process was further improved to make it more useful for partially water soluble monomers such as n-BMA and n-BA. The key parameters varied/changed for the present research are as follows:

- (a) At least one of the monomers in base micro emulsion must be partially or fully water soluble. In this study, methacrylic acid was in the base (or seed) microemulsion,
- (b) If an acidic monomer (methacrylic acid) is used in the seed microemulsion, it is important to maintain the pH of the seed microemulsion of 8-9 before addition of the initiator/activator (APS/TMEDA) to fully utilize the efficiency.⁴⁶ In the present research, pH of water in seed microemulsion was maintained slightly alkaline (9-10 at 25⁰C)⁴⁶ using 8-10 drops of diluted liquid ammonium hydroxide (50% in DI water),
- (c) Equal partitioning of co-surfactant (1-pentanol), the first part of the co-surfactant was added with monomer mixture in seed microemulsion and the second part was added with monomer mixture added dropwise in step 2. Partitioning of cosurfactant depends on the total monomer(s) present in the seed microemulsion, and it often holds the key to producing stable nanoparticle latexes
- (d) Amount of monomer(s) present in the seed microemulsion
- (e) Monomer(s) addition time, monomer droplet size, addition rate, and mixing rate, and

(f) Amount of initiator/activator

By properly controlling the above variables, stable pre-coalescence or post-coalescence crosslinked nanoparticle size latexes (diameters about 15-30 nm) were produced.

As shown in Table 4.2 and Figure 4.1 (a-e), addition of monomers with functional groups up to 2 wt% has minimal effect on particle size and polydispersity of the latexes. Even with 4 wt% of 1, 3-BGDMA and with 5 wt% of DAA, the polydispersity shows a very slight increase. The robustness of the modified microemulsion process was demonstrated with functional monomers since the polydispersity remained very low. Similarly, a negligible effect on the viscosity and glass transition temperature is observed up to 2 wt% additions of functional groups. With DAA a slight increase in viscosity and T_g is observed up to 5 wt%. Addition up to 4 wt% of 1, 3-BGDMA in pre-coalescence nanosize latex series showed substantial increases in T_g as well as viscosity.

Film formation by “pre-coalescence” and “post-coalescence” crosslinked latexes

Theoretical considerations of film formation by pre-coalescence and post-coalescence crosslinked latexes have been essentially previously published^{44, 45} and covered in Chapter 3 but are briefly included here for completeness.

(a) *Film formation by “pre-coalescence” crosslinked latexes:*

Films were cast from the internally (pre-coalescence) crosslinked latexes by conventional means. No coalescing solvent was used; film formation was accelerated by warming the films at 70°C overnight. Film thicknesses were about 50 μm. Theoretical considerations of film formation by pre-coalescence crosslinked latexes have been studied extensively by Zosel and Ley,⁴⁷ Tamai et al.,⁴⁸ Aradian et al.,⁴⁹ and Ghazaly et al.⁵⁰⁻⁵² Recently we published^{44, 45} a

systematic comparison of pre-coalescence crosslinked latexes with varying levels of crosslinking monomers. We demonstrated that with low levels (up to 2 wt%) of internal crosslinking, latex films are able to coalesce to form good films. At higher levels (above 2 wt%) of 1,-BGDMA often the interdiffusion of polymeric particles is impeded by crosslinking, hence, resulting in inferior film properties.

(b) *Film formation by “post-coalescence” crosslinked latexes:*

The DAA-containing latexes are combined with a stoichiometric amount of adipic dihydrazide (ADDH) crosslinker. Then the films were cast under the same conditions as for internally or pre-coalescence crosslinked latexes. Before the film is cast, premature reaction of ADDH with the reactive sites in the latex is minimal. The crosslinking reaction for the DAA monomer is shown in Figure 4.2. The ADDH is water soluble, and almost all of it remains separated from the reactive sites in the serum where it is. The relatively high (9–9.5) pH also suppresses the reaction. When the film is cast, however, the water evaporates, forcing ADDH to come in contact with the latex polymer surfaces when close packing of the latex particles has occurred; ammonia evaporates, lowering the pH to about 6.5; and then crosslinking accelerates.⁵³

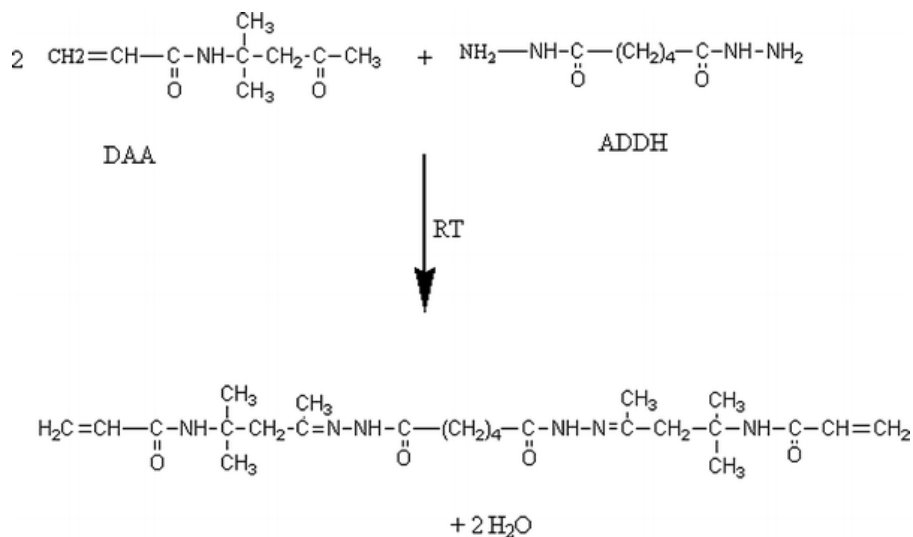


Figure 4.2: crosslinking reaction for DAA monomer

After the film is cast, the crosslinking reaction is known to proceed at a useful rate at room temperature. In this study we baked the films overnight at 70°C to assure a high level of conversion before testing and to avoid the use of coalescing solvents. Among the factors that will influence final properties of the films are the composition of the latexes and the relative rates of

- mixing of the crosslinker with the polymer,
- interdiffusion of the polymer molecules that originated in different latex particles,
- the chemical crosslinking reactions and diffusion of ADDH into the polymer,⁵⁴ and
- T_g of latex at a specific composition.

As demonstrated earlier,^{44, 45} to reach a high level of conversion the bake temperature should be well above the T_g of the specific latex composition. In this study, this is true for the low T_g latex (both pre-coalescence and post-coalescence crosslinked latexes). However, it may be borderline for high T_g latex (both pre-coalescence and post-coalescence crosslinked latexes). This was discussed in detail elsewhere.^{44, 45}

If the rate of the crosslinking reaction is too fast relative to mixing and interdiffusion, coalescence and interdiffusion will be slowed and perhaps retarded prematurely. The likely result will be excessively non-uniform films and less than optimal film properties. Some research reports^{44, 45, 53-57} suggest that the DAA/ADDH crosslinking combination has satisfactory relative rates and that good film properties can be attained.

Gel Content Results

Acetone extraction was employed to determine the gel content of the films from nanosize latexes as shown in Figure 4.3 (a, b). For comparison, gel content graphs of selected conventional latexes are also shown in the figure. In case of post-coalescence crosslinked films, not surprisingly, gel content was close to 100% for films containing DAA reactive sites. The results are in agreement with conventional size post-coalescence crosslinkable latexes. In case of pre-coalescence crosslinked nanosize latexes, the gel content values are much higher than their conventionally size counterparts. At 2 wt% gel content of nIL2 is 63.8, whereas IL-2 is 57.1. At 4 wt% level gel content of nIL-4 approaches 97.4%, whereas IL-4 is 64.2%. It's evident from the graph that in the case of conventional sized pre-coalescence crosslinked latexes at higher crosslinking levels, low values of gel fraction may reflect incomplete knitting of the particles during film formation, allowing small pieces to break loose and pass through filter. That is not the case with their nanosize counterparts. This could be due to the large surface area of nanosize latex particles facilitating uniform distribution of functional groups across the polymer network.

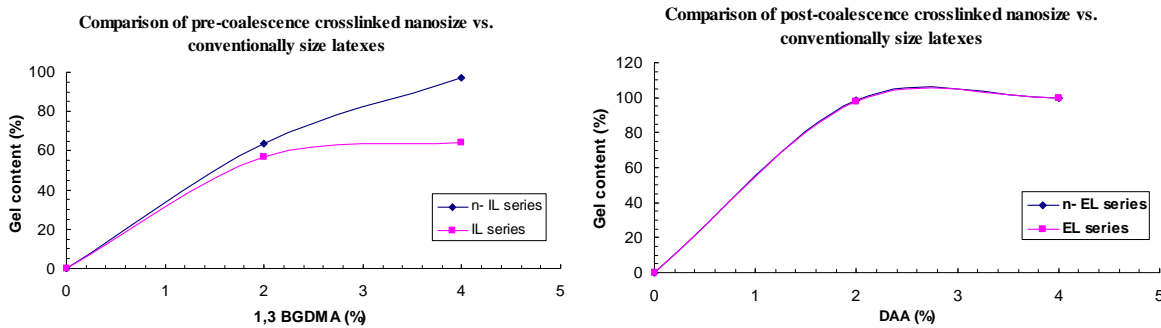


Figure 4.3 (a, b): Comparison of gel content of (a) pre-coalescence crosslinked nanosize vs. conventional latexes and (b) post-coalescence crosslinked nanosize vs. conventional latexes

End-use film properties

All the latexes were cast on aluminum panels and kept at 70 °C and 50% humidity for 8-10 hours and then stored at normal room conditions for a week before testing. The end-use properties are listed in Tables 3.4 and 3.5. Table 4.5 shows end-use properties of constituent nanosize latexes with pre-coalescence or post-coalescence crosslinking. These properties are compared with conventional size latexes as listed in Table 4.4.

In post-coalescence crosslinked nanolatexes as the level of crosslinking increase, solvent rub resistance significantly increases as expected. At 5 wt. % crosslinker all the properties, such as pencil hardness: B, solvent rub resistance: 100, block resistance: 4, 20 ° gloss: 52.2, and 60 ° gloss value: 86.4, are the highest. When nEL5 is compared to EL5 superior gloss, adhesion, hardness, and solvent rub resistance are observed in nEL5. This could be due to the large surface area of nanosize latexes providing uniform crosslinking of DAA across latex polymer chains. The poor resistance to water after 1 hour and 16 hours is likely due to the large amount of surfactant present on the surface of nEL5. For pre-coalescence latexes, most of the properties

remained largely unchanged except for a slight increase in solvent rub resistance at increasing levels of crosslinker. In general, post-coalescence crosslinked latex series have superior gloss and solvent resistance when compared to pre-coalescence latex counterparts. This is in harmony with our previous observations (described in Chapter 3) that in case of pre-coalescence crosslinked latexes, interdiffusion of polymer chains is impeded by crosslinking, showing deleterious effects on end-use properties.^{44, 45}

In general, comparisons of properties of nanosize latexes to their conventionally sized counterparts show improvement in gloss, adhesion, and solvent resistance. For all nanosize latexes, tape adhesion to aluminum increases from 4B (good) to 5B (excellent, the highest rating in this test). Solvent rub resistance greatly increases. Block resistance of conventional size latexes when compared with their nanosize counterparts is either comparable or slightly higher. In case of nanosize latexes, resistance to water is inferior compared to their conventional size counterparts. This may be due to the amount of surfactant present on the surface of nanosize latexes. Resistance to dilute sulfuric acid largely remained unchanged or slightly improved at 16 hours in case of nanosize latexes.

AFM Results

AFM tapping mode phase and height images of representative samples of latexes dried in an oven at 70°C and 50% relative humidity (RH) for 8-10 hours are show in Figures 4.4, 4.5, and 4.6. Figures 4.4 (a, b, and c) and 4.5 (a, b, and c) show tapping mode phase and height images of nL0, nIL4, and nEL5 at image size of 1µm x 1µm. Both the phase and height images of nL0 represent homogeneous structure when compared to those of nIL4 and nEL5. The effect of type of crosslinking and rate of crosslinking can be clearly seen when phase images of nIL4 and nEL5

are compared. The nEL5 images appear smooth and homogeneous compared to nIL4. Also, it is evident from the nIL4 phase image that the nanosize particles have retained their identity even after the films were force dried at 70°C, 50% RH. These observations suggest that rate of crosslinking reaction in nIL4 was fast enough to significantly retard homogenization of the film, at least near the surface. This is in harmony with our previous studies of conventional pre-coalescence or post-coalescence crosslinked latexes described in detail in Chapter 3.^{44, 45}

Figures 4.5 and 4.6 show comparison of tapping mode height images of nanoparticle latexes (at image size 1µm x 1µm) and conventional size constituents (at image size 1µm x 1µm). Figure 4.6 (a) shows peaks and valleys with lateral dimensions that are of a higher order of magnitude for neat L0 than nL0 in Figure 4.5(a). This indicates that with nanosize latexes, the surface becomes smooth and homogeneous. Significant effects on surface homogeneity are observed in case of functional latexes when comparing EL-5 (conventional) vs. nEL-5 (nano) or IL-4 (conventional) vs. nIL-4 (nano) where the nanoparticle latexes showed smooth and homogeneous surfaces in comparison to conventional counterparts. It is clear from these images that indeed nanosize particles, whether crosslinked or not, in general produces smooth films.

Table 4.6 shows average surface roughness values, Ra (in nm), measured using AFM and the surface smoothness values calculated from the roughness values. Further, the surface smoothness values are compared with the 20⁰ or 60⁰ gloss values. When comparing all the values for conventional vs. nanoparticle latexes, it is clear that indeed nanoparticle latexes in general showed smooth and homogeneous surface with higher gloss. Further, in case of post-coalescence crosslinked nanosize latex, nEL5, produces very smooth and homogeneous films, at least near to the surface. This is consistent with very high gloss values of nEL5 as shown in Table 4.6.

Table 4.4: End use properties of films cast from conventional latexes

Latex	Tape adhesion	Pencil hardness	MEK double rub resistance	Block Resistance	H ₂ SO ₄ spot test, pH=3.1 (open)			Distilled water spot test (open)			Gloss	
					15 min.	1 hour	16 hours	15 min.	1 hour	16 hours	20°	60°
L0	4B	4B	5	3 ± 1	E	E	F	E	E	G	18 ± 2.1	38.9 ± 5.1
EL-2	4B	2B	42		E	E	F	E	E	G	21 ± 0.3	38.2 ± 1.1
EL-5	4B	2B	83	9 ± 1	E	E	G	E	E	E	19 ± 1.6	36.7 ± 3.8
IL-2	5B	4B	6		E	G	F	E	E	F	12.2 ± 2.8	34.3 ± 1.2
IL-4	3B	4B	6	4 ± 1	E	G	F	E	E	F	11.6 ± 1.6	32.4 ± 2.9

Table 4.5: End use properties of films cast from nanosize latexes

Latex	Tape adhesion	Pencil hardness	MEK double rub resistance	Block Resistance	H ₂ SO ₄ spot test, pH=3.1 (open)			Distilled water spot test (open)			Gloss	
					15 min.	1 hour	16 hours	15 min.	1 hour	16 hours	20°	60°
nL0	5B	4B	15	3 ± 1	E	G	E	F	F	F	49 ± 7.9	79.4 ± 5.6
nIL2	5B	4B	17	1	G	F	P	G	E	P	40 ± 4.1	85.8 ± 0.8
nEL2	5B	4B	75	1	E	G	G	E	F	F	50.9 ± 3.6	77.9 ± 1
nIL4	5B	4B	20	2 ± 1	G	G	G	F	F	P	39 ± 3.9	87.6 ± 2.6
nEL5	5B	B	100	4 ± 1	E	E	E	G	F	F	52.2 ± 6.7	86.4 ± 2.6

Table 4.6: Comparison of surface smoothness and gloss values of nanoparticle latexes and their conventional counter parts

Latex Sample	AFM surface roughness: Ra (measured) (nm)	Surface smoothness: 1/Ra (calculated)(nm)	20 Gloss	60 Gloss
L0 (conventional)	1.2	0.83	18 ± 2.1	38.9 ± 5.1
IL-4 (conventional)	1.11	0.90	11.6 ± 1.6	32.4 ± 2.9
EL-5 (conventional)	1.14	0.87	19 ± 1.6	36.7 ± 3.8
nL0 (nano)	0.476	2.1	49 ± 7.9	79.4 ± 5.6
nIL4 (nano)	0.624	1.6	39 ± 3.9	87.6 ± 2.6
nEL5 (nano)	0.326	3.07	52.2 ± 6.7	86.4 ± 2.6

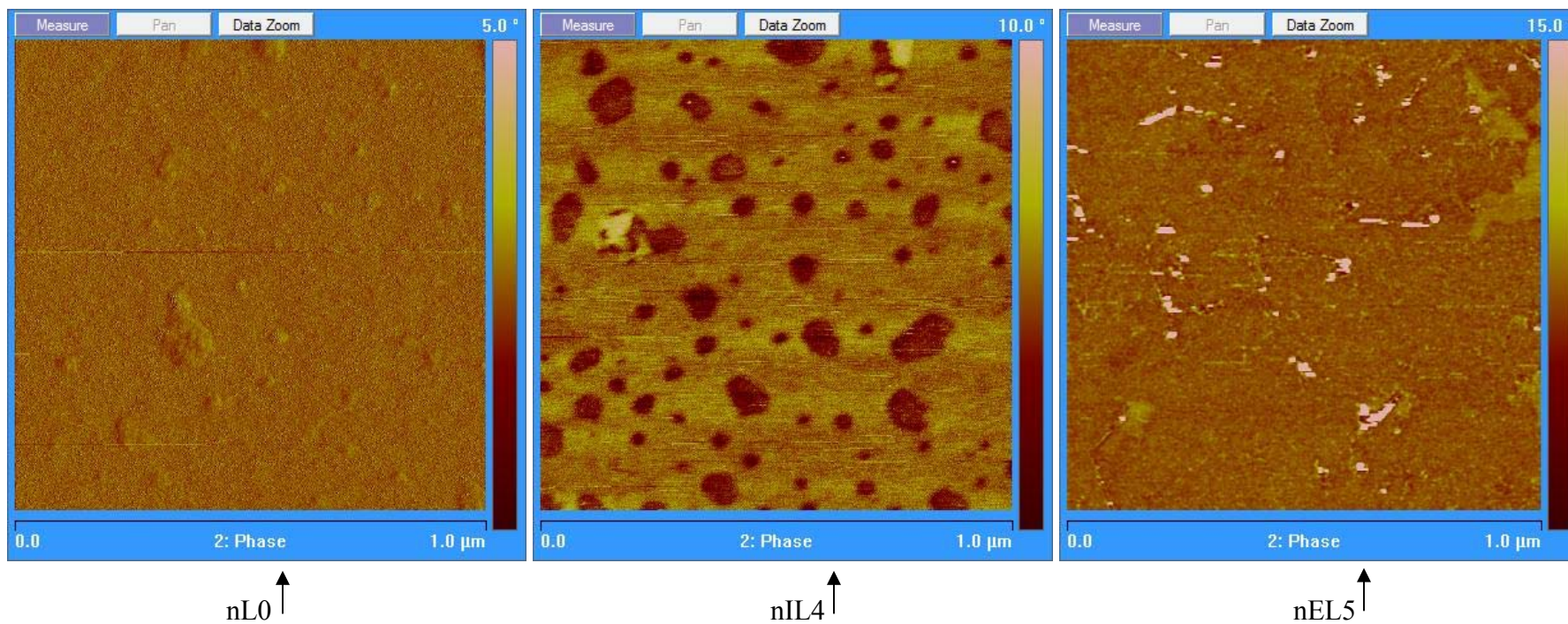


Figure 4.4(a, b, and c): AFM tapping mode phase images of (a) nL0, (b) nIL4, and (c) nEL5 at image size of 1μm X 1μm

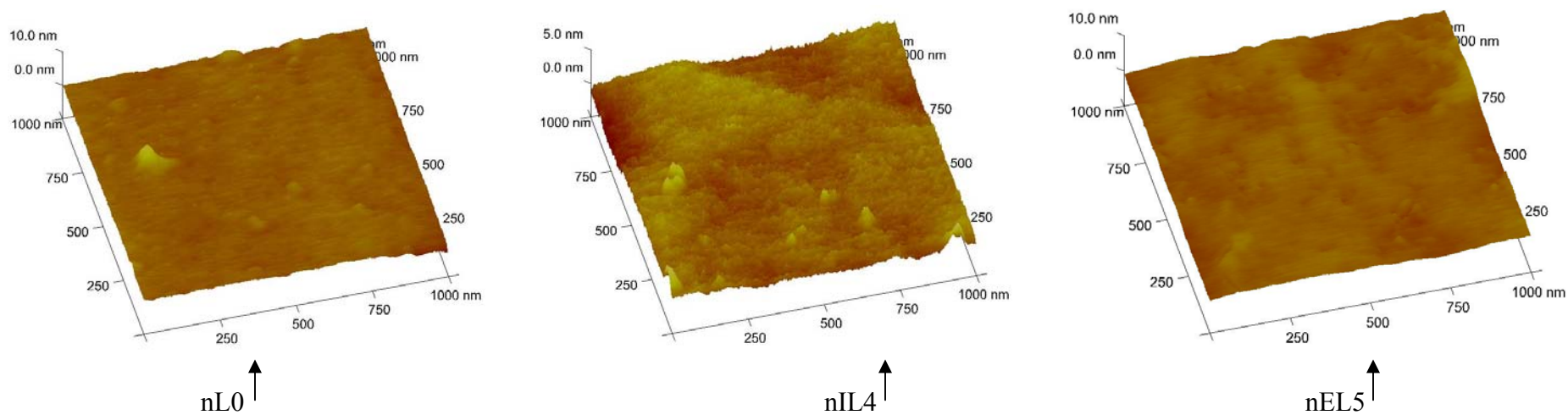


Figure 4.5(a, b, and c): AFM tapping mode height images of (a) nL0, (b) nIL4, and (c) nEL5 at image size of 1μm X 1μm

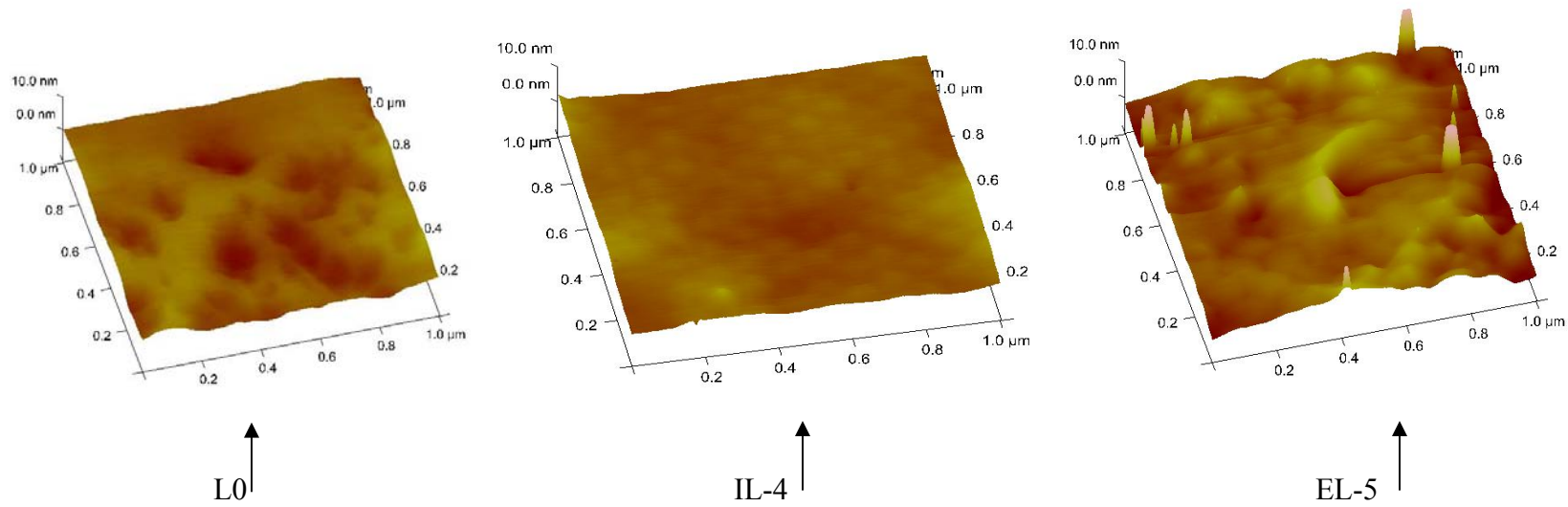


Figure 4.6(a, b, and c): AFM tapping mode height images of (a) L0, (b) nIL4, and (c) nEL5 at image size of 2um X 2um

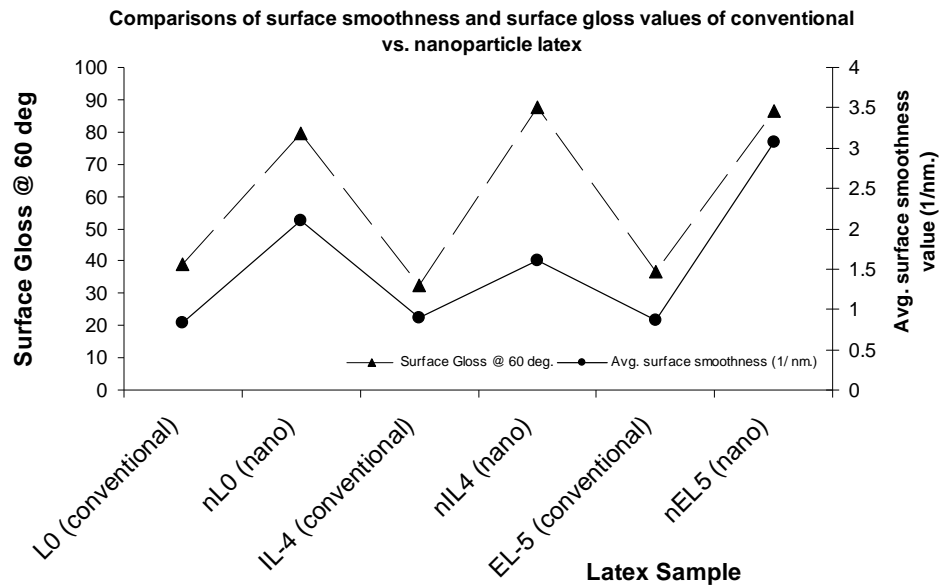


Figure 4.7: Comparison of surface smoothness and gloss values of nanoparticle latexes and their conventional counter parts

Fundamental Mechanical Properties

(a) Stress-Strain Curves

Average stress-strain curves of nanolatex pre-coalescence and post-coalescence series are shown in Figures 4.8 and 4.9, respectively. Each stress-strain curve represents an average of 5-6 replicates. Stress-strain data give important information about the ultimate mechanical properties of polymeric materials.^{44, 45} The values of Young's modulus, area under the stress-strain curve, strain at break, and stress at break are summarized in Table 4.7 for nanolatex series. For comparison, stress-strain analysis values for conventional latex series are shown in Table 4.8, and the respective curves for each post-coalescence and pre-coalescence conventional latex series are shown in Figures 4.10 and 4.11, respectively. It should be noted that for ease of comparisons the average stress-strain curves are used from Chapter 3. The area under the stress-strain curve is a measure of the flexibility and toughness of the film. As the area decreases, the film becomes less flexible and more brittle.

Table 4.7: Results of stress-strain analysis of nanosize latexes

Nanoparticle Latex	Young's Modulus (E'), MPa	Area Under Curve	Strain at Break(ϵ_b), %	Stress at Break(ϵ_b), MPa
nL0	2.2 ± 0.4	33 ± 1	81.5 ± 5.7	0.8
nIL2	6.4 ± 0.8	40.1 ± 15	86.4 ± 12	0.9 ± 0.2
nEL2	4.1 ± 0.1	71.8 ± 4.3	94.8 ± 4.3	1.5 ± 0.1
nIL4	5 ± 1.3	52.9	88.5	1.2
nEL5	11.4 ± 0.2	151 ± 20	78 ± 3.5	3.9 ± 0.2

Table 4.8: Results of stress-strain analysis of conventional size latexes

Conventional Latex	Young's Modulus (E'), MPa	Area Under Curve	Strain at Break(ϵ_b), %	Stress at Break(ϵ_b), MPa
L0	8.9 ± 0.6	172 ± 11	95.7 ± 6	2.7 ± 0.9
IL-2	18.1 ± 0.9	311 ± 14	106 ± 12	6.00 ± 0.2
EL-2	24.2 ± 1.5	221 ± 50	62.9 ± 9.1	6.63 ± 0.8
IL-4	49.7 ± 9.2	222 ± 6.3	57.9 ± 1.2	7.7
EL-5	45.3	196.5 ± 11	41.8 ± 0.7	9.5 ± 0.5

Stress-strain analysis of constituent nanosize latexes with pre-coalescence and post-coalescence crosslinking and comparisons with their conventional size counterparts:

For post-coalescence crosslinking nano latex series with increasing level of crosslinking, the values showed an increase indicating increased toughness in the sample. At 5 wt% of post-coalescence crosslinker nanolatex all four values, Y-modulus, area under the curve, stress at break and strain at break, are the highest when compared to all the other nano latex samples tested. This is an opposite trend when compared to the values of conventional latex with 5 wt% of post-coalescence crosslinker. In the latter case, only Young's modulus value showed an increase with significant decrease in area under the curve and strain at break, indicating brittleness in the sample. This could be attributed to the large surface area of nanosize latex particles facilitating uniform distribution of functional groups across the polymer network.

In case of pre-coalescence crosslinked nano latexes, Young's modulus showed marginal increase as the level of crosslinking increases. Area under the curve and strain at break largely remained unchanged (within the standard deviation of the test). Both pre-coalescence and post-coalescence crosslinked latexes at 2 wt% level of crosslinking showed higher values of strain at break. Also, when comparing the pre-coalescence crosslinking at 4 wt% vs. post-coalescence crosslinking at 5 wt%, the highest levels, in the nanolatex series – the post-coalescence crosslinking showed higher, almost twice, the modulus and the area under the curve values. Overall, when comparing the nanosize latex films with their conventional size counterparts, the Young's modulus and area under the curve values of nanosize latexes are very low. This could be attributed to the presence of the additional surfactant in the nanolatex series.

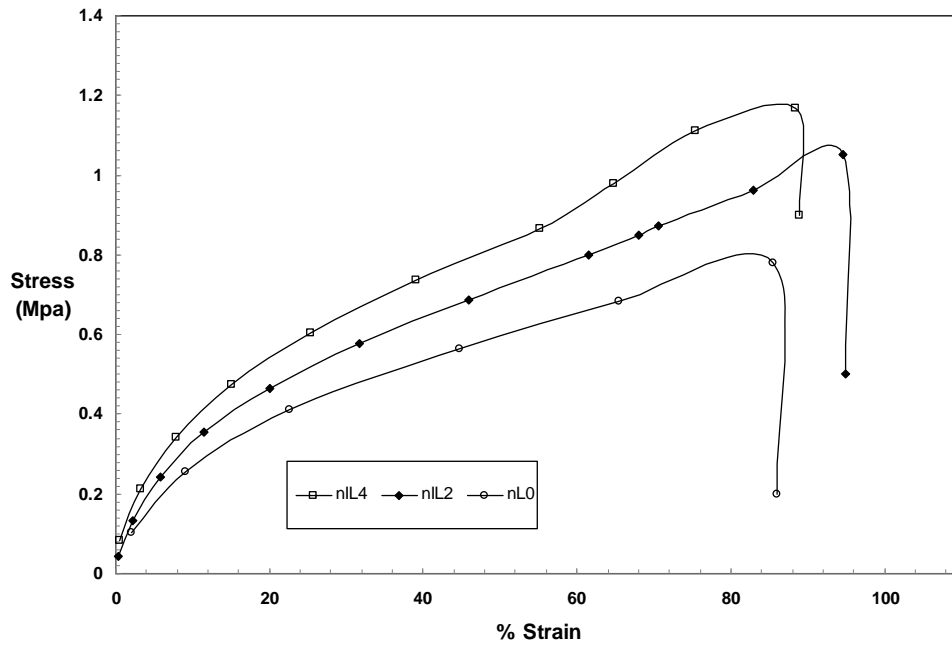


Figure 4.8: Comparison of average stress-strain curves for pre-coalescence crosslinked nanosize latex series

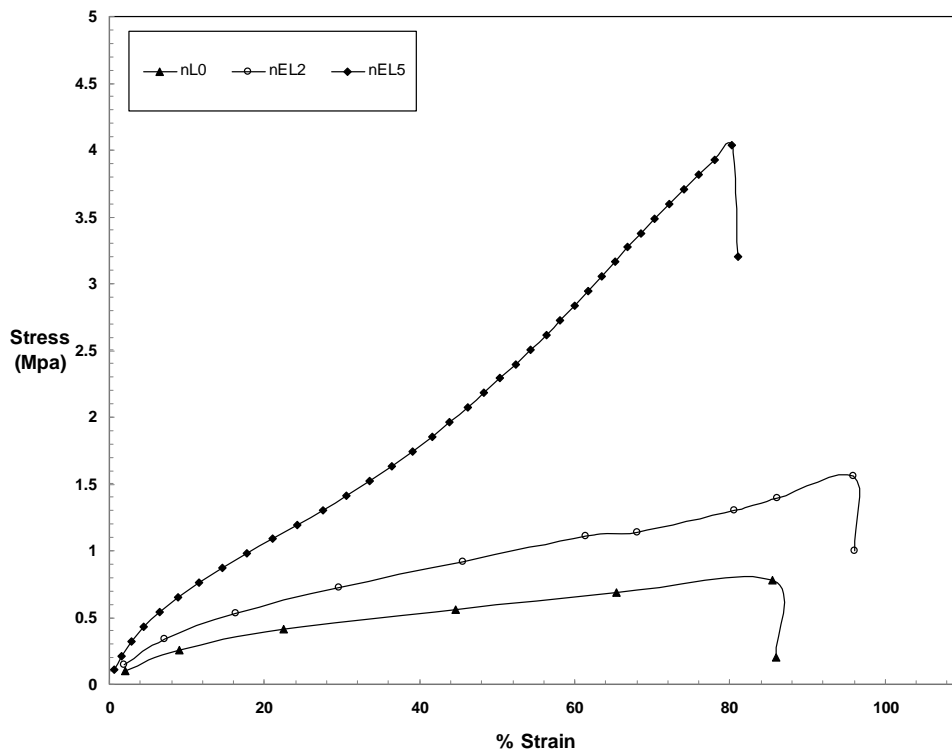


Figure 4.9: Comparison of average stress-strain curves for post-coalescence crosslinked nanosize latex series

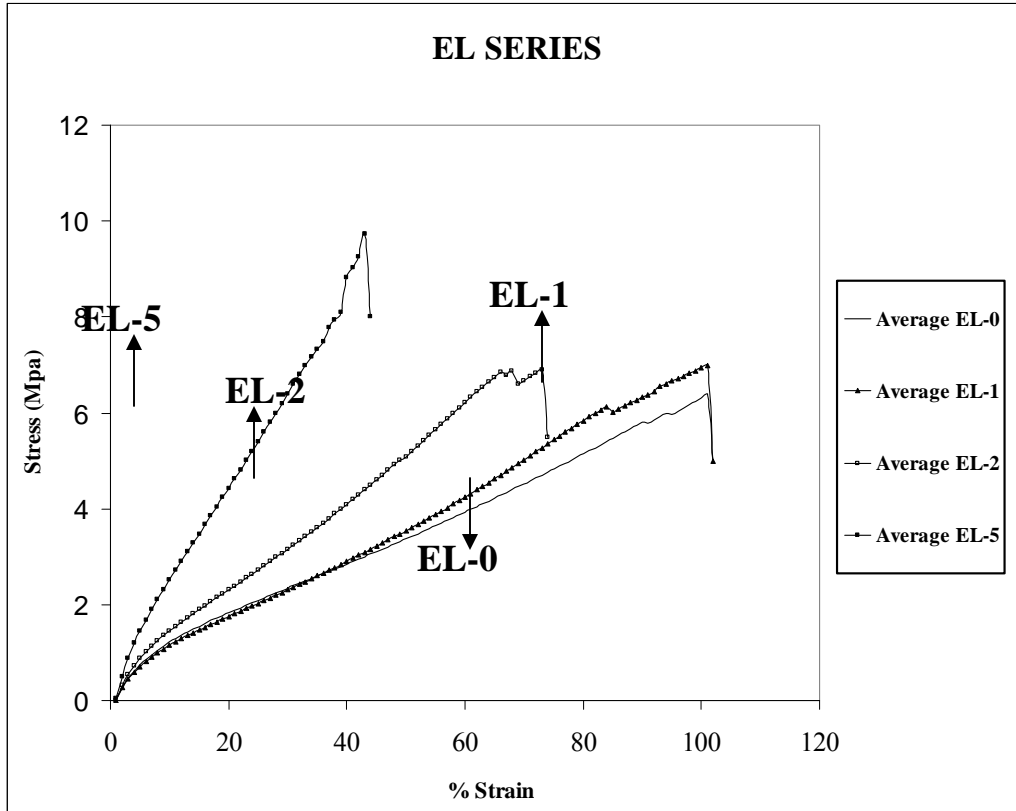


Figure 4.10: Comparison of average stress-strain curves for post-coalescence crosslinked conventional latex series (from Chapter 3)

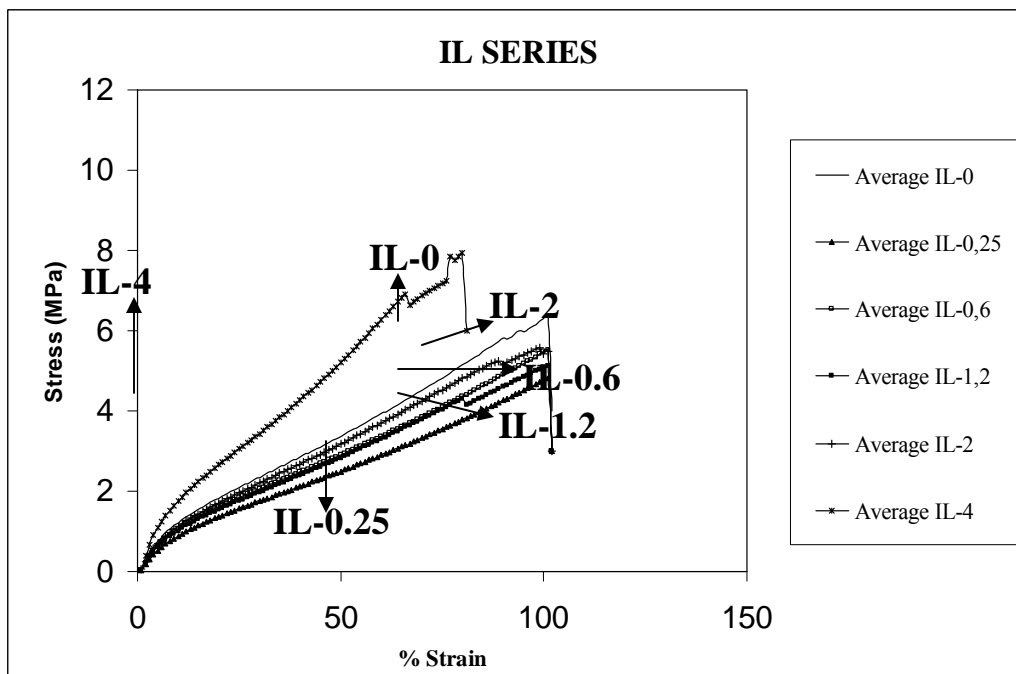


Figure 4.11: Comparison of average stress-strain curves for pre-coalescence crosslinked conventional latex series (from Chapter 3)

Dynamic mechanical properties

Dynamic mechanical characterization of heterogeneous polymers is dependent not only on the chemical composition of a material but also on physical or structural arrangement of the phases in a bulk polymer.^{44, 45} DMA analysis gives an insight into intrinsic mechanical properties of a polymer.^{44, 45} Figures 4.12-4.13 show respective storage and loss modulus curves of pre-coalescence nanolatex series and post-coalescence nanolatex series.

DMA provides information about the viscoelastic properties (storage modulus and loss modulus) of a polymer as a function of frequency and temperature.^{44, 45} The inflection point of the storage modulus is related to the T_g of the polymer.^{44, 45} It should be noted that the temperature corresponding to the inflection point of the tan delta curve is higher than the T_g value determined by MDSC, which is commonly observed.^{44, 45} The tan delta curve is calculated as ratio of the loss modulus and storage modulus. The point where the storage modulus curve flattens is an indicator of the rubbery plateau. Hill⁵⁸ points out that “for unpigmented crosslinked coating films the level of the storage modulus, E' , in the rubbery plateau region above T_g is an indicator of the level of crosslink density.” Hill⁵⁸ further points out that a wide variation in E' values has been observed from 4 MPa for lightly crosslinked systems to 200 MPa for very highly crosslinked films. For nanosize post-coalescence crosslinked latexes as shown in Table 4.10, in the 80-90 °C range, the values of E' are as follows: nL0, $E' = 0.9$ MPa, nEL2, $E' = 0.4$ MPa, and nEL5, $E' = 1.3$ MPa. In case of pre-coalescence crosslinked films for both nIL2 and nIL4, E' value in rubbery region is lower than E' value of nL0 in rubbery region. This difference in trends between nE-series and nI-series is consistent with our previous conclusions described in detail in Chapter 3.^{44, 45}

Also, when comparing the modulus values with their conventional size counterparts, nanoparticle latexes showed lower values. This could be due to presence of surfactant in nanosize latexes, which may lower the values of modulus in rubbery region.

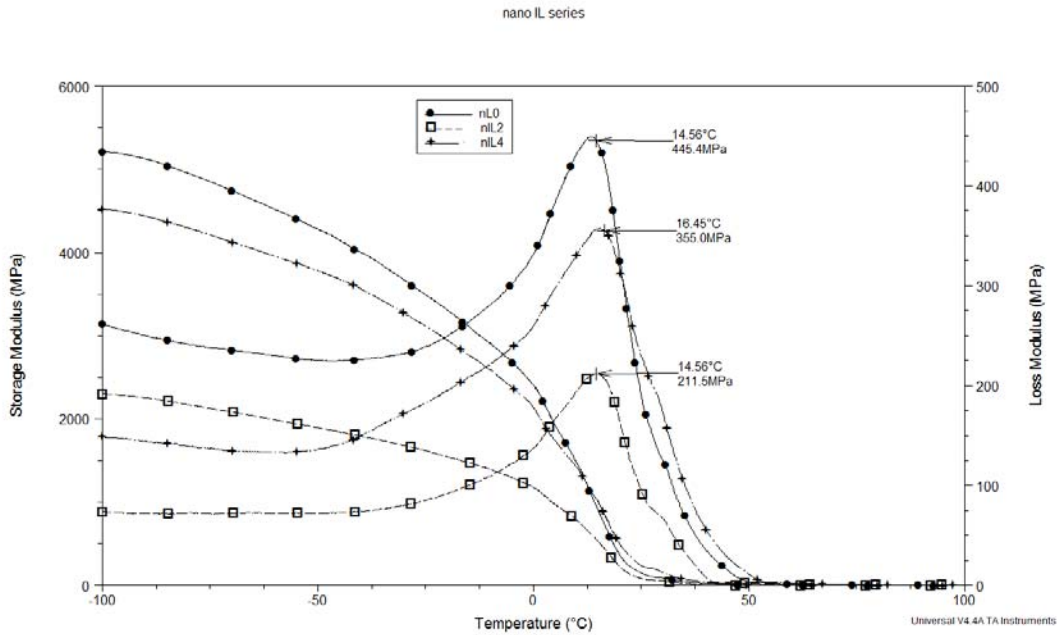


Figure 4.12: Comparison of storage and loss modulus curves of pre-coalescence crosslinker nanoparticle latex series

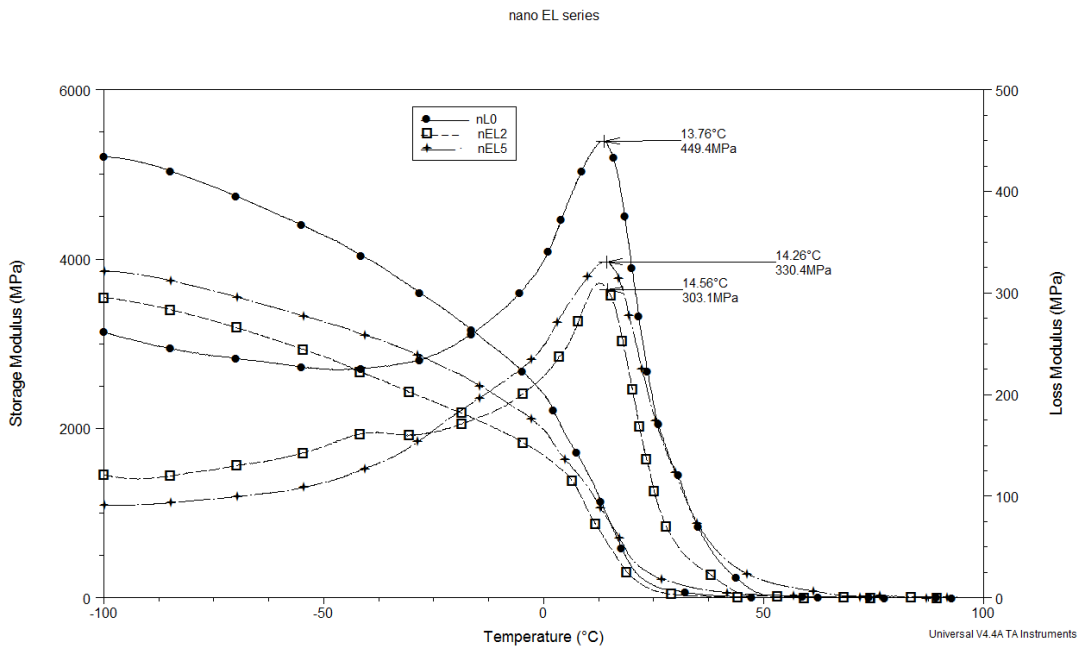


Figure 4.13: Comparison of storage and loss modulus curves of post-coalescence crosslinker nanoparticle latex series

Table 4.9: Comparison of DMA values with MDSC T_g values of conventionally size pre-coalescence or post-coalescence crosslinked latexes

Conventional Latex	MDSC T _g (°C)	DMA			DMA Tan delta		DMA storage modulus (Mpa), E', in rubbery (80-90 °C) region
		Storage modulus inflection point (°C)	Loss peak temperature (°C)	Tan delta peak Temperature (°C)	(L)HWHH	(R)HWHH	
L0	7.05	13.8	15.2	40.7	15.8	21.7	3.1
IL-2	5	18.7	18.2	42.7	10	13.1	1
EL-2	7	18.9	18.7	43.9	11.6	14.2	3
IL-4	14.6	26.3	24.3	50.3	16.92	21.6	5.2
EL-5	11.6	11.4	19.8	45.4	18.75	25	9

Table 4.10: Comparison of DMA values with MDSC T_g values of nano size pre-coalescence or post-coalescence crosslinked latexes

Nanoparticle Latex	MDSC T _g (°C)	DMA			DMA Tan delta		DMA storage modulus (Mpa), E', in rubbery (80-90 °C) region
		Storage modulus inflection point (°C)	Loss peak temperature (°C)	Tan delta peak Temperature (°C)	(L)HWHH	(R)HWHH	
nL0	4.77	13.1	13.8	32.5	18.65	18.85	0.9
nIL2	4.67	17.4	14.6	33.5	16.12	19.38	0.3
nEL2	3.13	9.4	14.6	35.8	18.01	25.79	0.4
nIL4	10.9	17.1	16.4	37.2	17.99	19.51	0.7
nEL5	5.15	15.9	14.3	41.4	14.04	32.36	1.3

Table 4.9 compares the MDSC T_g , DMA storage modulus inflection point, DMA loss peak temperature, tan delta peak temperature and half width/half height of tan delta peak. In the case of post-coalescence crosslinked latexes, with increasing % crosslinker, the shifting in tan delta peaks to higher temperature is negligible, but at the highest level of crosslinking, broadening as well as a shift to higher temperature is observed as reported in Table 4.6. The above observations are also reflected in half width and half height values of tan delta curves as shown in Table 4.6. The broadening of the tan delta peak is an indication of the development of a heterogeneous network structure and morphology as the crosslinker level increases.⁵⁸ This is consistent with our previous observations with post-coalescence conventional latex series as described in Chapter 3.^{44, 45}

Further, as the level of post-coalescence crosslinker increases, Y-modulus value increases at measurement temperatures of 25⁰C as shown in Figure 4.9 and Table 4.8. Also, as was observed in the case of conventional post-coalescence series, similarly with nanolatex post-coalescence series the tan delta peaks become broader (increase in half width and half height, Table 4.10), and the tan delta peak temperature increases, an indication of development of a more heterogeneous network structure and morphology. Thus, as the crosslinking level increases, the elastic modulus level obtained from stress-strain measurements increases and the DMA tan delta peak broadens. The rubbery plateau modulus obtained from DMA measurements increases at the 5% level, indicating a lightly crosslinked latex film. It should be noted that the MEK double rub resistance does increase as a function of crosslinking level, and the pencil hardness also increases with crosslinking level (see Table 4.5). These results lead us to conclude that at the appropriate crosslinker levels, an optimized hardness-flexibility balance can be achieved. Clearly the postcoalescence crosslinked latex particles are able to coalesce, interdiffuse, and

interpenetrate adequately before the crosslink density is high enough to impede the formation of films with desirable properties. All these observations indeed correlate with the observations noted (Chapter 3) in case of post-coalescence crosslinked conventional latex series.

In the case of the pre-coalescence crosslinked nanolatex samples, shifting of the tan delta peak to higher temperature (not as high as the post-coalescence crosslinked nanolatex at 5 wt%) can be seen at the highest crosslinking level in Table 4.10 with minimal broadening of the tan delta peak. This indicates that with increasing crosslinker level, a more heterogeneous structure is not developing, at least up to crosslinker levels of 4%. However, as the crosslinking level increases, the elastic modulus level obtained from stress-strain measurements increases up to 4% level and is the highest at 2% level. For nIL latex films, the rubbery plateau modulus obtained from DMA measurements does not show any significant increase for nIL2 or nIL4. This indicates that as the level of pre-coalescence crosslinker increases, internal particle crosslinking increases and inhibits interdiffusion and interparticle chain entanglement. It should be noted that the MEK double rub resistance showed a marginal increase as a function of crosslinking level, and the pencil hardness appears to be essentially independent of crosslinking level (see Table 4.5). These results indicate that the pre-coalescence particles are indeed internally crosslinked but only improve the properties of the latex films up to 2% level. However, at higher levels of crosslinking, such as at 4 wt% of pre-coalescence crosslinker, the properties are generally deleterious. Thus, in case of pre-coalescence crosslinking, the interdiffusion is impeded because too much crosslinking occurs before sufficient interparticle chain entanglement and particle coalescence can occur. All of these observations indeed correlate with the observations noted (Chapter 3) in case of pre-coalescence crosslinked conventional latex series.^{44, 45}

Conclusions

This study serves as a fundamental and practical contribution to nanoparticle latex research, forming a basis for exploring potential commercial applications of functional nanosize latexes made using an improved modified microemulsion polymerization technique.

- The key findings of the research are summarized below:

- An improved process has been developed for making thermoplastic nanoparticle latexes in the 15-30 nm diameter range using monomers with low water solubility.
- The gel content values of post-coalescence crosslinked nanosize latexes are in agreement with our previous observations for conventional size latexes. However, the gel content values of pre-coalescence crosslinked nanosize latexes are higher than their conventional counterparts. The large surface areas and small sizes of nanosize latex particles may facilitate the uniform distribution of functional groups across the polymer network.
- The experimental data show that films made from nanosize latexes in general have superior gloss, solvent resistance, adhesion when compared to their conventional size counterparts. For all nanosize latexes, tape adhesion to aluminum increases from 4B (good) to 5B (excellent, the highest rating in this test). Solvent rub resistance greatly increases. Block resistance of conventional size latexes when compared with their nanosize counterparts is either comparable or slightly higher. In case of nanosize latexes, resistance to water is inferior compared to their conventional size counterparts. This may be due to the amount of surfactant present on and near the surface of nanosize latex films. Resistance to diluted sulfuric acid largely remained unchanged or slightly improved at 16 hours in case of nanosize latexes.

- AFM tapping mode phase images clearly showed the effect of type and rate of crosslinking on the resulting film morphology. The rate of the crosslinking reaction in pre-coalescence crosslinked (4wt% level) low T_g nanoparticle latex was fast enough to significantly retard homogenization of the film, at least near to the surface, and is consistent with previous observations for the conventional size counterpart. Comparing tapping mode height images of nanosize vs. conventional size counterparts, in general, we see that nanosize latex films produce smoother surfaces.
- Stress-strain results showed that with increasing levels of post-coalescence crosslinker in nanosize latexes, Young's modulus increased. In the case of pre-coalescence crosslinked latexes, Young's modulus showed marginal increase as the level of crosslinking increases. Area under the curve and strain at break largely remained unchanged (within the standard deviation of the test). At 2 wt% level of crosslinking in both pre-coalescence and post-coalescence crosslinked nanolatexes, higher values of strain at break is observed. Overall, when comparing the nanosize latex films with their conventional size counterparts, the Young's modulus and area under the curve values of nanosize latexes are very low. This could be attributed to presence of the additional surfactant in the nanolatex series.
- DMA analysis results showed that in the case of post-coalescence crosslinker, nanoparticle latex samples exhibited a decrease and broadening of the tan delta peak with increasing levels of crosslinker, indicating an increase in heterogeneous network structure and morphology. At the 5% crosslinker level, the rubbery plateau modulus values indicate that these systems are lightly crosslinked. For the pre-coalescence crosslinked nanoparticle latex samples, shifting of tan delta peak to higher temperatures occurs at the

increasing crosslinking level, although not as greatly as in the case of post-coalescence crosslinked nanoparticle latexes. DMA analysis showed that the pre-coalescence particles are indeed internally crosslinked, but internal crosslinking only improves the properties of the latex films up to the 2% level and mostly showed no improvement or in most cases deleterious properties at higher crosslinking levels (4 wt%). Thus, in case of pre-coalescence crosslinking, the interdiffusion is apparently impeded because too much crosslinking occurs before sufficient interparticle chain entanglement and particle coalescence can occur. All of these observations indeed correlate with the observations noted (Chapter 3) in case of conventional latex series.^{44, 45}

References:

1. Moser, W. R., *Advance Catalysts and Nanostructured Materials : Modern Synthetic Methods*. Academic Press: San Diego, CA, 1996.
2. Jena, P., *Clusters and Nanostructured Materials*. In Behera, S. N., Ed. Nova Science Publishers: New York, 1996.
3. Chow, G.-M., *Nanotechnology: Molecularly Designed Materials*. In Gonsalves, K. E., Ed. American Chemical Society: Washington, D.C., 1996.
4. Siegel, R. W., *Polymeric Material Science Engineering* 1995, 73, 26.
5. Gref, R. M., Y. ; Peracchia, M.T.; Trubetskoy, V.; Langer, R.; Torchilin, V., *Science* 1995, 267, 458.
6. Stupp, S. I. L., V.; Walker, K.; Li, L.S.; Huggins, K.E.; Kesser, M.; Amstutz, A., *Science* 1997, 276, 384.
7. Kaiyi, L.; Zhaoqun, W., A novel method for preparing monodispersed polystyrene nanoparticles. *Front.Chem.China* 2007, 2, (1), 17-20.
8. He, G.; Pan, Q., Synthesis of Polystyrene and Polystyrene/Poly (methyl methacrylate) Nanoparticles. *Macromolecular Rapid Communications* 2004, 25, (17), 1545-1548.
9. Stoffer, J. O.; Bone, T. J., Polymerization in Water-in-Oil Microemulsion Systems I. *Journal of Polymer Science, Polymer Chemistry Edition* 1980, 18, (8).
10. Stoffer, J. O.; Bone, T. J., Polymerization in water-in-oil microemulsion systems. II. SEM investigation of structure *Journal of Dispersion Science and Technology* 1980, 1, (4), 393-412.
11. Atik, S. S.; Thomas, J. K., Polymerized Microemulsions. *J. American Chemical Society* 1981, 103, (14), 4279-4280.
12. Atik, S. S.; Thomas, J. K., Photochemistry in polymerized microemulsion systems *Journal of the American Chemical Society* 1982, 104, (12), 5868-74.
13. Atik, S. S.; Thomas, J. K., Photoinduced reactions in polymerized microemulsions *Journal of the American Chemical Society* 1983, 105, (14), 4515.
14. Antonietti, M.; Bremser, W.; Muschenborn, D.; Rosenauer, C.; Schupp, B.; Schmidt, M., Synthesis and size control of polystyrene latexes via polymerization in microemulsion *Macromolecules* 1991, 24, (25), 6636-43.
15. Candau, F.; Leong, Y. S.; Fitch, R. M., Kinetic study of the polymerization of acrylamide in inverse microemulsion *Journal of Polymer Science, Polymer Chemistry Edition* 1985, 23, (1), 193-214.
16. Candau, F.; Leong, Y. S.; Fitch, R. M., Effect of solution components on the termination mechanism in acrylamide microemulsion polymerizations *Journal of Polymer Science, Part A: Polymer Chemistry* 1989, 27, (7), 2179-88.
17. Capek, I.; Potisk, P., Microemulsion polymerization of butyl acrylate. IV. Effect of emulsifier concentration *Journal of Polymer Science, Part A: Polymer Chemistry* 1995, 33, (10), 1675-83.
18. Corpart, J. M.; Selb, J.; Candau, F., Characterization of high charge density ampholytic copolymers prepared by microemulsion polymerization *Polymer* 1993, 34, (18), 3873-86.

19. Feng, L.; Ng, K. Y. S., In situ kinetic studies of microemulsion polymerizations of styrene and methyl methacrylate by Raman spectroscopy *Macromolecules* 1990, 23, (4), 1048-53.
20. Gan, L. M.; Chew, C. H.; Lee, K. C.; Ng, S. C., Polymerization of methyl methacrylate in ternary oil-in-water microemulsions *Polymer* 1993, 34, (14), 3064-9.
21. Gan, L. M.; Chew, C. H.; Lye, I.; Ma, L.; Li, G., Effect of water-soluble cosurfactants on microemulsion polymerization of styrene *Polymer* 1993, 34, (18), 3860-4.
22. Gan, L. M.; Chew, C. H.; Lee, K. C.; Ng, S. C., Formation of polystyrene nanoparticles in ternary cationic microemulsions *Polymer* 1994, 35, (12), 2659-64.
23. Guo, J. S.; Sudol, E. D.; Vanderhoff, J. W.; El-Asser, M. S., Particle nucleation and monomer partitioning in styrene oil-in-water microemulsion polymerization *Journal of Polymer Science, Part A: Polymer Chemistry* 1992, 30, (5), 691-702.
24. Guo, J. S.; Sudol, E. D.; Vanderhoff, J. W.; El-Asser, M. S., Modeling of the styrene microemulsion polymerization *Journal of Polymer Science, Part A: Polymer Chemistry* 1992, 30, (5), 703-12.
25. Kuo, P. L.; Turro, N. J.; Tseng, C. M.; El-Aasser, M. S.; Vanderhoff, J. W., Photoinitiated polymerization of styrene in microemulsions *Macromolecules* 1987, 20, (6), 1216-21.
26. Larpent, C.; Tadros, T. F., Preparation of microlatex dispersions using oil-in-water microemulsions *Colloid & Polymer Science* 1991, 269, (11), 1171-83.
27. Ming, W.; Zhao, J.; Lu, X.; Wang, C.; Fu, S., Novel Characteristics of a Polystyrene Microsphere Prepared by Microemulsion Polymerization *Macromolecules* 1996, 29, (24), 7678-7682.
28. Rodriguez-G., L. A.; Mendizabal, E.; Puig, J. E.; Kaler, E. W., Polymerization of methyl methacrylate in 3-component cationic microemulsion *Journal of Applied Polymer Science* 1993, 48, (5), 775-86.
29. Texter, J.; Oppenheimer, L. E.; Minter, J. R., Microemulsion polymerization in the water, bis(2-ethylhexyl) sulfosuccinate sodium salt (Aerosol-OT), tetrahydrofurfuryl methacrylate system *Polymer Bulletin (Berlin, Germany)* 1992, 27, (5), 487-94.
30. Wu, C., Laser Light Scattering Determination of the Surfactant Interface Thickness of Spherical Polystyrene Microlatexes. *Macromolecules* 1994, 27, (24), 7099-102.
31. Guo, A. L., G.; Tao, J., *Macromolecules* 1996, 29, 2487.
32. Henselwood, F. L., G., *ibid* 1997, 30, 488.
33. Li, M. J., M.; Zhu, L.; Wu, C., *Macromolecules* 1997, 30, 2201.
34. Okubo, M. F., N.; Ito, A., *Journal of Applied Polymer Science* 1997, 66, 1461.
35. Okubo, M. S., R.; Fukami, N.; Ito, A., *Colloid & Polymer Science* 1997, 275, 170.
36. Gan, L. M.; Chew, C. H.; Lian, N.; Li, G. Z., Polymerization of Styrene in a Winsor I-like System *Langmuir* 1994, 10, (7), 2197-201.
37. Loh, S. E.; Gan, L. M.; Chew, C. H.; Ng, S. C., Polymerization of methyl methacrylate in Winsor I-like system *Journal of Macromolecular Science, Pure and Applied Chemistry* 1996, A33, (3), 371-84.
38. Ming, W.; Jones, F. N.; Fu, S., High solids-content nanosize polymer latexes made by microemulsion polymerization. *Macromolecular Chemistry and Physics* 1998, 199, (6), 1075-1079.

39. Ming, W.; Jones, F. N.; Fu, S., Synthesis of nanosize poly(methyl methacrylate) microlatexes with high polymer content by a modified microemulsion polymerization. *Polymer Bulletin* 1998, 40, (6), 749-756.
40. Ming, W.; Jones, F. N.; Fu, S., High Solids-content Nanosize Polymer Latexes Made by Microemulsion Polymerization. *Macromol. Chem. Phys.* 1998, 199, 1075-1079.
41. Ming, W.; Jones, F. N.; Fu, S., Synthesis of nanosize poly(methyl methacrylate) microlatexes with high polymer content by a modified microemulsion polymerization. *Polym. Bull.* 1998, 40, (6), 749-756.
42. Ming, W.; Zhao, Y.; Cui, J.; Fu, S.-K.; Jones, F. N., "Formation of Irreversible Nearly Transparent Physical Polymeric Hydrogels During a Modified Microemulsion Polymerization," *Macromol* 1999, 32, 528-530.
43. Ming, W.; Zhao, Y.; Fu, S.; Jones, F. N. In *Polym. Mater. Sci. Eng.*, 1999; ACS: 1999; p 514.
44. Joshi, R.; Lefevre, E.; Patel, C.; Provder, T.; Crombez, R.; Shen, W.; Jones, F. N., Thermoanalytical and morphological studies of cross-linked latex films by advanced techniques. *Journal of Thermal Analysis and Calorimetry* 2008, 93, (1), 19-26.
45. Joshi, R. G.; Provder, T.; Ziemer, P. D.; Mao, W.; Shen, W.; Jones, F. N., Investigation of the effect of precoalescence or postcoalescence crosslinking on film formation, properties, and latex morphology. *Journal of Coatings Technology and Research* 2008 (online first, DOI: 10.1007/s11998-008-9115-7).
46. Chang-Mei, K. E.; Hou-Zhi, W.; Wei, D.; Yan, W.; Jun, X. U.; Hui, D.; Mei-jie, X.; Hui-zhong, Z.; Xuan-ke, L., High solids-content nanosize polymeric microlatexes made by microemulsion copolymerization at ambient temperature. *Journal of Wuhan University of Technology - Mater. Sci. Ed.* 2004, 19, (1), 30-34.
47. Zosel, A.; Ley, G., "Influence of crosslinking on structure, mechanical properties, and strength of latex films". *Macromolecules*, 1993, 26, 2222-2227.
48. Tamai, T.; Pinenq, P.; Winnik, M. A., "Effect of cross-linking on polymer diffusion in poly(butyl methacrylate-co-butyl acrylate) latex films". *Macromolecules* 1999, 32, 6102-6110.
49. Aradian, A.; Raphael, E.; G., d. G. P., "A scaling theory of the competition between interdiffusion and cross-linking at polymer interfaces". *Macromolecules* 2002, 35, 4036-4043.
50. Ghazaly, H. M.; Daniels, E. S.; Dimonie, V. L.; El-Aasser, M. S.; Klein, A., "Synthesis and characterization of a macromonomer crosslinker". *J. Appl. Polym. Sci.* 2000, 77, 1362-1368.
51. Ghazaly, H. M.; Daniels, E. S.; Dimonie, V. L.; Klein, A.; El-Aasser, M. S., "Miniemulsion copolymerization of n-butyl methacrylate with crosslinking monomers". *J. Appl. Polym. Sci.* 2001, 81, 1721-1730.
52. Ghazaly, H. M.; Daniels, E. S.; Dimonie, V. L.; Klein, A.; Sperling, L. H.; El-Aasser, M. S., "Properties of N-butyl methacrylate copolymer latex films derived from crosslinked latex particles" *J. Appl. Polym. Sci.* 2003, 88, 42-49.
53. Kessel, N.; Illsley, D. R.; Keddie, J. L., "The Influence of Interdiffusion and Crosslinking in the Film Formation of an Acrylic Latex" *J. Coat. Technol. Res.* 2008, (online first, DOI:10.1007/s11998-008-9096-6).
54. Emmons, W. D., (to Rohm and Haas) "Ambient or low-temperature curable coatings,". U.S. Patent 4,210,565, 1980.

55. "Diacetone acrylamide, N-(1,1 dimethyl-3-oxobutyl)-acrylamide," *Kyowa Hakko U.S.A. Inc. Technical information sheet* 2008 (retrieved), p 4.
56. Taylor, J. W.; Winnik, M. A., "Functional Latex and Thermoset Latex Films," *JCT Research* 2004, 1, (3), 163-190.
57. Robinson, G. F.; Shemancik, R. C.; Speight, R. D.; Wong, P. T.; Znidersic, K. M. (to Akzo Nobel), "Coating Compositions and Coatings Formed Therefrom." US Patent 6,605,359, 2003.
58. Hill, L. W., "Dynamic Mechanical and Tensile Properties". In *Paint and Coatings Testing Manual: Fourteenth Edition of the Gardner-Sward Handbook*, Koleske, J. V., Ed. ASTM: Ann Arbor, MI, 1995; pp 534–546.

Chapter 5

Blends of conventional size and nanoparticle size acrylic latexes*

Introduction

Synthetic latexes have been industrially important for over 60 years and have attracted considerable academic interest. Latex blends, physically mixing two different latexes with homogeneous particle morphologies, have attained a great deal of attention in last two decades.¹⁻²¹ This strategy is known to eliminate or reduce the use of coalescing aids (or plasticizers), which are considered volatile organic compounds (VOCs) in a coating formulation.^{7, 20} Another effective approach is the use of structured latexes by changing the particle morphology in a single particle i.e. core/shell type latexes covered extensively in the literatures.^{9, 10, 12, 15, 19} There have been many thousands of publications and patents on latex blend research.^{1-15, 17-21} Drying behavior and mechanical properties of blends of a low glass transition temperature (T_g) polymer based latex (commonly viewed as film former or a continuous phase) and a high T_g polymer based latex (commonly viewed as filler or a dispersed phase) have been thoroughly investigated in the past. Many other factors, individually or combined, covered in the literature^{1-15, 17-21} govern the film properties and film formation of latex blends, such as mechanical properties of neat constituents and their morphologies, compatibility between the two mixing phases or the interfacial activity between the two mixed phases, particle size and particle size ratios of blend components, weight fraction, distribution and packing factor of dispersed phase, or their blend ratios. Further, it was shown that incorporation of a functional group can enhance the miscibility between the two phases, hence, the overall film properties of resulting latex blends.^{2, 17}

*Winner of the Prestigious "A.L. Gordon Award" at 2008 FutureCoat! Conference sponsored by Federation of Societies for Coatings Technology, in Chicago, IL, USA.

*Presented at Prestigious "Matiello Symposium" at 2009 CoatingsTech Conference sponsored by FSCT-NPCA, in Indianapolis, IN, USA.

*2 Patents filed, Joshi, R.G. et al., "Conventional Latex/Nanolatex Blends", US (12578442) and PCT (60536) on Oct 13, 2009 (Eastern Michigan University)

Although many investigators have studied blends of latexes, including blends of latexes with different particle sizes, surprisingly few, if any, of the thousands of publications contain systematic studies of blends of thermoplastic nanoparticles in the 15-30 nm diameter range with larger thermoplastic latexes (diameters of about 100 to 1000 nm) – the subject of this research. Also, two significant variables, the glass transition temperature (T_g) of the large and small polymer particles (they can be the same or different) and the effects of chemical crosslinking, pre-coalescence (internal) vs. post-coalescence crosslinking (external), are key factors in this research.

In Chapter 3, the effect of pre-coalescence or post-coalescence crosslinking on conventionally sized latex film formation, properties, and latex morphology was covered.^{22, 23} As described Chapter 3, “Pre-coalescence crosslinked latexes” or “intraparticle crosslinking latexes” refers to latex particles that are crosslinked before the film formation or the coalescence stage. In this study, 1, 3-butylene glycol dimethacrylate (1, 3-BGDMA) was used as the pre-coalescence crosslinker. The “post-coalescence crosslinked latexes” or “interparticle crosslinking latexes” referred to the latexes that are prepared with reactive sites such as hydroxyl groups and are crosslinked during film formation by an external crosslinker that is added to the coating formulation but not co-polymerized in the latex. Many combinations of reactive sites and crosslinkers have been described in literature.²⁴ In this study diacetone acrylamide (DAAM) was used as the monomer to place reactive sites within the latex and adipic dihydrazide (ADDH) as the post-coalescence crosslinker. This combination of site and crosslinker has been described in trade literature²⁵ and in numerous patents²⁶⁻²⁹ and is being utilized by some major coatings and ink companies in their product formulations.

In Chapter 4, preparation of comparable nanosize latexes containing 0 – 4 wt. % of pre-coalescence crosslinker (1, 3-BGDMA) and 0 – 5 wt. % of reactive monomer for post-coalescence crosslinker (DAA) is covered. Both the pre-coalescence and post-coalescence nanosize latex series were prepared using improved modified microemulsion copolymerization process using target glass transition temperature of 5 °C. As described in Chapter 4, Ming's modified microemulsion process³⁰⁻³³ was basically used to make nanoparticle latexes with further improvements to enable use of functional monomers and monomers with low water solubility.

This chapter describes a study in which the nanosize latexes (from Chapter 4) were blended with previously reported^{22, 23} conventional latexes (from Chapter 3) in different weight ratios ranging from 7.5/92.5 to 70/30 nano/conventional latexes. The films cast from these latexes were characterized using a variety of end-use tests and advanced instruments such as a dynamic mechanical analyzer (DMA), modulated differential scanning calorimeter (MDSC), and atomic force microscope (AFM). Information from such instruments should greatly enhance our understanding of the relation between physical and morphological properties of coatings. The overall goal was to understand the relationship among the variables of (a) particle size and distribution level, (b) type and level of crosslinker, and (c) blending and blend ratios and the effect upon the resultant fundamental and end-use film properties and latex film morphology.

Experimental Details

Preparation of pre-coalescence or post-coalescence crosslinked conventional latexes^{22, 23}

(described in detail in Chapter 3):

The conventional latex samples employed here have been described previously.³¹ In brief, latexes were synthesized with varying levels of pre-coalescence crosslinker (internal) and post-coalescence (external) crosslinkable sites. Two sets of latexes were prepared, one with a target glass transition temperature (T_g) of about 7 °C and the other with a target T_g of about 22 °C. Compositions and characteristics of these latexes are shown in Table 5.1. It should be noted here that the surfactant/monomer wt. ratio used for conventional latex synthesis is 3/100. The latexes are coded I for pre-coalescence or internal, E for post-coalescence or external, L for low T_g , H for high T_g , and a number for the weight % of crosslinker or reactive site in the monomer line up. Thus, for example, IL-4 means an internally (or pre-coalescence) crosslinked, low T_g latex with 4.0 wt. % of 1, 3-BGDMA and EH-5 means an externally (or post-coalescence) crosslinked, high T_g latex with 5.0 wt. % of DAA.

Preparation of nanosize latexes (with or w/o functional group) using improved modified microemulsion copolymerization³⁰⁻³³ (described in detail in Chapter 4):

Nanosize latexes were synthesized with varying levels of pre-coalescence (internal) and post-coalescence (external) crosslinkable sites as described previously. The latexes were prepared with the target glass transition temperature (T_g) of 5 °C. The compositions and characteristics of these latexes are shown in Table 5.2. It should be noted here that the surfactant/monomer wt. ratio used for nanoparticle latex synthesis is 1/10.5. The nanosize latexes are coded I for pre-coalescence or internal, E for post-coalescence or external, L for low T_g and, a number for the weight % of crosslinker or reactive site in the monomer line up. Thus, for

example nIL-2 means pre-coalescence crosslinked latex with 2 wt. % of 1, 3-BGDMA and nEL-5 means post-coalescence crosslinked latex with 5 wt. % of DAA.

Preparation of latex blends using functional pre-coalescence (internally crosslinked) and post-coalescence (crosslinkable) conventional latexes with nanosize polymer latexes with or without functional groups:

The conventional latexes, listed in Table 5.1, and the nanoparticle latexes, listed in Table 5.2, were mixed in a variety of ratios, on wt/wt basis, with gentle stirring in a glass beaker. The resulting latex blends are listed in Table 5.3. The blends are coded as first two/three alphanumeric for conventional latexes (as described above) and the second three/four alphanumeric for nanolatexes (as described above) separated using a hyphen. For example, H0_nL0 showed blend of high T_g conventional latex with no crosslinker with low T_g nanolatex with no crosslinker. Many latex blends were employed and large amounts of experimental work have been generated. For the purpose of this chapter, in order to make the results more understandable, the ten most representative examples in seven different concentrations are shown in Table 5.3.

Table 5.1: Characteristics of conventionally sized (with or without crosslinker) latexes^{22, 23} (Chapter 3)

Latex	Composition	% Non-Volatiles	Particle Size, nm	Glass Transition Temperature (°C) by MDSC	Glass Transition Temperature (°C) by Fox Equation	pH	Gel Content	Viscosity η (mPa•s)
L0	<i>nBA/nBMA//MAA=21/77/2</i>	47.0	134	7.05	5.06	9.8	0.0	280
EL-5	<i>nBA/nBMA/DAA/MAA=21/72/5/2</i>	46.3	137	11.6	---	9.7	100.0	1320
IL-4	<i>nBA/nBMA/1,3-BGDMA/MAA=21/73/4/2</i>	46.8	123	14.6	---	9.2	64.2	70
H0	<i>nBA/nBMA/ /MAA=9/89/2</i>	46.9	126	26.3	14.4	9.1	0.0	120
EH-5	<i>nBA/nBMA/DAA/MAA=9/84/5/2</i>	46.0	129	29.7	---	9.8	97.9	1010
IH-4	<i>nBA/nBMA/1,3-BGDMA/MAA=9/85/4/2</i>	47.6	125	33	---	9.2	62.9	120

Table 5.2: Characteristics of nanosize (with or without crosslinker) latexes (Chapter 4)

Nanosize Latex	Composition	% Non-Volatiles	Particle Size, nm	Polydispersity	Glass Transition Temperature (°C) using MDSC	Glass Transition Temperature (°C) using Fox Equation	pH	Gel Content	Viscosity η (mPa•s)
nL0	<i>nBA/nBMA//MAA=21/77/2</i>	10.8	23.2	0.09	4.77	5.06	9.3	0.0	13
nEL2	<i>nBA/nBMA/DAA/MAA=21/75/2/2</i>	10.7	23	0.087	3.13	---	9.7	98.1	13
nEL5	<i>nBA/nBMA/DAA/MAA=21/72/5/2</i>	10.6	21.7	0.12	5.15	---	9.5	99.9	17
nIL2	<i>nBA/nBMA/1,3-BGDMA/MAA=21/75/2/2</i>	10.9	23.2	0.089	4.67	---	9.1	63.8	13
nIL4	<i>nBA/nBMA/1,3-BGDMA/MAA=21/73/4/2</i>	10.9	22.2	0.1	10.9	---	9.8	97.4	15

Table 5.3: Characteristics of ten most representative latex blends

Latex blend	Composition (%wt.)		Brief description
	Conventionally size latex	Nanosize latex	
L0_nL0	100,92.5,85,70,50,30,0	0,7.5,15,30,50,70,100	L0 (Soft conventional latex, zero crosslinker) with $T_g = 7^\circ\text{C}$, particle diameter 134 nm and nL0 (Soft nanoparticle latex, zero crosslinker), $T_g = 4.77^\circ\text{C}$, particle diameter 23.2 nm
L0_nEL2	100,92.5,85,70,50,30,0	0,7.5,15,30,50,70,100	L0 (Soft conventional latex, zero crosslinker) with $T_g = 7^\circ\text{C}$, particle diameter 134 nm and nEL2 (Soft nanoparticle latex with 2% crosslinkable monomer), $T_g = 3.13^\circ\text{C}$, particle diameter 23 nm
L0_nIL4	100,92.5,85,70,50,30,0	0,7.5,15,30,50,70,100	L0 (Soft conventional latex, zero crosslinker) with $T_g = 7^\circ\text{C}$, particle diameter 134 nm and nIL4 (Soft nanoparticle latex with 4% crosslinkable monomer within the particles,), $T_g = 10.9^\circ\text{C}$, particle diameter 22 nm
H0_nL0	100,92.5,85,70,50,30,0	0,7.5,15,30,50,70,100	H0 (Hard conventional latex, zero crosslinker) with $T_g = 26^\circ\text{C}$, particle diameter 126 nm, and nL0 (Soft nanoparticle latex, zero crosslinker), $T_g = 4.77^\circ\text{C}$, particle diameter 23.2 nm
H0_nEL5	100,92.5,85,70,50,30,0	0,7.5,15,30,50,70,100	H0 (Hard conventional latex, zero crosslinker) with $T_g = 26^\circ\text{C}$, particle diameter 126 nm, and nEL5 (Soft nanoparticle latex with 5% crosslinkable monomer), $T_g = 5.15^\circ\text{C}$, particle diameter 21.7 nm
H0_nIL2	100,92.5,85,70,50,30,0	0,7.5,15,30,50,70,100	H0 (Hard conventional latex, zero crosslinker) with $T_g = 26^\circ\text{C}$, particle diameter 126 nm, and nIL2 (Soft nanoparticle latex with 2% crosslinkable monomer), $T_g = 4.67^\circ\text{C}$, particle diameter 23.2 nm
EL5_nL0	100,92.5,85,70,50,30,0	0,7.5,15,30,50,70,100	EL5 (Soft conventional latex with 5% crosslinkable monomer) with $T_g = 5^\circ\text{C}$, particle diameter 137 nm, and nL0 (Soft nanoparticle latex, zero crosslinker), $T_g = 4.77^\circ\text{C}$, particle diameter 23.2 nm
IL4_nL0	100,92.5,85,70,50,30,0	0,7.5,15,30,50,70,100	IL4 (Soft conventional latex with 4% crosslinkable monomer within the particles) with $T_g = 13^\circ\text{C}$, particle diameter 123 nm, and nL0 (Soft nanoparticle latex, zero crosslinker), $T_g = 4.77^\circ\text{C}$, particle diameter 23.2 nm
EH5_nL0	100,92.5,85,70,50,30,0	0,7.5,15,30,50,70,100	EH5 (Hard conventional latex with 5% crosslinkable monomer) with $T_g = 23^\circ\text{C}$, particle diameter 129 nm, and nL0 (Soft nanoparticle latex, zero crosslinker), $T_g = 4.77^\circ\text{C}$, particle diameter 23.2 nm
IH4_nL0	100,92.5,85,70,50,30,0	0,7.5,15,30,50,70,100	IH4 (Hard conventional latex with 4% crosslinkable monomer within the particles) with $T_g = 33^\circ\text{C}$, particle diameter 125 nm, and nL0 (Soft nanoparticle latex, zero crosslinker), $T_g = 4.77^\circ\text{C}$, particle diameter 23.2 nm

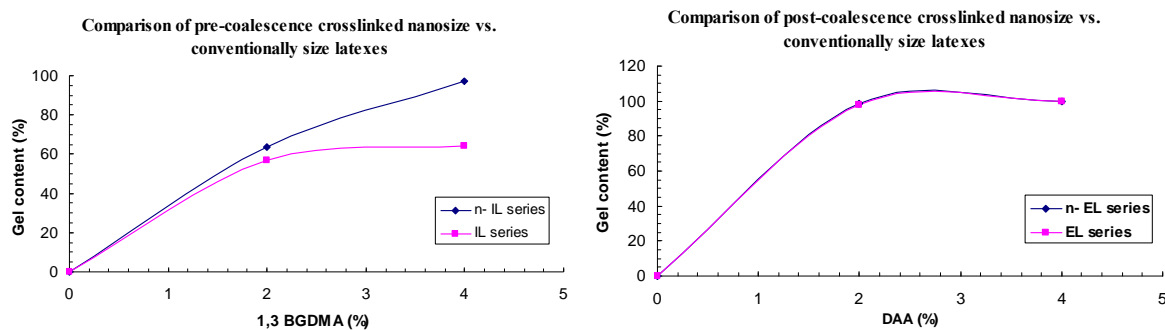


Figure 5.1 (a, b): Comparison of gel content of (a) pre-coalescence crosslinked nanosize vs. conventional latexes and (b) post-coalescence crosslinked nanosize vs. conventional latexes

Characterization of Latexes

Latex Properties

(a) Conventional Latexes (with or without functional groups)^{22, 23} (Chapter 3):

The weight percentage of non-volatile solids content (% NVM) was measured using ASTM D 4758-87. Viscosity was measured by ASTM D 4287 at 20 °C using a Brookfield Viscometer, Model DV-1, using Spindle #4 at 20 rpm. pH was measured with a Fischer Acumet Model 620 pH meter and with pH paper.

For particle size (diameter) and particle size distribution measurements, each latex was diluted to a transmission factor of 0.5-1.0 (about 0.05-0.1 wt% solids) and measured at 25 °C using the light-scattering instrument, MICROTAC Series 9200. Three tests were performed within 180 sec. to obtain an average value of a volume distribution.

For gel content measurements, an empty extraction thimble was dried at 85°C in an oven for 2 h, cooled in a desiccator overnight, and weighed. Latex films (prepared on glass and detached) were dried in a desiccator overnight, cut into small pieces, weighed, and put into the thimble. After a 12-h extraction with acetone in a Soxhlet extractor, the thimble was dried in an oven at 85°C for 2 h, cooled in a desiccator overnight, and weighed. The gel content was calculated from the initial and final weights, assuming that gelled material remained in the thimble. The results are show in Figure 5.1(a, b) and Table 5.1.

(b) Nanosize latexes (with or without functional groups) (Chapter 4):

The weight percentage of non-volatile solids content (% NVM) was measured using ASTM D 4758-87. Viscosity was measured by ASTM D 4287 at 25 °C using a using a Brookfield Viscometer, model CAP 2000+, using Spindle #1 at 113 rpm. pH was measured with a Fischer Acumet Model 620 pH meter and with pH paper.

Particle size (diameter) and particle size distribution of nanosize latexes were determined using dynamic light scattering method with a 90 PLUS Particle Analyzer (Brookhaven Instruments Co.) at room temperature, after the nanosize latex samples were diluted to a solid content of about 0.1 wt.%. A 10 MM potassium nitrate (KNO₃) solution was used as diluent. The latex samples were filtered using Whatman Puradisc 25 AS filters with 200nm pore size before running for particle size analysis. For each sample at least 3 runs (each run of 10 min. duration) for a total of 30 min. were done. The average effective diameters and polydispersity from the intensity distribution were obtained directly from the measurement results and reported.

For gel content measurements of nanosize latexes, a similar procedure was followed as described earlier for gel content measurements of conventional latex. The results are shown in Figure 5.1(a, b), Table 5.2.

It should be noted that for particle size measurement, different instruments were used to measure the particle size and distribution of conventional and nanolatex samples. In selected cases, results from the MICROTRAC Series 9200 light scattering instrument and the Brookhaven 90 PLUS Particle Size Analyzer were found to correlate well.

Film Properties:

The minimum film formation temperature (MFT), crack point and knife point, was determined using a Rhopoint MFFT Bar - 90, Rhopoint Instruments. Briefly, the instrument was equilibrated over a specific temperature range (determined based on the glass transition temperature of latex sample) for about 20 minutes. Five replicates are laid down in quick succession using a 75 micron (3 mils) one inch cube applicator. The tracks were laid down left to right. A clearly defined limit of coalescence will show in about 90-120 minutes, and the MFT temperature can then be read using the cursor scale. The crack point, the temperature onset of

formation that is crack-free, was determined using a fingernail. The knife point, the temperature onset of film integrity where the film no longer cracks upon disturbing or peeling the film, was determined using a plastic or metallic spatula by carefully peeling away the film starting from the crack point.

Specimens were prepared on aluminum panels by drawing the latexes down using a square wet film applicator (Paul N. Gardner Co., Inc.) with 0.25 mm (wet) clearance on aluminum panels. The panels were dried in an oven at 70 °C and 50% humidity for 24 hours and then stored at normal room conditions for a week before testing. No coalescing solvents were used. Dry film thicknesses were approximately 50 µm. Before casting these films, a stoichiometric amount of adipic dihydrazide (ADDH) was added to the E-series latexes.

Dry film thickness was measured at 25°C by Elcometer-345-Digital Coating thickness Gauge (Elcometer Instruments Ltd.).

Solvent resistance was determined by methyl ethyl ketone (MEK) rubbing. The load was applied by a ball peen hammer with a 448 g head wrapped with cheesecloth soaked with MEK. The reported end point was the number of double rubs required to break through the film and expose bare metal.

Chemical resistance tests were conducted at 25 °C following ASTM D 1308. A 1-mL sample of each test reagent (water, dilute sulfuric acid at pH 3) was pipeted (a 5-mL pipet graduated in 0.1 mL) onto the horizontal panel and immediately covered with a watch glass. After a specific time interval, the spot was wiped clean and the film was examined immediately for defects. Intervals used were 15 min, 1 h, and 16 h.

Pencil hardness was tested at 25 °C following the procedure of ASTM 3363.

Tape adhesion was measured by ASTM D 3359. The films were cut with a cross-cut kit (Precision Gage & Tool Company) before testing.

Block Resistance was measured by ASTM D 4946. Briefly, latex films were cast on a sealed test chart and the films were dried in an oven at 70 °C and 50% humidity for 8-10 hours and then stored at normal room conditions for a week before testing. After conditioning, six 3.8 x 3.8 cm. sections from the films were exactly cut as mentioned in the ASTM method. 3 sets of 2 film squares facing each other were placed in the oven, exactly as described in the ASTM method, at 50 °C for 30 minutes. The specimens were cooled at room temperature for about 30 min. and blocking was measured. The average of three reading with standard deviation is reported.

Specular Gloss at 20° and 60° was measured using ASTM D 523 test method. Latex films were applied to glass panels, conditioned in an oven at 70 °C and 50% humidity for 8-10 hours and then stored at normal room conditions for a week before testing. Gloss was measured using BYK Gardner, BYK micro-TRI-gloss meter.

Thermal and Mechanical Properties:

For glass transition temperature (T_g) measurement, specimens for latex blends were prepared on glass panels by drawing the latexes down using a square wet film applicator (Paul N. Gardner Co., Inc) with 0.30 mm (wet) clearance on glass panels. The glass panels were dried in an oven at 70 °C and 50% humidity for 8-10 hours and then stored at normal room conditions for a week before testing. The T_g of the dried films was determined by TA instrument - TA 2920 MDSC with RCS (Refrigerant Cooling System) accessory under nitrogen purge at flow rate of 50 mL/min. For testing, the samples were kept in closed aluminum non-hermetic pans.

Temperature scans were done from -90 °C to 100 °C at 2 °C/min with a modulation of +/- 1.00 °C at every 60 seconds under nitrogen. The MDSC was equilibrated at -90 °C for 5 min.

Dynamic Mechanical analyses were conducted using TA Instruments Model Q800 Dynamic Mechanical Analyzer (DMA) with the LNCS accessory. Specimens for stress-strain and dynamic mechanical studies were prepared on glass panels as described in MDSC studies section. A film cutter (supplied by TA instruments) was used to cut, at constant depth, rectangular specimens about 15-20 mm long, 3-6 mm wide, and 0.1-0.2 mm thick from the cured films.

The stress-strain studies were done at room temperature (~25 °C) in air on the Q800 DMA with the thin film tension clamp in a controlled force mode with a ramped force of 3N/min up to 18N/min and the resultant % strain was observed. DMA measurements of dried specimen were done at 1 Hz with a thin film tension clamp over the temperature range of -100 °C to 120 °C, using liquid nitrogen as a coolant. The flow rate of liquid nitrogen into the DMA depends upon the starting temperature desired and is controlled by the ramp rate or heating rate of 3 °C/min.

Measurements with AFM:

A Digital Instruments Multimode SPM with a NanoScope IIIa controller and an E-scanner (X-Y scanning limit of 15 µm and a Z limit of 2 µm), operated in the tapping mode, was used to observe surface morphologies of selected specimens. The latex samples were conditioned in an oven at 70 °C and 50% humidity for 8-10 hours and then stored at normal room conditions for a week before imaging. Both height and phase data were captured at image size of 1 × 1 µm for all samples. For every sample, two sets of images were captured. For each uncrosslinked conventional latex blend, nanolatex at six different concentrations (wt %), 0%, 15%, 30%, 50%,

70%, and 100%, were captured. For each pre-coalescence or post-coalescence crosslinked latex blend, nanolatex at five different concentrations (wt %), 0%, 15%, 30%, 50%, and 100% were captured.

Results and discussion

Theoretical considerations of film formation and properties by latex blends

A useful model of film formation by latexes involves three major, overlapping, stages.^{20, 24, 34-36} The third stage of film formation involves interdiffusion of polymer chains from different latex particles. Interdiffusion knits vestigial particles together and is essential if the polymer film is to realize the mechanical properties of which its composition is capable. Complete interdiffusion is not necessary, however; it is only necessary for the molecules from adjacent particles to interpenetrate to a distance comparable to the root-mean-square radius of gyration (R_G) of the individual molecules,³⁴ typically a smaller distance than the diameters of the original latex particles.

In this model, latexes with high T_g (above room temperature) are difficult to coalesce and interdiffuse, thus resulting in poor film formation. On the other hand, low T_g (below room temperature) latex polymers will easily interdiffuse resulting in better film formation but can not provide sufficient hardness and will have poor block resistance. Many investigators described^{2, 5-8, 11, 14, 18, 20} blending hard-soft and/or large-small particles latexes to achieve better film formation with improved film properties. Winnik and Feng²⁰ studied drying behavior of hard-soft latex blends, their mechanical properties and effect of surfactant on drying process. The group found that hard and soft latexes dried more slowly than the corresponding soft latexes alone. They investigated the transparency of latex films as a function of soft phase and particle diameter. They also reported that in the blend films, hard particles act as reinforcement fillers

and provide great improvement to the mechanical properties of films formed. Geurts et al.⁷ recently proposed a theoretical model for latex blend in which the hard polymer builds an internal film structure along the edges of the particles of the soft polymer, wherein the soft polymer forms a coherent film under ambient conditions, and the internal structure of the hard polymeric material present in a limited amount provides the required hardness.

Schmidt et al.¹⁶ produced bimodal size blends of poly (styrene-co-butyl acrylate) particles and claimed that the bimodal size latex produces film with superior luster due to the improved packing efficiency of bimodal latex particles. Eckersley and Helmer⁵ demonstrated that particle size ratio of soft/hard constituent latexes has a significant effect on end-use properties and resulting morphology of latex blends. They reported that when $R_{\text{soft}}/R_{\text{hard}} \gg 1$ (where R is the radius of the latex particle), the hard phase acts as reinforcing filler, thus increasing bulk modulus of the film. Farris and Agarwal¹ published a complete study of the mechanical properties and morphology of acrylic latex blends. The results of the study showed that phase inversion to a continuous hard matrix from the soft one occurs around 30-40% of hard phase content. Tang et al.¹⁷ reported that compatibility between two polymer phases distribution and packing behavior of dispersed hard particles in a continuous soft matrix, can greatly affect resulting mechanical properties of latex blends. They showed that surface modification of the hard phase can greatly influence the particle distribution in the continuous phase, and dynamic mechanical properties of blends through the mechanism of glassy interphase formation. Colombini et al.^{3,4} thoroughly investigated viscoelastic properties and morphology of latex blends. They reported that the mechanical behavior of latex blends is governed by the mechanical properties of the neat constituents, the morphology, the interfacial activity between the phases, and the effect of polymerization route on the amount of interphases

and blend composition. Xu et al.³⁷ demonstrated that crosslinking could help produce cohesive films of incompatible polymers. In general, the latex polymers used in most of the above studies had particle sizes ranging from 40nm to 400 nm and contained no functional (crosslinkable or crosslinked) group.

In this research, the large (~120 to 130 nm) and small (~ 20 to 25nm) particles are sized so that the nanoparticles can fill the hollow spaces between the larger particles during the late stages of particle coalescence and the early stages of interdiffusion assuming unimpeded interdiffusion of polymer chains between latex particles.

Film formation by “pre-coalescence” and “post-coalescence” crosslinked latexes

Theoretical considerations of film formation by pre-coalescence and post-coalescence crosslinked latexes have been extensively covered in Chapters 3 and 4 but are briefly included here for completeness.

(a) Film formation by “pre-coalescence” crosslinked latexes:

Films were cast from the internally (pre-coalescence) crosslinked latexes by conventional means. No coalescing solvent was used; film formation was accelerated by warming the films at 70°C overnight. Film thicknesses were about 50 µm. Theoretical considerations of film formation by pre-coalescence crosslinked latexes have been studied extensively by Zosel and Ley,³⁸ Tamai et al.,³⁹ Aradian et al.,⁴⁰ and Ghazaly et al.⁴¹⁻⁴³ In Chapter 3 a systematic comparison of pre-coalescence crosslinked latexes with varying levels of crosslinking monomers was covered. It was demonstrated that with low levels (up to 2 wt%) of internal crosslinking, latex films are able to coalesce to form good films. At higher levels (above 2 wt%) of 1,-

BGDMA, often the interdiffusion of polymeric particles is impeded by crosslinking, hence, resulting in inferior film properties.

(b) *Film formation by “post-coalescence” crosslinked latexes:*

The DAA-containing latexes are combined with a stoichiometric amount of adipic dihydrazide (ADDH) crosslinker. Then the films were cast under the same conditions as for internally or pre-coalescence crosslinked latexes. Before the film was cast, premature reaction of ADDH with the reactive sites in the latex was minimal.^{21-26, 44, 46} The crosslinking reaction for the DAA monomer is shown below. The ADDH is water soluble, and almost all of it remains separated from the reactive sites in the serum where it is. The relatively high (9–9.5) pH also suppresses the reaction. When the film is cast, however, the water evaporates, forcing ADDH to come in contact with the latex polymer surfaces when close packing of the latex particles has occurred; ammonia evaporates, lowering the pH to about 6.5 and then crosslinking accelerates.⁴⁴

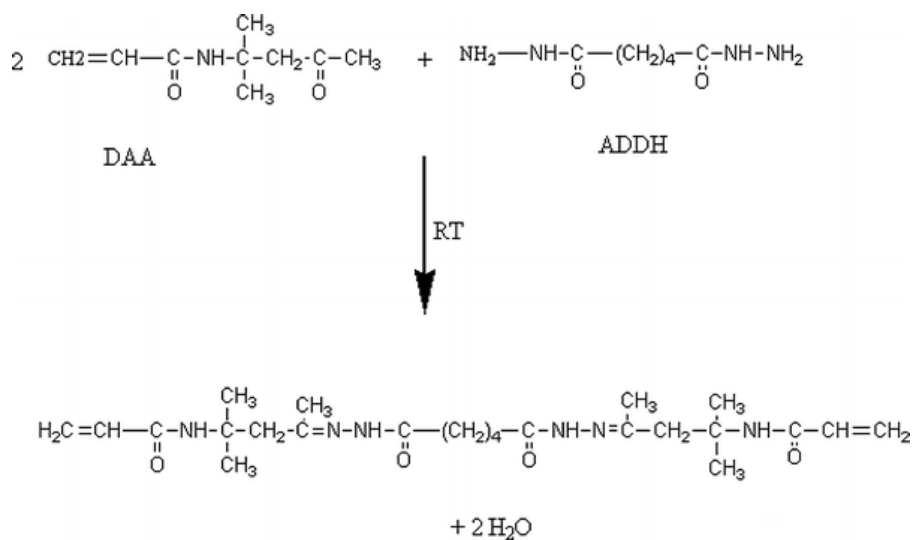


Figure 5.2: crosslinking reaction for DAA monomer

After the film is cast, the crosslinking reaction is known to proceed at a useful rate at room temperature. In this study the latex films were baked overnight at 70°C to assure a high level of conversion before testing and to avoid the use of coalescing solvents. Among the factors that will influence final properties of the films are the composition of the latexes, and the relative rates of

- mixing of the crosslinker with the polymer,
- interdiffusion of the polymer molecules that originated in different latex particles,
- the chemical crosslinking reactions and diffusion of ADDH into the polymer,²⁶ and
- T_g of latex at a specific composition.

As demonstrated earlier,^{22, 23} to reach a high level of conversion the bake temperature should be well above the T_g of the specific latex composition. In this study, this is true for the low T_g latex (both pre-coalescence and post-coalescence crosslinked latexes). However, it may be borderline for high T_g latex (both pre-coalescence and post-coalescence crosslinked latexes). This was discussed in detail elsewhere.^{22, 23}

If the rate of the crosslinking reaction is too fast relative to mixing and interdiffusion, coalescence and interdiffusion will be slowed and perhaps retarded prematurely. The likely result will be excessively non-uniform films and less than optimal film properties. Some researchers^{22-26, 29, 44} report that the DAA/ADDH crosslinking combination has satisfactory relative rates and good film properties can be attained.

Minimum film formation (MFT) crack point and knife point temperature, MDSC T_g :

MFT crack point [MFTc] and knife point [MFTk] of latex blends with different weight ratios of nanolatex (with or without functional group) in conventional size functional latexes are

shown in Table 5.4. Table 5.5 shows the respective glass transition temperatures, T_g , of latex blends measured using MDSC. For comparisons, their respective neat constituents, conventional and nanoparticle latexes are included in each table.

Overall, for all latex blends samples, at different ratios of nano/conventional latexes, similar trends are observed when comparing the results of MFTk, MFTc data and their respective MDSC T_g . In general, when the T_g 's of the components were different, and the T_g 's of the films fell in between. The data were not entirely linear; however, the blends displayed a modest upward bias from linearity. The results from Tables 5.4(a), (b) and Table 5.5 showed that increasing the levels of nanolatex in the blends – particularly at 15 wt% or more, in general, showed a significant decrease in the crack point, knife point, and MDSC T_g temperatures. At 7.5 wt% of nanolatex in the blend, negligible effects are observed when compared to their conventional size neat constituents.

When a low T_g non-crosslinked conventional latex (L0) is blended with a nanolatex, either (a) with non-crosslinked (L0_nL0 blend) or (b) with 4% pre-coalescence crosslinker (L0_nIL4 blend), a marginal decrease in crack point, knife point, and MDSC T_g is observed. When a 2% post-coalescence crosslinked nanoparticle latex is blended with a non-crosslinked conventional latex, L0_nEL2 blend, a significant decrease in the minimum film formation temperatures and glass transition temperature was observed, particularly at or above 30 wt% of nanolatex in the blend. As shown in tables below, L0: MFTc = 1.25⁰C, MFTk= 11.9⁰C, and MDSC T_g is = 7⁰C when compared to L0_nEL2: at 30% nEL2, MFTc = <0⁰C, MFTk = 10.9⁰C, and MDSC T_g = 4.95⁰C.

When a low T_g pre-coalescence crosslinked latex was blended with a non-crosslinked nanolatex, IL4_nL0 blend, a significant decrease in the MFTs and MDSC T_g was observed in blends with 50 wt% or more nanolatex. In the case of low T_g post-coalescence crosslinked latex when blended with a non-crosslinked nanolatex, EL5_nL0 blend, surprisingly negligible differences were observed as a function of wt% nanolatex for MFT and most T_g values.

In the case of a high T_g conventional latex, crosslinked or non-crosslinked, when blended with a low T_g nanoparticle latex, crosslinked or non-crosslinked, showed sharp decreases in crack point, knife point, and MDSC T_g values, particularly at or above 15 wt% of nanolatex present in the blends. For example, H0_nL0 at 0% nanolatex showed $MFT_c = 19.6^\circ\text{C}$, $MFT_k = 22^\circ\text{C}$ that decreases to 16.85°C at 15% nL0, 14.3°C at 30% nL0, 12.1°C at 50% nL0 and $MFT_c = 5.2^\circ\text{C}$, $MFT_k = 9.7^\circ\text{C}$ at 70% nL0 present in the MFTk blend. Similarly, in case of EH5_nL0 at 0% nL0 the $MFT_c = 20.2^\circ\text{C}$, $MFT_k = 27.4^\circ\text{C}$, MDSC $T_g = 29.7^\circ\text{C}$; all continued to decrease at increasing levels of nL0 in the blend. In fact, at 70% nL0 present: $MFT_c = 13.8^\circ\text{C}$, $MFT_k = 19.7^\circ\text{C}$, and MDSC $T_g = 22.1^\circ\text{C}$. From these results it can be speculated that the nanosize latexes may facilitate the coalescence process in high T_g conventional size latex particles. This speculation is supported by the fact that some nanoparticle latexes have molecules compressed into volumes that are smaller than their normal RMS radius of gyration, a thermodynamically uncomfortable situation, and coalescence gives the molecules an opportunity to gain their normal dimensions, a thermodynamically favored transition. Earlier research by Fu et al.⁴⁵ and Ming et al.³⁰⁻³³ support the speculation. Typically, in commercial practice, coalescing aids or plasticizers are used to temporarily depress or reduce MFT of high T_g latexes. Use of nanosize latexes to reduce MFT of high T_g latexes could potentially reduce or conceivably eliminate air-polluting solvents from a typical latex paint formulation.

Table 5.4 (a): MFT crack point (MFTc) of latex blends:

Latex blend sample (conventional size latex_nanosize latex)	% nano by wt.						
	0%	7.5%	15%	30%	50%	70%	100%
L0_nL0	1.25 ± 0.1	1.6 ± 0.2	0.55 ± 0.1	0.43 ± 0.1	0.46 ± 0.1	<0	<0
L0_nIL4	1.25 ± 0.1	1.5 ± 0.4	1.63 ± 0.5	1.48 ± 0.2	1.35 ± 0.1	<0	<0
L0_nEL2	1.25 ± 0.1	0.65 ± 0.1	0.25 ± 0.3	<0	<0	<0	<0
H0_nL0	19.6 ± 1.1	19.2 ± 0.6	16.85 ± 0.5	14.3 ± 0.9	12.1 ± 0.2	5.2 ± 0.3	<0
H0_nIL2	19.6 ± 1.1	19.3 ± 0.8	19.1 ± 0.3	14 ± 0.7	14.4 ± 0.1	8.9± 0.2	<0
H0_nEL5	19.6 ± 1.1	18.9 ± 0.9	17.6 ± 1.5	16.3 ± 0.5	14.6± 0.3	13.5± 0.8	<0
EL5_nL0	<0	<0	<0	<0	<0	<0	<0
IL4_nL0	6.8 ± 0.1	6.1± 0.3	5.7 ± 0.2	4.8± 0.4	4.2± 0.2	<0	<0
EH5_nL0	20.2 ± 1.3	19.4± 0.3	18.7 ± 0.7	19± 0.2	14.2± 0.5	13.8± 0.6	<0
IH4_nL0	29.3 ± 0.7	28.2± 0.7	26.4 ± 1.2	25.2± 0.8	24.5± 0.9	<0	<0

Table 5.4 (b): MFT knife point (MFTk) of latex blends:

Latex blend sample (conventional size latex nanosize latex)	% nano by wt.						
	0%	7.5%	15%	30%	50%	70%	100%
L0_nL0	11.9 ± 0.1	13.2 ± 0.3	13.6 ± 0.2	12.2± 0.2	12.8 ± 0.1	10.1 ± 0.3	9.7 ± 0.2
L0_nIL4	11.9 ± 0.1	11.6 ± 0.2	11.8 ± 0.6	11.3 ± 0.4	11.5 ± 0.3	10 ± 0.5	13.2 ± 0.1
L0_nEL2	11.9 ± 0.1	11.3 ± 0.3	11.75 ± 0.1	10.9 ± 0.5	8.93 ± 0.3	8.8 ± 0.2	7.33 ± 0.5
H0_nL0	22 ± 1	21.6 ± 0.3	19.3 ± 0.5	16.7 ± 0.3	14.5 ± 0.6	7.6 ± 0.3	9.7 ± 0.2
H0_nIL2	22 ± 1	21.7 ± 0.3	21.5 ± 0.6	16.4 ± 0.9	16.8 ± 0.8	11.3 ± 0.5	9.2 ± 0.1
H0_nEL5	22 ± 1	21.3 ± 0.9	23 ± 0.6	18.7 ± 0.4	17 ± 0.3	15.9 ± 0.2	10.1 ± 0.1
EL5_nL0	7.1 ± 0.1	8.5 ± 0.1	8.1 ± 1.4	7.9 ± 0.7	7.5 ± 0.6	8.8 ± 0.1	9.7 ± 0.2
IL4_nL0	14.6 ± 0.3	14.7 ± 0.1	13.7 ± 0.5	12.9 ± 0.9	12.5 ± 0.8	8.7 ± 0.3	9.7 ± 0.2
EH5_nL0	27.4 ± 0.7	24.4 ± 0.8	24.9 ± 0.4	24.1 ± 1.1	20.1 ± 0.6	19.7 ± 0.1	9.7 ± 0.2
IH4_nL0	> 33	32.2 ± 1.2	31.8 ± 2.4	28.3 ± 1.8	27.6 ± 1.7	11.5 ± 0.1	9.7 ± 0.2

Table 5.5. MDSC T_g of latex blends:

Latex blend sample (conventional size latex nanosize latex)	% nano by wt.						
	0%	7.5%	15%	30%	50%	70%	100%
L0_nL0	7.05	7.4	6.38	6.23	6.26	4.9	4.77
L0_nIL4	7.05	7.10	7.17	7.10	7.08	5.5	10.9
L0_nEL2	7.05	7.2	7.62	4.95	4.8	4.6	3.13
H0_nL0	26.3	25.9	23.5	21.0	18.8	11.9	4.77
H0_nIL2	26.3	26.1	25.7	20.8	21.2	15.7	4.67
H0_nEL5	26.3	25.7	24.5	23.1	21.4	20.3	5.15
EL5_nL0	11.6	10.5	10.1	9.9	9.77	4.7	4.77
IL4_nL0	14.6	12.8	11.62	11	10.8	4.7	4.77
EH5_nL0	29.7	26.7	25.8	26.5	22.5	22.1	4.77
IH4_nL0	33	32.8	31.9	29.8	29.1	4.11	4.77

End-use film properties

All the latex blends samples were cast on pre-treated aluminum panels and baked at 70 °C and 50% humidity for 8-10 hours and then stored at normal room conditions for a week before testing. The goal of baking was to assure high coalescence and conversion before testing and to avoid the complication of coalescing solvents. The end-use properties are listed in Tables 5.6-5.10. For comparison, their respective neat conventional latex and nanoparticle latexes are included in the tables.

Table 5.6: Cross- cut Adhesion (ASTM D 3359) of latex blends:

	L0_nL0	L0_nIL4	L0_nEL2	H0_nL0	H0_nIL2	H0_nEL5	EL5_nL0	IL4_nL0	EH5_nL0	IH4_nL0
0%	4B	4B	4B	4B	4B	4B	4B	3B	5B	3B
7.5%	5B	5B	5B	5B	5B	5B	5B	5B	5B	3B
15%	5B	5B	5B	5B	5B	5B	5B	5B	4B	1B
30%	5B	5B	5B	5B	5B	5B	5B	5B	5B	2B
50%	5B	5B	5B	5B	5B	5B	5B	5B	5B	4B
70%	5B	5B	5B	5B	5B	5B	5B	5B	5B	3B
100%	5B	5B	5B	5B	5B	5B	5B	5B	5B	5B

Table 5.7: Pencil Hardness (ASTM D 3363) of latex blends:

%nano by wt.	Latex blend sample (conventional size latex nanosize latex)									
	L0_nL0	L0_nIL4	L0_nEL2	H0_nL0	H0_nIL2	H0_nEL5	EL5_nL0	IL4_nL0	EH5_nL0	IH4_nL0
0%	4B	4B	4B	4B	4B	4B	2B	4B	B	5B
7.5%	4B	3B	3B	HB	F	F	HB	B	H	2H
15%	2B	HB	B	B	HB	HB	B	HB	HB	F
30%	2B	HB	B	B	HB	B	B	F	H	B
50%	4B	B	B	B	B	B	B	B	H	B
70%	4B	B	B	B	B	B	3B	2B	B	3B
100%	4B	4B	4B	4B	4B	B	4B	4B	4B	4B

Table 5.8: Solvent Resistance (MEK 2 Rub) of latex blends:

%nano by wt.	Latex blend sample (conventional size latex nanosize latex)									
	L0_nL0	L0_nIL4	L0_nEL2	H0_nL0	H0_nIL2	H0_nEL5	EL5_nL0	IL4_nL0	EH5_nL0	IH4_nL0
0%	5	5	5	7	7	7	83	6	106	4
7.5%	6	12	15	9	13	16	112	12	120	10
15%	5	12	24	10	12	20	110	10	125	12
30%	6	30	25	16	13	18	113	10	115	10
50%	6	10	22	20	15	20	100	13	110	12
70%	7	10	20	18	12	15	70	8	75	14
100%	15	20	75	15	17	100	15	15	15	15

Table 5.9: Elevated Temperature Block Resistance (ASTM D 4946) of latex blends:

%nano by wt.	Latex blend sample (conventional size latex_ nanosize latex)									
	L0_nL0	L0_nIL4	L0_nEL2	H0_nL0	H0_nIL2	H0_nEL5	EL5_nL0	IL4_nL0	EH5_nL0	IH4_nL0
0%	3 ± 1	3 ± 1	3 ± 1	9	9	9	9 ± 1	4 ± 1	9	9
7.5%	9	8	9	10	10	10	10	9	10	10
15%	3 ± 1	5 ± 1	8 ± 1	10	9	10	9	5 ± 1	9	9
30%	6 ± 1	4 ± 1	7 ± 1	9	9	9	9	4 ± 1	10	9
50%	4 ± 1	5	6 ± 1	8 ± 1	9 ± 1	9	10	5 ± 1	10	10
70%	4 ± 1	5 ± 1	6	7 ± 1	8	8	9 ± 1	5 ± 1	9	9
100%	3 ± 1	2 ± 1	1	3 ± 1	1	4 ± 1	3 ± 1	3 ± 1	3 ± 1	3 ± 1

Table 5.10: Acid - Open Spot Test (ASTM D 1308) of latex blends:

%nano by wt.	Latex blend sample (conventional size latex_ nanosize latex)																													
	L0_nL0			L0_nIL4			L0_nEL2			H0_nL0			H0_nIL2			H0_nEL5			EL5_nL0			IL4_nL0			EH5_nL0			IH4_nL0		
	15 min.	1 hr.	16 hr.	15 min.	1 hr.	16 hr.	15 min.	1 hr.	16 hr.	15 min.	1 hr.	16 hr.	15 min.	1 hr.	16 hr.	15 min.	1 hr.	16 hr.	15 min.	1 hr.	16 hr.	15 min.	1 hr.	16 hr.	15 min.	1 hr.	16 hr.	15 min.	1 hr.	16 hr.
0	E	E	F	E	E	F	E	E	F	E	G	F	E	G	F	E	G	F	E	E	G	E	G	F	E	G	F	E	G	P
7.5%	E	E	G	E	E	E	E	E	E	E	E	E	E	G	G	E	E	G	E	E	E	E	G	E	E	G	F	E	G	G
15%	E	E	G	E	E	E	E	E	E	E	E	E	E	E	E	E	E	E	E	E	G	E	E	E	G	G	F	E	G	G
30%	E	G	E	G	G	G	E	E	E	E	E	E	G	G	G	G	E	F	E	G	G	E	E	E	E	E	G	G	G	G
50%	E	G	E	G	G	G	E	E	E	E	E	E	G	G	F	E	E	G	E	E	G	E	E	E	E	E	E	E	G	G
70%	E	G	E	G	G	G	E	G	G	E	G	E	G	F	P	E	E	G	E	E	G	E	E	G	E	G	G	E	G	E
100%	E	G	E	G	G	G	E	G	G	E	G	E	G	F	P	E	E	E	E	G	E	E	E	E	G	E	E	E	G	E

E: Excellent, no change; G: Good, slightly white, but recovered quickly; F: Fair, whitening, becomes transparent after 24 hours; P: Poor, permanent damage.

Table 5.11: Water - Open Spot Test (ASTM D 1308) of latex blends:

%nano by wt.	Latex blend sample (conventional size latex_ nanosize latex)																													
	L0 nL0			L0 nIL4			L0 nEL2			H0 nL0			H0 nIL2			H0 nEL5			EL5 nL0			IL4 nL0			EH5 nL0			IH4 nL0		
	15 min.	1 hr.	16 hr.	15 min.	1 hr.	16 hr.	15 min.	1 hr.	16 hr.	15 min.	1 hr.	16 hr.	15 min.	1 hr.	16 hr.	15 min.	1 hr.	16 hr.	15 min.	1 hr.	16 hr.	15 min.	1 hr.	16 hr.	15 min.	1 hr.	16 hr.	15 min.	1 hr.	16 hr.
0	E	E	G	E	E	G	E	E	G	E	E	G	E	E	G	E	E	G	E	E	E	E	E	F	E	G	G	E	E	P
7.5%	E	E	E	E	E	G	E	E	G	E	E	G	E	E	G	E	E	G	E	E	E	E	E	G	E	G	G	E	E	G
15%	E	E	E	E	E	E	E	E	G	E	G	F	E	E	G	E	E	F	E	E	E	E	E	E	E	G	G	E	G	G
30%	E	E	E	G	E	E	E	G	G	E	G	F	E	G	G	G	E	E	E	G	E	E	E	E	E	G	G	E	E	G
50%	E	E	E	E	E	E	E	G	G	E	G	G	E	E	F	G	E	F	E	E	E	E	E	E	E	G	G	E	E	G
70%	G	G	G	G	G	G	E	G	G	G	F	F	G	E	F	G	G	F	G	G	G	G	G	G	G	F	F	G	G	G
100%	F	F	F	F	F	P	E	F	F	F	F	F	G	E	P	G	F	F	F	F	F	F	F	F	F	F	F	F	F	F

E: Excellent, no change; G: Good, slightly white, but recovered quickly; F: Fair, whitening, becomes transparent after 24 hours; P: Poor, permanent damage.

Table 5.12: Specular Gloss (ASTM D 523) of latex blends:

%nano by wt.	Specular Gloss test results (ASTM D 523)																					
	Latex blend sample (conventional size latex_ nanosize latex)																					
	L0 nL0		L0 nIL4		L0 nEL2		H0 nL0		H0 nIL2		H0 nEL5		EL5 nL0		IL4 nL0		EH5 nL0		IH4 nL0			
	20°	60°	20°	60°	20°	60°	20°	60°	20°	60°	20°	60°	20°	60°	20°	60°	20°	60°	20°	60°		
0%	18.1 ± 2.1	38.9 ± 5.1	18.1 ± 2.1	38.9 ± 5.1	18.1 ± 2.1	38.9 ± 5.1	19.2 ± 1.3	34.6 ± 1.3	19.2 ± 1.3	34.6 ± 1.3	19.2 ± 1.3	34.6 ± 1.3	19.1 ± 1.6	36.7 ± 3.8	11.6 ± 1.6	32.4 ± 2.9	23.2 ± 5.6	50.1 ± 2.3	19 ± 0.3	37.8 ± 2.3		
7.5%	14.7 ± 0.1	50.6 ± 1.6	15.3 ± 0.9	50 ± 1.2	14.3 ± 0.6	53.4 ± 0.2	49.3 ± 1.6	77.5 ± 1.3	58.6 ± 1.2	81.8 ± 0.1	61.3 ± 0.4	81.1 ± 0.3	24.2 ± 5.1	56.3 ± 7.3	14.4 ± 2.8	53.7 ± 6	43.6 ± 2.9	73.3 ± 7.5	14.5 ± 1.9	50.2 ± 0.2		
15%	38.7 ± 3.4	72.5 ± 1.6	35.4 ± 0.6	76 ± 1.8	46.1 ± 2.6	68.1 ± 7.1	73.2 ± 1.6	92.7 ± 2.9	59.8 ± 2.4	80.1 ± 2	73.2 ± 2.3	97.1 ± 3.1	42.7 ± 2.3	70 ± 2.1	47.6 ± 3.3	65.8 ± 3.1	68.2 ± 2.7	82.2 ± 2.6	41.7 ± 0.6	73.5 ± 0.9		
30%	42.6 ± 4.3	68.8 ± 4.5	48.2 ± 0.3	73.2 ± 2.3	47.2 ± 5.6	76.3 ± 2.9	57.8 ± 2.4	80.4 ± 0.8	41.8 ± 1.8	74.6 ± 4	58.6 ± 3.8	84.2 ± 2.6	52.6 ± 4	78.6 ± 2.6	48.8 ± 0.8	70.6 ± 3.4	54.8 ± 2.2	78.2 ± 1.6	49.6 ± 2.8	80.5 ± 3		
50%	15.2 ± 2.9	46.6 ± 3	38.1 ± 6	73.3 ± 4	36.5 ± 1.1	77.7 ± 2	64.6 ± 1.4	86.1 ± 2.3	46.8 ± 0.9	77.9 ± 0.1	64.8 ± 2	88.2 ± 2.4	48.8 ± 1.3	82.5 ± 0.5	40.6 ± 0.5	78.3 ± 2.5	46.7 ± 3.4	80.4 ± 1.8	54.8 ± 2.6	87.6 ± 2		
70%	15.6 ± 0.3	45.8 ± 2.1	42.5 ± 4.2	71.5 ± 2.8	38.4 ± 6.2	73.2 ± 3.9	27.5 ± 0.1	67.5 ± 0.3	40.3 ± 0.7	79.1 ± 0.4	35.3 ± 0.1	75.8 ± 0.4	45.7 ± 2.6	79.4 ± 0.9	31.8 ± 2.6	74.5 ± 3.6	31.7 ± 1	71 ± 1.6	44.6 ± 2.4	71.6 ± 2.9		
100%	49.3 ± 7.9	79.4 ± 5.6	39.3 ± 3.9	87.6 ± 2.6	50.9 ± 3.6	77.9 ± 1	49.3 ± 7.9	79.4 ± 5.6	40.3 ± 4.1	85.8 ± 0.8	52.2 ± 6.7	86.2 ± 2.6	49.3 ± 7.9	79.4 ± 5.6	49.3 ± 7.9	79.4 ± 5.6	49.3 ± 7.9	79.4 ± 5.6	49.3 ± 7.9	79.4 ± 5.6		

Table 5.6 shows crosscut adhesion test results for all latex blends samples with different concentration ranges. The results indicate that in general the addition of nanosize latexes increases the tape adhesion to aluminum 4B (good) to 5B (excellent, the highest rating in this test). For nine of the ten blends, adhesion of all films containing nanoparticles was 5B. The exceptions were films that included a highly crosslinked (pre-coalescence; e.g., IH4) latex. However, the very crude nature of the crosscut adhesion test (ASTM) does not allow an assessment of how much adhesion was improved. The difference between 4B (good) and 5B (the top rating) can be modest or large. Further, the data can be rationalized on the basis that nanoparticles are much better able to conform to irregularities in the substrate surface than conventional latex particles, especially when the nanoparticles have T_g 's below the film formation conditions.

The pencil hardness results are shown in Table 5.7 for all latex blend series with different concentrations of nanoparticle latexes. In general the pencil hardness grade improves, particularly at 7.5 to 30 % by wt. of nanoparticle polymers. The pencil hardness values do correlate to some degree with T_g , but more strongly to the level of nanoparticles (or particle packing) and secondly, to the degree of crosslinking (or degree of chain entanglement between the particles) in the film brought about by crosslinking either in the conventional or nanoparticles latexes. See Table 5.7 for values of pencil hardness of H, 2H, and HB, which generally optimizes at 7.5%, 15% and 30% concentration of nanoparticles. The effect of crosslinking and T_g on pencil hardness is strongly seen in EH5_nL0 concentrations. To give another example: the blended film with 15% post-coalescence crosslinked nanolatex (H0_nEL5, 15%) was superior to films cast from 100% post-coalescence cross-linked conventional latex (EL5) with no nanoparticles. MDSC T_g 's of the films in Table 5.5 were 24.5 °C (H0_nEL5, 15%) and 11.6 °C

(EL5, 100%). The blended film was significantly superior in tensile properties and in pencil hardness. This result is appealing because it achieves superior film properties with an 85% reduction of the amount of crosslinker required in conventional technology. It should also be noted here that in general, properties of coatings depend on both the bulk properties of film and its surface, and near-surface, properties. To give an example, pencil hardness depends upon compressive strength and tear strength of the bulk material and often on adhesion to the substrate and on slipperiness of the outer surface.

The solvent resistance (MEK 2 rubs) test results are shown in Table 5.8. In general, it is noteworthy that the solvent resistance of the all-thermoplastic blends improved modestly, again suggesting that the nanoparticles are able to improve the coalescence and interpenetration of the polymer molecules during film formation, independent of crosslinking. However, the auxiliary effect of crosslinking on solvent resistance (MEK 2 rubs) was most strongly seen in EL5_nL0 (low T_g blends) and EH5_nL0 (high T_g blends) as well as in 100% nanoparticle nEL5 and nEL2 films. This improvement in properties is due to chain entanglement and interdiffusion between particles due to external crosslinking. Interestingly the modest level of nanoparticle addition improves MEK rubs even where there is no crosslinking, such as H0_nL0 series or at the modest levels of total crosslinking for example H0_nEL5. In both of these cases, the T_g of the mixture is high, around 20+. This factor in addition to the packing affects the crosslinking.

Table 5.9 shows elevated temperature block resistance values of the latex blends. In general, the block resistance correlates primarily to the blend T_g (high), secondarily to crosslinking in the nanoparticle or conventional latex particle, and thirdly to particle packing in the blend at some specific nanoparticle composition. This last point with respect to particle packing is illustrated by IL4_nL0 (7.5%); and L0_nL0, L0_nIL4, at 7.5%. The most unusual

result was for L0_nEL2 series of blends at up to 70% of nEL2 addition. The highest block number is at 7.5%, L0_nEL2 (9 - excellent) and the second highest block number is at 15% of nEL2 in latex blend (8 - very good) when compared to 100% L0 (block number rating 3 – poor). Typically the block resistance of low T_g latexes is poor. This is one of the reasons why low T_g latexes are blended with high T_g latexes. This is not the case here. The unusually high block ratings of the L0_nEL2 blend series produce an unexpected result. One explanation could be based on the percolation theory as explained by Eckersley and Helmer.⁵ They demonstrated that high particle size ratio of constituent latexes has a significant effect on block resistance and other end-use properties of latex blend. This could also be happening in this case since the large particle size latexes are ~ 120nm vs. nanosize latexes are ~ 20-25nm, a size ratio of 5 to 6. Also, homogeneous distribution of functional group across the polymer particle and effect of extra surfactant from nanoparticle, conceivably thermodynamic effect of allowing constrained molecules in nanoparticles to extend to RMS dimensions can play significant role in improving final properties of the latex blends.

Table 5.12 shows 20° and 60° specular gloss values of the latex blends. In general, the gloss values (20° and 60°) tend to optimize at 15 and 30% concentration of nanoparticles when compared to the 0% nanoparticle composition, which in many cases is close to values obtained at 100% nanoparticles, which ideally should provide the optimum gloss levels because of particle packing in the nanosize regime. Thus the 15 to 30% concentration range is more or less equivalent to gloss achieved at 100% nanoparticles. It is clear that inclusion of nanoparticles increases specular gloss at 20° and 60° . The increase in gloss is noteworthy because it overcomes a long-standing limitation of conventional latexes, their inability to form films with high gloss.

Further, the increase in the specular gloss can be explained on the basis that nanoparticles tend to populate the surface as the films form, making the surfaces smoother.

To verify this explanation, atomic force microscopy (AFM) images of the films were taken. The results were mixed. Often the images gave a clear visual impression of smoother films with nanoparticles, but not always. The AFM micrographs are shown in Figures 5.2-5.12, for each latex blend with different concentrations of nanolatex. Perusal of these images suggests a correlation between visual impression and measured gloss, although the correlation is imperfect. Note that the smoothest appearing image (disregarding the artifacts) is the 85/15 blend, which has the highest gloss. However, it is difficult to explain why the films with higher nanoparticle levels appear rougher and had lower gloss.

The atomic force microscope's software includes a program that enables calculation of average roughness (Ra) of the surface. This calculation was performed for all specimens. Examples of the outcomes are shown in Figures 5.13-5.23. In these figures, the reciprocal of Ra (termed average "relative surface smoothness") is plotted along with the gloss readings at 20° and 60° against % of nanoparticles by weight. The results show reasonably good correlation. In other cases the correlation is usually similar, but sometimes not as good. Overall, nanolatex at 15% concentration showed the highest gloss and smoothness that correlated well with the visuals of the images from AFM.

Figure 5.3. L0_nL0 (from left to right - nanolatex concentration: 0%, 15%, 30%, 50%, 70%, and 100%):

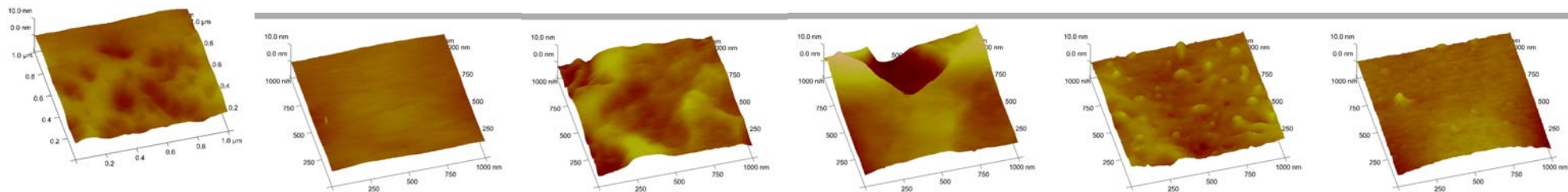


Figure 5.4. L0_nIL4 (from left to right - nanolatex concentration: 0%, 15%, 30%, 50%, 70%, and 100%):

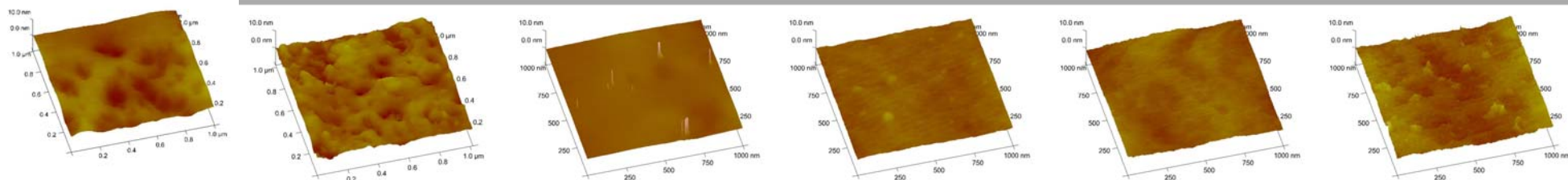


Figure 5.5. L0_nEL2 (from left to right - nanolatex concentration: 0%, 15%, 30%, 50%, 70%, and 100%):

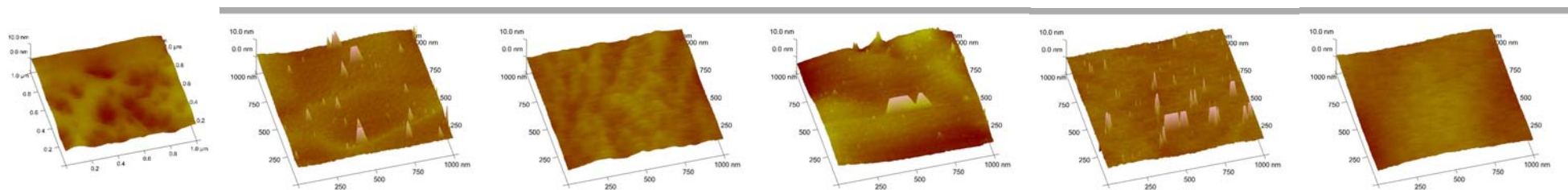


Figure 5.6. H0_nL0 (from left to right - nanolatex concentration: 0%, 15%, 30%, 50%, 70%, and 100%):

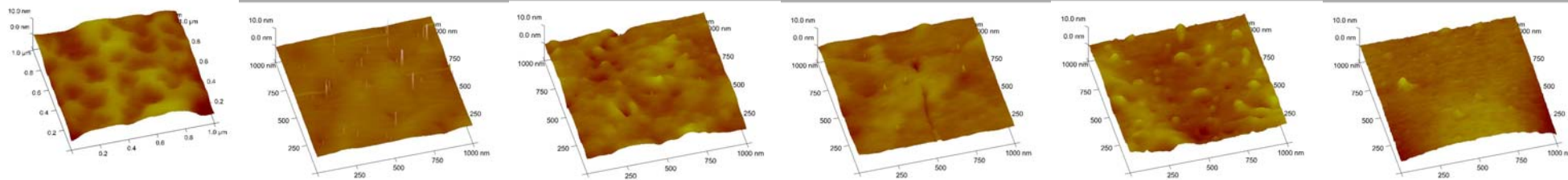


Figure 5.7. H0_nIL2 (from left to right - nanolatex concentration: 0%, 15%, 30%, 50%, 70%, and 100%):

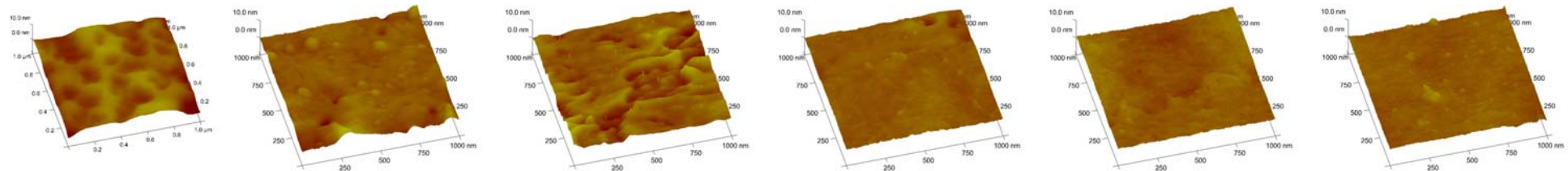


Figure 5.8. H0_nEL5 (from left to right - nanolatex concentration: 0%, 15%, 30%, 50%, 70%, and 100%):

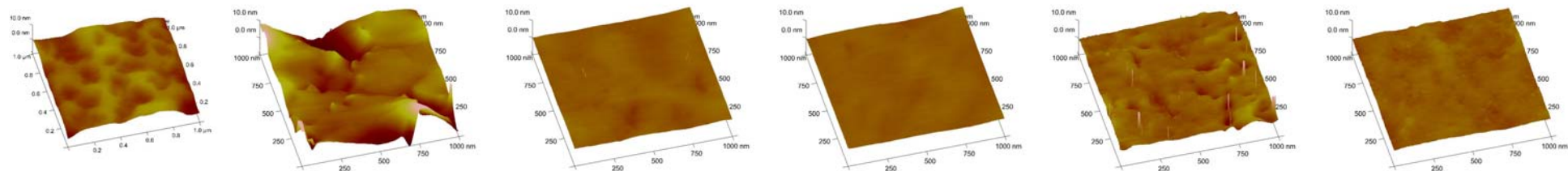


Figure 5.9. EL5_nL0 (from left to right - nanolatex concentration: 0%, 15%, 30%, 50%, 70%, and 100%):

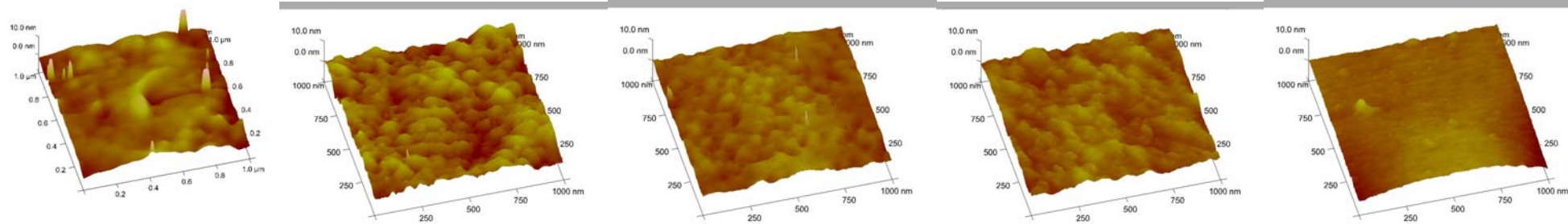


Figure 5.10. IL4_nL0 (from left to right - nanolatex concentration: 0%, 15%, 30%, 50%, 70%, and 100%):

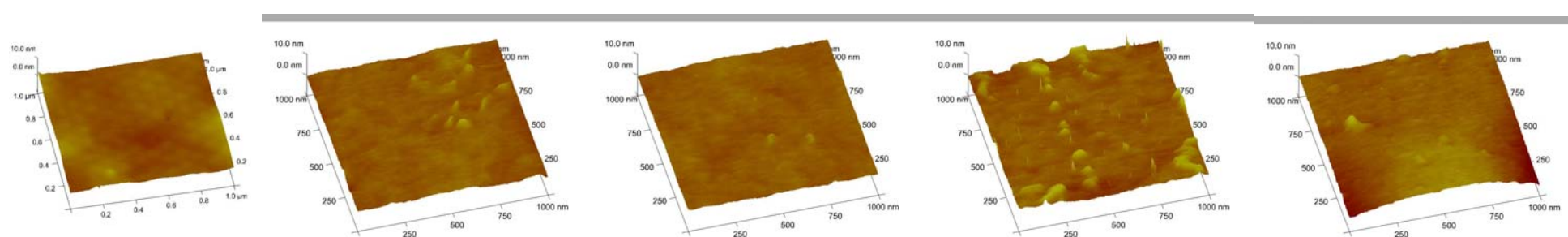


Figure 5.11. EH5_nL0 (from left to right - nanolatex concentration: 0%, 15%, 30%, 50%, 70%, and 100%):

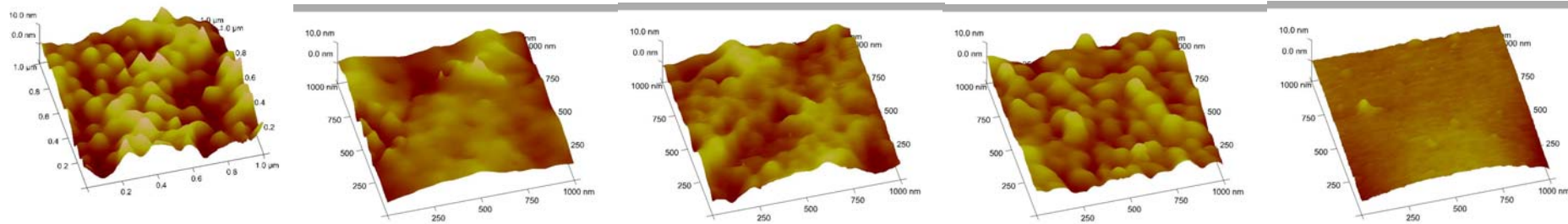
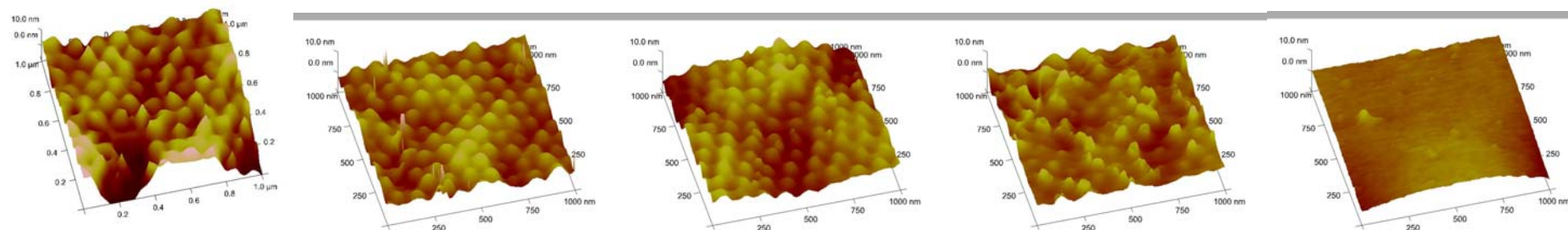


Figure 5.12. IH4_nL0 (from left to right - nanolatex concentration: 0%, 15%, 30%, 50%, 70%, and 100%):



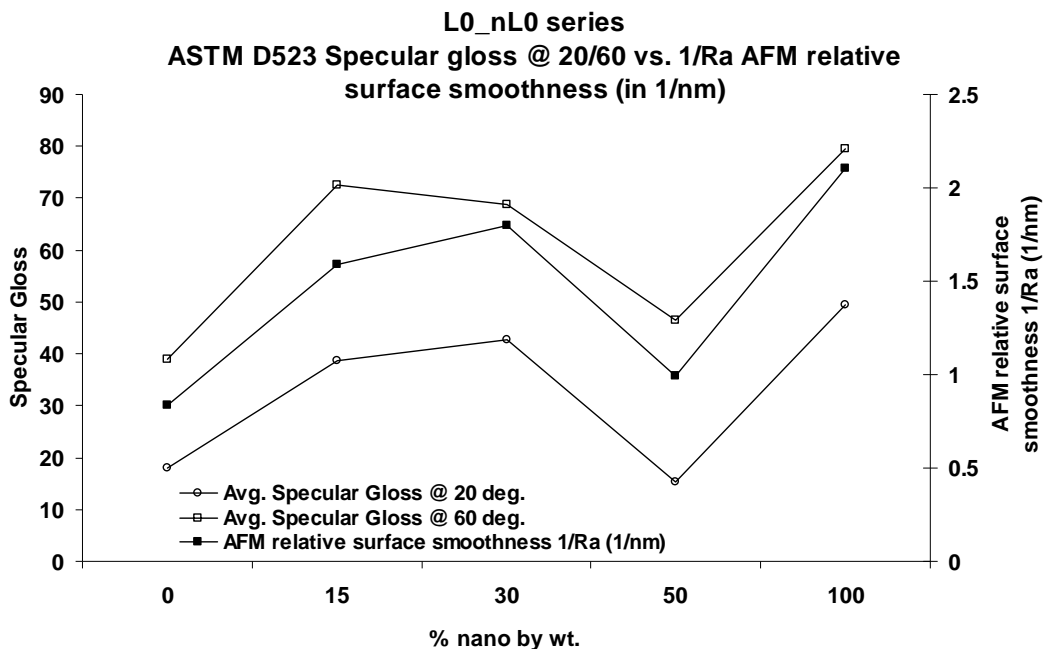


Figure 5.13. Plots of relative average surface smoothness and specular gloss at 20° and 60° vs. % nanoparticles by weight. (L0_nL0 series)

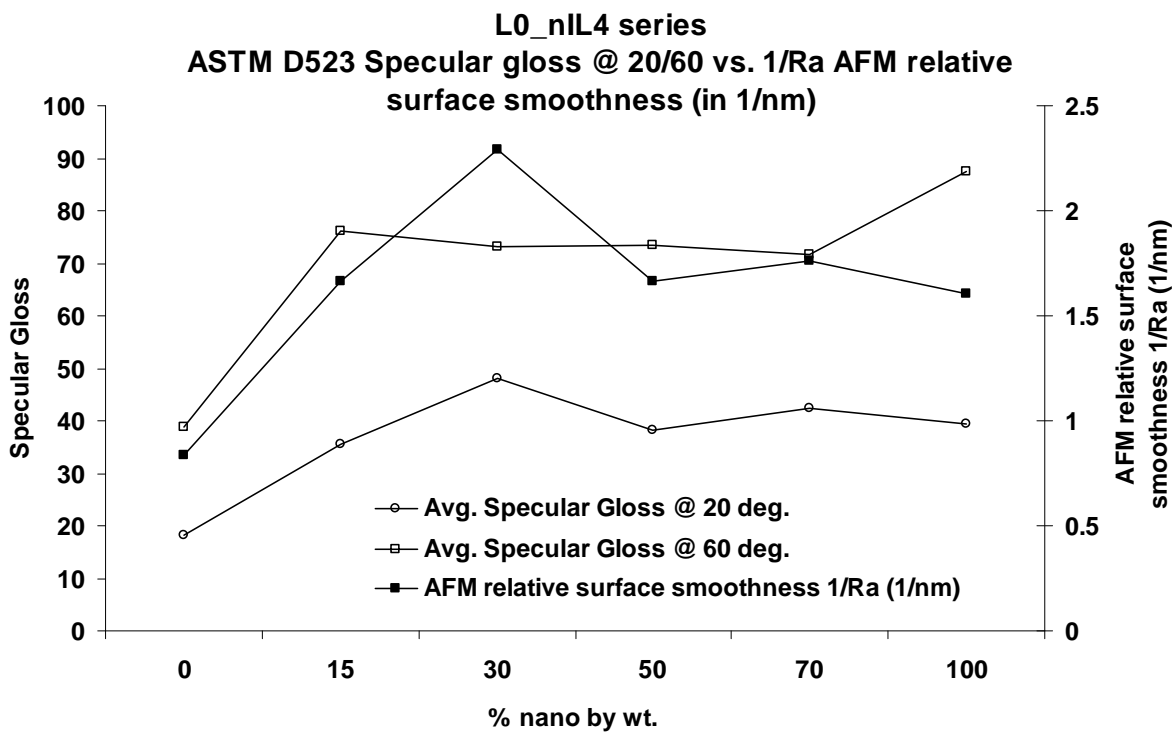


Figure 5.14. Plots of relative average surface smoothness and specular gloss at 20° and 60° vs. % nanoparticles by weight. (L0_nIL4 series)

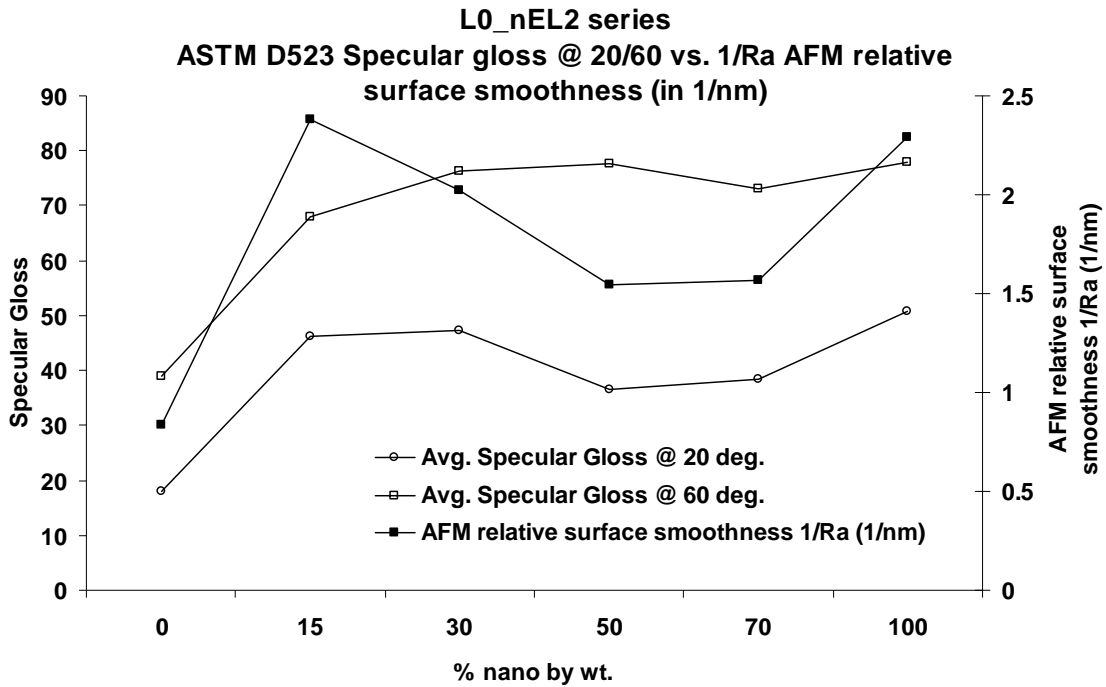


Figure 5.15. Plots of relative average surface smoothness and specular gloss at 20° and 60° vs. % nanoparticles by weight. (L0_nEL2 series)

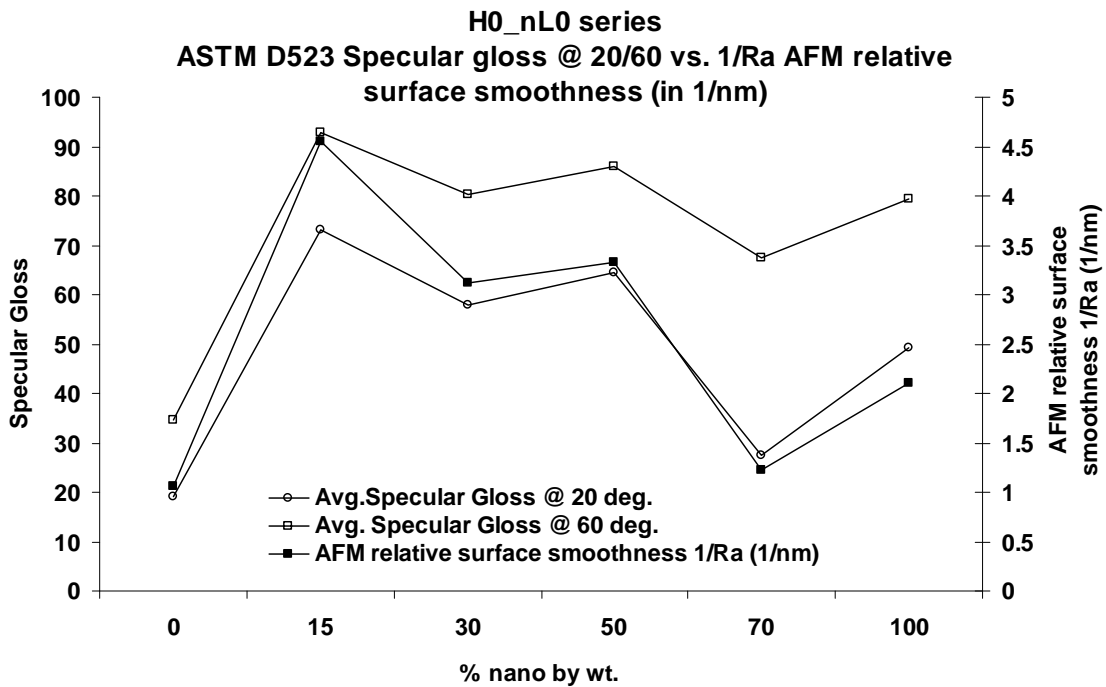


Figure 5.16. Plots of relative average surface smoothness and specular gloss at 20° and 60° vs. % nanoparticles by weight. (H0_nL0 series)

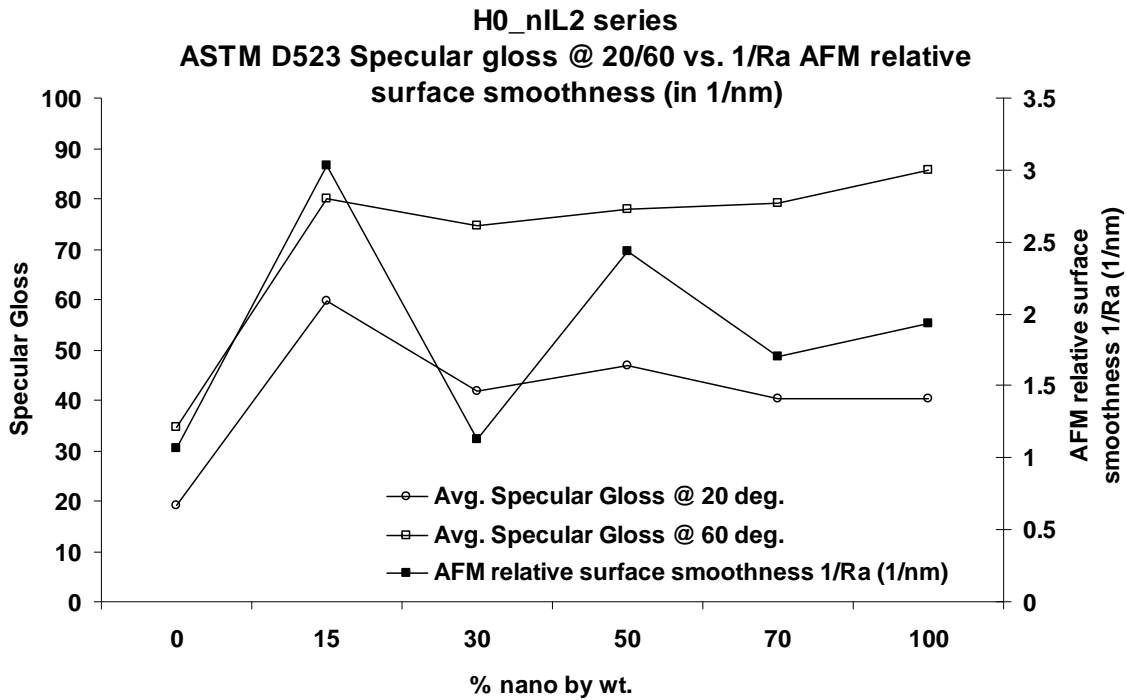


Figure 5.17. Plots of relative average surface smoothness and specular gloss at 20° and 60° vs. % nanoparticles by weight. (H0_nIL2 series)

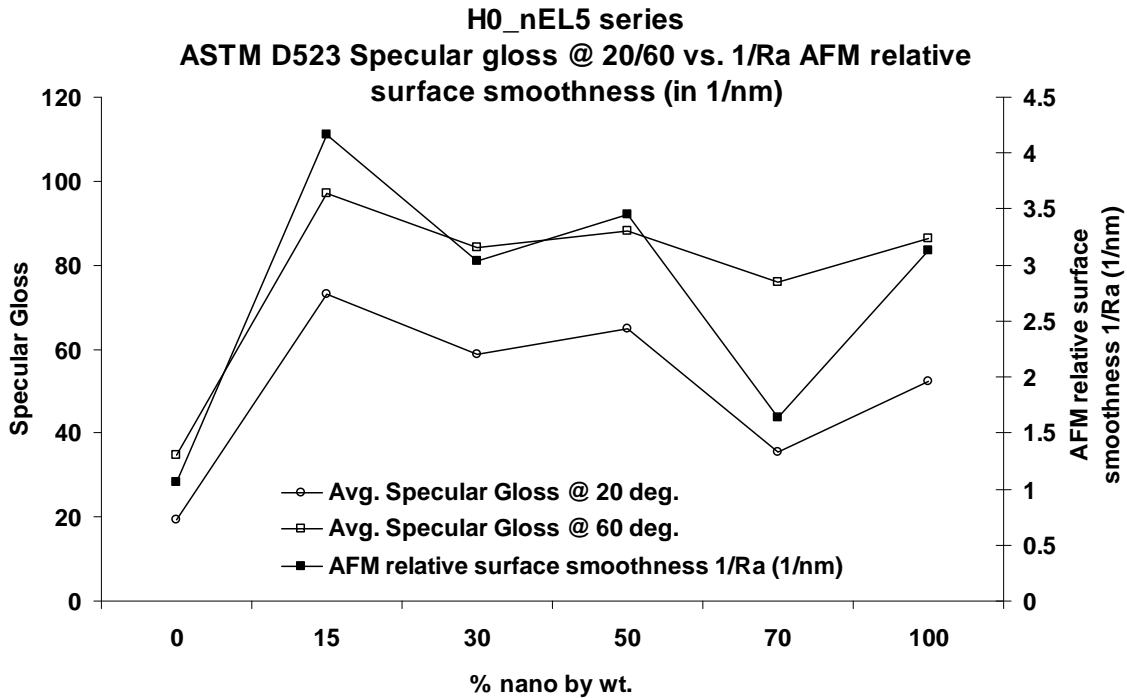


Figure 5.18. Plots of relative average surface smoothness and specular gloss at 20° and 60° vs. % nanoparticles by weight. (H0_nEL5 series)

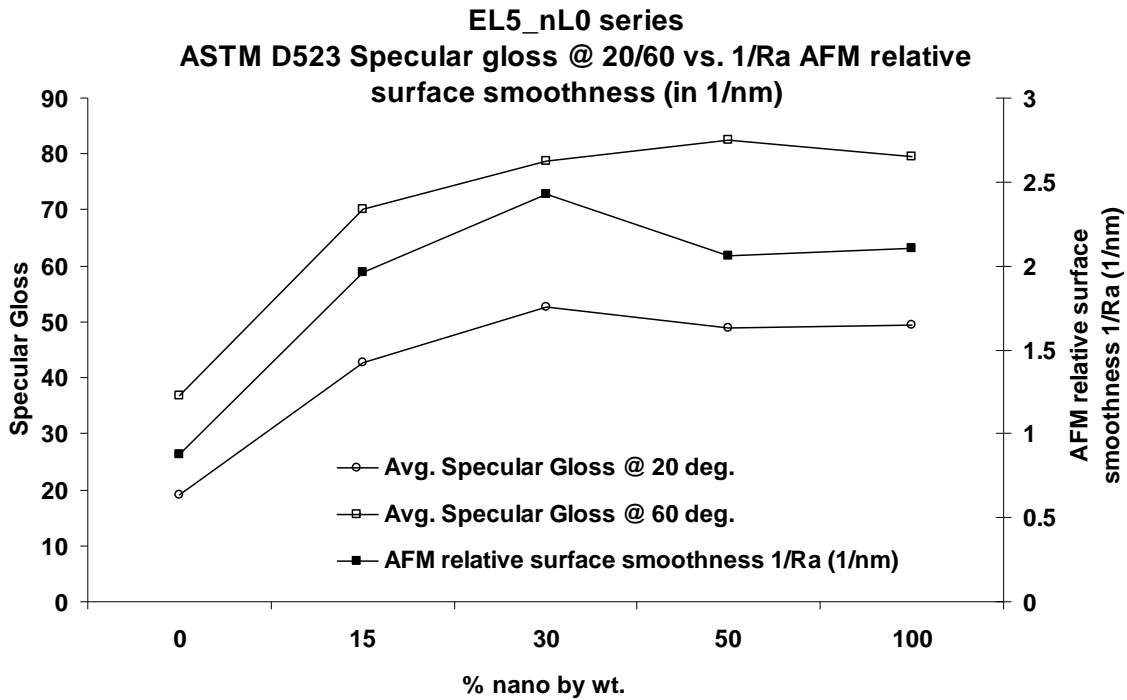


Figure 5.19. Plots of relative average surface smoothness and specular gloss at 20° and 60° vs. % nanoparticles by weight. (EL5_nIL0 series)

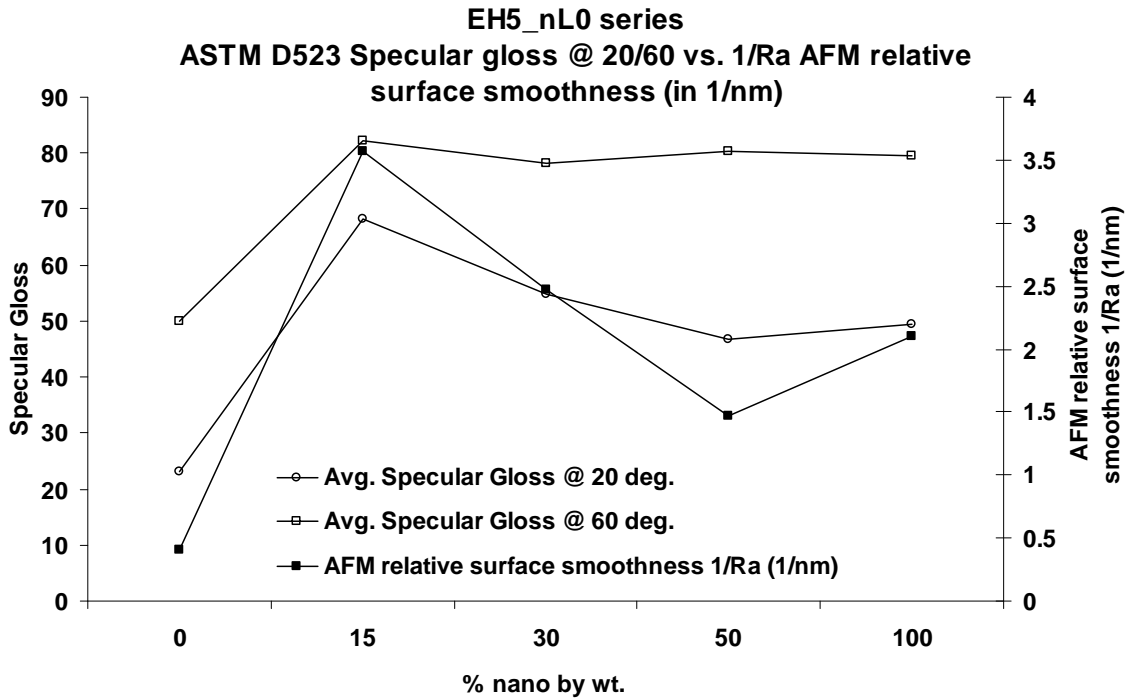


Figure 5.20. Plots of relative average surface smoothness and specular gloss at 20° and 60° vs. % nanoparticles by weight. (EH5_nIL0 series)

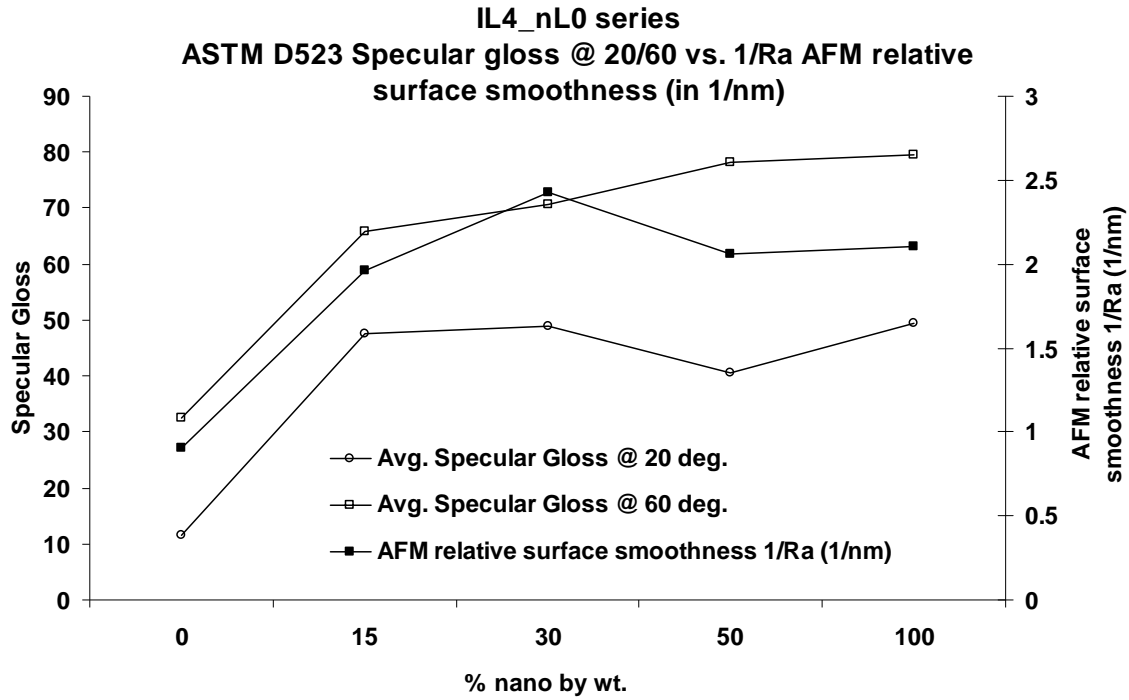


Figure 5.21. Plots of relative average surface smoothness and specular gloss at 20° and 60° vs. % nanoparticles by weight. (IL4_nIL0 series)

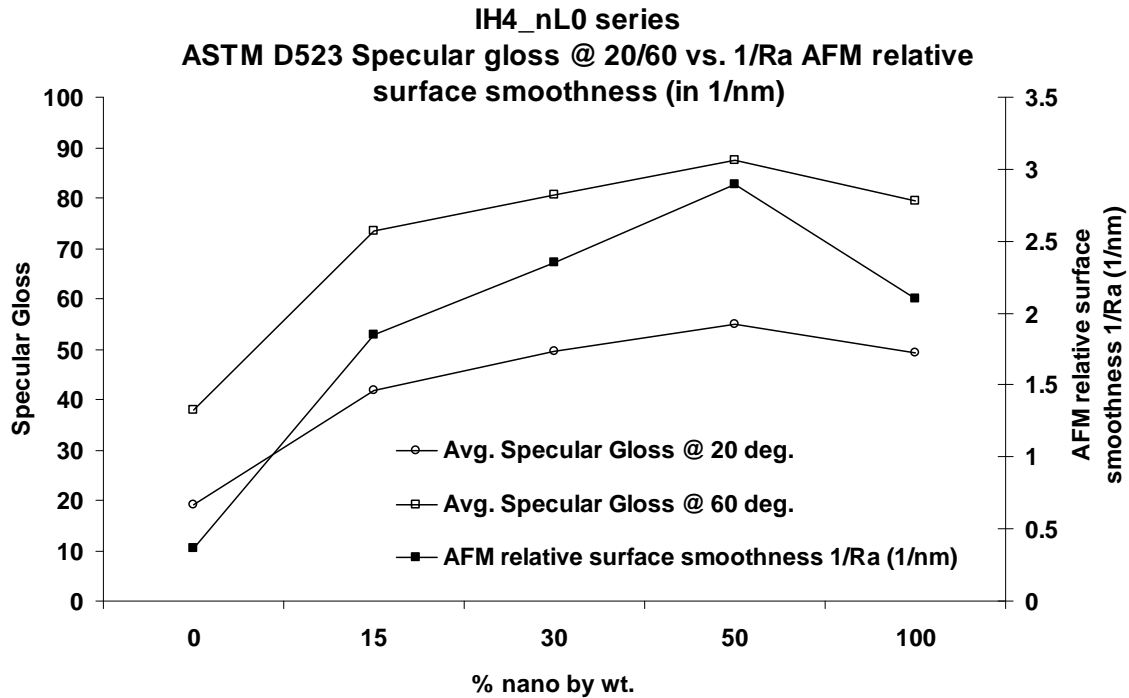


Figure 5.22. Plots of relative average surface smoothness and specular gloss at 20° and 60° vs. % nanoparticles by weight. (IH4_nIL0 series)

Overall, correlating all the above figures and data clearly indicates that nanoparticles tend to populate the outer surface of the film, increasing gloss, and the film substrate interface, improving adhesion. As Provder et al.⁴⁶ pointed out, the AFM analysis clearly suggests that the packing model theory would be applicable to the bulk of the film; however, at the very surface of the film, which is seen by AFM, the morphology could be different. In this case, auto-stratification could also be occurring with an excess of nanoparticles at the surface compared to the bulk film. These observations are consistent with Leary et al.'s (ICI Paints, Australia) research^{6, 11, 14} that demonstrated that such auto-stratification can occur in a bimodal population if the ratio of modes (large diameter to small diameter) was on the order of 5 or so. Indeed, the candidates presented in this research showed a size ratio of 5 to 6 (large particle size latexes are ~ 120nm vs. nanosize latexes are ~ 20-25nm).

Table 5.13: Formulation matrix based on end-use properties results

Latex blend	Properties improve up to (concentration of nano by wt.)	Best properties at (concentration of nano by wt.)
L0_nL0	30% by wt. of nano	At 15, 30 wt.% nano
L0_nIL4	70% by wt. of nano	At 15, 30 wt.% nano
L0_nEL2	70% by wt. of nano	At 15, 30 wt.% nano
H0_nL0	70% by wt. of nano	At 15, 50 wt.% nano
H0_nIL2	70% by wt. of nano	At 15, 50 wt.% nano
H0_nEL5	70% by wt. of nano	At 15, 50 wt.% nano
IL4_nL0	50% by wt. of nano	At 15, 30 wt.% nano
EL5_nL0	50% by wt. of nano	At 30 wt.% nano
EH5_nL0	50% by wt. of nano	At 15 wt.% nano
IH4_nL0	50% by wt. of nano	At 50 wt.% nano

Table 5.13 provides a quick general summary of (a) at what concentration of nanolatex the properties improve and (b) which is the best concentration of nanolatex that provides the best properties in general. This table serves as a fundamental matrix or aid for a coatings formulator

to make selections based on the end-use requirements to formulate a latex blend. As shown in the table for most of the latex blends, the best properties are achieved at 15% of nanolatex concentration. Further, at 30% concentration of nanolatex in the blends, the properties are improved for most of the latexes. This showed that the optimum concentration range for nanolatex in a latex blend is up to 30 wt% to achieve a maximum.

Fundamental Mechanical Properties

Stress-Strain Curves

Average stress-strain curves comparing neat constituents vs. their blends are shown in Figures 5.23-5.32. Each stress-strain curve represents an average of 5-6 replicates. Stress-strain data give important information about the ultimate mechanical properties of polymeric materials.^{22, 23} The values of Young's modulus, area under the stress-strain curve, strain at break, and stress at break are summarized in Tables 5.14-5.23. The area under the stress-strain curve is a measure of the flexibility and toughness of the film. As the area decreases, the film becomes less flexible and more brittle.

Table 5.14: Latex blend series L0_nL0

%nano by wt.	Young's Modulus (E'), MPa	Area Under Curve	Strain at Break(ϵ_b), %	Stress at Break(ϵ_b), MPa
0%	8.9 ± 0.6	172 ± 11	95.7 ± 6	2.7 ± 0.9
7.5%	7.58 ± 0.9	67.7 ± 4.6	85.1 ± 0.3	1.5 ± 0.2
15%	10.1 ± 1.2	83 ± 14	83.6 ± 12	2 ± 0.2
30%	5 ± 0.1	46.8 ± 6	76.2 ± 1.8	1.2 ± 0.1
50%	6.7 ± 0.6	39.2 ± 1.4	76.2 ± 2.7	1 ± 0.04
70%	4.5 ± 0.7	30.2 ± 0.4	71 ± 1.2	0.8 ± 0.03
100%	2.2 ± 0.4	33 ± 1	81.5 ± 5.7	0.8 ± 0.1

Table 5.15: Latex blend series L0_nIL4

%nano by wt.	Young's Modulus (E'), MPa	Area Under Curve	Strain at Break(ϵ_b), %	Stress at Break(ϵ_b), MPa
0%	8.9 ± 0.6	172 ± 11	95.7 ± 6	2.7 ± 0.9
7.5%	5.4 ± 1.2	49.6 ± 9.1	68.8 ± 6.2	1.31 ± 0.1
15%	9.7 ± 0.2	72.9 ± 8.8	78.5 ± 3.8	1.9 ± 0.2
30%	4.9 ± 1.1	57.5 ± 6.6	83.3 ± 8.3	1.3 ± 0.1
50%	5.5 ± 0.1	47.2 ± 2.5	77.9 ± 2.6	1.1 ± 0.1
70%	8.9 ± 0.8	51.5 ± 8.3	85.6 ± 8.5	1.2 ± 0.1
100%	5 ± 1.3	52.9 ± 5.9	88.5 ± 3.5	1.2 ± 0.1

Table 5.16: Latex blend series L0_nEL2

%nano by wt.	Young's Modulus (E'), MPa	Area Under Curve	Strain at Break(ϵ_b), %	Stress at Break(ϵ_b), MPa
0%	8.9 ± 0.6	172 ± 11	95.7 ± 6	2.7 ± 0.9
7.5%	7.3 ± 1.7	56.6 ± 9.8	75.9 ± 2.3	1.43 ± 0.1
15%	10.2 ± 2	154 ± 27	94 ± 6.3	3.13 ± 0.2
30%	6.4 ± 1.2	60.7 ± 1.2	81 ± 4.3	1.42 ± 0.1
50%	6.81 ± 1.4	53.5 ± 3.7	79.3 ± 7.9	1.31 ± 0.1
70%	4.3 ± 1.1	75.1 ± 7.5	93.9 ± 3.4	1.6 ± 0.1
100%	4.1 ± 0.1	71.8 ± 4.3	94.8 ± 4.3	1.5 ± 0.1

Table 5.17: Latex blend series H0_nL0

%nano by wt.	Young's Modulus (E'), MPa	Area Under Curve	Strain at Break(ϵ_b), %	Stress at Break(ϵ_b), MPa
0%	15.9 ± 1.1	175 ± 2.8	98.8 ± 0.1	3.55 ± 0.1
7.5%	46.1 ± 3.2	177.8 ± 11	79.1 ± 7.8	4.6 ± 0.1
15%	149 ± 45.4	528 ± 95	78 ± 7.7	13.9 ± 0.6
30%	66.9 ± 15	201.4 ± 4	81.1 ± 0.4	4 ± 0.1
50%	38 ± 21	125 ± 15	80.9 ± 1.8	3.1 ± 0.1
70%	44 ± 9	117 ± 23	77.8 ± 2.2	2.9 ± 0.2
100%	2.2 ± 0.4	33 ± 1	81.5 ± 5.7	0.8 ± 0.1

Table 5.18: Latex blend series H0_nIL2

%nano by wt.	Young's Modulus (E'), MPa	Area Under Curve	Strain at Break(ϵ_b), %	Stress at Break(ϵ_b), MPa
0%	15.9 ± 1.1	175 ± 2.8	98.8 ± 0.1	3.55 ± 0.1
7.5%	89 ± 30	198 ± 11	89 ± 4.3	4.5 ± 0.4
15%	194 ± 4.9	530 ± 101	81 ± 11	12.7 ± 0.3
30%	31.6 ± 3	124 ± 6	81 ± 2	3 ± 0.2
50%	19.1 ± 0.7	107 ± 5	83 ± 2.1	2.6 ± 0.1
70%	36.3 ± 8	94.2 ± 2.8	84.8 ± 3.3	2.2 ± 0.1
100%	6.4 ± 0.8	40.1 ± 15	86.4 ± 12	0.9 ± 0.2

Table 5.19: Latex blend series H0_nEL5

%nano by wt.	Young's Modulus (E'), MPa	Area Under Curve	Strain at Break(ϵ_b), %	Stress at Break(ϵ_b), MPa
0%	15.9 ± 1.1	175 ± 2.8	98.8 ± 0.1	3.55 ± 0.1
7.5%	81.8 ± 12	189 ± 12	91 ± 2.3	4.13 ± 0.1
15%	206 ± 1	983 ± 175	85.2 ± 2.4	23.4 ± 2
30%	53.3 ± 5.2	183 ± 8.9	91 ± 3.2	3.9 ± 0.1
50%	33.4 ± 3.3	151 ± 11	88.1 ± 2.1	3.5 ± 0.1
70%	25.6 ± 12	133 ± 19	85 ± 2.2	3.1 ± 0.2
100%	11.4 ± 0.2	151 ± 20	78 ± 3.5	3.9 ± 0.2

Table 5.20: Latex blend series EL5_nL0

%nano by wt.	Young's Modulus (E'), MPa	Area Under Curve	Strain at Break(ϵ_b), %	Stress at Break(ϵ_b), MPa
0%	45.3 ± 9.2	196.5 ± 11	41.8 ± 0.7	9.5 ± 0.5
7.5%	36.6 ± 0.1	149 ± 34	68 ± 5.4	4.4 ± 0.7
15%	94.7 ± 26	541 ± 12	71.6 ± 6.2	15.4 ± 1.8
30%	47.4 ± 4	160 ± 11	65.4 ± 0.3	5 ± 0.4
50%	24.9 ± 10	156 ± 25	69.8 ± 5.5	4.4 ± 0.3
70%	25.3 ± 0.5	118 ± 27	79.8 ± 3.4	2.9 ± 0.6
100%	2.2 ± 0.4	33 ± 1	81.5 ± 5.7	0.8 ± 0.1

Table 5.21: Latex blend series IL4_nL0

%nano by wt.	Young's Modulus (E'), MPa	Area Under Curve	Strain at Break(ϵ_b), %	Stress at Break(ϵ_b), MPa
0%	49.7 ± 9.2	222 ± 6.3	57.9 ± 1.2	7.7 ± 0.5
7.5%	14.2 ± 3.1	83 ± 9.3	87.5 ± 5	1.9 ± 0.1
15%	29.8 ± 0.7	239 ± 7.7	95.5 ± 3.4	5 ± 0.2
30%	14.2 ± 0.1	87.2 ± 3.9	87.2 ± 2	1.94 ± 0.2
50%	13.7 ± 1.1	75.5 ± 1.7	84 ± 1.2	1.7 ± 0.1
70%	9.6 ± 2.5	55.4 ± 11	73 ± 10	1.5 ± 0.1
100%	2.2 ± 0.4	33 ± 1	81.5 ± 5.7	0.8 ± 0.1

Table 5.22: Latex blend series EH5_nL0

%nano by wt.	Young's Modulus (E'), MPa	Area Under Curve	Strain at Break(ϵ_b), %	Stress at Break(ϵ_b), MPa
0%	159 ± 11	174 ± 11	38.8 ± 1.5	8.9 ± 0.2
7.5%	100 ± 2	183 ± 9	61.4 ± 2.3	6.05 ± 0.2
15%	222 ± 3	429 ± 12	56.1 ± 5.6	16.2 ± 0.1
30%	135 ± 17	186 ± 2	72 ± 7.1	5.2 ± 0.5
50%	114 ± 23	142 ± 9.8	68 ± 8.6	4.2 ± 0.4
70%	35.5 ± 0.5	127 ± 11	80.2 ± 5.1	3.18 ± 0.2
100%	2.2 ± 0.4	33 ± 1	81.5 ± 5.7	0.8 ± 0.1

Table 5.23: Latex blend series IH4_nL0

%nano by wt.	Young's Modulus (E'), MPa	Area Under Curve	Strain at Break(ϵ_b), %	Stress at Break(ϵ_b), MPa
0	213 ± 5.7	186 ± 9	38.2 ± 2	9.83
7.5%	*	*	*	*
15%	150 ± 30	355 ± 12	74.9 ± 4.6	9.9
30%	*	*	*	*
50%	107 ± 5.5	143 ± 8	33.3 ± 1.2	8.6 ± 0.9
70%	63.9 ± 6.9	198 ± 10	80 ± 0.2	5 ± 0.1
100%	2.2 ± 0.4	33 ± 1	81.5 ± 5.7	0.8 ± 0.1

Note: Asterisk in Table indicates sample was too brittle to test

Figures 5.23-5.32 show comparison of different neat constituent versus blend concentrations. Surveying all data in tables and figures, we see that, when L0 is blended with nL0, there is a general decrease in Young's modulus values as expected for a very soft film.

However, a slight increase in Young's modulus is observed at 15% concentration of nanoparticles. Also, at increasing concentration of nanoparticle latex, the respective area under the curve values decrease, indicating less flexibility or brittleness in the samples. Comparing pre-coalescence versus post-coalescence crosslinked nanosize latex blends with L0, similar trends are observed. Also, in both these cases at 15% concentration of nanoparticles, increase in Young's modulus values is observed.

When nanosize latexes with or without crosslinker blended with H0 (hard matrix), results were unexpected. The Young's modulus values showed outstanding improvements in the concentration ranges between 7.5-30% of nanoparticles, particularly at 15% concentration. The Young's modulus of 100% H0 (15.9 MPa) showed 9-fold increase (149 MPa) with only 20% decrease in strain-to-break when blended with 15% nL0. This is not expected. These results are striking because the compositions of the two types of particles are the same, and no crosslinking is involved. The main difference is particle size. Typically when soft particles (dispersed phase) are blended in a hard matrix (continuous phase), the modulus values should go down depending upon the composition. This is not the case here. Farris and Agarwal¹ studied the fundamental mechanical behavior of hard/soft latex blends. They demonstrated that blends of hard/soft conventional size latex mostly reflect characteristics of their continuous phase. Another explanation could be based on the percolation theory as explained by Eckersley and Helmer.⁵ The nonfunctional low T_g nanoparticles may be filling in voids between the large particles so that the large particles can coalesce better and, thus, increase the overall mechanical strength of the films.

What happens when we subject the nanoparticles to pre-coalescence or post-coalescence crosslinking? In case of functional nanolatex, further improvements in the values can be

obtained. At 15% concentration of nIL2, the increase in Young's modulus of H0 was 12 folds (194 MPa) with only 18% decrease in strain-to-break and at 15% concentration of nEL5, the increase in Young's modulus of H0 was the highest, 13 fold (206 MPa), with only 15% decrease in strain-to-break values. Similarly, a respective increase in the area under the curve and stress at break is observed, indicating increased toughness in samples.

Similar significant increases in Young's modulus values are observed when nonfunctional nanosize low T_g latexes blended with post-coalescence crosslinked conventional size latex. The Young's modulus values for EL5: 45 MPa vs. EL5_nL0: 94.7 MPa and EH5: 159 MPa vs. EH5_nL0: 222 MPa. In addition, the area under the curve and strain-to-break values also showed respective improvements in both the above samples. This indicates increased toughness in the samples. In the case of nL0 when blended with pre-coalescence crosslinked conventional latexes, the Young's modulus values decreases: IL4: 49.7 MPa vs. IL4_nL0 (15%): 29.8 MPa, IH4: 213 MPa vs. IH4_nL0 (15%): 150 MPa. However, the area under the curve and the strain-at-break values showed respective increase in both the blends indicating flexibility in samples with optimum Young's modulus values. When correlating the values from MFTs and MDSC T_g of the above samples, this is a beneficial feature, especially in case of high T_g pre-coalescence latex, when blended with low T_g nanoparticle latexes – The low T_g nanoparticle latex will help coalesce the high T_g pre-coalescence latex particles and provide efficient film formation.

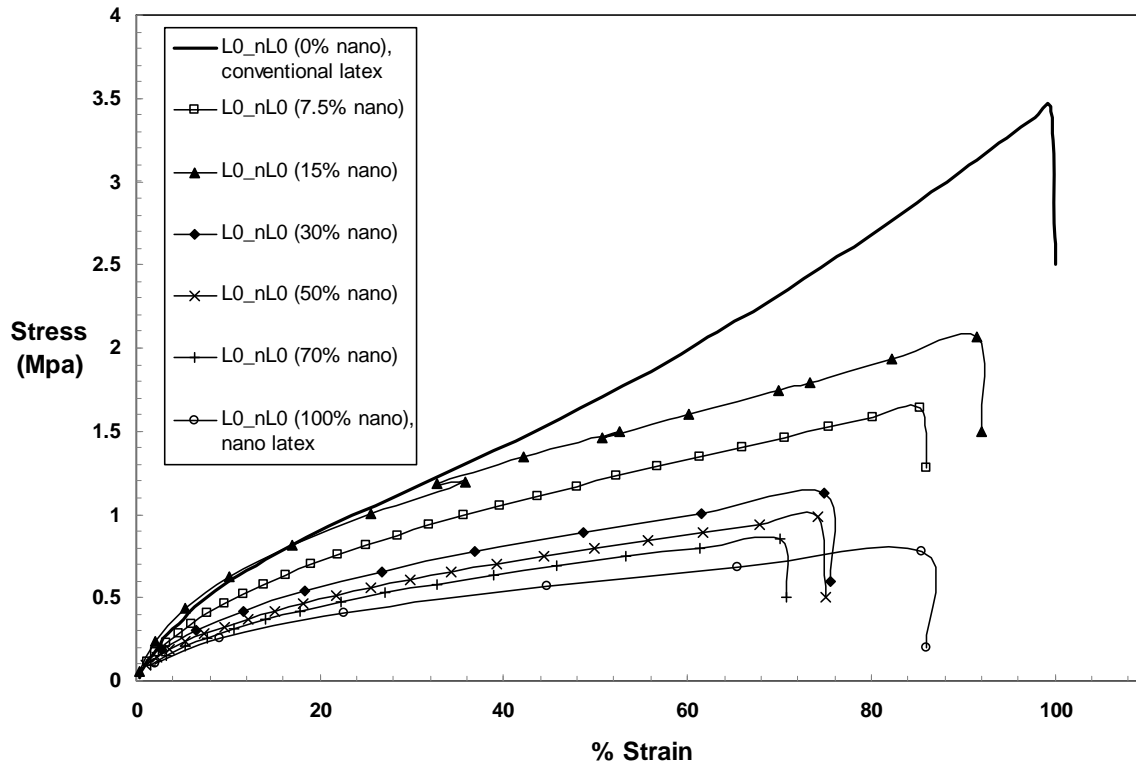


Figure 5.23. Comparison of average stress-strain curves for L0_nL0 series

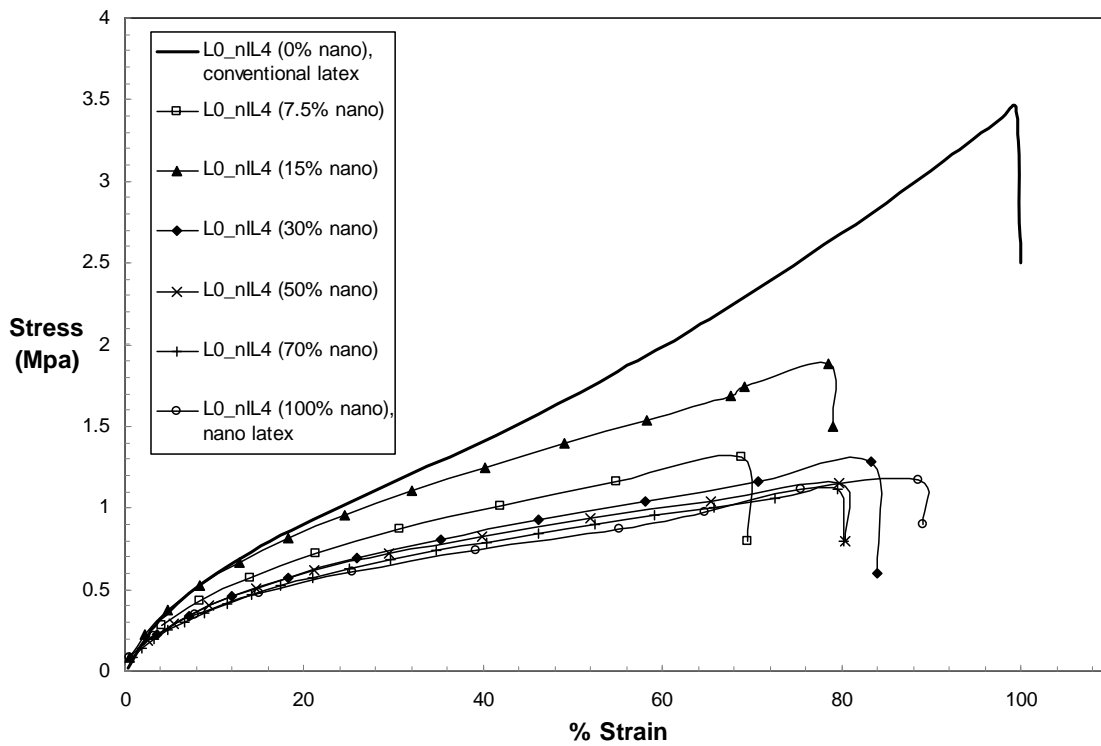


Figure 5.24. Comparison of average stress-strain curves for L0_nIL4 series

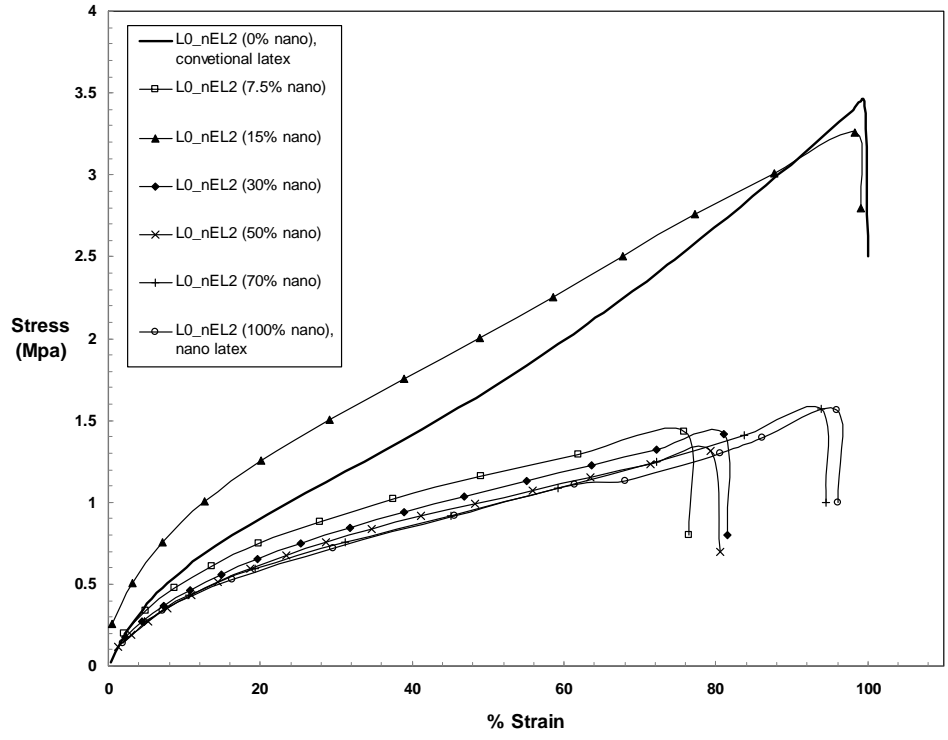


Figure 5.25. Comparison of average stress-strain curves for L0_nEL2 series

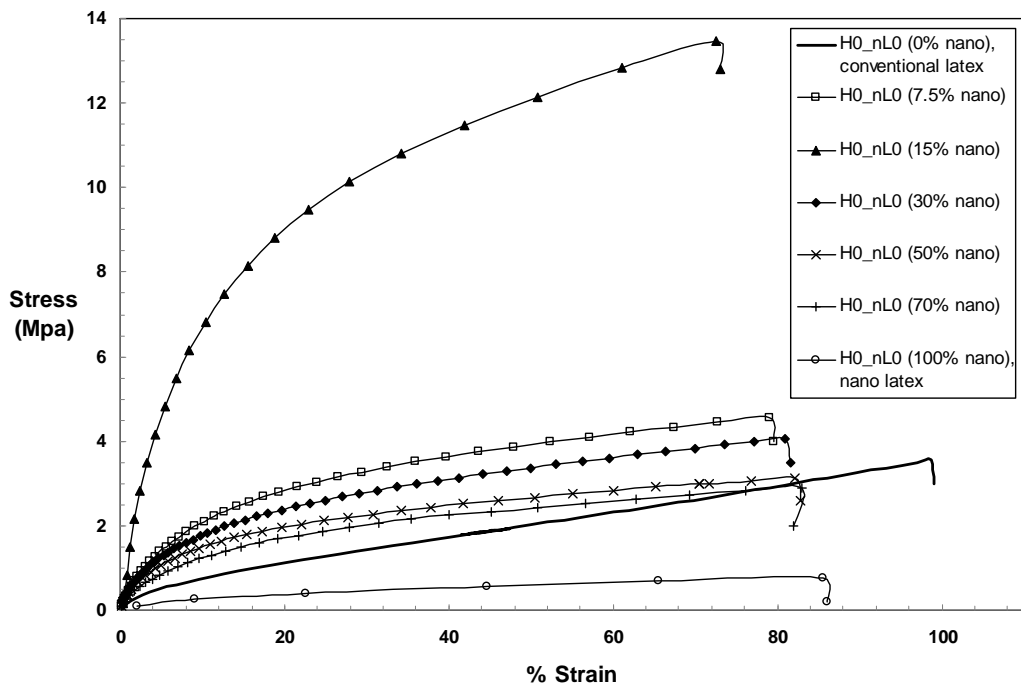


Figure 5.26. Comparison of average stress-strain curves for H0_nL0 series

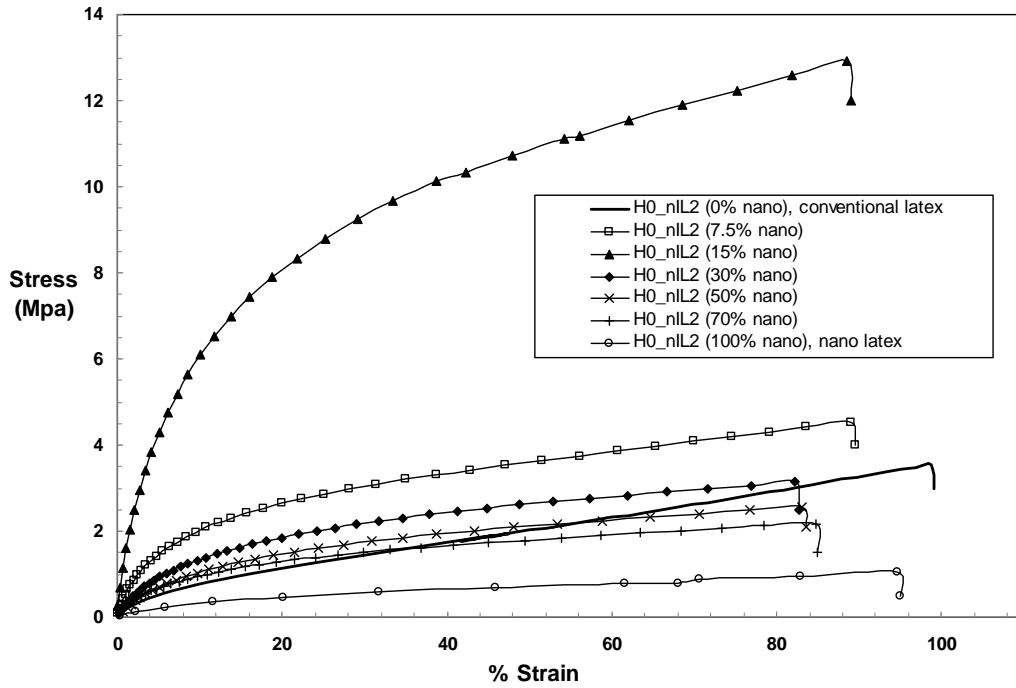


Figure 5.27. Comparison of average stress-strain curves for H0_nIL2 series

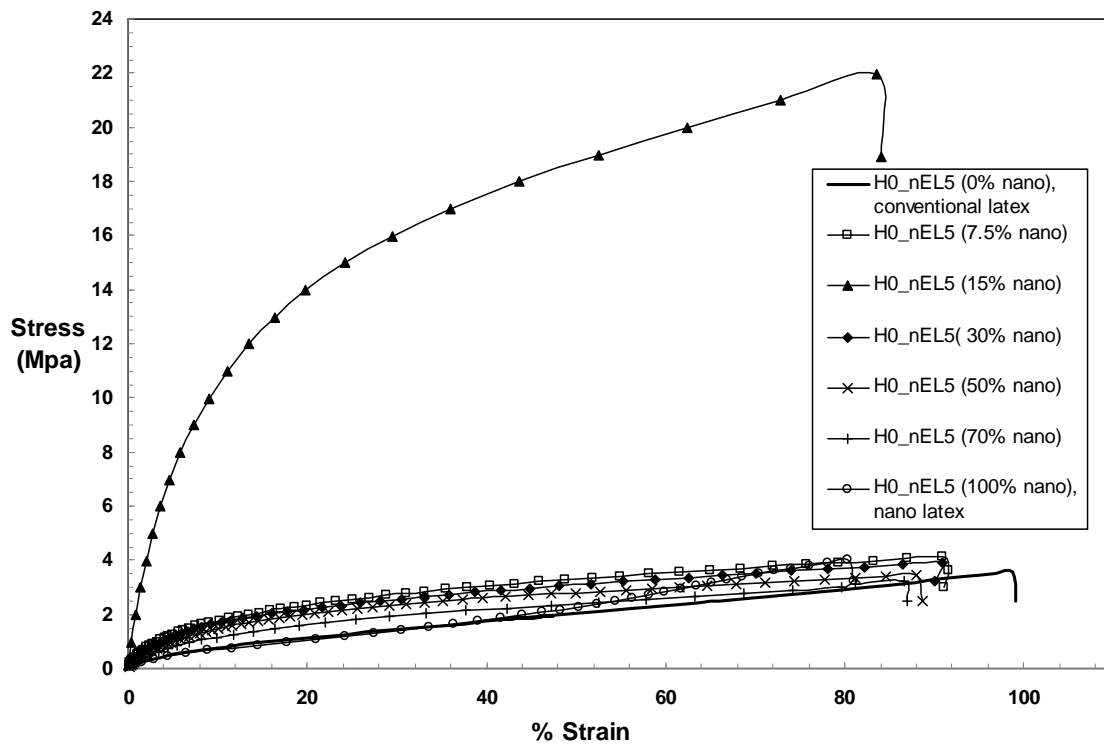


Figure 5.28. Comparison of average stress-strain curves for H0_nEL5 series

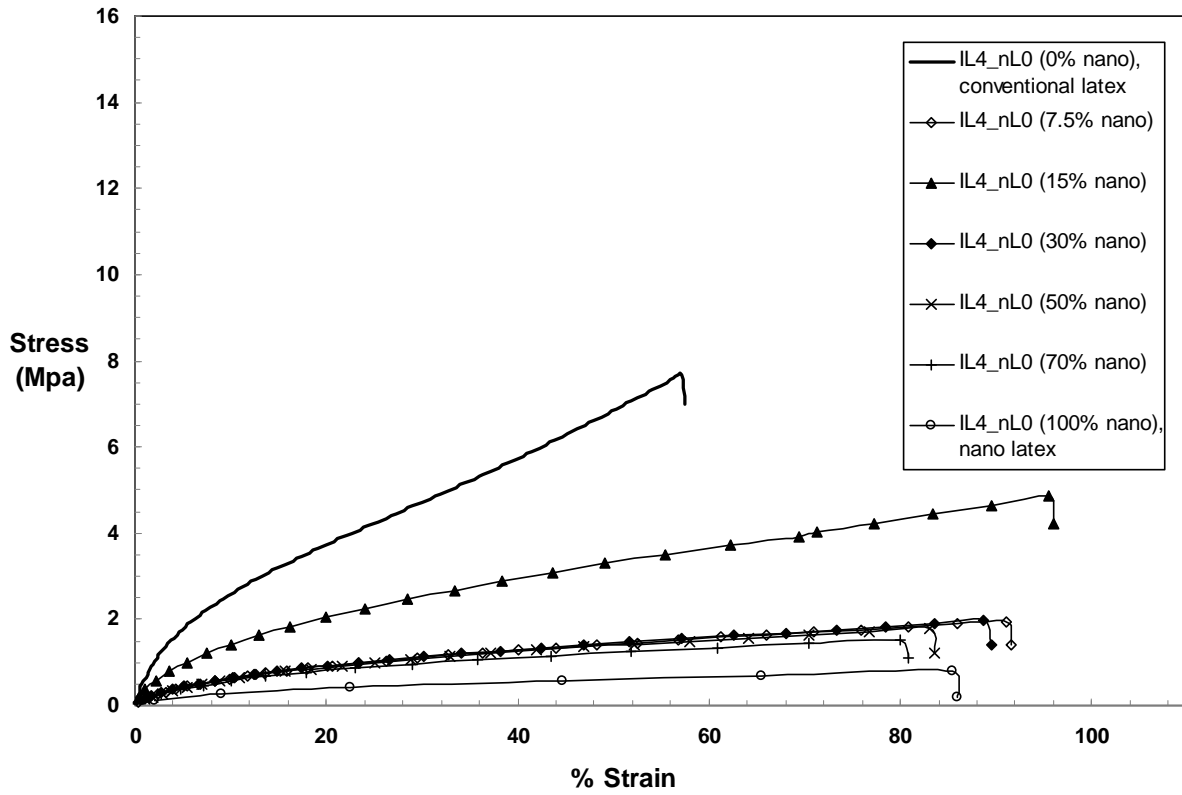


Figure 5.29. Comparison of average stress-strain curves for IL4_nL0 series

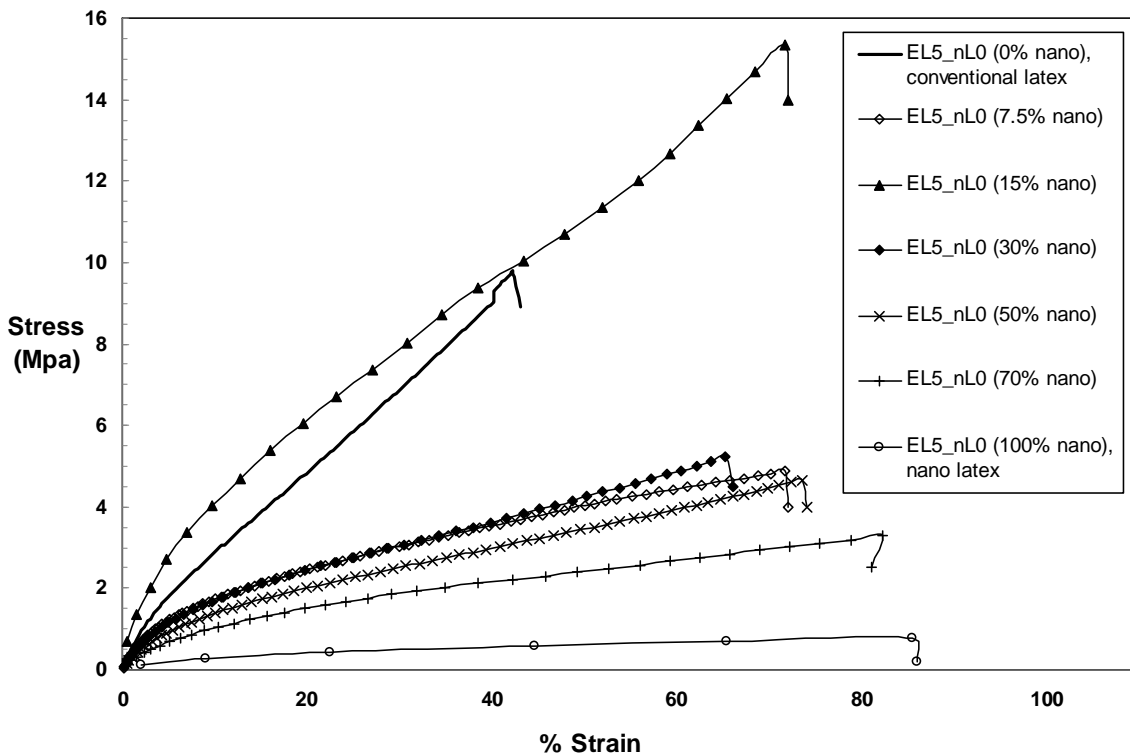


Figure 5.30. Comparison of average stress-strain curves for EL5_nL0 series

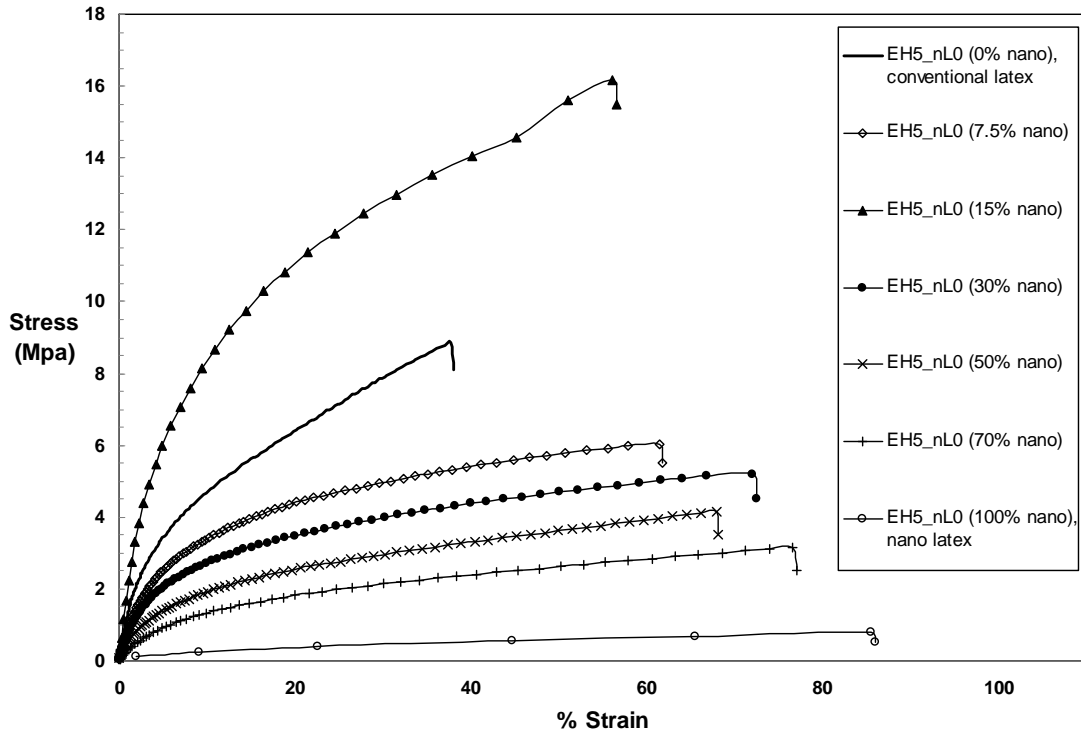


Figure 5.31. Comparison of average stress-strain curves for EH5_nL0 series

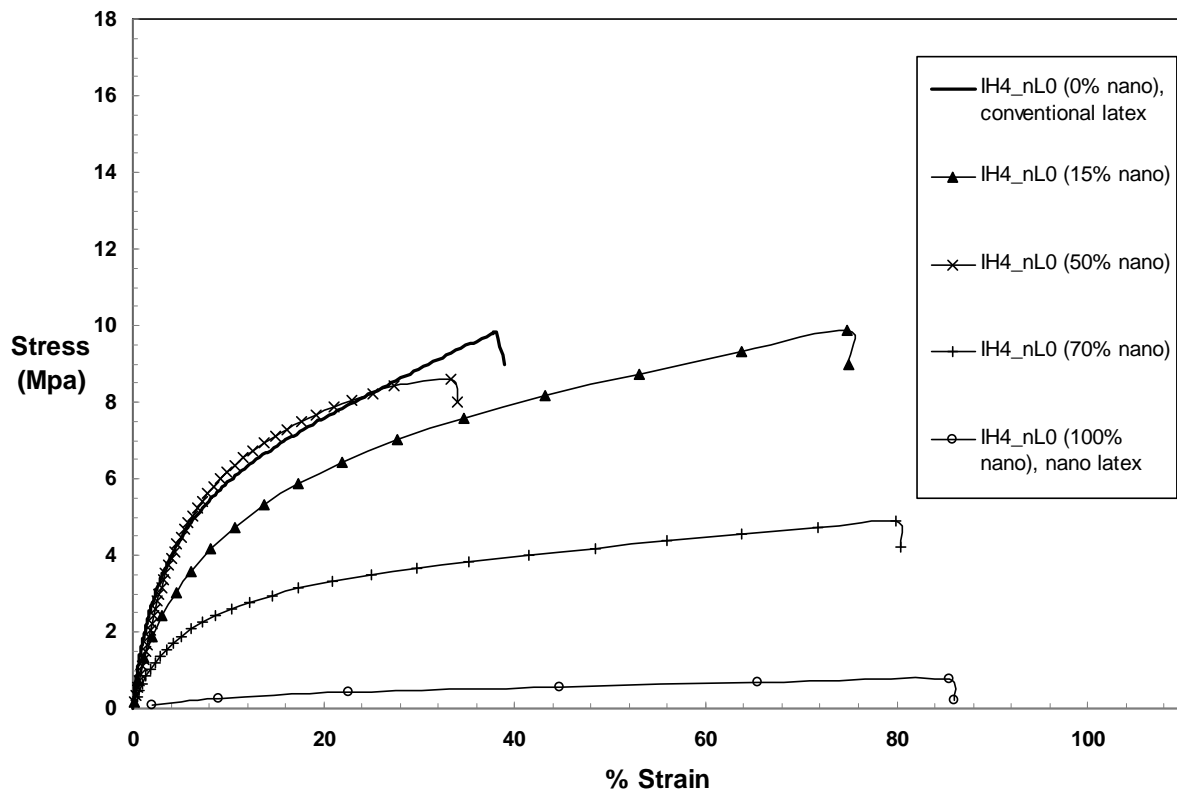


Figure 5.32. Comparison of average stress-strain curves for IH4_nL0 series

In general, the stress-strain analysis showed that in most cases, the 85/15 blends give the most improved results. Properties of other blend ratios, at 7.5% and at 30% concentration, are also often enhanced. It is noteworthy that the pencil hardness of all the blends is sharply increased relative to the conventional latex film. It is also interesting that the solvent resistance of the all-thermoplastic blends improved modestly, again suggesting that the nanoparticles were able to improve the coalescence and interpenetration of the polymer molecules during film formation, independent of crosslinking.

In summary, based on end-use properties and stress-strain data, it is clear that in most cases the 85/15 blends gave a great balance of overall properties. The other effective blends ratios are at 7.5% and at 30% in most cases. Further, surveying all data, it is clear that the film properties depend on (a) T_g , (b) crosslinking, and (c) blend ratio. Properties of most coatings are significantly influenced by T_g and crosslinking, which is not surprising. What is surprising is the strong dependence on blend ratio and the very positive synergies in property improvement that are observed.

As suggested by Jones et al.,⁴⁶ the above observations lead us to theorize about why the blends, especially the 85/15 blends, perform so well. The conjecture is based on the classical model of film formation by thermoplastic latexes; this model is simplistic but useful.^{20, 24, 34-36} It postulates three overlapping stages of film formation: (1) evaporation of volatiles, (2) particle deformation to a continuous film (or sometimes referred to as “coalescence”), (3) molecular interpenetration to knit the particles together (also called “fusion” or “further coalescence”). The third stage is critical to achieving full potential film properties. Based on this model, a picture of what might be happening with blends follows:

- During evaporation, nanoparticles (22-23 nm) presumably fill the interstices among the 120-140 nm conventional particles.
- If the larger particles were rigid, uniform spheres and were able to adopt a close-packed geometry, we estimate that there would be room for only 4 to 6 nanoparticles per large particle. The diameter ratio of a 130 nm particle to a 22 nm particle is about the same as that of a volley ball (10 inches) to a golf ball (1.68 inches). As indicated above, the ratio of conventional particles to nanoparticles in an 85/15 blend is roughly 1/25, as visualized in Figure 5.A.



Figure 5.A. Volleyball (conventional particles ~120-130nm) vs. golf ball (nanoparticles ~ 20-25 nm)⁴⁶

- However, the conventional particles are not uniform in size, and they are unlikely to be able to form a neat, close-packed array in the presence of nanoparticles, especially since the evaporation step is rapid. Thus there is probably room for more than 4 to 6 nanoparticles in a reasonably homogenous array after water evaporation.
- At high levels of nanoparticles, however, the nanoparticles would be forced to cluster, and the array at the end of stage 1 would become less homogeneous.

- Assuming a reasonably uniform distribution of large and small particles in the film at the start of stage 2, there are three mechanisms by which nanoparticles could facilitate coalescence and molecular interpenetration as the films form:
 1. The nanoparticles would partly fill voids, sharply reducing the amount of shrinkage needed to achieve film uniformity during stage 2.
 2. Coalescence is thought to be driven partly by reductions in surface energy during the process. Nanoparticles would enhance this effect because their surface areas are much larger on an equal weight basis.
 3. Conceivably, some molecules within the nanoparticles may be constrained within the particles and unable to extend to their preferred RMS dimensions. If this were true, it would provide an additional driving force for molecular interpenetration needed to develop full film properties.
- If there is, indeed, an optimum ratio of conventional particles to nanoparticles, it is not known how to measure it directly. The data presented here suggest that it may be somewhere between 1/15 and 1/30 for particles of the sizes studied here.
- The dynamical mechanical property results in the next section show a measurable maximum in the storage modulus values in the rubbery region at 85/15 conventional particle/nanoparticle concentration ratio for both crosslinkable and uncrosslinkable nanoparticles. This supports the speculation that at this concentration, a film structure is formed which optimizes end-use and fundamental properties of the nanoparticle blends.

- When the nanoparticles are crosslinkable after coalescence, the outcome might be a framework of crosslinked nanoparticles surrounding uncrosslinked vestiges of the conventional particles analogous to a semi-interpenetrating polymer network.

Dynamic mechanical properties

Dynamic mechanical characterization of heterogeneous polymers is dependent not only on the chemical composition of a material but also on physical or structural arrangement of the phases in a bulk polymer.^{22, 23} DMA analysis gives an insight into intrinsic mechanical properties of a polymer.^{22, 23} DMA provides information about the viscoelastic properties (storage modulus and loss modulus) of a polymer as a function of frequency and temperature.^{22, 23} The inflection point of the storage modulus is related to the T_g of the polymer.^{22, 23} It should be noted that the temperature corresponding to the inflection point of the tan delta curve is higher than the T_g value determined by MDSC, which is commonly observed.^{22, 23} The tan delta curve is calculated as the ratio of the loss modulus to the storage modulus. The point where the storage modulus curve flattens is an indicator of the rubbery plateau. Figures 5.33-5.42 show comparison of different neat constituent versus their blends concentrations. Each figure includes two sub-figures: (a) comparison of loss modulus curves and (b) comparison of storage modulus curves. Tables 5.24-5.33 show comparison of MDSC T_g , DMA storage modulus inflection point, DMA loss peak temperature, tan delta peak temperature, half width/half height of tan delta peak, and storage modulus values in rubbery region (80-90°C). In general, the MDSC T_g , DMA storage modulus inflection point, DMA loss peak temperature values, showed similar trends and good correlation.

Hill⁴⁷ points out that “for unpigmented crosslinked coating films the level of the storage modulus, E' , in the rubbery plateau region above T_g is an indicator of the level of crosslink

density.” Hill⁴⁷ further points out that a wide variation in E' values has been observed from 4 MPa for lightly crosslinked systems to 200 MPa for very highly crosslinked films. For latex blends, E' values in rubbery region depict a complex scenario. The E' values, in 80-90 °C range, are lower compared to their neat conventional size constituents. Thus, none of the latex blends films are lightly crosslinked per Hill’s criteria.⁴⁷ However, upon close examination of the storage modulus values in the rubbery region for the blends, it can be seen that the values go through a small but measurable maximum at the 15 wt.% concentration of nanoparticles. The only exception to this is the blend EH5-nL0, where the maximum occurs at 7.5 wt.% concentration of nanoparticles. This small but measurable maximum value of the storage modulus at 15 wt.% of nanoparticles correlates well with other end-use and fundamental property results indicating that optimum property improvements in nanoparticle blends occur around 15 wt.% of nanoparticles. This observation supports the speculation that a unique film structure is formed at this concentration of nanoparticles.

In the case of blends of low T_g conventional latex L0, with increasing levels of nL0 concentration, clear broadening (refer to increase of half width/half height values) and shifting of tan delta peak to lower temperature is evident in Figure 5.33 and Table 5.24. Going from 0% to 7.5% to 15% nanoparticle concentration showed a shift in tan delta to lower temperature, but the clear broadening of the tan delta peak can be seen at levels at or above 30% concentration. In case of pre-coalescence (nIL4) or post-coalescence (nEL2) nanolatex blended with L0, the trends in the tan delta peak are not clear. Mostly for both blends, at higher concentration of pre-coalescence or post-coalescence nanoparticles, the broadening in tan delta curves is observed. Surprisingly, at 15% concentration of pre-coalescence or post-coalescence nanoparticles, the tan delta peak shifts towards higher temperature. Similarly, in the cases EL5_nL0 blends, EH5_nL0

blend, IH4_nL0 blend, and IL4_nL0 blends, no clear trend was observed. For most of the blends, shifting of tan delta peaks to lower temperature was observed. Tan delta peak broadening was clearly observed for EL5_nL0 blend; at 7.5%, 30%, and 50% nL0 concentration of nL0 and for IL4_nL0 blend: at 15% and 30% concentration of nL0, for EH5_nL0 blend: at 30% nL0 concentration and for IH4_nL0: at 50% concentration.

An opposite trend is observed with the blends of H0_nL0. At increasing levels of nanoparticles in the blend, the tan delta peak shifts towards higher temperature and broadening in the tan delta peak is also evident. The broadening of the tan delta peak is an indication of development of a heterogeneous network structure and morphology.⁴⁷ Indeed, in the case of H0_nL0 blends, the tan delta peaks become broader and the peak value decreases, an indication of development of more heterogeneous network structure and morphology. Further, at 15% concentration of nanoparticle latex, the peak shifts to the highest temperature compared to all the other samples. At 15% concentration of nL0, the elastic modulus level obtained from stress-strain measurements increases, and DMA tan delta peak broadens. As mentioned earlier, these results are striking because the compositions of the two types of particles are the same, and no crosslinking is involved. The main difference is particle size. This proves that, in addition to glass transition temperature (and crosslinking), blend ratio is a significant variable. Also, these observations are consistent with all the other test results and solidifies our theory about why the blends, especially the 85/15 blends, perform so well.

In the case of pre-coalescence or post-coalescence crosslinked nanolatex, when blended with a high T_g no crosslinker latex in a different concentrations, similar effects are observed. In general, at increasing concentration of nanoparticle latex, tan delta peaks shift to higher temperatures, clear broadening of the tan delta peaks are observed, and at 15% concentration of

the functional nanoparticles in the blend, the tan delta peak showed the highest temperature shift and broadening.

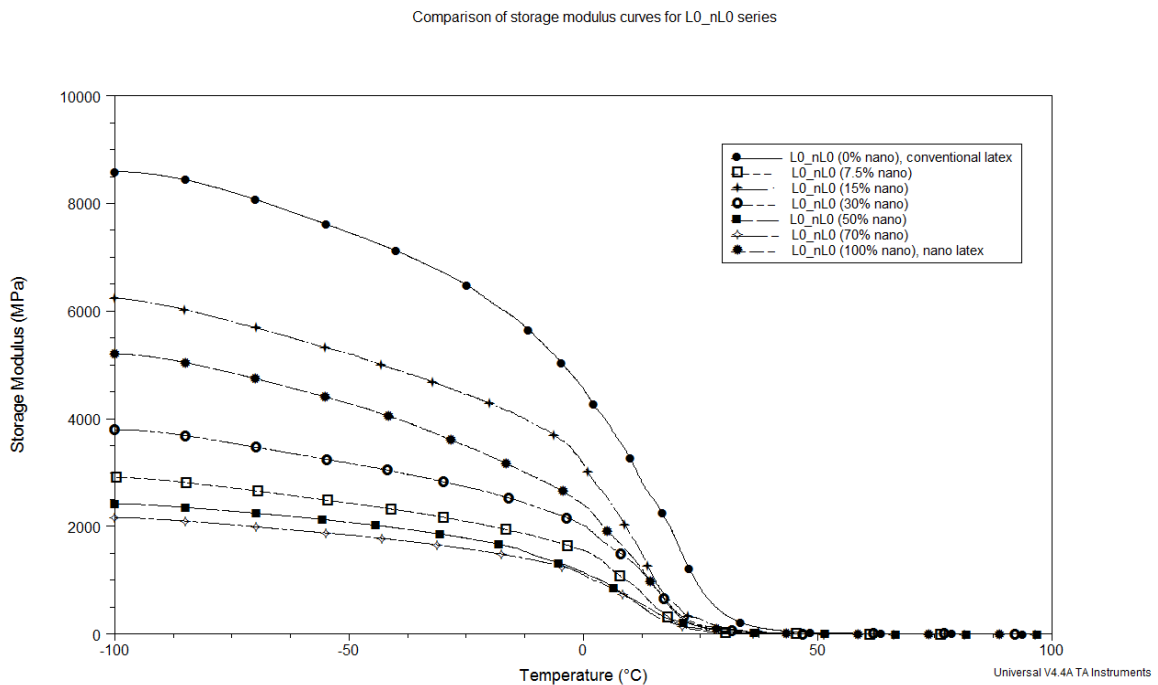
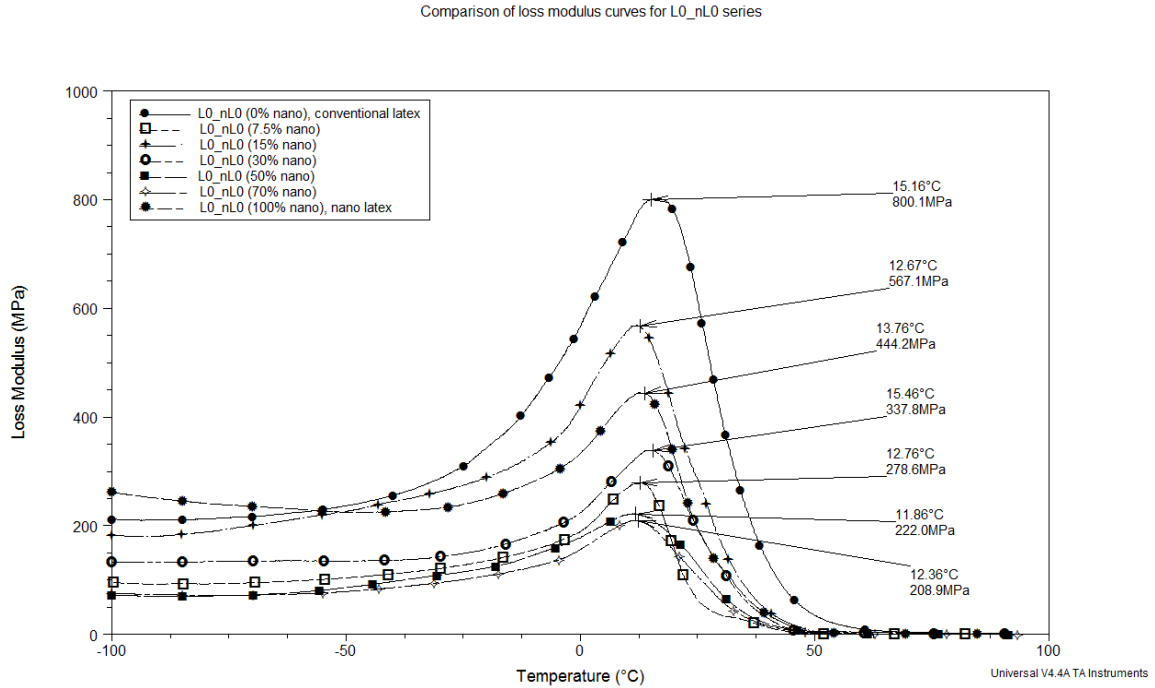
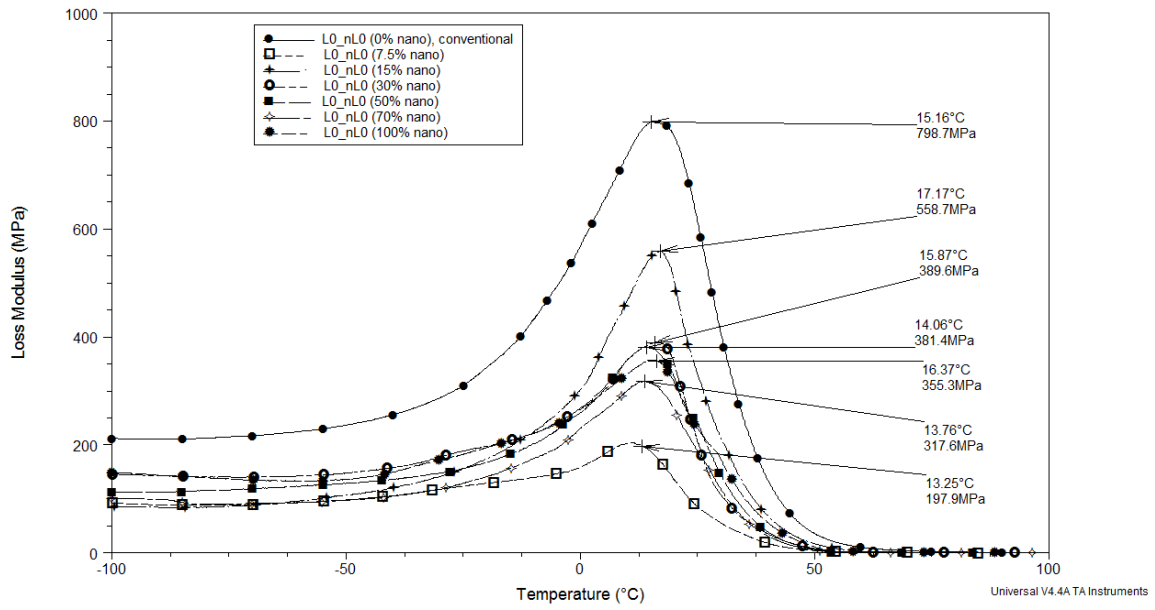


Figure 5.33: (a) Comparison of loss modulus curves and (b) Comparison of storage modulus curves for L0_nL0 series

Comparison of loss modulus curves for L0_nIL4 series



Comparison of storage modulus curves for L0_nIL4 series

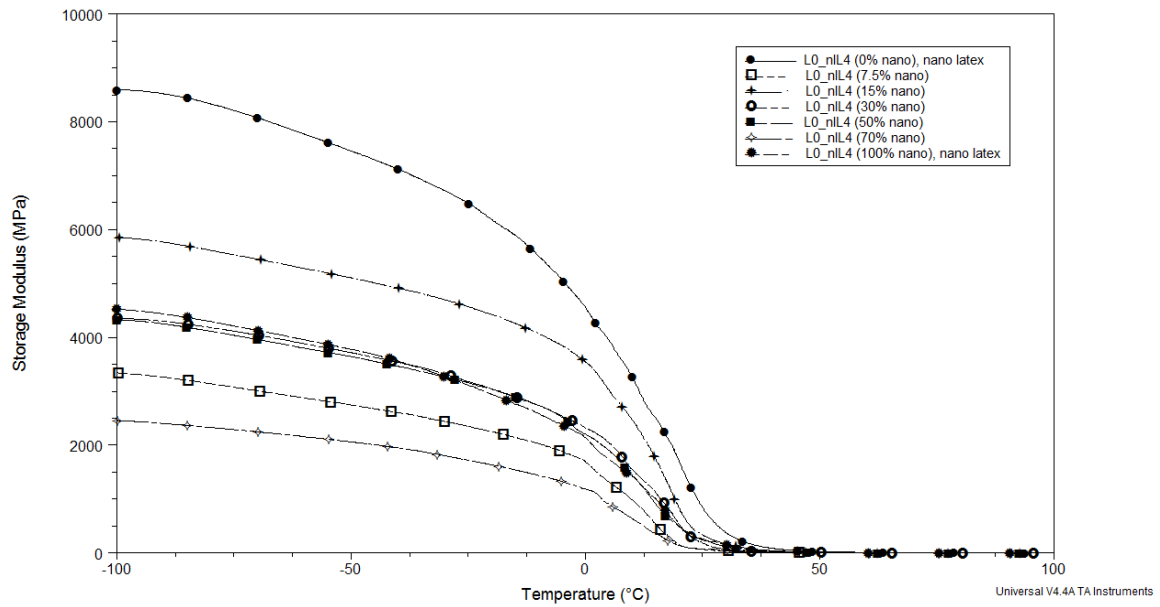
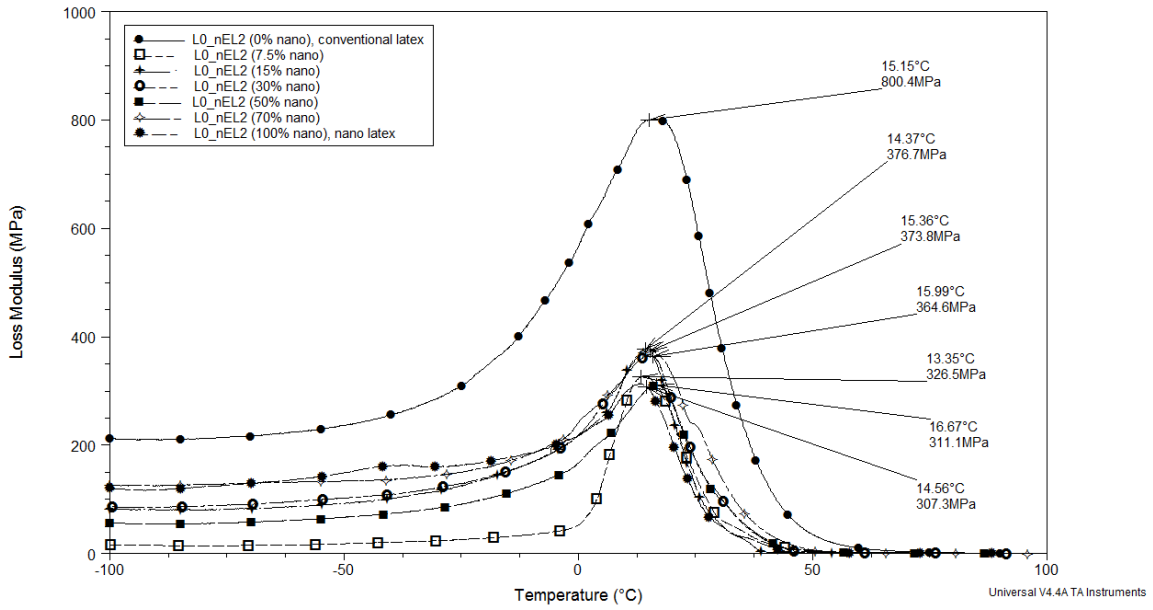


Figure 5.34: (a) Comparison of loss modulus curves and (b) Comparison of storage modulus curves for L0_nIL4 series

Comparison of loss modulus curves for L0_nEL2 series



Comparison of storage modulus curves for L0_nEL2 series

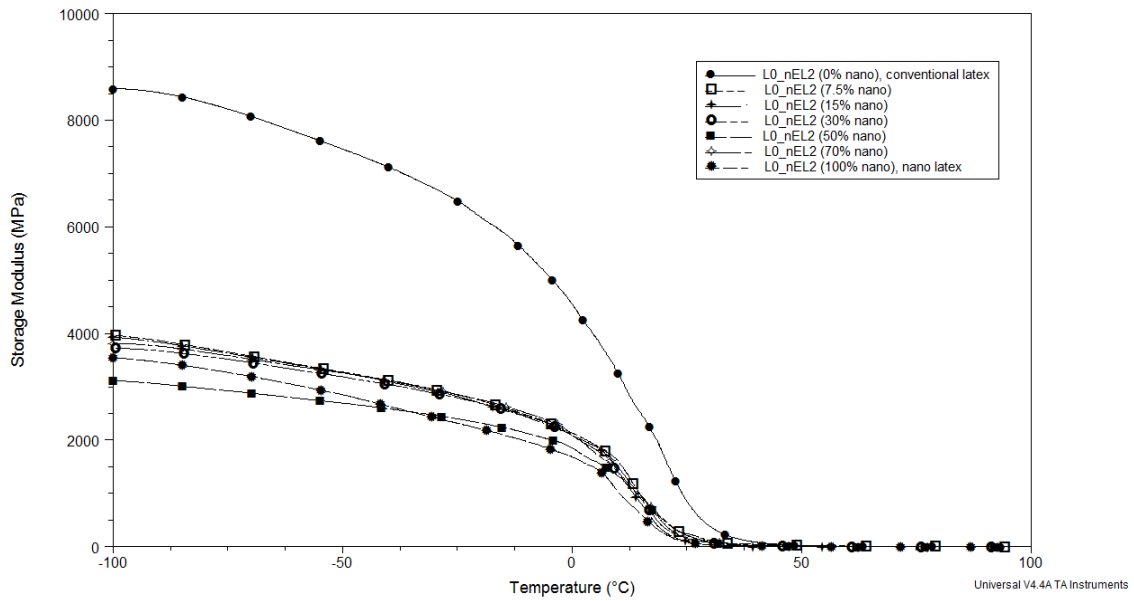
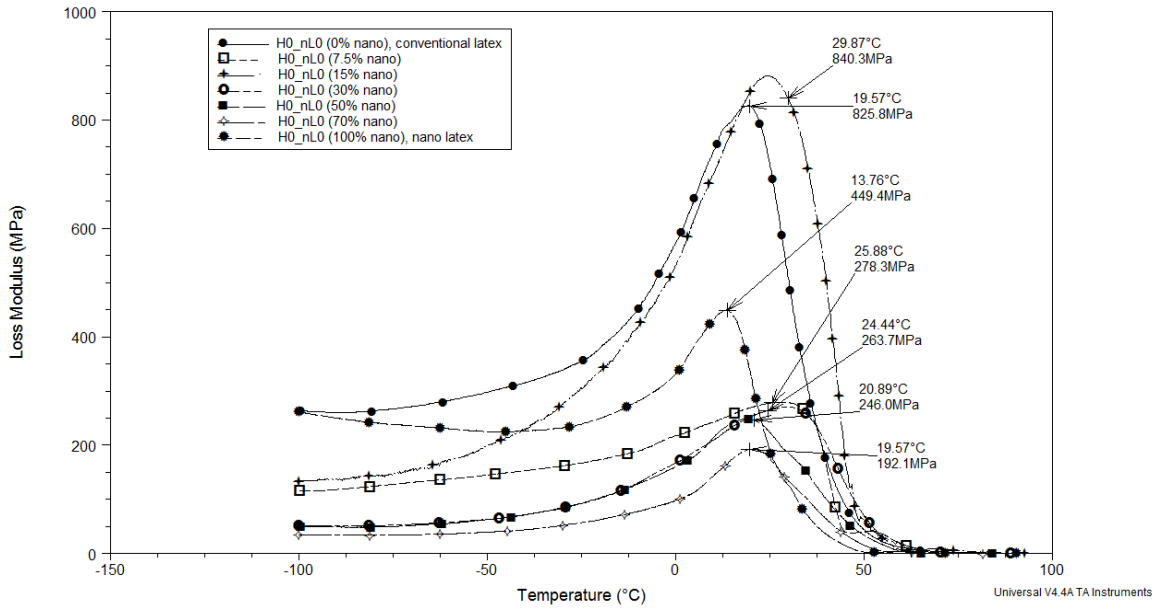


Figure 5.35: (a) Comparison of loss modulus curves and (b) Comparison of storage modulus curves for L0_nEL2 series

Comparison of loss modulus curves for H0_nL0 series



Comparison of storage modulus curves for H0_nL0 series

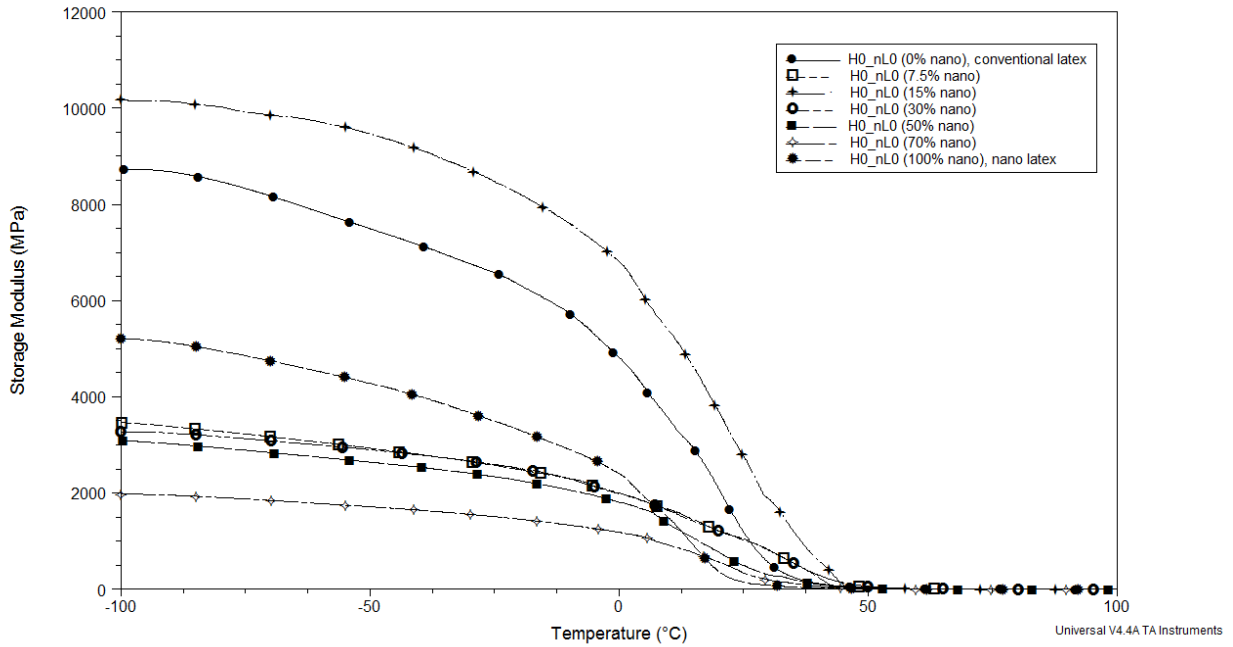
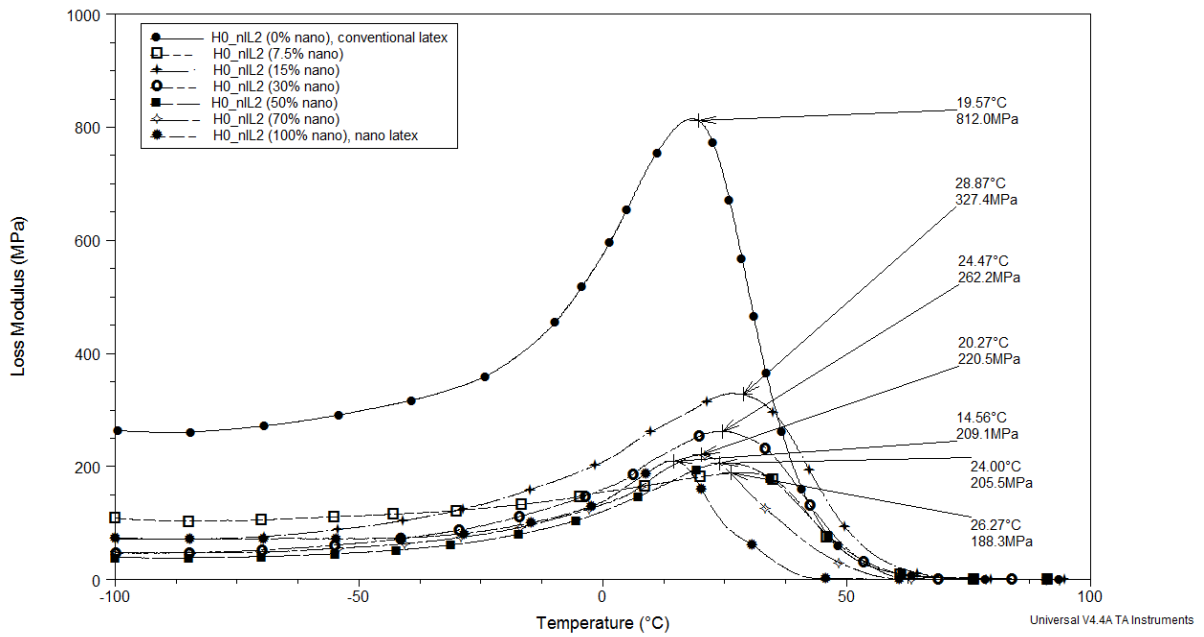


Figure 5.36: (a) Comparison of loss modulus curves and (b) Comparison of storage modulus curves for H0_nL0 series

Comparison of loss modulus curves of H0_nIL2 series



Comparison of storage modulus curves for H0_nIL2 series

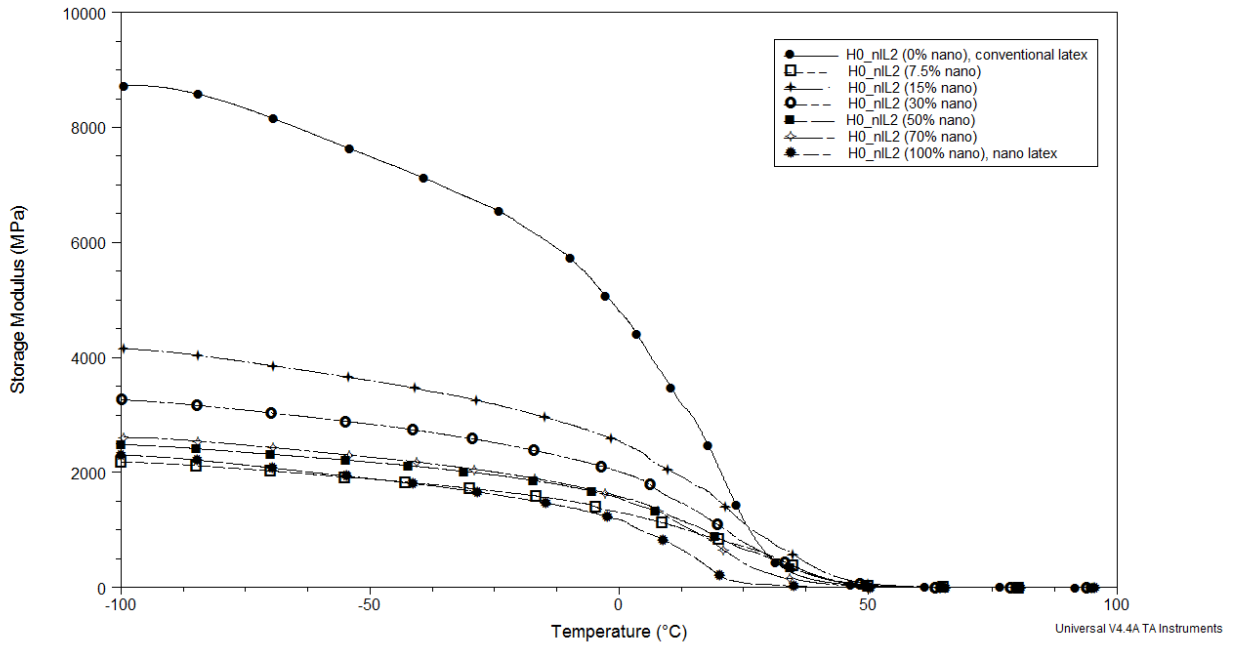
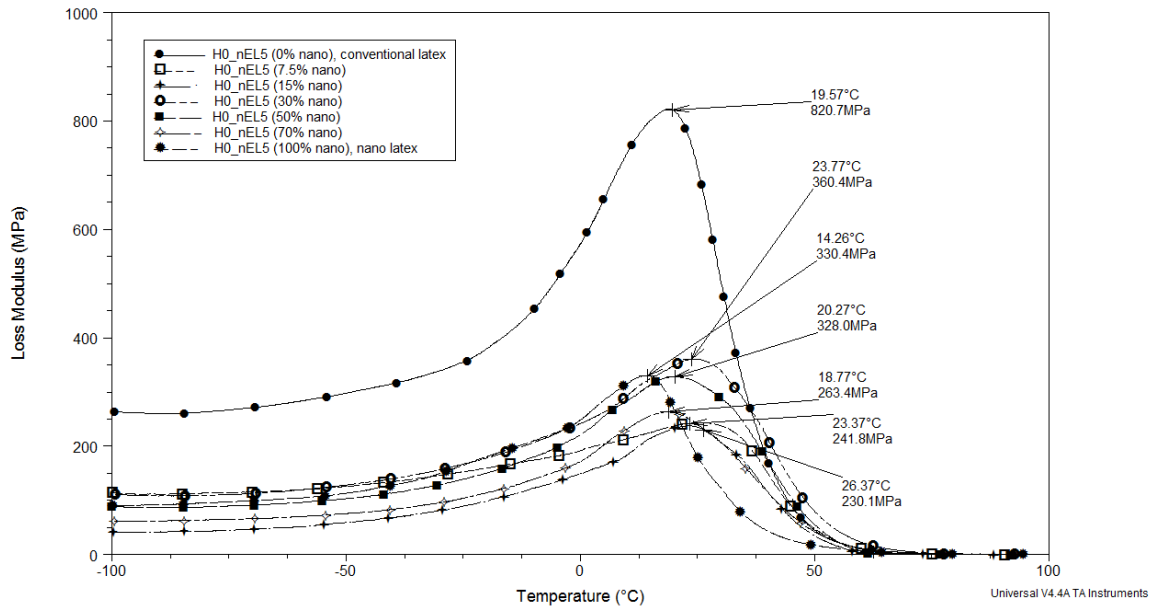


Figure 5.37: (a) Comparison of loss modulus curves and (b) Comparison of storage modulus curves for H0_nIL2 series

Comparison of loss modulus curves of H0_nEL5 series



Comparison of storage modulus curves for H0_nEL5 series

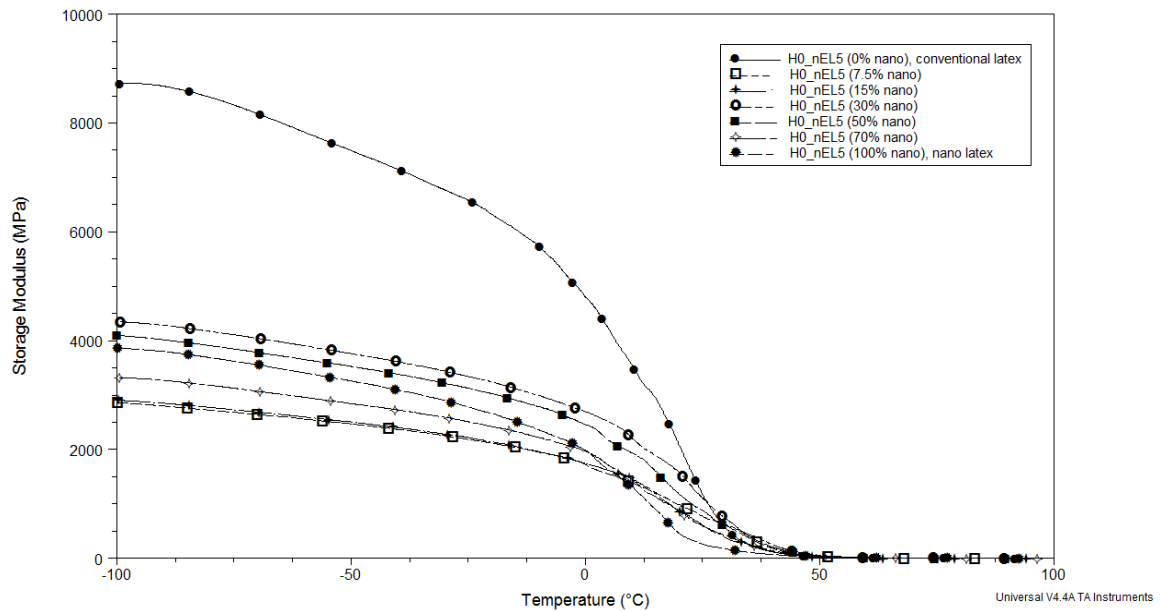
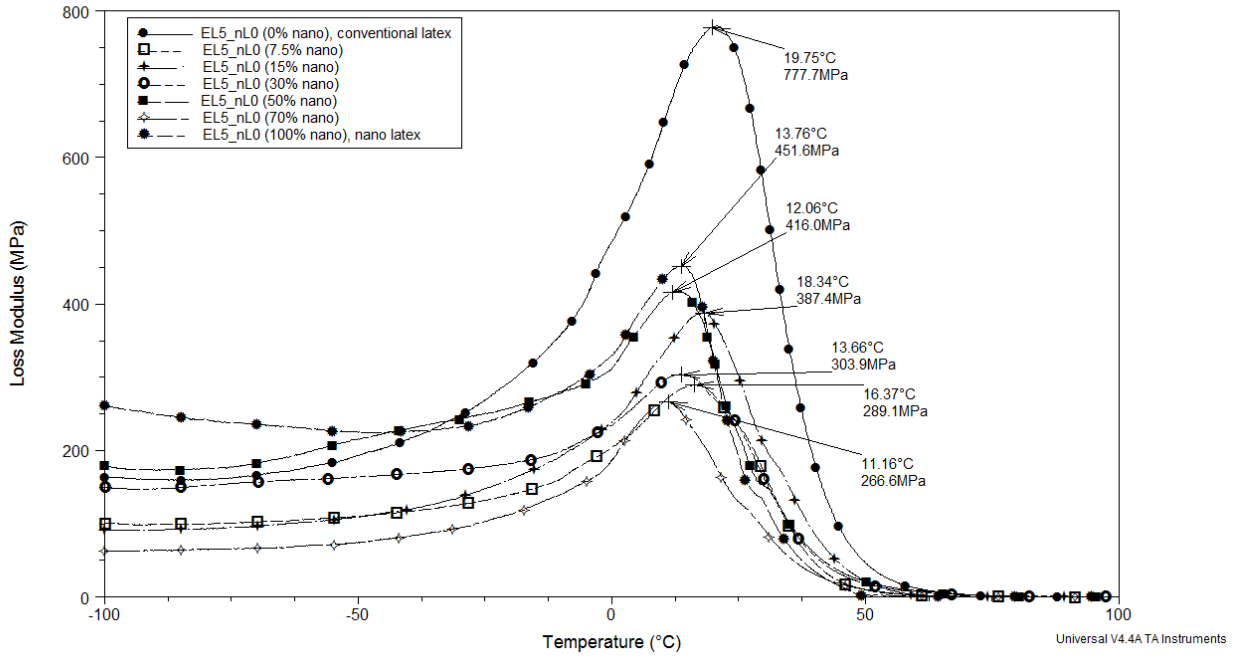


Figure 5.38: (a) Comparison of loss modulus curves and (b) Comparison of storage modulus curves for H0_nEL5 series

Comparison of loss modulus curves for EL5_nL0 series



Comparison of storage modulus curves of EL5_nL0 series

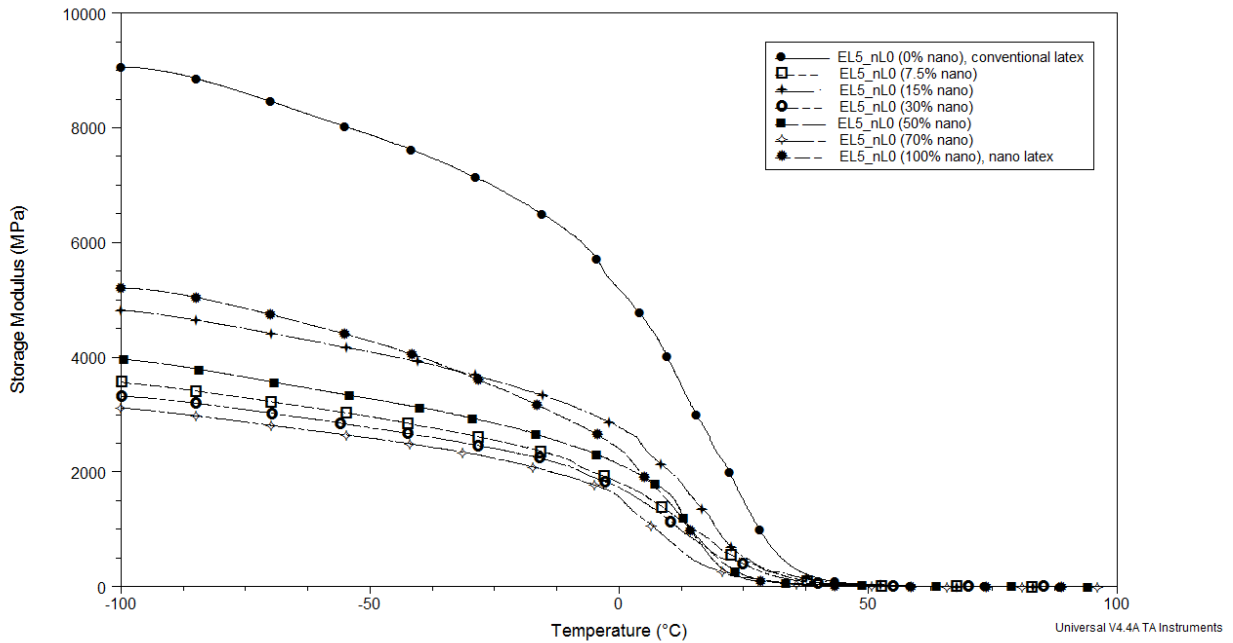
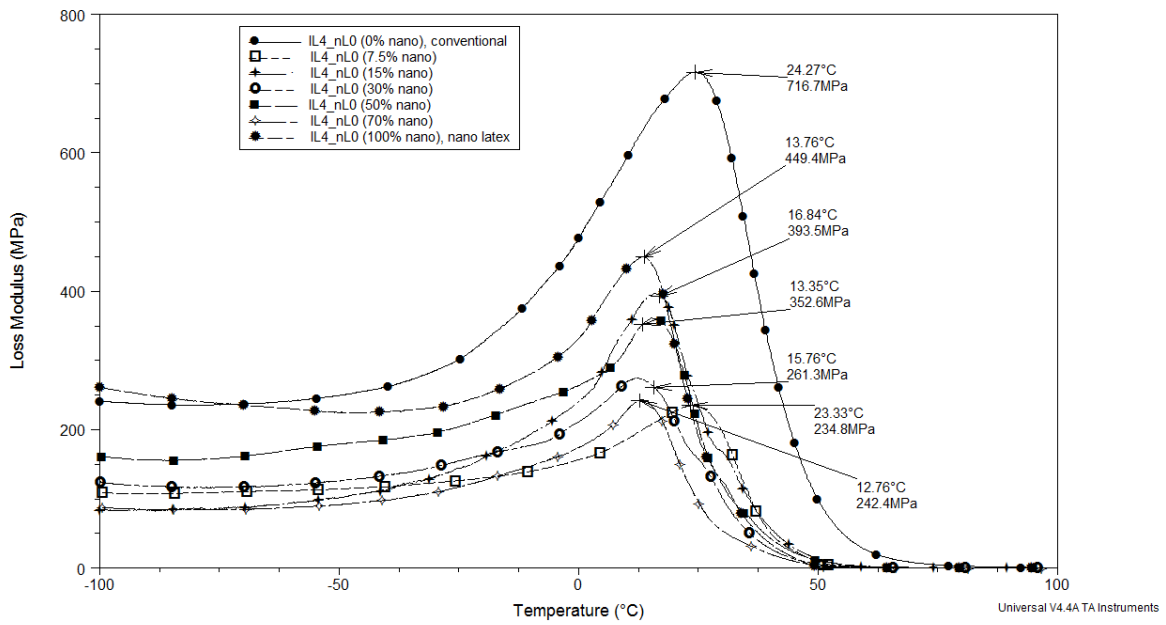


Figure 5.39: (a) Comparison of loss modulus curves and (b) Comparison of storage modulus curves for EL5_nL0 series

Comparison of loss modulus curves for IL4_nL0 series



Comparison of storage modulus curves for IL4_nL0 series

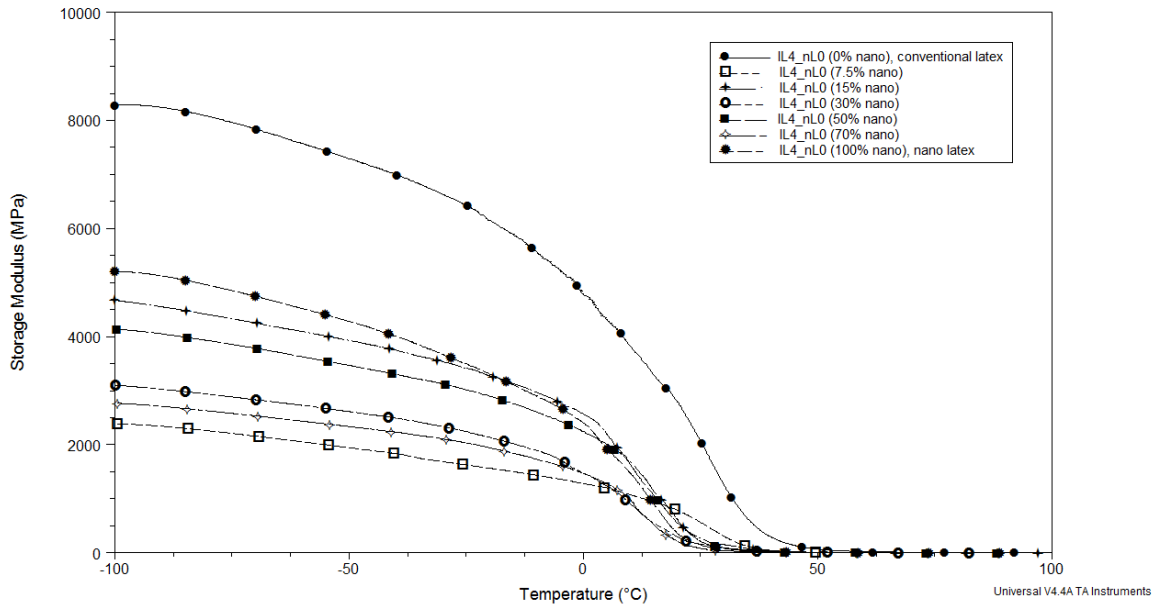
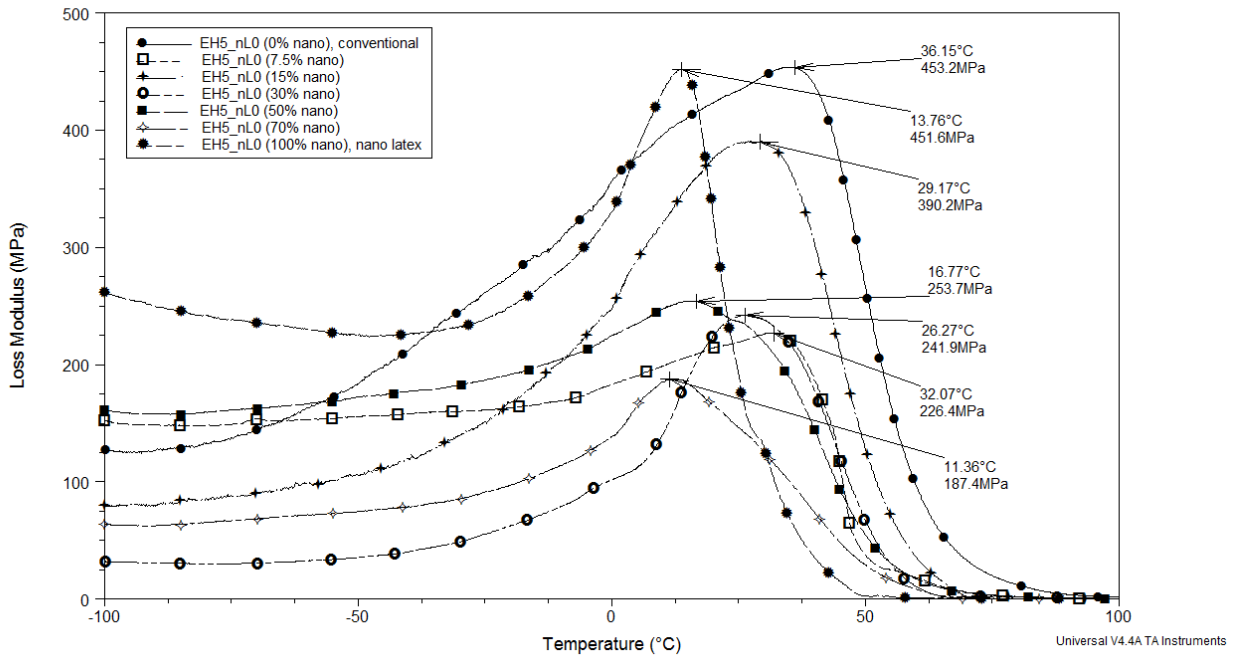


Figure 5.40: (a) Comparison of loss modulus curves and (b) Comparison of storage modulus curves for IL4_nL0 series

Comparison of loss modulus curves for EH5_nL0 series



Comparison of storage modulus curves for EH5_nL0 series

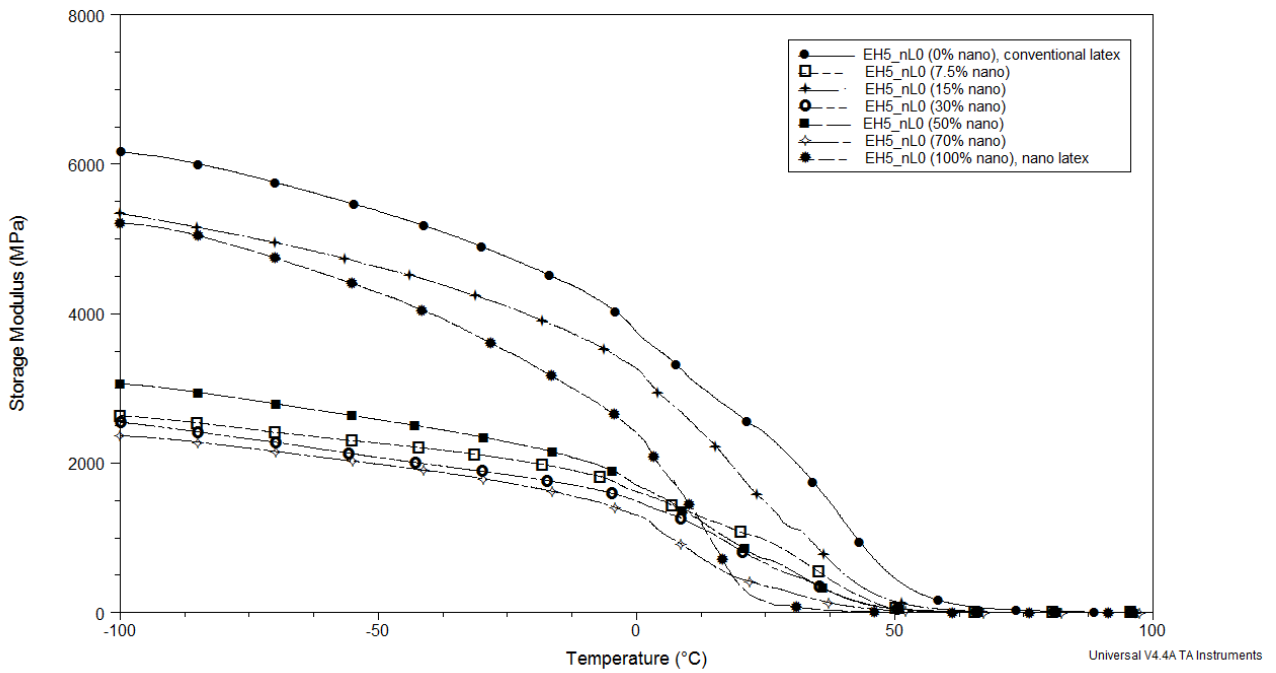
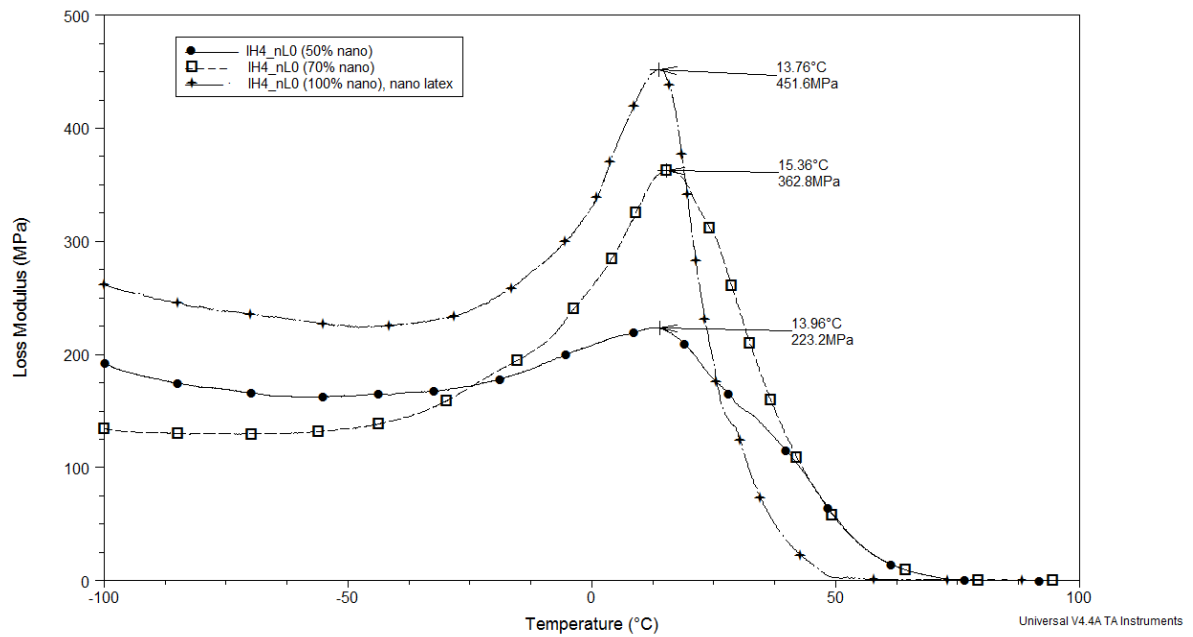


Figure 5.41: (a) Comparison of loss modulus curves and (b) Comparison of storage modulus curves for EH5_nL0 series

Comparison of loss modulus curves for IH4_nL0 series



Comparison of storage modulus curves of IH4_nL0 series

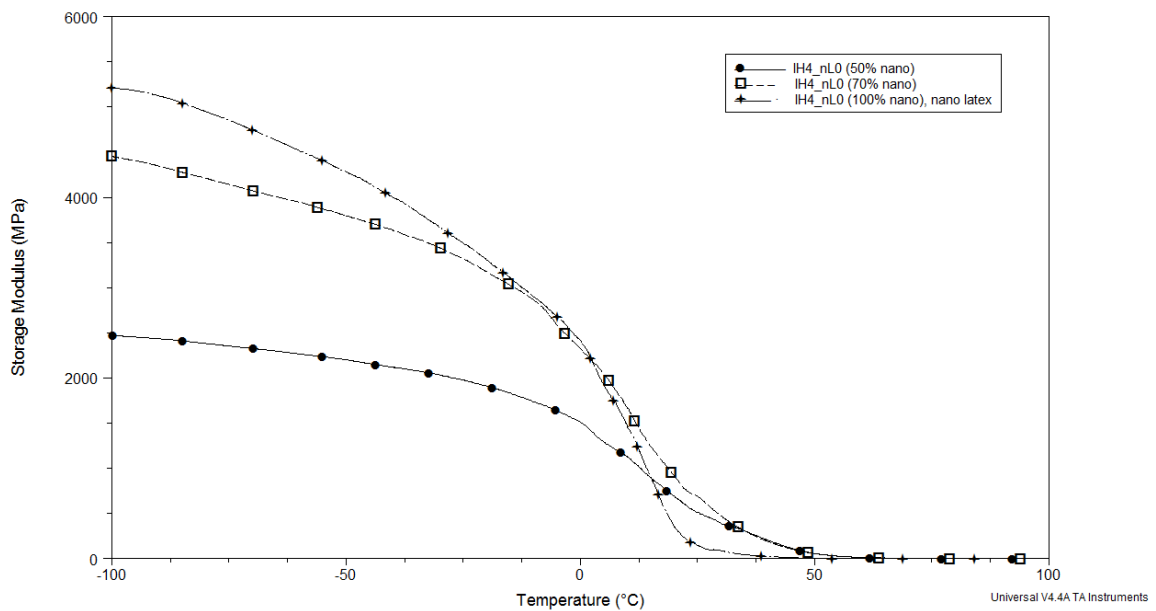


Figure 5.42: (a) Comparison of loss modulus curves and (b) Comparison of storage modulus curves for IH4_nL0 series

Table 5.24: Latex blend series L0_nL0

%nano by wt.	MDSC T _g (°C)	DMA			DMA Tan delta		DMA storage modulus (Mpa), E', in rubbery (80-90 °C) region
		Storage modulus inflection point (°C)	Loss peak temperature (°C)	Tan delta peak Temperature (°C)	(L)HWHH	(R)HWHH	
0%	7.05	13.8	15.2	40.7	15.8	21.7	3.1
7.5%	7.4	11.4	12.8	35.9	17.49	26.26	0.7
15%	6.38	13.9	12.7	37.6	17.93	19.57	1.8
30%	6.23	13.8	15.5	38	19.62	30.38	1.1
50%	6.26	7.4	11.9	36.7	14.65	32.01	0.6
70%	4.9	12.7	12.4	35	16.26	27.59	0.3
100%	4.77	13.1	13.8	32.5	18.65	18.85	0.9

Table 5.25: Latex blend series L0_nIL4

%nano by wt.	MDSC T _g (°C)	DMA			DMA Tan delta		DMA storage modulus (Mpa), E', in rubbery (80-90 °C) region
		Storage modulus inflection point (°C)	Loss peak temperature (°C)	Tan delta peak Temperature (°C)	(L)HWHH	(R)HWHH	
0%	7.05	13.8	15.2	40.7	16.88	19.62	3.1
7.5%	7.1	13.6	13.2	39.9	11.45	19.05	0.7
15%	7.17	17.9	17.3	43.9	17.6	21.52	1.2
30%	7.1	17.5	15.9	39.3	16.81	25.93	0.6
50%	7.08	13.7	14.1	35.8	20.5	32.65	0.3
70%	5.5	13.4	13.8	35.1	20.9	19.75	0.2
100%	10.9	17.1	16.4	37.2	17.99	19.51	0.7

Table 5.26: Latex blend series L0_nEL2

%nano by wt.	MDSC T _g (°C)	DMA			DMA Tan delta		DMA storage modulus (Mpa), E', in rubbery (80-90 °C) region
		Storage modulus inflection point (°C)	Loss peak temperature (°C)	Tan delta peak Temperature (°C)	(L)HWHH	(R)HWHH	
0%	7.05	13.8	15.2	40.7	16.88	19.62	3.1
7.5%	7.2	9	13.4	36.8	9.83	22.17	0.5
15%	7.62	10.5	14.4	44.7	13.45	13.05	1.6
30%	4.95	16.4	16.1	35.4	17.21	30.64	0.3
50%	4.8	17.5	16.7	33.1	15.49	31.36	0.2
70%	4.6	12.3	15.4	38.4	16.54	33.46	0.7
100%	3.13	9.4	14.6	35.8	18.01	25.79	0.4

Table 5.27: Latex blend series H0_nL0

%nano by wt.	MDSC T _g (°C)	DMA			DMA Tan delta		DMA storage modulus (Mpa), E', in rubbery (80-90 °C) region
		Storage modulus inflection point (°C)	Loss peak temperature (°C)	Tan delta peak Temperature (°C)	(L)HWHH	(R)HWHH	
0%	26.3	20.8	19.6	43.9	15.33	22.17	3
7.5%	25.9	28.2	25.9	56.8	12.8	20.2	1.2
15%	23.5	33.1	29.9	58.1	17.7	16.8	2.5
30%	21	22.9	24.4	52.4	17.16	23.44	0.7
50%	18.8	23	21	48.5	19.71	21.89	0.3
70%	11.9	9.9	19.6	45.6	20.32	26.68	0.2
100%	4.77	13.1	13.8	32.5	18.65	18.85	0.9

Table 5.28: Latex blend series H0_nIL2

%nano by wt.	MDSC T _g (°C)	DMA			DMA Tan delta		DMA storage modulus (Mpa), E', in rubbery (80-90 °C) region
		Storage modulus inflection point (°C)	Loss peak temperature (°C)	Tan delta peak Temperature (°C)	(L)HWHH	(R)HWHH	
0%	26.3	20.8	19.6	43.9	15.02	22.38	3
7.5%	26.1	21.8	26.3	56.6	17.06	22.54	1
15%	25.7	34	28.9	57.6	16.48	22.02	1.8
30%	20.8	20.2	24.5	50.2	18.97	17.63	0.5
50%	21.2	19.9	24.1	49.8	20.1	21.2	0.4
70%	15.7	18.9	20.3	47.4	20.75	15.05	0.3
100%	4.67	17.4	14.6	33.5	16.12	19.38	0.3

Table 5.29: Latex blend series H0_nEL5

%nano by wt.	MDSC T _g (°C)	DMA			DMA Tan delta		DMA storage modulus (Mpa), E', in rubbery (80-90 °C) region
		Storage modulus inflection point (°C)	Loss peak temperature (°C)	Tan delta peak Temperature (°C)	(L)HWHH	(R)HWHH	
0%	26.3	20.8	19.6	43.9	16.72	21.08	3
7.5%	25.7	24.8	23.4	54.1	17.03	22.67	0.7
15%	24.5	33.7	26.4	55.6	15.48	22.02	0.8
30%	23.1	22.8	23.8	53.1	18.81	22.89	0.5
50%	21.4	16	20.3	48.1	16.72	21.38	0.3
70%	20.3	16.3	18.8	46.3	21.07	23.83	0.3
100%	5.15	15.9	14.3	41.4	14.04	32.36	1.3

Table 5.30: Latex blend series EL5_nL0

%nano by wt.	MDSC T _g (°C)	DMA			DMA Tan delta		DMA storage modulus (Mpa), E', in rubbery (80-90 °C) region
		Storage modulus inflection point (°C)	Loss peak temperature (°C)	Tan delta peak Temperature (°C)	(L)HWHH	(R)HWHH	
0%	11.6	11.4	19.8	45.4	18.75	25	9
7.5%	10.5	11.1	16.4	37.2	23.04	35.42	1.2
15%	10.1	18.7	18.3	40.4	15.58	26.08	4.5
30%	9.86	10.7	13.7	39.3	22.92	35.42	1.2
50%	9.77	13.3	12.1	29.6	21.9	31.3	0.6
70%	4.7	2.4	11.2	31.8	25	25	0.6
100%	4.77	13.1	13.8	32.5	18.65	18.85	0.9

Table 5.31: Latex blend series IL4_nL0

%nano by wt.	MDSC T _g (°C)	DMA			DMA Tan delta		DMA storage modulus (Mpa), E', in rubbery (80-90 °C) region
		Storage modulus inflection point (°C)	Loss peak temperature (°C)	Tan delta peak Temperature (°C)	(L)HWHH	(R)HWHH	
0%	14.6	26.3	24.3	50.3	16.92	21.58	5.2
7.5%	12.8	27.1	23.3	46.1	16.4	27.6	0.3
15%	11.6	19.8	16.8	42.4	22.09	15.41	0.6
30%	11	12.4	15.8	40.4	18.21	26.49	0.5
50%	10.8	11.4	13.3	35.6	20.58	29.42	0.2
70%	4.7	10.4	12.8	39.2	18.64	29.21	0.2
100%	4.77	13.1	13.8	32.5	18.65	18.85	0.9

Table 5.32: Latex blend series EH5_nL0

%nano by wt.	MDSC T _g (°C)	DMA			DMA Tan delta		DMA storage modulus (Mpa), E', in rubbery (80-90 °C) region
		Storage modulus inflection point (°C)	Loss peak temperature (°C)	Tan delta peak Temperature (°C)	(L)HWHH	(R)HWHH	
0%	29.7	38.5	36.2	63.9	22.6	26.3	13
7.5%	26.7	34.6	32.1	60.8	24.45	25.55	3.5
15%	25.8	18.3	29.2	56.9	18.66	26.09	2.2
30%	26.5	17.4	26.3	55.8	19.2	32.9	1.7
50%	22.5	13.5	16.8	54.4	19.84	27.03	1.2
70%	22.1	4.9	11.4	49.7	20.98	24.27	0.6
100%	4.77	13.1	13.8	32.5	18.65	18.85	0.9

Table 5.33: Latex blend series IH4_nL0

%nano by wt.	MDSC T _g (°C)	DMA			DMA Tan delta		DMA storage modulus (Mpa), E', in rubbery (80-90 °C) region
		Storage modulus inflection point (°C)	Loss peak temperature (°C)	Tan delta peak Temperature (°C)	(L)HWHH	(R)HWHH	
0%	33	*	*	*	*	*	*
7.5%	32.8	*	*	*	*	*	*
15%	31.9	*	*	*	*	*	*
30%	29.8	*	*	*	*	*	*
50%	29.1	13	14	58.6	19.77	24.03	0.5
70%	4.11	11.4	15.4	57.2	24.05	23.05	0.7
100%	4.77	14.9	13.8	32.5	18.65	18.85	0.9

Note: Asterisk in Table indicates sample was too brittle to test

Conclusions:

The overall results of the present study described in this chapter suggest these conclusions:

- Blending conventional latexes with nanoparticle latexes may be a useful approach to near-zero VOC coating formulations. The blends combine substantial improvements in certain film properties with a modest decrease in minimum filming temperatures (MFT). None of the properties we tested were seriously degraded by blending. Further, from all data it can be clearly stated that the nanoparticles are functioning as coalescing aids. This could be due to number reasons such as better packing, release of surplus surface energy from the nanoparticles, action of extra surfactant that comes along with the nanoparticles, and conceivably thermodynamic effect of allowing constrained molecules in nanoparticles to extend to RMS dimensions.
- Film properties are strongly influenced by T_g , crosslinking, particle size and distribution, blending, and blend ratios.
- Independent of T_g and crosslinking, blending at the optimum ratio has a large effect on bulk film properties such as modulus and hardness and also a beneficial effect on solvent resistance and block resistance. Improved molecular interpenetration (the third stage of film formation) is a suggested explanation.
- Crosslinking the nanoparticles can be combined with blending to further enhance properties.
- AFM images and the surface smoothness graphs showed that the nanoparticles with T_g 's of 5 °C appear to populate both film surfaces, increasing gloss and adhesion.

- The optimum level of 22 nm nanoparticles in 130 nm conventional particles is thought to be somewhere around 15/1 to 30/1 on a number of particles basis. For a 15 wt % nanoparticle blend this ratio is roughly 25/1.
- Substantial property improvements also occur at 7.5 wt % and 30 wt% nanoparticles.

References

1. Agarwal, N.; Farris, R. J., Mechanical Properties of Acrylic Based Latex Blends. *POLYMER ENGINEERING AND SCIENCE* 2000, 40, (2), 376-390.
2. Boyars, B., Daniels, E.S., Storer, R., Klein, A., The Influence of Latex Blend Composition on Crosslinking and Mechanical Properties. *Journal of Applied Polymer Science* 2007, 104, 3774-3779.
3. Colombini, D., Ljungberg, N., Hassander, H., Karlsson, O.J., The effect of the polymerization route on the amount of interphase in structured latex particles and their corresponding films. *Polymer* 2005, 46, 1295-1308.
4. Colombini, D., Hassander, H., Karlsson, O.J., Maurer, F.H., Effects of Thermal Annealing on the viscoelastic Properties and Morphology of Bimodal Hard/Soft Latex Blends. *Journal of Polymer Science: Part B: Polymer Physics* 2005, 43, 2289-2306.
5. Eckersley, S. T.; Helmer, B. J., Mechanistic Considerations of Particle Size Effects on Film Properties of Hard/Soft Latex Blends. *Journal of Coatings Technology* 1997, 69, (864), 97-107.
6. Geoffrey, B. A.; Bignell, D. S.; Cook, I. B.; Leary, B.; Lyons, C. J. (to ICI Australia Operations Proprietary Ltd.) "Addition polymer particles". U.S. Patent 5244737, 1993.
7. Geurts, J., Bouman, J., Overbeek, A., New Waterborne Acrylic Binders For Zero VOC paints. *J.Coat.Technol.Res.* 2008, 5, (1), 57-63.
8. Geurts, J. M., Lammers, M., German A.L., The Effect of Bimodality of the Particle Size Distribution on Film Formation of Lattices. *Colloids Surf. A: Physiochem. Eng. Aspects* 1996, 108, (2-3), 295-303.
9. Hagen, R., Salmen, L., Karlsson, O., Wesslen, B., Viscoelastic Properties and Film Morphology of Heterogeneous Styrene-Butadiene Latexes. *J.Appl.Polym.Sci.* 1996, 62, (7), 1067-1078.
10. Heuts, M. P. J., Febre Le, R.A., Hilst Van, J.L.M., Overbeek, G.C., Influence of Morphology on Film Formation of Acrylic Dispersions. *Am.Chem.Soc.Symp.Ser.* 1996, 648, 271-285.
11. Jocelyn, M. C.; William, M. C.; William, P. H.; Leary, B.; Henry, C. S.; Thamala, C. W. (to Orica Australia PTY Ltd.) "Aqueous polymer dispersion". U.S. Patent 6777489 2004.
12. Juhue, D.; Lang, J., Film Formation from Dispersion of Core-Shell Latex Particles. *Macromol.* 1995, 28, 1306-1308.
13. Keddie, J. L., Film Formation of Latex. *Mater. Sci.Eng. Rep.* 1997, 21, (3), 101-170.
14. Leary, B.; Lyons, C. J., "A Novel Composite Polymer Latex Technology". *Australian Journal of Chemistry* 1989, 42, (12), 2055-2070.
15. Lepizzera, S., Lhommeau, C., Dilger, G., Pith, T., Lambla, M., Film Forming Ability and Mechanical Properties of Coalesced Latex Blends. *Journal of Polymer Science: Part B: Polymer Physics* 1997, 35, 2093-2101.
16. Schmidt, A.; Gunter, K.; Werner, C. (to Bayer Aktiengesellschaft) "Aqueous dispersions based on (meth)acrylic acid alkyl ester polymers with two pronounced, substantially non-overlapping peaks in the particle size distribution within specific particle size ranges, and a process for the preparation and use thereof". United States Patent 4384056, 1983.

17. Tang, J., Daniels, E.S., Dimonie V.L., Vratsanos, M.S., Klein, A., El-Aasser, M.S., Mechanical Properties of Films Prepared from Model High-Glass-Transition-Temperature/Low-Glass-Transition Temperature Latex Blends. *Journal of Applied Polymer Science* 2002, 86, 2788-2701.
18. Tzitzinou, A., Keddie, J.L., Geurts, J.M., Peters, A.C.I.A., Satguru, R., Film Formation of Latex Blends with Bimodal Particle Size Distributions: Consideration of Particle Deformability and Continuity of the Dispersed Phase. *Macromol* 2000, 33, 2695-2708.
19. Vandezande, G. A.; Rudin, A., Novel Composite Latex Particles for Use in Coatings. *J.Coat.Technol.* 1994, 66, (828), 99-108.
20. Winnik, M. A.; Feng, J., Latex Blends: An Approach to Zero VOC Coatings. *Journal of Coatings Technology* 1996, 68, (852), 39-50.
21. Wu, W.; Olesen, K. R.; Miner II, A. R.; Schneider, J. A., "Vinyl Acetate-Ethylene and Acrylic Latexes to Achieve Targeted Performance Properties" *JCT Coatings Tech.* 2008, pp 44-52.
22. Joshi, R.; Lefevre, E.; Patel, C.; Provder, T.; Crombez, R.; Shen, W.; Jones, F. N., Thermoanalytical and morphological studies of cross-linked latex films by advanced techniques. *Journal of Thermal Analysis and Calorimetry* 2008, 93, (1), 19-26.
23. Joshi, R. G.; Provder, T.; Ziemer, P. D.; Mao, W.; Shen, W.; Jones, F. N., Investigation of the effect of precoalescence or postcoalescence crosslinking on film formation, properties, and latex morphology. *Journal of Coatings Technology and Research* 2008 (online first, DOI: 10.1007/s11998-008-9115-7).
24. Taylor, J. W.; Winnik, M. A., "Functional Latex and Thermoset Latex Films,". *JCT Research* 2004, 1, (3), 163-190.
25. "Diacetone acrylamide, N-(1,1dimethyl-3-oxobutyl)-acrylamide," *Kyowa Hakko U.S.A. Inc. Technical information sheet* 2008 (retrieved), p 4.
26. Emmons, W. D., (to Rohm and Haas) "Ambient or low-temperature curable coatings,". U.S. Patent 4,210,565, 1980.
27. Geelhaar, H. J.; Penzel, E.; Ley, G., (to BASF) "Binders for paints," U.S. Patent 4,267,091, 1981.
28. Krajnik, J. M.; Lam, V. H.; Sabo, L. O.; Camerson, J. M.; Mittleman, M. L.; Wise, K. M., (to Sherwin-Williams) "Waterborne coating compositions,". U.S. Patent Application 20020103278, 2002.
29. Robinson, G. F.; Shemancik, R. C.; Speight, R. D.; Wong, P. T.; Znidarsic, K. M. (to Akzo Nobel), "Coating Compositions and Coatings Formed Therefrom." US Patent 6,605,359, 2003.
30. Ming, W.; Jones, F. N.; Fu, S., High Solids-content Nanosize Polymer Latexes Made by Microemulsion Polymerization. *Macromol. Chem. Phys.* 1998, 199, 1075-1079.
31. Ming, W.; Jones, F. N.; Fu, S., Synthesis of nanosize poly(methyl methacrylate) microlatexes with high polymer content by a modified microemulsion polymerization. *Polym. Bull.* 1998, 40, (6), 749-756.
32. Ming, W.; Zhao, Y.; Cui, J.; Fu, S.-K.; Jones, F. N., "Formation of Irreversible Nearly Transparent Physical Polymeric Hydrogels During a Modified Microemulsion Polymerization," *Macromol* 1999, 32, 528-530.
33. Ming, W.; Zhao, Y.; Fu, S.; Jones, F. N. In *Polym. Mater. Sci. Eng.*, 1999; ACS: 1999; p 514.

34. Winnik, M. A., "The formation and properties of latex films". In *Emulsion Polymerization and Emulsion Polymers*, Lovell, P. A.; El-Aasser, M. S., Eds. Wiley: New York, 1997; pp 467–518.
35. Winnik, M. A., "Interdiffusion and Crosslinking in Thermoset Latex Films". *J. Coat. Technol.* 2002, 74, (925), 49-63.
36. Winnik, M. A., "Crosslinking and Polymer Interdiffusion in Latex Films". *Polym. Prep.* 2003, 44, (1), 100-101.
37. Xu, J.; Dimonie, V. L.; Sudol, D. E.; El-Aasser, M. S., Crosslinking of isocyanate functional acrylic latex with telechelic polybutadiene. I. Synthesis and characterization. *J. Appl. Polym. Sci.* 1997, 69, (5), 965-975.
38. Zosel, A.; Ley, G., "Influence of crosslinking on structure, mechanical properties, and strength of latex films". *Macromolecules*, 1993, 26, 2222–2227.
39. Tamai, T.; Pinenq, P.; Winnik, M. A., "Effect of cross-linking on polymer diffusion in poly(butyl methacrylate-co-butyl acrylate) latex films". *Macromolecules* 1999, 32, 6102-6110.
40. Aradian, A.; Raphael, E.; G., d. G. P., "A scaling theory of the competition between interdiffusion and cross-linking at polymer interfaces". *Macromolecules* 2002, 35, 4036-4043.
41. Ghazaly, H. M.; Daniels, E. S.; Dimonie, V. L.; El-Aasser, M. S.; Klein, A., "Synthesis and characterization of a macromonomer crosslinker". *J. Appl. Polym. Sci.* 2000, 77, 1362–1368.
42. Ghazaly, H. M.; Daniels, E. S.; Dimonie, V. L.; Klein, A.; El-Aasser, M. S., "Miniemulsion copolymerization of n-butyl methacrylate with crosslinking monomers". *J. Appl. Polym. Sci.* 2001, 81, 1721-1730.
43. Ghazaly, H. M.; Daniels, E. S.; Dimonie, V. L.; Klein, A.; Sperling, L. H.; El-Aasser, M. S., "Properties of N-butyl methacrylate copolymer latex films derived from crosslinked latex particles" *J. Appl. Polym. Sci.* 2003, 88, 42-49.
44. Kessel, N.; Illsley, D. R.; Keddie, J. L., "The Influence of Interdiffusion and Crosslinking in the Film Formation of an Acrylic Latex" *J. Coat. Technol. Res.* 2008, (online first, DOI:10.1007/s11998-008-9096-6).
45. JIANG, W.; YANG, W.; ZENG, X.; FU, S., Structure and Properties of Poly(methyl methacrylate) Particles Prepared by a Modified Microemulsion Polymerization. *Journal of Polymer Science: Part A: Polymer Chemistry* 2004, 42, 733-741.
46. Jones, F. N.; Joshi, R. G.; Provder, T.; Shen, W. In *Blending Polymer Nanoparticles with Conventional Latexes*, CoatingsTech Conference, Indianapolis, IN, 2009; FSCT-NPCA: Indianapolis, IN, 2009.
47. Hill, L. W., "Dynamic Mechanical and Tensile Properties". In *Paint and Coatings Testing Manual: Fourteenth Edition of the Gardner-Sward Handbook*, Koleske, J. V., Ed. ASTM: Ann Arbor, MI, 1995; pp 534–546.

Chapter 6

Conclusions

This study serves as a fundamental and practical contribution to latex research, forming a basis for exploring potential applications of crosslinked and nanoparticle size latexes and their blends as a binder in paints, coatings, or adhesives. The main goal of the present study was to investigate the effect(s) of type (pre-coalescence or post-coalescence) and level of crosslinking, particle size and distribution, glass transition temperature (T_g), and blends of conventional and nanoparticle latexes and their different weight ratios on latex film formation process, end-use properties, fundamental thermal and mechanical properties, and latex morphology.

The key highlights of present research are shown below:

- When comparing post-coalescence versus pre-coalescence crosslinking, the research data (Chapter 3) clearly showed that at increasing levels of crosslinking (up to 5 wt. %) post-coalescence crosslinking showed improvement in latex end-use and mechanical properties due to sufficient interdiffusion of the polymer chains between the particles to interdiffuse and interpenetrate adequately before the crosslink density was high enough to impede formation of films with desirable end-use properties. On the other hand, pre-coalescence crosslinking studied showed that up to a certain level (up to 0.6% to 1.2%) the latex properties are neutral or even favorable for overall properties. However, at levels higher than 0.6% to 1.2%, the polymer chains within particles became increasingly resistant to interdiffusion between particles and perhaps to coalescence, resulting into inferior film properties.
- Studying the effect of type of crosslinking on glass transition temperature, the test data clearly demonstrated that at increasing levels of pre-coalescence crosslinking, the T_g

increases. At 4 wt. % level (highest) of pre-coalescence crosslinked latexes, the T_g was increased by $10^{\circ}\text{C} \pm 2^{\circ}\text{C}$. In the case of post-coalescence crosslinked latexes, up to 5 wt. % level (highest) very slight effect was observed on T_g .

- An improved process was developed for making thermoplastic nanoparticle latexes in the 15-30 nm diameter range using monomers with low water solubility (Chapter 4).
- Studying the effects of particle size and distribution (Chapter 4), the experimental data showed that films made from nanosize latexes (avg. particle size = 20 to 25 nm) in general have superior gloss, solvent resistance, and adhesion and produce smoother films when compared to their conventional size counterparts (avg. particle size = 120-130nm). However, due to amount of surfactant present on and near the surface of nanosize latex films, they showed inferior water resistance and lower Young's modulus and area under the curve values when compared to the conventional size counterparts.
- Studying blends of conventional and nanoparticle latexes (Chapter 5) showed that in addition to T_g , crosslinking, particle size and distribution, film properties are also strongly influenced by blending and blend ratios. Independent of T_g and crosslinking, blending at the optimum ratio has a large effect on bulk film properties such as modulus and hardness, and also a beneficial effect on solvent resistance and block resistance. The optimum level of 22 nm nanoparticles in 130 nm conventional particles is thought to be somewhere around 15/1 to 30/1 on a number of particles basis. At 15 wt % nanoparticle blend ratio (roughly 25/1, nano/conventional), significant improvements in bulk properties such as Young's modulus (up to 13 fold increase) and surface properties such as specular 60° gloss value [from 35 (indicating a rough surface, as usual for films cast from latexes) to 92 (indicating a very smooth surface, unprecedented from films cast

from latexes)] was observed. At 7.5 wt% and 30 wt% of nanoparticles, the blends showed substantial improvements in latex properties.

- Our research data (Chapter 5) clearly demonstrated that blending conventional and nanoparticle latexes may be a useful approach to near-zero VOC coating formulations. The blends combined substantial improvements in certain film properties with a modest decrease in minimum filming temperatures (MFT). None of the properties tested were seriously degraded by blending. Further, from all data it can be clearly stated that the nanoparticles were functioning as coalescing aids. This could be due to number reasons such as better packing, release of surplus surface energy from the nanoparticles, action of extra surfactant that comes along with the nanoparticles, conceivably thermodynamic effect of allowing constrained molecules in nanoparticles to extend to RMS dimensions.

In the future, one of the major areas of research could be formulating the crosslinked and nanoparticle latexes and their blends in paints and coatings as binders and studying their effects on paint properties. Another area of future interest could be formulating nanosize latexes as additives (up to 5 wt% to 10 wt %) in paint formulation with other acrylic binders. Studying the effects of blends of pre-coalescence and post-coalescence crosslinked latexes in different weight ratios on latex film formation and properties could also be an area of potential future interest. Studying real-time film formation of nanoparticle latexes and their blends with conventional size (crosslinked or uncrosslinked latexes) will be useful study to understand the role of nanoparticle latexes as coalescing aids.